APPLIED STOCHASTIC OPTIMAL CONTROL FOR SPACECRAFT GUIDANCE

A Dissertation
Presented to
The Academic Faculty

By

Jack Ridderhof

In Partial Fulfillment
of the Requirements for the Degree
Doctor of Philosophy in
Aerospace Engineering

Georgia Institute of Technology

May 2021

APPLIED STOCHASTIC OPTIMAL CONTROL FOR SPACECRAFT GUIDANCE

Thesis committee:

Dr. Panagiotis Tsiotras, Advisor
School of Aerospace Engineering
Georgia Institute of Technology

Dr. Soumyo Dutta
Langley Research Center
National Aeronautics and Space Administration

Dr. Koki Ho
School of Aerospace Engineering
Georgia Institute of Technology

Dr. Behcet Açıkmeşe
Department of Aeronautics and Astronautics
University of Washington

Dr. Glenn Lightsey
School of Aerospace Engineering
Georgia Institute of Technology

Dr. John Carson III
Johnson Space Center
National Aeronautics and Space Administration

Date approved: April 9, 2021

The most important questions of life are indeed, for the most part,

really only problems of probability.

Pierre-Simon Laplace

For my parents

ACKNOWLEDGMENTS

It's often said that graduate students adopt the style and perspective of their academic advisors. I hope this is true. It's hard for me to imagine where I would be today without what I have learned from my advisor Panagiotis Tsiotras, and I would like to express my thanks for his help, guidance, and insight over the past five years. I would also like to thank my other thesis committee members Koki Ho, Glenn Lightsey, Soumyo Dutta, Behcet Açıkmeşe, and John Carson for their valuable perspective, comments, and discussions.

Four years ago, NASA took a chance by awarding me a Space Technology Research Fellowship, setting me on my current trajectory. I would like to extend my sincere thanks to everyone in the NSTRF program for this wonderful opportunity. In particular, I would like to thank my NSTRF advisor Soumyo Dutta, who has been my guide to applied research and to EDL writ large.

I would also like to thank the many other amazing engineers and researchers at NASA with whom I have had the opportunity to work with and learn from, including Richard Otero, David Way, and Breanna Johnson. I am especially thankful to Allen Chen for his mentorship, shared office space, and insight on the systems engineering angle to EDL. The lessons I have learned while working with these NASA engineers and researchers have crucially and positively shaped this dissertation.

Going as far back as elementary school, I have been surrounded by many wonderful and inspiring teachers. To name only a few: my middle school science teacher Ms. Caldwell, high school physics teacher Mr. Burmester, and high school robotics mentor Dr. Lockhart. Thank you.

Finally, I would like to thank my parents, and my brothers, for always being there.

TABLE OF CONTENTS

LIST OF TABLES

LIST OF FIGURES

LIST OF ACRONYMS

CS covariance steering

EDL entry, descent, and landing

GRF Gaussian random field

iCS iterative covariance steering

LC linear covariance

LQG Linear Quadratic Gaussian

MSL Mars Science Laboratory

NPC numerical-predictor corrector

PDG Powered Descent Guidance

SDE stochastic differential equation

SUMMARY

Optimal control theory has been successfully applied to a wide range of a problems in spacecraft trajectory optimization. Historically, the identification and management of uncertainty in spaceflight applications has been a separate endeavor from optimal trajectory design, with the exception of heuristic margins applied on the deterministic optimal trajectory. Following a stochastic optimal control approach, on the other hand, leads to the direct consideration of uncertainty for the design of closed-loop trajectories with probabilistic constraints. Resulting control laws are designed with respect to all possible trajectory and control input realizations, and the performance is evaluated over measures of the aggregate, or expected, state and control trajectories.

This dissertation focuses on specific applications of stochastic optimal control for spacecraft guidance, namely: powered descent guidance (PDG), atmospheric entry guidance, and aerocapture guidance. In addition, extensions are developed, which have further applications for spacecraft guidance, to the general theory of applying convex optimization to jointly steer the mean and covariance of stochastic systems, subject to probabilistic constraints.

For minimum-fuel PDG, the problem of setting non-conservative thrust margins is addressed by application of minimum-variance, covariance-constrained stochastic optimal control. The resulting closed-loop PDG process does not, with high probability, either saturate thrust commands or deviate too far from the desired landing site. Next, entry guidance in an atmosphere with spatially-dependent random variations in the atmospheric density is posed as a chance-constrained stochastic optimal control problem; the resulting targeting accuracy is shown to be better than the current state-of-the-art Apollo-derived entry guidance. Finally, in order to address the problem of aerocapture guidance around a planet with an unknown atmosphere, a successive convex programming-based method is developed to solve chance-constrained stochastic optimal control problems for systems acting in

the presence of a Gaussian random field. In a numerical example of an aerocapture mission with bank angle control, the developed method is used to solve for a control law that explicitly minimizes the 99^{th} percentile of the required Δv, subject to constraints on the probability distribution of the closed-loop bank angle during atmospheric flight.

CHAPTER 1
INTRODUCTION

Before the Viking 1 lander touched down in Chryse Planitia on July 20, 1976, marking the second successful landing of a spacecraft on Mars, and the start of the first successful surface mission on Mars[1], the project engineers were able to predict that the landing site would be, with about 99% confidence, within a 280 km by 100 km ellipse, referred to as the landing ellipse [2]. Over 36 years later, the landing site for the Mars Science Laboratory (MSL) rover Curiosity was predicted to be within a 20 km by 7 km ellipse with the same confidence, more than an order of magnitude improvement over the Viking landing ellipse [3]. Keeping with the trend towards improved accuracy, on February 18, 2021 the Mars 2020 Perseverance rover landed only approximately 2 km from the targeted touch-down point in Jezero Crater, within the predicted 7.1 km by 6.5 km 99% confidence ellipse [4]. Looking forward, current human Mars mission architectures require the landing site to be within a few meters of a designated position, and advanced robotic missions to scientifically interesting landing sites, such as a proposed sample return mission, require similar precision [5].

The improvement in the landing accuracy from Viking to MSL was the result of a range of advancements in entry, descent, and landing (EDL) technology. To name a few: more accurate interplanetary navigation decreased the uncertainty in the spacecraft states prior to entry into the Martian atmosphere [6]; an Apollo-derived entry guidance was able to fly out errors in the interplanetary delivery states and desensitize the entry trajectory to uncertainties in the atmosphere and in the vehicle aerodynamic characteristics [3]; and a guided powered descent phase removed the remaining kinetic energy of the descent vehicle

[1]The Mars 3 spacecraft successfully landed first on December 2, 1971, but stopped transmitting seconds after landing [1].

before the Curiosity rover was lowered to the surface by the Sky Crane maneuver [7].

Modeling, quantifying, and managing uncertainty is a central problem to be solved as part of the design of a successful EDL system. In the state-of-the-art approach, extensive Monte Carlo simulations are run to evaluate system performance, which is measured in terms of probabilities [8]. The landing ellipse is one example of a statistical performance metric. Monte Carlo simulations are also used for system-level decision making, by comparing functions of the probability distributions of select figures-of-merit resulting from competing design decisions [9]. For example: Adjusting a certain guidance parameter may decrease the average landed position error, but unacceptably increases the probability of exceeding a peak loading constraint during entry.

Guidance algorithms used for EDL have been, historically, based on flight heritage and are relatively simple in theory and implementation. Both the entry and powered descent guidance used for MSL and Mars 2020 are based on Apollo flight-proven algorithms and both only require basic arithmetic in onboard calculations. The EDL literature, in contrast, largely focuses on a class of guidance algorithms referred to as numerical-predictor correctors (NPCs), which are, in a sense, a special case of model predictive control (MPC).

On the theoretical side, probability and stochastic process theory provides a basis for understanding the evolution of uncertain systems, such as the entry, descent, and landing of a spacecraft. Constructing guidance laws to desirably steer the probability distribution of the uncertainty falls under the domain of stochastic optimal control. As we will show in the following chapters, the recently developed theory of covariance steering has many possible applications in spaceflight and EDL. In this method, one treats the covariance of an uncertain state as the object to-be-controlled, and probabilistic constraints on the trajectory are realized as joint constraints on the mean and covariance of the uncertain state. The probability distribution of an uncertain system is then explicitly controlled by selection of nominal control inputs and corresponding state feedback gains. Furthermore, under certain assumptions, this synthesis of feedback control laws for probabilistically-

constrained systems can be posed as a convex optimization problem.

There is, at present, a gap between the practice of EDL and the modern theory of control under uncertainty. The central aim of this dissertation is to take a step in the direction of filling this gap. As we will show in the following chapters, the application of theory to EDL is more complicated than simple substitution a particular set of equations of motion. Instead, care must be taken when identifying the problem to be solved, and nuances from the application domain drive the development of the relevant theory.

While the focus of this dissertation is on the application of stochastic optimal control for EDL, we also study the general theory for control under uncertainty, and the problem of aerocapture guidance in particular. Thus, our application is on the more broad topic of spacecraft guidance, rather than only EDL guidance.

In the following section, we review the powered descent, atmospheric entry, and aerocapture guidance problems and provide the necessary background for the existing solution methods. We also review recent developments from stochastic optimal control theory, and remark on necessary theoretical extensions required for application to EDL and aerocapture.

1.1 Background and Literature Review

1.1.1 Powered Descent Guidance

During the powered descent phase of a planetary landing mission, a descent vehicle uses the thrust from the rocket engines to remove the excess kinetic energy and steer the vehicle to the desired landing site. The Powered Descent Guidance (PDG) controller is responsible for determining and executing the sequence of thrust vectors for the vehicle to follow in order to reach the landing site, while satisfying certain constraints, such as avoiding subsurface flight or not exceeding a maximum velocity.

The majority of current PDG strategies still follow the powered descent architecture developed for the Apollo program. This PDG scheme represents trajectories as polynomials

parameterized in time. The Apollo PDG algebraically solved for the polynomial coefficients in order to meet prescribed boundary conditions [10]. The thrust commands were then set to track the acceleration profile obtained by twice differentiating the polynomial representing the descent path. The Apollo polynomial guidance was later adapted for the Mars Science Laboratory (MSL) PDG [11, 12, 7]. While this polynomial guidance is computationally efficient, it is not fuel-optimal [13]; that is, the guidance solution requires more fuel than necessary in order to complete the maneuver.

Minimum-fuel PDG, on the other hand, has, until recently, been primarily the focus of academic research [14, 15]. In the special case when the descent trajectory is strictly vertical, the minimum-fuel control sequence is such that the vehicle first descends in free-fall, and then, at a particular time that can be computed algebraically, the maximum throttle is applied until touchdown [16]. Hence, the optimal control strategy has a bang-bang structure. For the general case of a three-dimensional descent trajectory, however, there is no known algebraic representation of the minimum-fuel solution, although properties of optimal solutions can be derived from the Minimum Principle. Specifically, the minimum-fuel optimal thrust profile is nonsingular with a max-min-max structure [17].

Fortunately, due to recent theoretical developments and technological advances in onboard computational capabilities, it is now possible to compute minimum-fuel PDG trajectories onboard the spacecraft as the solution to a numerical optimization problem [18]. One such method is due to the theory of lossless convexification, which allows for the minimum-fuel PDG to be posed as a convex optimization problem. As a result, the globally optimal powered descent trajectory can be computed by convex optimization with guaranteed convergence [19, 20]. The G-FOLD algorithm, which is based on the theory of lossless convexification, has been demonstrated in test flights [21]. Furthermore, when the descent trajectory is solved as a convex optimization problem, it is possible to enforce convex path constraints, such as minimum glide slope or maximum off-vertical thrust direction [19]. Recent works have included more complex state-triggered and line-of-sight

constraints [22, 23]. Iterative methods extending lossless convexification theory have been applied to handle nonlinear drag forces [24] and vehicle attitude dynamics [25]. The convergence guarantees stemming from the problem convexity make these previous methods ideally suited for on-board closed-loop trajectory generation, although to-date the approach has only been used to autonomously generate a reference trajectory on-board, which is then tracked using a linear controller [21].

On a different research direction, an indirect method has been developed to solve on-board for minimum-fuel descent trajectories, which includes optimization over the time-of-flight and the maneuver start time [26]. This indirect method determines the optimal thrust profile from the solution to a multivariate root-finding problem, which can be computed quickly onboard. This approach thus enables an implicit form of closed-loop control wherein the optimal thrust profile is continuously resolved during the descent maneuver. On the other hand, this indirect method does not have a guarantee of convergence and does not include constraints on the glide slope or thrust-pointing angle. See also Refs. [27, 28, 29, 30, 31].

Both the lossless convexification method as well as the indirect method can enable closed-loop control during powered descent by either continuously resolving for a nominal trajectory or by using closed-loop tracking, however neither approach accounts for stochasticity. As has been shown in [32, 33], accounting for stochasticity yields better performance than simply applying deterministic closed-loop guidance. This initially may seem surprising, but it is easy to see why this is the case. While closing the loop, a purely deterministic framework can be overly optimistic about the future of disturbances (i.e., there will be none) and hence it will be more aggressive in its effort to suppress the current disturbances. A stochastic treatment, on the other hand, pays equal attention to both the current and future disturbances when closing the loop. For this reason, we will follow a stochastic approach with the primary objective to fill this gap between deterministic open-loop (or even closed-loop) guidance and stochastic feedback control. In other words, by

introducing stochasticity we are able to obtain less conservative solutions that save fuel.

If the fuel-optimal PDG trajectory is given before the mission starts or even if it is solved once before the initiation of the powered descent maneuver, then the computed open-loop descent trajectory must be tracked using feedback control in order to reject external disturbances and to minimize the effect of unmodeled dynamics [21]. The engine throttle along a fuel-optimal powered descent trajectory, however, should always either be at the maximum or at the minimum allowable value [17]. On the other hand, and since the magnitude of the closed-loop thrust commands are not known when designing the open-loop trajectory, conservative margins must be included on the open-loop throttle commands. Fuel-optimality must then be traded against the control authority allocated for closed-loop thrust corrections by setting margins on the open-loop throttle. The open-loop PDG solution therefore implicitly depends on the intensity of the external disturbances. Indeed, even if closed-loop control is achieved by continuously resolving for the optimal, open-loop trajectory, the robustness of the trajectory to disturbances can be improved by including control margins [34, 35].

1.1.2 Entry Guidance

The successful MSL mission demonstrated, for the first time, guided atmospheric entry at a planet other than Earth. The vehicle flew with a trimmed angle of attack for positive lift with an L/D of 0.24, and a reaction control system banked the vehicle to modulate the vertical lift based on the predicted range-to-target [3]. Following parachute deployment and a powered descent phase, the Curiosity rover was deployed approximately 2 km from the target landing site [3]. Looking forward, future exploration missions will require even greater landing accuracy, perhaps on the order of meters, in order to preposition supplies or to study interesting geological phenomena [36, 37]. Improvements to entry guidance performance will be a crucial component supporting this increased landing accuracy.

The MSL entry guidance was derived from the Apollo final phase entry guidance, which

includes a separate logic to independently set the magnitude of the bank angle (for range control) and the sign of the bank angle (for lateral control) [38, 39]. In this scheme, range control is affected by scaling the vertical component of the lift vector, by means of setting the bank angle magnitude as shown in Figure 3.1, based on the predicted effect this change will have on the range flown. Discrete bank-reversal events are triggered when the navigated crossrange error exceeds a threshold. Underlying the Apollo final phase guidance, as well as many modern approaches to entry guidance, is a mapping from *constant* control input corrections to changes in the final downrange position. In the case of the Apollo final phase range control, this mapping is approximated to first order (i.e., linearized) about a given reference trajectory, which, in turn, allows for the vertical lift correction to be written as a linear function of the current state deviation from this reference trajectory [38, 39]. The resulting onboard range control algorithm then only requires performing simple arithmetic after looking up the current set of feedback gains and nominal state values from a stored table.

The majority of modern proposed entry guidance algorithms follow the same basic principle as the Apollo final phase algorithm, in the sense that the controls applied at any particular time should be those that, if held constant, will steer the vehicle to a target state. However, due to improvements in onboard computational capabilities, guidance algorithms are no longer reliant on the linear approximation employed for Apollo [40]. Instead, the equations of motion can be numerically integrated onboard to obtain a trajectory resulting from a particular control input, and this process can be repeated for different candidate controls. The requirement that the candidate control be constant, which is a necessary assumption in the derivation of the Apollo final phase feedback gains, is removed when using numerical integration; however, the control function is still often low (one or two) dimensional as to support rapid and reliable onboard convergence [35]. This approach is referred to as numerical-predictor corrector (NPC) guidance [35, 41, 42]. The Shuttle entry guidance, in contrast, tracked a drag profile as a function of the planet-relative velocity, and

the projected range was computed as a function of the drag profile [43, 44]. Subsequent research has expanded on drag-profile tracking entry guidance for Earth and Mars entry [45, 46, 47].

While in flight, the vehicle will most likely deviate from the planned trajectory due to external disturbances and parametric uncertainties. Thus, the actual control inputs will not be equal to the predicted control inputs, and the actual trajectory will not be the same as the predicted trajectory. The performance of an entry guidance algorithm is thus often measured statistically following repeated random Monte Carlo trials, which include variations to the atmosphere and initial vehicle states, in addition to a large number of additional randomized parameters. Holding constant the statistics of the Monte Carlo inputs, and taking the number of trials to be a very large number, this procedure establishes a mapping from the *algorithm* used for entry guidance to the *statistics* of the closed-loop entry trajectory, which in this context is now a random process rather than a deterministic function of time. One may then consider the entry guidance problem as finding a *guidance algorithm*, or in certain cases a *guidance law*, which results in desirable statistics of the closed-loop entry trajectory. Unfortunately, the mapping established by Monte Carlo from the entry guidance algorithm to the trajectory statistics is, in general, a "black-box," which can obscure the causal effect of guidance parameters on state dispersions.

1.1.3 Aerocapture Guidance

Aerocapture is an orbital aeroassist maneuver during which a spacecraft uses a planet's atmosphere to decelerate from a hyperbolic orbit into a captured elliptical orbit around the planet, thus reducing the fuel required for orbital missions around other planets. Concept studies have shown that using aerocapture in place of an all-propulsive system can increase the delivered mass to a science orbit around Neptune by 1.4 times [48, 49, 50], can decrease the required launch mass for a Mars robotic mission by 3-4 times [51], and can decrease the required mass for a Titan robotic mission by between 40 and 80% [52, 53]. Furthermore,

studies have shown aerocapture to be an enabling technology for a baseline human Mars mission architecture and for a small-sat Venus orbiter mission [5, 54, 55, 56].

As for planetary entry, bank angle modulation can be used for control during the atmospheric flight segment of an aerocapture maneuver [57, 55, 58], but other guidance and control architectures have also been investigated. The direct force control (DFC) method (also referred to as α-β control or uncoupled range control) independently sets the angle of attack and the angle of sideslip to affect the longitudinal and lateral dynamics [59, 60]. Discrete-event drag modulation, wherein segments of the vehicle are jettisoned to change the vehicle ballistic coefficient, has recently gained attention as a simple and effective aerocapture strategy [61, 62, 56, 63].

In the literature, the majority of aerocapture architectures use numerical-predictor corrector (NPC) guidance. Similar to predictor-corrector entry guidance, predictor-corrector aerocapture guidance systems continuously recompute, in flight, open-loop controls — which are parameterized to be low-dimensional — that minimize a performance index.

The NPC logic for aerocapture with bank angle control follows from deterministic optimal control theory. The optimal bank angle sequence for an aerocapture maneuver is to first fly full lift-up until a particular time, and then to fly full lift-down for the remainder of the atmospheric flight segment. Prior to this roll-over event, the NPC guidance iteratively solves for the time to preform the roll-over. Then, following the roll-over, the guidance iteratively solves for the constant bank-angle command to minimize the predicted exit-condition error [64]. Thus, for both phases of flight, the NPC must only solve for a single parameter describing the predicted trajectory. The resulting mission architecture is shown in Figure 1.1.

Similarly, NPC guidance for DFC solves for low-dimensional angle of attack and angle of sideslip functions [59], and discrete-event drag modulation NPCs solve for the jettison time [61, 63]. Most aerocapture NPC implementations estimate the atmospheric density during flight, and the predicted trajectories assume that the density, as a function of altitude,

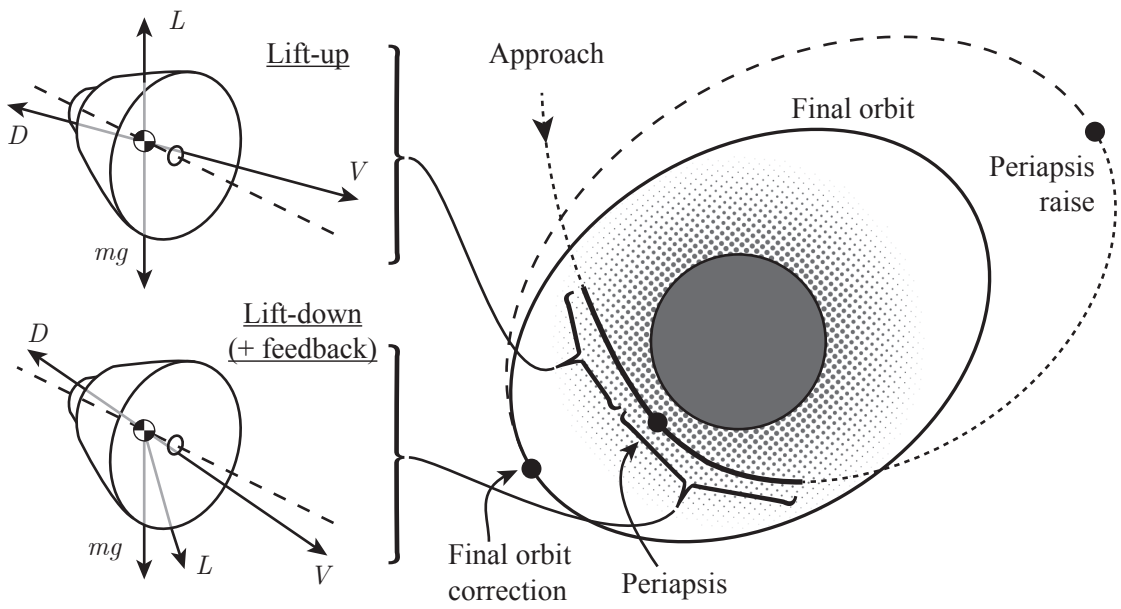

Figure 1.1: Bank angle control for aerocapture using numerical-predictor corrector guidance

is equal to the onboard best estimate [64, 61, 63].

While no existing aerocapture NPC methods explicitly consider uncertainty in the problem formulation, recent works have sought to address the role of uncertainty in aerocapture guidance. The effect of atmospheric scale height uncertainty on the optimal open-loop roll-over time, for bank angle control, was addressed in Ref. [65], and it was observed that certain roll-over times result in less sensitive trajectories. The author proposed a Gaussian random field (GRF) model for atmospheric density uncertainty in Ref. [66], and studied the effect of the roll-over time on the probability distribution of fuel cost. In Ref. [67], a GRF model of the atmospheric density, based on MarsGRAM [68], was utilized, in conjunction with the Karhunen–Loève and polynomial chaos expansions, for aerocapture uncertainty quantification.

1.1.4 Covariance Steering

In recent years, the controlled evolution of the state statistics of linear systems has been extensively studied, and authors have proposed methods to solve for control laws which

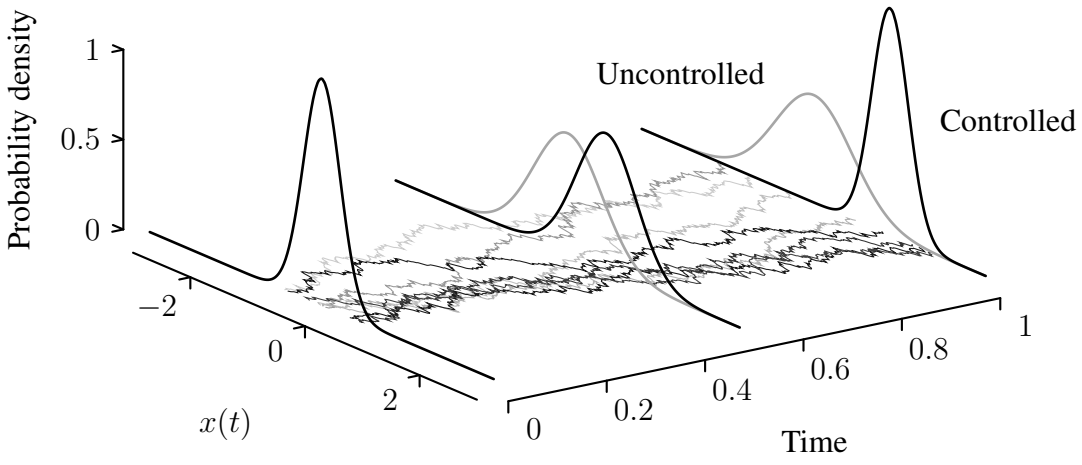

Figure 1.2: Sample paths and probability density evolution of the Ornstein–Uhlenbeck random process $x(t)$. The mean and variance of the controlled process are separately steered by the nominal control and the feedback gain.

directly control the state probability distribution [69, 70, 71]. For a general nonlinear stochastic system, one may equivalently consider either the random dynamics of sample paths or the deterministic evolution of the state probability distribution, which satisfies a partial differential equation (PDE) [72]. The control problem can be formulated as one of simultaneously steering each sample trajectory, and as a consequence, we can analytically study the difference between open and closed-loop control [72].

When the system is linear with additive Brownian noise, the PDE describing the state probability distribution can be decomposed into two independent ordinary differential equations (ODEs) for both the mean and the covariance of the state. The nominal, or feedforward, control appears as the input to steer the evolution of the expected state, whereas the feedback gain appears as the input to steer the evolution of the state covariance. Thus, one may solve for the nominal control to steer the mean of the state distribution, while also solving for the feedback gain to steer the covariance [72]. From this perspective, stochastic control is concerned with controlling the *deterministic* dynamics describing the system uncertainty (e.g., covariance) rather than controlling a collection of uncertain sample trajectories. An example of the controlled evolution of the probability density of the Ornstein–Uhlenbeck random process is shown in Figure 1.2.

The problem of solving for state feedback gains to control the state covariance evolution is referred to as the *covariance steering* (CS) problem.

The special case of linear time-varying stochastic systems with additive Brownian noise has been extensively studied in the literature. The infinite horizon covariance control problem for linear time invariant systems has been researched since the late 80's. In [73, 74] the authors investigated the state-feedback gains that *assign* a state covariance value to the system, i.e., the system state covariance converges asymptotically to the assigned value. The finite horizon case has only recently gained attention [75, 76, 77, 78, 79, 80]. It has been shown that if the system is controllable, then the state covariance is also controllable [72]. That is, for an initial covariance $P_0 > 0$ at time t_0, there exists a state feedback gain defined on the interval $[t_0, t_f]$ that steers the covariance to any final value $P_f > 0$ for any time $t_f > t_0$. The solution to the linear continuous-time CS problem with expected quadratic cost was given by Chen et al. [75, 69, 81], and the solution was found to be closely related to the classical linear quadratic feedback control. The linear discrete-time CS problem with quadratic cost has also been studied and a similar close connection to linear quadratic control has been shown [79].

Since the trajectory of a stochastic system is uncertain, it follows that constraint violation is also uncertain, and thus, for a particular control law, there is a corresponding probability that a constraint is satisfied. In fact, for Gaussian distributed systems, there is a nonzero probability that the state lies within any particular set in the state space, and thus it is impossible to ensure constraint satisfaction with absolute certainty. Instead, the *probability* that a constraint is violated may be bounded. Constraints on probabilities, such as the violation of a deterministic constraint, are referred to as *chance constraints* [82]. Stochastic optimization with chance constraints is accordingly referred to as chance-constrained optimization [83]. For instance, suppose that the state x must lie within a set $\mathcal{R}$, which

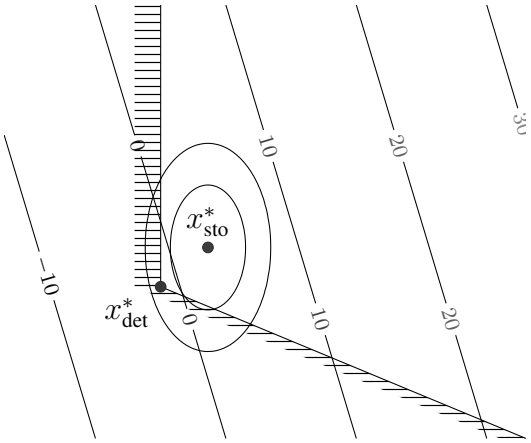

Figure 1.3: Example chance-constrained optimization. The deterministic optimal value x^*_{det} lies on the constraint boundary, while the mean stochastic optimal value x^*_{sto} lies within the constrained region with sufficient probability. Contours around x^*_{sto} denote level sets of its probability density function.

leads to

$$\text{deterministic constraint:} \qquad x \in \mathcal{R}, \tag{1.1}$$

$$\text{chance constraint:} \qquad \mathbb{P}(x \notin \mathcal{R}) \leq \beta, \tag{1.2}$$

where β is a prescribed maximum probability of constraint violation. An example of chance-constrained optimization is shown in Figure 1.3, wherein the mean of an uncertain state is optimized while the covariance is unaffected by the optimization.

More generally, chance-constrained optimization can be performed by setting both the mean and higher moments of a random decision variable. The control of stochastic dynamical systems, for example, can be effected via feedforward or feedback control, both of which have different affects on the state probability distribution. Indeed, for the case of linear discrete-time stochastic systems, it has been shown that the reference trajectory and the feedback controller are coupled in the presence of chance constraints [71].

It is not difficult to imagine a situation in which the nominal and feedback controls are coupled. For example, as an uncertain system approaches a constraint, there are two actions that can be taken: steer the mean state away from the constraint (by changing the nominal

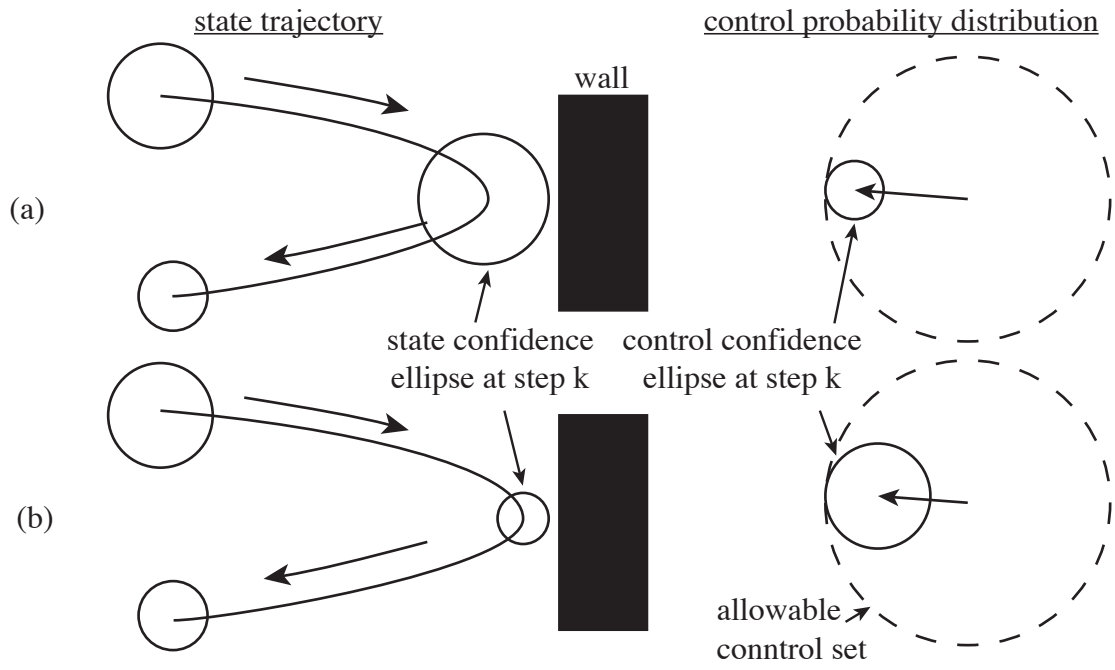

Figure 1.4: Constraint induced coupling between the mean and covariance trajectories.

control), or steer the covariance to reduce the probability of violating the constraint (by increasing the feedback gain). Similarly, if the control input is bounded, then the nominal and the feedback controls are also coupled by chance constraints, since setting the nominal control to be near the maximum allowable value restricts the allowable variance of the closed-loop control. This concept is graphically shown in Figure 1.4, where for case (a) more control effort is used to steer the mean and in case (b) more control effort is allocated to steer the covariance.

For the case that the state chance-constrained region is a convex polytope, the combined optimal nominal control and feedback gains can be solved by convex programming [71]. The latter work draws connections between covariance control and a large class of stochastic control problems for which chance constraints are utilized in order to guarantee performance under uncertainty [84, 85], such as stochastic model predictive control (SMPC) [86, 83] and vehicle path planning in belief space [82, 87].

A convex formulation of the maximum control magnitude chance constraint, as shown in Figure 1.4, was provided by the author in Ref. [88].

Output Feedback Covariance Steering

The aforementioned works on chance-constrained covariance steering assume that the value of the state is perfectly known to the controller, and thus the control actions can depend on the state. But if the state is instead only accessed indirectly though measurements, then the control actions must be taken on the basis of the measured output values. That is, the controller uses *output feedback*.

For unconstrained linear stochastic systems with additive Brownian noise, the separation theorem provides that the optimal control and the optimal estimator are obtained independently, leading to linear quadratic Gaussian (LQG) optimal control [89]. Furthermore, the certainty equivalence principle states that the optimal control does not depend on the uncertainty, but rather is equivalently obtained by assuming the uncertain state is deterministic and known [90, 89]. But in the presence of constraints, as was shown by the author in Ref. [91], the control does indeed depend on the underlying uncertainty, including the observation model, in the presence of constraints, which motivates our study of output feedback covariance steering.

Extending the covariance steering problem to include imperfect state knowledge requires a careful treatment of the uncertainty in the initial state. For the present formulation, we decompose the uncertainty in the initial state, measured by the state covariance P_0, into two components: that which will eventually be known at the initial time, $\hat{P}_{0^-}$, and that which will remain unknown at the initial time, $\tilde{P}_{0^-}$ (formal definitions will be given later, in Section 4.3). For the complete state knowledge case, the entirety of the initial state uncertainty fell into the former category, since we had assumed that the unknown initial state will be known to the controller when the first control is issued. We refer to this component of the state as the filtered, or estimated, state. The component of the state that remains unknown is the estimation error.

In practice, the differentiation between the covariance of the estimated state and the covariance of the estimation error follows from the system behavior from the time when

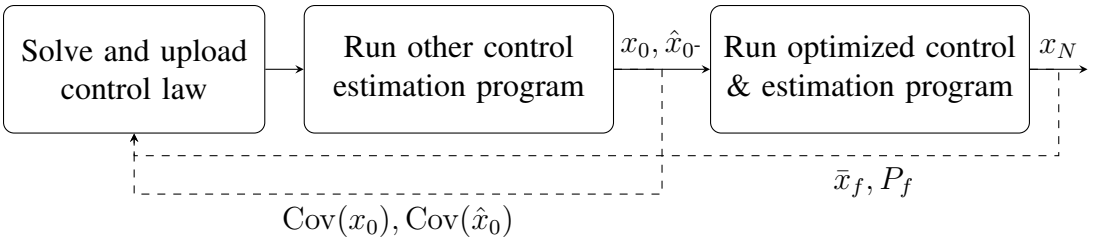

Figure 1.5: Example structure of problem with initial state uncertainty. The true state at the initial time is x_0, its estimate is $\hat{x}_{0^-}$, the final state is x_N, and the final target mean and maximum covariance, which define constraints on the control design, are $\bar{x}_f$ and P_f.

controller is designed until the time when the first control input under consideration is determined. Consider, for example, the problem of designing a control law for a spacecraft docking maneuver, and suppose that the control law must be uploaded to the spacecraft several hours before the maneuver is set to begin. Furthermore, suppose that the spacecraft is subjected to random disturbances, and therefore, when designing the control law, we only know the probability distribution of the possible spacecraft states at the maneuver start time. A block diagram of this setup is shown in Figure 1.5. If, on the one hand, the spacecraft will be collecting measurements and performing accurate onboard estimation leading up to the maneuver, then at the maneuver start time the estimated state will be close to the true state, as is shown on the left of Figure 1.6. Note the similarity of this case to the complete state knowledge case. On the other hand, if the spacecraft does not collect measurements after the control law is uploaded, then the best onboard estimate of the state will remain close to the prior best estimate: the mean; this situation is shown in the center of Figure 1.6. Finally, for the case that some imperfect measurements will be taken, then the initial state uncertainty will be composed of both error sources, as is shown on the right of Figure 1.6.

The problem of output-feedback covariance steering has been visited in [92, 93], where the problem had no constraints other than a terminal boundary constraint. Thus, these works only dealt with the control of the state covariance and did not consider mean dynamics, whereas the approach presented in this dissertation deals with state chance constraints

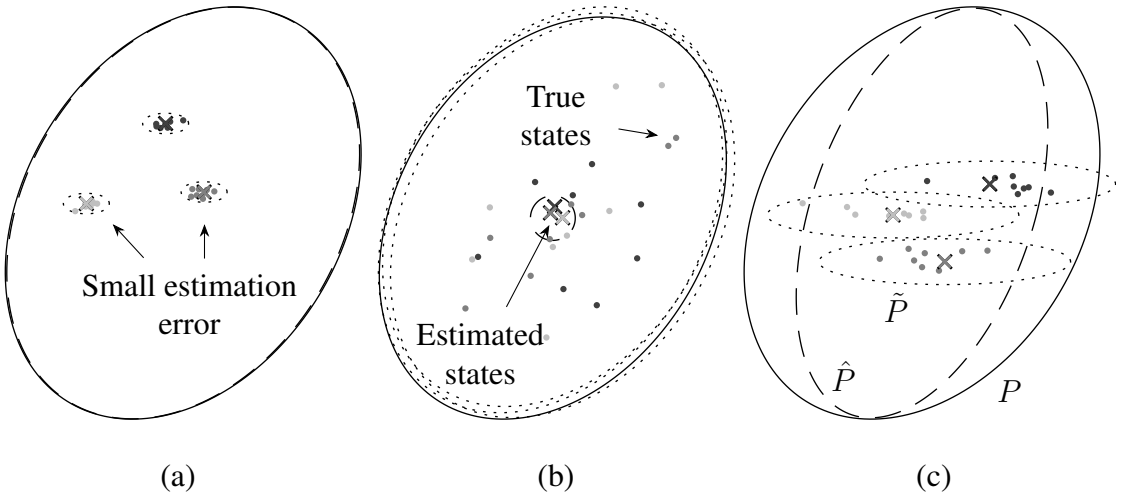

Figure 1.6: Samples with varying balance between estimated state uncertainty and estimation error uncertainty. Total state covariance P_0 is solid, estimated state covariance $\hat{P}_{0\text{-}}$ is dashed, and estimation error covariance $\tilde{P}_{0\text{-}}$ is dotted. From left to right: large $\hat{P}_{0\text{-}}$, large $\tilde{P}_{0\text{-}}$, mixed $\hat{P}_{0\text{-}}$ and $\tilde{P}_{0\text{-}}$.

and simultaneously steers the mean and the covariance of the system state, and thus, can be applied to more realistic scenarios.

A similar problem setup as the one addressed in this dissertation has also been visited from the SMPC community [94], where an output feedback controller was designed to deal with chance constraints. Although the approach in [94] successfully computes control commands that satisfy all the constraints, the control policy suffers from conservativeness due to the convex relaxation of the covariance dynamics.

Nonlinear Covariance Steering

The problem of chance-constrained covariance steering for nonlinear continuous-time stochastic systems was addressed by the author in Refs. [70, 88], wherein a successive linearization approach was developed. We refer to this approach as iterative covariance steering (iCS).

Other authors have addressed nonlinear stochastic optimal control via stochastic differential dynamic programming (SDDP) [95, 96, 97, 98]. The SDDP formulation, which computes the solution to a nonlinear stochastic optimal control problem by successive back-

ward and forward evaluations of the value function and of the dynamics approximated to second order, has been shown to be very successful for a wide variety of problems including low-thrust spacecraft trajectory control. Furthermore, SDDP has been extended to handle state and control chance constraints [99]. SDDP and iCS have been applied to low-thrust spacecraft guidance in Refs. [95, 96, 88].

In contrast to SDDP and other stochastic control methods, the iCS method approximates the dynamics to first order and assumes that the state is Gaussian distributed. This allows for each optimization to be solved as a convex program, which, in turn, allows for the inclusion of state and control constraints as well as providing guarantees on each iterative solution. On the other hand, many systems are not adequately represented by this linear-Gaussian approximation, and so trajectory design for these systems would be better handled by the SDDP approach using a second order approximation of the dynamics and the unscented transform for the evolution of the state distribution.

1.2 Dissertation Objective and Contributions

From a high level, this dissertation aims to bridge the gap between the recent theoretical developments in stochastic optimal control described in Subsection 1.1.4 and the spacecraft guidance applications also described in Subsections 1.1.1–1.1.3. Chapter summaries given in the following section provide a detailed description of the application-specific objectives and products of this research. An outline of specific contributions is given below.

- Powered descent guidance
  - Develop stochastically-derived throttle margins for application to minimum-fuel PDG
- Entry Guidance
  - Derive stochastic differential equation-based atmosphere model for altitude-dependent random density variations

  - Derive rapid quantification method for entry vehicle dispersions due to atmosphereic density variations
  - Pose and solve entry guidance in a randomly perturbed atmosphere as a chance-constrained stochastic optimal control problem

- Aerocapture guidance
  - Derive general formulation of chance-constrained covariance steering with state-dependent disturbances due to a Gaussian random field
  - Solve, via successive convex programming, for a state-history feedback law that explicitly minimizes the upper percentile of Δv required to complete an aerocapture mission around a planet with the atmospheric density modeled as a Gaussian random field

- Low-thrust spacecraft guidance
  - Derive convex formulation of maximum control magnitude chance constraint
  - Develop successive convex programming algorithm to solve nonlinear chance-constrained covariance steering problems

- General chance-constrained covariance steering theory
  - Derive convex programming solution to chance-constrained covariance steering with output feedback
  - The above contributions for aerocapture guidance and low-thrust spacecraft guidance are derived for general systems

1.3 Summary of Dissertation

The following chapters in this dissertation are summarized below.

- **Chapter 2: Powered Descent Guidance**

  If during a guided powered descent maneuver the descent vehicle deviates from the planned trajectory, then the vehicle may need to adjust the commanded thrust in order to still reach the target landing site or to avoid violating mission constraints. However, often the nominal thrust command at any time along a minimum-fuel powered descent trajectory is either at the maximum or the minimum throttle, and as a result the corrective thrust command may be outside the allowable throttle range. A margin must therefore be added between the planned throttle command and the engine throttle limits, but this margin may be overly conservative to the detriment of performance. In Chapter 2, the powered descent trajectory is modeled as a stochastic process in order to non-conservatively adjust the bounds on the feed-forward optimal thrust magnitude command to allow for sufficient feedback authority. The margin on the nominal throttle is computed as a function of the covariance of the closed-loop thrust commands so that if the nominal throttle is within the limits, plus the margin, then the closed-loop throttle is within the allowable limits with high probability. The proposed method can be solved onboard without iteration.

- **Chapter 3: Stochastic Entry Guidance**

  In Chapter 3, closed-loop entry guidance in a randomly perturbed atmosphere, using bank angle control, is posed as a stochastic optimal control problem. The entry trajectory, as well as the closed-loop controls, are both modeled as random processes with statistics determined by the entry dynamics, the entry guidance, and the probabilistic structure of altitude-dependent atmospheric density variations. The entry guidance, which is parameterized as a sequence of linear feedback gains, is designed to steer the probability distribution of the entry trajectories while satisfying bounds on the allowable control inputs and on the maximum allowable state errors. Numerical simulations of a Mars entry scenario demonstrate improved range targeting performance when using the developed stochastic guidance scheme as compared to the existing

Apollo final phase algorithm.

- **Chapter 4: Covariance Steering Theory**

  In Chapter 4, the existing theory of chance-constrained covariance steering is reviewed and the following extensions are presented: a convex formulation of a maximum Euclidean magnitude chance constraint, chance-constrained covariance steering with output feedback, and nonlinear continuous-time covariance steering via successive convex programming. For the output-feedback problem, the filtered state is obtained via a Kalman filter, and the problem is formulated as a deterministic convex program in terms of the distribution of the filtered state. We observe that, for the output-feedback problem, in the presence of constraints on the state covariance, and in contrast to classical Linear Quadratic Gaussian (LQG) control, the optimal feedback control depends on both the process noise and the observation model. Nonlinear covariance steering is applied to a numerical example for a low-thrust Earth-to-Mars transfer.

- **Chapter 5: Covariance Steering with Spatially-Dependent Uncertainty**

  The chance-constrained covariance steering theory presented in Chapter 4 assumes the stochasticity to be time-dependent with known statistics. Disturbances affecting a vehicle during atmospheric flight for either entry or aerocapture missions, on the other hand, cannot be simply modeled by a time sequence of independent random vectors. We present a solution for covariance steering with spatially (i.e., state) dependent disturbances in Chapter 5, wherein the problem of optimizing affine feedback laws that explicitly steer the mean and covariance of an uncertain system state in the presence of a Gaussian random field is considered. Spatially-dependent disturbances are successively approximated with respect to a nominal trajectory by a sequence of jointly Gaussian random vectors. Sequential updates to the nominal control inputs are computed via convex optimization that includes the effect of affine

state feedback, the perturbing effects of spatial disturbances, and chance constraints on the closed-loop state and control. The developed method is applied to solve for an affine feedback law to minimize the 99^{th} percentile of Δv required to complete an aerocapture mission around a planet with a randomly disturbed atmosphere.

- **Chapter 6: Conclusions**

  In Chapter 6, we summarize the contributions presented in this dissertation and present possible future research directions.

CHAPTER 2
POWERED DESCENT GUIDANCE

The material in this chapter is based on Refs. [100, 101].

2.1 Introduction

In this chapter, we address the interdependency between open-loop minimum-fuel PDG and closed-loop tracking control by studying the powered descent trajectory as a stochastic process. The descent vehicle states, and by extension the closed-loop thrust commands, are then described by random vectors with known distributions. In this setting, the nominal (i.e., open-loop) thrust steers the mean of the state distribution while the feedback gain steers the dispersion (i.e., the covariance) of the state distribution [72, 100, 71]. The margins imposed on the nominal throttle commands thus have a natural interpretation: If the nominal control satisfies the throttle margin, then the closed-loop control satisfies the maximum and minimum throttle constraints with high probability. This definition of the control margin can still be applied for the case that the open-loop trajectory is resolved during the maneuver, in the sense that the control margin provides a probabilistic guarantee on resolvability.

Furthermore, the closed-loop thrust corrections are provided as the minimum-variance control solution such that the covariance of the descent vehicle state at the end of the maneuver is no greater than a given maximum value [75, 100]. This formulation has several implications for minimizing the fuel-cost of the nominal trajectory. First, the variance of the feedback control influences the throttle margin, since if the uncertainty of the future closed-loop thrust increases, then a larger margin must be imposed on the nominal thrust. This, in turn, increases the fuel cost. Second, there is a trade-off between the closed-loop control variance and the final state variance. For a given intensity of external disturbances,

the uncertainty in the vehicle states at the end of the maneuver can be decreased by taking more aggressive corrective control actions. In the standard Linear Quadratic (LQ) optimal control formulation, this trade-off is achieved by manually tuning the weight matrices for the final state error and for the running control cost [15]. For the present problem, in contrast, we apply a recent result from constrained stochastic optimal control in order to solve for the minimum-variance control while meeting a final state covariance constraint [75, 69, 81], which removes the need to hand-tune weight matrices and is thus is better suited for on-board implementation.

Contributions

The main contributions of this chapter are summarized below. First, we extend the aforementioned existing theory on covariance control [75, 69, 81] to allow for non-constant, bounded mass values, as is the case for the vehicle mass after thrusting. This result is then applied to solve for the feedback gains such that the covariance of the closed-loop trajectory at a final time is constrained by a user-defined upper bound. Second, we provide a method for determining the throttle margins as a function of the closed-loop control covariance that can be computed onboard with convergence guarantees. The throttle margins are then provided as the input to a deterministic minimum-fuel PDG problem; this approach contrasts the classical method of closed-loop guidance for which the feedback gains are computed after the determination of the open-loop trajectory [15]. Third, we provide a link between minimum-variance feedback control and minimum-fuel powered descent trajectories by showing that decreasing the variance of future feedback controls allows for smaller throttle margins, which in turn decreases the fuel cost.

Organization

The chapter is organized as follows. In Section 2.2, minimum-fuel PDG is introduced as a stochastic optimal control problem. In Subsection 2.3.1, we separate the system dynamics

into a deterministic mean part and a stochastic deviation from the mean part. The feedback control is derived in Subsection 2.3.2, the throttle margin is constructed in Subsection 2.3.3, the mean control is posed as a deterministic PDG problem in Subsection 2.3.4, and an algorithm for the proposed closed-loop PDG is presented in Subsection 2.3.5. The organization of Section 2.3 is shown graphically in Figure 2.2. Finally, we present a numerical example for a powered descent maneuver at Mars in Section 2.4 and we compare the results with a traditional approach that does not account for the closed-loop control variance when determining the throttle margins.

2.2 Problem Formulation

Consider a spacecraft in powered descent modeled as a point-mass with mass m and with position and velocity $x = (r, v) \in \mathbb{R}^3 \times \mathbb{R}^3$ in a surface-fixed inertial frame. At the initial time $t = 0$, the mass $m(0) = m_0 > 0$ is assumed to be fixed and known. The initial position and velocity $x(0) = x_0 = (r_0, v_0)$, which we refer to as the state, is assumed to be a random vector distributed as

$$x_0 \sim \mathcal{N}(\bar{x}_0, P_{x_0}), \tag{2.1}$$

where the positive semi-definite matrix P_{x_0} and the vector $\bar{x}_0$ are both fixed and known. Random force disturbances acting on the vehicle are modeled as a 3-dimensional Brownian motion $w(t)$ scaled by a positive constant γ. The spacecraft motion is thus described by the stochastic differential equation (SDE)

$$\mathrm{d}\begin{bmatrix} r \\ v \\ m \end{bmatrix} = \begin{bmatrix} v \\ u/m + g \\ -\alpha \|u\| \end{bmatrix} \mathrm{d}t + \begin{bmatrix} 0 \\ \gamma/m \\ 0 \end{bmatrix} \mathrm{d}w(t), \tag{2.2}$$

where $g \in \mathbb{R}^3$ is the gravitational acceleration, α is a positive mass-flow parameter, and $u \in \mathbb{R}^3$ is the control thrust given at each time t by the affine feedback law

$$u(t) = \bar{u}(t) + K(t)\tilde{x}(t), \tag{2.3}$$

where $\tilde{x} = x - \mathbb{E}(x)$ is the state deviation from the mean, $\bar{u} = \mathbb{E}(u)$ is the mean control, and K is a feedback gain matrix to be determined. We assume that the mean control is sufficiently larger than the feedback control so that we may approximate

$$\mathbb{E}(\|u\|) \approx \|\bar{u}\| . \tag{2.4}$$

From this assumption, it follows that the mass is an approximate deterministic function of the mean control, given as the solution to the ordinary differential equation (ODE)

$$\dot{m} = -\alpha \|\bar{u}\| , \tag{2.5}$$

with the initial value $m(0) = m_0$. After a still to-be-determined time-of-flight $t_f > 0$, we require that the mean and the covariance of the spacecraft state satisfy the terminal constraints

$$\mathbb{E}(x_{t_f}) = \bar{x}_f, \tag{2.6a}$$

$$\mathrm{Cov}(x_{t_f}) \leq P_{x_f}, \tag{2.6b}$$

where the final state mean $\bar{x}_f$ is a given vector and the maximum final state covariance P_{x_f} is a given positive-definite matrix. The spacecraft's engines have a minimum and maximum throttle that cannot be exceeded, and therefore the control is constrained to lie inside the set

$$\Omega = \{u : \rho_1 \leq \|u\| \leq \rho_2\}, \tag{2.7}$$

where $\rho_2 > \rho_1 > 0$ are the maximum and minimum throttle limits. Since the state is initially Gaussian distributed, there will be a nonzero probability that the throttle constraint is violated when the feedback gain K is nonzero. We therefore require that the control remains within the set Ω with high probability. During flight, the thrust commands are saturated in the event that the throttle constraint is violated. That is, we require that

$$\mathbb{P}(u(t) \in \Omega) \geq 1 - \beta \ \text{ for all } \ t \in [0, t_f], \tag{2.8}$$

where $1 \geq \beta > 0$ is a prescribed constant specifying the maximum probability of control saturation. The parameter β allows for the system designer to specify a balance between robustness to disturbances and fuel cost: as will be shown analytically in Section 2.3.4 and numerically in Section 2.4, lower values of β will result in a larger throttle margin and a correspondingly higher fuel cost. The mean state $\bar{x} = \mathbb{E}(x)$ and mean control $\bar{u}$ are further constrained by

$$(\bar{x}(t), \bar{u}(t)) \in \mathcal{X} \times \mathcal{U} \ \text{ for all } \ t \in [0, t_f], \tag{2.9}$$

where $\mathcal{X}$ is the convex set restricting the glide slope angle θ to be less than the maximum glide slope angle $\theta_0 \leq \pi/2$, defined as

$$\mathcal{X} = \{(\bar{r}, \bar{v}) : \theta(\bar{r}) \leq \theta_0 \leq \pi/2\}, \tag{2.10}$$

where $\theta(\bar{r})$ is the angle between the mean position vector $\bar{r}$ and the local vertical, and where $\mathcal{U}$ is the cone of thrust vectors with off-vertical angle no more than a given maximum angle ϕ_0 (see Figure 2.1), that is,

$$\mathcal{U} = \{\bar{u} : \|\bar{u}\| \cos\phi_0 + g^{\mathsf{T}}\bar{u}/\|g\| \leq 0\}. \tag{2.11}$$

We are interested in solving the following optimal control problem to safely land the spacecraft while minimizing fuel consumption.

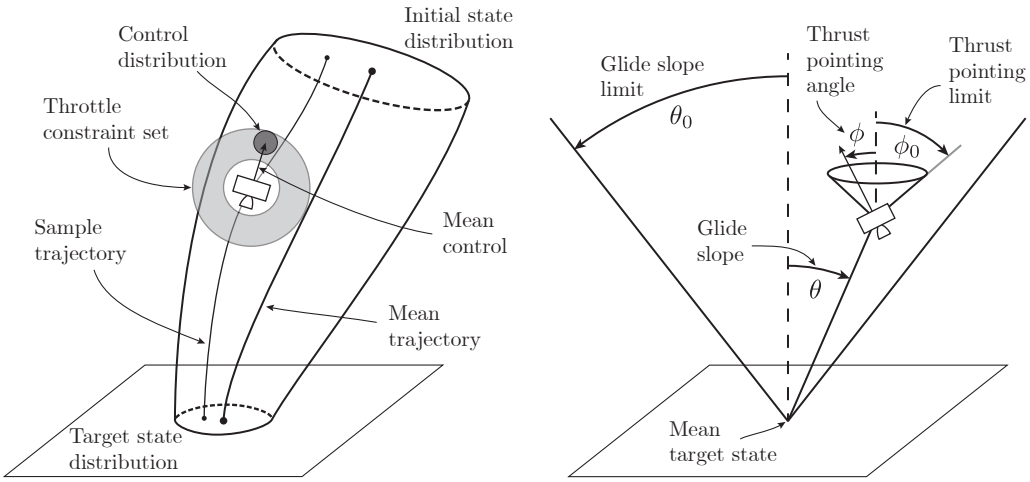

Figure 2.1: (Left:) Schematic of powered descent with the state modeled as a random vector. (Right:) Definitions of glide slope and thrust pointing limits.

Problem 2.1. *Find the time-of-flight $t_f > 0$, the mean control $\bar{u}(t)$ for $t \in [0, t_f]$, and the feedback gain $K(t)$ for $t \in [0, t_f]$ that minimize the expected fuel cost*

$$J(\bar{u}, t_f) = \int_0^{t_f} \|\bar{u}(t)\| \, \mathrm{d}t, \tag{2.12}$$

subject to the dynamics (2.2) with the control law (2.3), the initial state distribution (2.1), the throttle constraint (2.8), the mean path constraints (2.9), and the final state distribution constraint (2.6).

2.3 Problem Analysis

2.3.1 Separation of Deterministic and Stochastic Dynamics

Since the mass is deterministic due to the assumption (2.4), we can take the expectation of the dynamics (2.2) to obtain an ODE for the mean dynamics given by

$$\begin{bmatrix} \dot{\bar{r}} \\ \dot{\bar{v}} \\ \dot{m} \end{bmatrix} = \begin{bmatrix} \bar{v} \\ \bar{u}/m + g \\ -\alpha \|\bar{u}\| \end{bmatrix}, \tag{2.13}$$

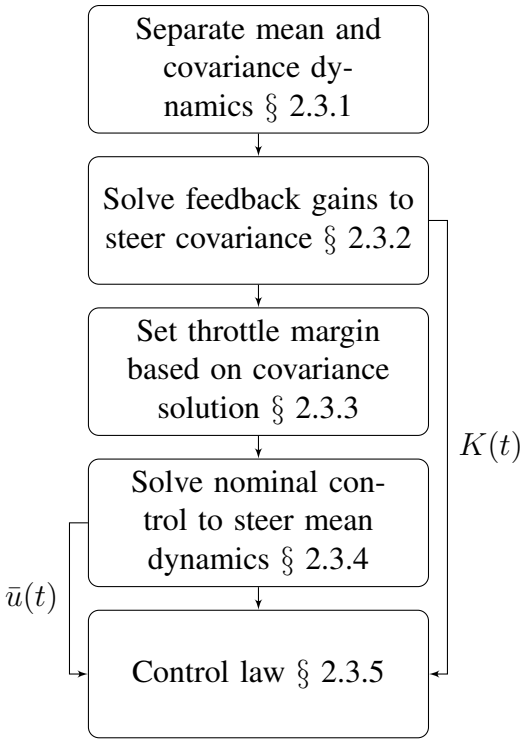

Figure 2.2: Organization of solution procedure.

with the initial conditions $(\bar{r}(0), \bar{v}(0)) = \bar{x}_0$ and $m(0) = m_0$. Then, by subtracting the mean dynamics (2.13) from the original dynamics (2.2), and substituting the control law (2.3), we obtain the SDE

$$\mathrm{d}\tilde{x} = (A + BK/m)\tilde{x}\mathrm{d}t + (\gamma/m)B\mathrm{d}w_t, \tag{2.14}$$

for the state deviation dynamics with the initial condition $\tilde{x}(0) = x_0 - \bar{x}_0$, and where

$$A = \begin{bmatrix} 0 & I \\ 0 & 0 \end{bmatrix}, \qquad B = \begin{bmatrix} 0 \\ I \end{bmatrix}. \tag{2.15}$$

The mass dynamics do not depend on the deviation state $\tilde{x}$, and therefore the deviation state dynamics are linear. It follows that the state x remains normally distributed over the entire problem horizon with mean $\bar{x}$ and covariance $P_x = \mathbb{E}(\tilde{x}\tilde{x}^\intercal)$, which comes as the solution

to the differential Riccati equation

$$\dot{P}_x = (A + BK/m)P_x + P_x(A + BK/m)^\intercal + (\gamma/m)^2 BB^\intercal, \tag{2.16}$$

with the initial condition $P_x(0) = P_{x_0}$. Furthermore, since the feedback control $\tilde{u} = K\tilde{x}$ is also a zero-mean normal random vector with covariance $P_u = KP_xK^\intercal$, we have that the control is distributed as

$$u \sim \mathcal{N}(\bar{u}, KP_xK^\intercal). \tag{2.17}$$

2.3.2 Optimal Covariance Control

The covariance dynamics (2.16) depend on the spacecraft mass m, which is a function on the mean control $\bar{u}$. Therefore, the deviation state dynamics, and hence the state and the control covariance evolution, depend on the choice of the mean control. On the other hand, the set of allowable values for the mean control which satisfy the throttle constraint (2.8) depends on the control covariance, and hence, by (2.16), on the feedback gain K. In order to break this circular dependency, we will first solve for a feedback gain that will steer the covariance dynamics (2.16) to a final state covariance that satisfies the terminal constraint (2.6b) for any value of the mass that is bounded by

$$m_\ell(t) \leq m(t) \leq m_u(t) \;\text{ for all }\; t \in [0, t_f], \tag{2.18}$$

where $m_\ell(t)$ and $m_u(t)$ are given functions of time. For instance, since the throttle is bounded by ρ_1 and ρ_2, it follows from (2.5) that the mass will always be bounded as in (2.18) with the bounds given by

$$m_\ell(t) = m_0 - \rho_2 \alpha t, \tag{2.19}$$

$$m_u(t) = m_0 - \rho_1 \alpha t, \tag{2.20}$$

for $t \geq 0$. We first consider the following problem to find the feedback gain K^ℓ which steers the covariance dynamics in the case the mass m is equal to it's lower bound m_ℓ over the entire problem horizon.

Problem 2.2. *For a fixed time-of-flight $t_f > 0$ and for the mass given as $m(t) = m_\ell(t)$ for $t \in [0, t_f]$, find the feedback gain $K(t)$ for $t \in [0, t_f]$ that steers the state covariance dynamics (2.16) to the final state covariance $P_x(t_f) = P_{x_f}$, while minimizing the cost*

$$\tilde{J}(K) = \int_0^{t_f} \mathrm{tr}(RKP_xK^\mathsf{T} + QP_x)\mathrm{d}t, \tag{2.21}$$

where $R = R(t) > 0$ and $Q = Q(t) \geq 0$ are given matrix-valued functions for $t \in [0, t_f]$. We denote the solution to this problem by the pair (K^ℓ, P_x^ℓ), where $P_x^\ell = P_x^\ell(t)$ is the solution to (2.16) with the gain $K^\ell = K^\ell(t)$ and mass $m_\ell = m_\ell(t)$.

A solution to Problem 2.2 is guaranteed to exist provided that the pair (A, B) is controllable [72], which, by inspection of (2.15), holds for the present problem. Furthermore, the feedback gain K^ℓ that solves Problem 2.2 is given in terms of the solution to a backwards matrix Riccati equation with the initial condition provided as a closed-form function of P_{x_0}, P_{x_f}, and γ; see Ref. [81, Theorem 1]. Thus, Problem 2.2 can be solved onboard. The cost (2.21) penalizes the state and control deviation the nominal trajectory, which, as we will show in Section 2.3.3, corresponds to how much throttle margin must be allowed to allow for closed-loop controls.

Next, we use the solution (K^ℓ, P_x^ℓ) of Problem 2.2 to construct a new feedback gain K such that the terminal covariance constraint (2.6b) will be be satisfied for any mass function satisfying (2.18). By definition, P_x^ℓ solves the equation

$$\dot{P}_x^\ell = (A + BK^\ell/m_\ell)P_x^\ell + P_x^\ell(A + BK^\ell/m_\ell)^\mathsf{T} + (\gamma/m_\ell)^2 BB^\mathsf{T}, \tag{2.22}$$

with boundary conditions $P_x^\ell(0) = P_{x_0}$ and $P_x^\ell(t_f) = P_{x_f}$. Therefore, if we set K as a

function of m, m_ℓ, and K^ℓ in such a way that the state covariance P_x is always less than or equal to P_x^ℓ, then we will have that

$$P_x(t_f) \leq P_x^\ell(t_f) = P_{x_f}. \tag{2.23}$$

Before we state our main result we will need a comparison formula for Riccati equations, which is taken from Ref. [102] with minor modifications.

Lemma 2.3.1. *[102, Theorem 2.1] Let P_i, $i = 1, 2$, be a solution of*

$$\dot{P}_i = \mathcal{A}_i^\intercal(t)P_i + P_i\mathcal{A}_i(t) + \mathcal{Q}_i(t) \tag{2.24}$$

on the interval $[0, t_f]$. If $P_1(0) = P_2(0)$, and if

$$\begin{bmatrix} \mathcal{Q}_1 - \mathcal{Q}_2 & \mathcal{A}_1 - \mathcal{A}_2 \\ (\mathcal{A}_1 - \mathcal{A}_2)^\intercal & 0 \end{bmatrix} \geq 0, \quad t \in [0, t_f], \tag{2.25}$$

then $P_2(t) \leq P_1(t)$ for all $t \in [0, t_f]$.

Theorem 2.3.2. *Let P_x be the solution to (2.16) with feedback gain K given by*

$$K(t, m) = \frac{m}{m_\ell(t)}K^\ell(t), \quad t \in [0, t_f], \tag{2.26}$$

where $m \geq m_\ell(t)$ for all $t \in [0, t_f]$. Then $P_x(t) \leq P_x^\ell(t)$ for all $t \in [0, t_f]$.

Proof. First, we rewrite (2.22) as

$$\dot{P}_x^\ell = m_\ell^{-2}\big[(m_\ell^2 A - m_\ell BK^\ell)P_x^\ell + P_x^\ell(m_\ell^2 A - m_\ell BK^\ell)^\intercal + \gamma^2 BB^\intercal\big]. \tag{2.27}$$

Substituting the feedback gain (2.26) into (2.16) yields

$$\dot{P}_x = m_\ell^{-2}\big[(m_\ell^2 A - m_\ell BK^\ell)P_x + P_x(m_\ell^2 A - m_\ell BK^\ell)^\intercal + (\gamma m_\ell/m)^2 BB^\intercal\big]. \tag{2.28}$$

Then, using

$$\mathcal{A}_1 = \mathcal{A}_2 = m_\ell^2 A - m_\ell B K^\ell, \tag{2.29}$$

$$\mathcal{Q}_1 = \gamma^2 B B^\mathsf{T}, \quad \mathcal{Q}_2 = \gamma^2 \frac{m_\ell^2}{m^2} B B^\mathsf{T}, \tag{2.30}$$

we may rewrite (2.27) and (2.28) as

$$\dot{P}_x^\ell = m_\ell^{-2}(\mathcal{A}_1 P_x^\ell + P_x^\ell \mathcal{A}_1^\mathsf{T} + \mathcal{Q}_1), \tag{2.31}$$

$$\dot{P}_x = m_\ell^{-2}(\mathcal{A}_2 P_x + P_x \mathcal{A}_2^\mathsf{T} + \mathcal{Q}_2). \tag{2.32}$$

Since $m \geq m_\ell$ and $BB^\mathsf{T} \geq 0$, it follows that

$$\mathcal{Q}_1 - \mathcal{Q}_2 = \gamma^2 B B^\mathsf{T} \left(1 - \frac{m_\ell^2}{m^2}\right) \geq 0, \tag{2.33}$$

and therefore, for all $t \in [0, t_f]$,

$$\begin{bmatrix} \mathcal{Q}_1 - \mathcal{Q}_2 & 0 \\ 0 & 0 \end{bmatrix} \geq 0. \tag{2.34}$$

Finally, we apply Lemma 2.3.1 with $P_1 = P_x^\ell$ and $P_2 = P_x$ to conclude that $P_x(t) \leq P_x^\ell(t)$ for all $t \in [0, t_f]$. □

Corollary 2.3.3. *Let P_x be the solution to (2.16) with the feedback gain K as in (2.26), and assume that the mass is bounded by (2.18). Then, the control covariance matrix $P_u = K P_x K^\mathsf{T}$ is bounded from above by*

$$P_{u,max} = \frac{m_u^2}{m_\ell^2} K^\ell P_x^\ell K^{\ell^\mathsf{T}}, \tag{2.35}$$

where (K^ℓ, P_x^ℓ) is the solution to Problem 2.2.

Proof. Substituting the feedback gain K from (2.26) into $P_u = KP_xK^\mathsf{T}$, and using the fact that the mass m is bounded from above by m_u, along with the fact that $P_x \leq P_x^\ell$, we obtain

$$P_u = KP_xK^\mathsf{T} = \frac{m^2}{m_\ell^2}K^\ell P_x K^{\ell\mathsf{T}} \leq \frac{m_u^2}{m_\ell^2}K^\ell P_x^\ell K^{\ell\mathsf{T}} = P_{u,\max}. \tag{2.36}$$

□

We note that in the special case in which the mass is known precisely when solving Problem 2.2, then we can set a prior bound on the mass such that $m_u = m = m_\ell$, from which it follows that $P_u = P_{u,\max}$. More generally, the difference between P_u and $P_{u,\max}$ decreases monotonically as the ratio of the upper to the lower bound on mass decreases.

2.3.3 Mean Throttle Margin

In general, solving for the optimal control with respect to the probabilistic throttle constraint (2.8) is intractable. Therefore, we develop the following relaxation. Given a control covariance P_u and maximum saturation probability β as in (2.8), we wish to find the largest subset $\Omega_\delta = \Omega_\delta(P_u, \beta)$ of admissible controls given by

$$\Omega_\delta = \{\bar{u} : \rho_1 + \delta \leq \|\bar{u}\| \leq \rho_2 - \delta\}, \tag{2.37}$$

with the property that

$$u \sim \mathcal{N}(\bar{u}, P_u) \text{ and } \bar{u} \in \Omega_\delta \implies \mathbb{P}(u \in \Omega) \geq 1 - \beta. \tag{2.38}$$

We refer to the parameter δ as the *throttle margin*. In general, finding the smallest throttle margin such that (2.38) holds is a nonlinear optimization problem with constraints given in terms of three-dimensional integrals, and thus is not computationally feasible for onboard applications. We therefore solve the following problem: find the smallest value of the radius for a 3-dimensional ball centered at $\bar{u}$ that has probability of containing u of at least

equal to $1-\beta$. This radius will, in turn, provide a conservative value for the throttle margin δ in (2.37), as shown geometrically in Figure 2.3.

Lemma 2.3.4. *Let $\tilde{u} \sim \mathcal{N}(0, P_u)$ and let σ_u^2 be the maximum eigenvalue of P_u. Then, for all $\delta \geq 0$,*

$$\mathbb{P}(\|\tilde{u}\| \leq \delta) \geq \operatorname{erf}\left(\frac{\delta}{\sigma_u\sqrt{2}}\right) - \frac{2\delta}{\sigma_u\sqrt{2\pi}} e^{-\delta^2/2\sigma_u^2}. \tag{2.39}$$

Proof. It can be shown [103] that for any $a \geq 0$,

$$\mathbb{P}(\tilde{u}^\intercal P_u^{-1}\tilde{u} \leq a^2) = \operatorname{erf}\left(\frac{a}{\sqrt{2}}\right) - \frac{2a}{\sqrt{2\pi}} e^{-a^2/2}. \tag{2.40}$$

To obtain the desired result we find the radius δ of a ball that contains the ellipsoid $\{\tilde{u} : \tilde{u}^\intercal P_u^{-1}\tilde{u} \leq a^2\}$. First, we diagonalize the control covariance matrix by $P_u = UDU^\intercal$, where U is orthogonal and D is a diagonal matrix of the eigenvalues λ_i of P_u. Since $\sigma_u^2 \geq \lambda_i$, it follows that

$$D^{-1} = \frac{1}{\sigma_u^2}\operatorname{diag}(\sigma_u^2/\lambda_i) \geq \frac{1}{\sigma_u^2} I. \tag{2.41}$$

From the previous expression it follows that

$$\tilde{u}^\intercal P_u^{-1}\tilde{u} = \tilde{u}^\intercal U D^{-1} U^\intercal \tilde{u} \geq \|\tilde{u}\|^2 / \sigma_u^2. \tag{2.42}$$

The inequality $\tilde{u}^\intercal P_u^{-1}\tilde{u} \leq a^2$ implies that

$$\|\tilde{u}\|^2 / \sigma_u^2 \leq \tilde{u}^\intercal P_u^{-1}\tilde{u} \leq a^2. \tag{2.43}$$

For $\delta^2 = a^2\sigma_u^2$, this implies $\|\tilde{u}\|^2 \leq \delta^2$ and thus $\|\tilde{u}\| \leq \delta$. Therefore $\{\tilde{u} : \tilde{u}^\intercal P_u^{-1}\tilde{u} \leq a^2\} \subseteq \{\tilde{u} : \|\tilde{u}\| \leq \delta\}$, and hence $\mathbb{P}(\tilde{u}^\intercal P_u^{-1}\tilde{u} \leq a^2) \leq \mathbb{P}(\|\tilde{u}\| \leq \delta)$. The result follows by substituting $a = \delta/\sigma_u$ into (2.40):

$$\mathbb{P}(\|\tilde{u}\| \leq \delta) \geq \mathbb{P}(\tilde{u}^\intercal P_u^{-1}\tilde{u} \leq \delta^2/\sigma_u^2) \geq \operatorname{erf}\left(\frac{\delta}{\sigma_u\sqrt{2}}\right) - \frac{2\delta}{\sigma_u\sqrt{2\pi}} e^{-\delta^2/2\sigma_u^2}. \tag{2.44}$$

□

Theorem 2.3.5. *Let $u \sim \mathcal{N}(\bar{u}, P_u)$, and let Ω_δ be defined as in (2.37) where the throttle margin δ satisfies*

$$\operatorname{erf}\left(\frac{\delta}{\sigma_u\sqrt{2}}\right) - \frac{2\delta}{\sigma_u\sqrt{2\pi}}e^{-\delta^2/2\sigma_u^2} \geq 1-\beta, \tag{2.45}$$

where σ_u^2 be the maximum eigenvalue of P_u. Then (2.38) holds.

Proof. If $\bar{u} \in \Omega_\delta$ and $\|\tilde{u}\| \leq \delta$, then

$$\|u\| = \|\bar{u}+\tilde{u}\| \leq \|\bar{u}\| + \|\tilde{u}\| \leq \rho_2 - \delta + \delta = \rho_2, \tag{2.46}$$

$$\|u\| = \|\bar{u}+\tilde{u}\| \geq \|\bar{u}\| - \|\tilde{u}\| \geq \rho_1 + \delta - \delta = \rho_1. \tag{2.47}$$

Hence $\{u : \bar{u} \in \Omega_\delta,\ \|\tilde{u}\| \leq \delta\} \subseteq \Omega$, which implies that $\mathbb{P}(u \in \Omega) \geq \mathbb{P}(\|\tilde{u}\| \geq \delta)$ when $\bar{u} \in \Omega_\delta$. Lastly, if δ satisfies inequality (2.45), we conclude from Lemma 2.3.4 that $\mathbb{P}(u \in \Omega) \geq 1-\beta$. □

Proposition 2.3.6. *If there exists a value of δ that satisfies inequality (2.45), then the minimum value of δ satisfying (2.45) is the unique solution to*

$$\operatorname{erf}\left(\frac{\delta}{\sigma_u\sqrt{2}}\right) - \frac{2\delta}{\sigma_u\sqrt{2\pi}}e^{-\delta^2/2\sigma_u^2} - 1 + \beta = 0. \tag{2.48}$$

Proof. Take $\xi(\delta)$ to be the left hand side of inequality (2.45). We have that $\xi(0) = 0$. Then, taking the derivative, we obtain

$$\frac{\mathrm{d}\xi}{\mathrm{d}\delta}(\delta) = \frac{2\delta^2}{\sigma_u^3\sqrt{2\pi}}e^{-\delta^2/2\sigma_u^2}, \tag{2.49}$$

which is strictly positive for $\delta > 0$. Hence $\xi(\delta)$ is monotonically increasing for positive δ, and so the minimum value of δ that satisfies (2.45) is the unique solution to (2.48). □

Therefore, given a control covariance P_u and maximum saturation threshold β, we can obtain the set Ω_δ by solving a one-dimensional zero-finding problem for (2.48), which can

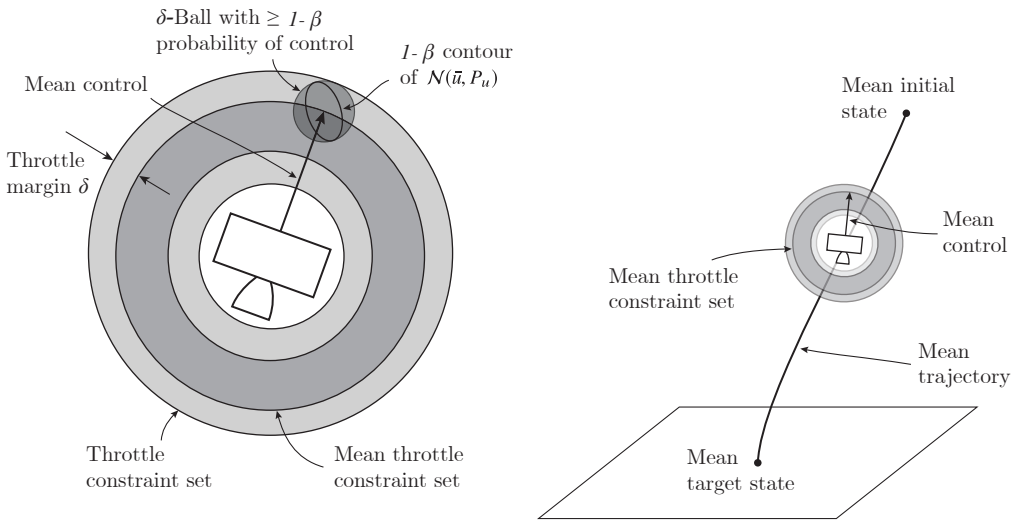

Figure 2.3: Conversion from stochastic to deterministic problem with throttle margin.

be performed onboard. We henceforth denote dependence of variables on P_u and β by a subscript δ, since the thrust margin δ is a function of P_u and β, that is, $\delta = \delta(t;\beta) = \delta(P_u(t);\beta)$.

2.3.4 Optimal Mean Control

Suppose that, for a given time-of-flight $t_f > 0$, we have solved for both the feedback gain K from (2.26) and the corresponding maximum control covariance $P_{u,\max}$ from (2.35). The throttle margin $\delta(t)$ is then computed from (2.48) to obtain the mean control constraint set $\Omega_{\delta(t)}$. We are now prepared to solve for the mean control by substituting the probabilistic thrust constraint (2.8) in Problem 2.1 with the deterministic constraint

$$\bar{u}(t) \in \Omega_{\delta(t)} \quad \text{for all} \quad t \in [0, t_f]. \tag{2.50}$$

The mean control problem is formalized as follows.

Problem 2.3. *For a fixed time-of-flight $t_f > 0$ and given throttle margin $\delta(t)$ for $t \in [0, t_f]$, find the mean control $\bar{u}(t)$ for $t \in [0, t_f]$ that minimizes the expected fuel cost (2.12) subject to the mean dynamics (2.13), the mean throttle constraint (2.50), the mean path constraints*

(2.9), and the final mean state constraint (2.6).

Remark 1. *Problem 2.3 is a standard, deterministic PDG problem, and therefore may be solved by existing methods, such as Ref. [19].*

The mean control solving Problem 2.3 satisfies the mean throttle constraint (2.50), and therefore, by Theorem 2.3.5, the original probabilistic thrust constraint (2.8) is satisfied.

Furthermore, we obtain the optimal time-of-flight as

$$t_f^* = \arg\min J_\delta^*(t_f), \tag{2.51}$$

where $J_\delta^*(t_f)$ denotes the optimal cost for Problem 2.3 with the throttle margin δ and time-of-flight t_f; that is, for a given throttle margin $\delta = \delta(t)$ and time-of-flight $t_f > 0$, the resulting optimal cost for Problem 2.3 is $J_\delta^*(t_f)$. The function $J_\delta^*(t_f)$ is unimodal [19], and therefore, for a fixed throttle margin, the optimal time-of-flight can be found by a simple line search. It is well known that the control solving Problem 2.3 is bang-bang, which we formally state in the following theorem.

Theorem 2.3.7. *The optimal thrust profile $\bar{u}^*$ solving Problem 2.3 has a max-min-max structure with no singular arcs. That is, for any time-of-flight $t_f > 0$ (including $t_f = t_f^*$),*

$$\|\bar{u}^*(t)\| = \begin{cases} \rho_2 - \delta(t), & 0 \le t \le t_1, \\ \rho_1 + \delta(t), & t_1 < t \le t_2, \\ \rho_2 - \delta(t), & t_2 < t \le t_f, \end{cases} \tag{2.52}$$

for all $t \in [0, t_f]$.

Proof. See Refs. [14, 19, 17]. □

Corollary 2.3.8. *Let δ_1 and δ_2 be piecewise continuous, positive functions defined over the interval $[0, t_f]$ such that $\delta_1(t) \le \delta_2(t)$ for all $t \in [0, t_f]$. If, in addition, $\delta_1(t) < \delta_2(t)$ for any nonzero time interval, then $J_{\delta_1}^*(t_f) < J_{\delta_2}^*(t_f)$.*

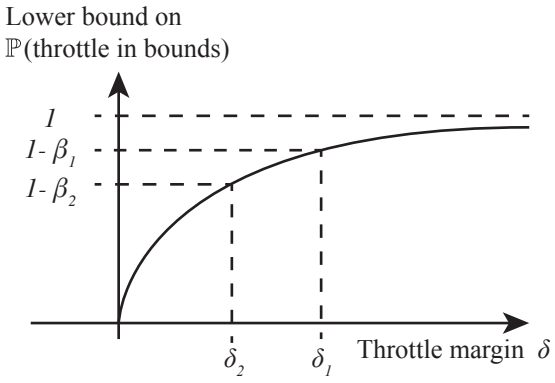

Figure 2.4: Diagram of $\xi(\delta)$ as in (2.48) and (2.49).

Proof. Let $t_f > 0$ be fixed, and let $\bar{u}_2^*$ be the control solving Problem 2.3 with the throttle margin δ_2. First, we observe that the control $\bar{u}_2^*$ satisfies the throttle constraint with the margin δ_1, since $\rho_1 + \delta_1 \leq \|\bar{u}_2^*\| \leq \rho_2 - \delta_1$ for all time. Since $J_{\delta_1}^*(t_f)$ is the minimum cost for all controls that satisfy this constraint, it follows that

$$J_{\delta_1}^*(t_f) \leq J(\bar{u}_2, t_f) = J_{\delta_2}^*(t_f). \tag{2.53}$$

It remains to show that equality does not hold. Indeed, if the throttle margin is given by δ_1, then $\rho_1 + \delta_1 < \|\bar{u}_2^*\| < \rho_2 - \delta_1$ on a nonzero interval implies that the control $\bar{u}_2^*$ is singular on a nonzero interval. This contradicts Theorem 2.3.7, and thus $\bar{u}_2^*$ is not an optimal control for Problem 2.3 with margin δ_1, which implies that the inequality in (2.53) is strict. □

Corollary 2.3.9. *Increasing the maximum probability of throttle saturation β decreases the fuel cost.*

Proof. As β increases, then, by (2.48) and (2.49), the throttle margin δ decreases; see Figure 2.4. Suppose first that the time-of-flight is held constant while β is increased. Then the throttle margin will decrease at every time instant, and thus, by Corollary 2.3.8, the fuel cost will decrease. It follows that the fuel will also decrease when the time-of-flight is left as an optimization variable. □

Corollary 2.3.8 is a formal statement of the intuitive result that decreasing the throttle

margin at any point along the trajectory will decrease the fuel cost. Furthermore, since our definition (2.48) of the throttle margin depends on the control covariance, Corollary 2.3.8 implies a connection between minimum-variance feedback control and constrained minimum-fuel control: if the control variance increases, then the fuel cost increases. We also observe, as a consequence of Corollary 2.3.8, that the noise intensity γ and maximum probability of control saturation β influence the fuel cost. Indeed, either increasing γ or decreasing β will increase the throttle margin, and hence will increase the fuel cost. These observations were confirmed by our numerical experiments reported in Section 2.4.

2.3.5 Closed-loop Powered Descent Guidance

The results of the preceding sections are summarized in the following algorithm.

Algorithm 1: Closed-loop powered descent guidance

Input: $t_f, m_0, \beta, \gamma > 0$, $P_{x_0}, P_{x_f} > 0$, $\bar{x}_0$, and $m_\ell(t), m_u(t)$ for $t \in [0, t_f]$
Output: Control law $u(t, x)$

1 Solve Problem 2.2 to obtain $P_x^\ell(t)$ and $K^\ell(t)$ for $t \in [0, t_f]$;
2 Set $K(t, m) = mK^\ell(t)/m_\ell(t)$;
3 Solve (2.48) with $\sigma_u = \sqrt{\lambda_{\max}(P_{u,\max}(t))}$, where $P_{u,\max}$ given as in (2.35), to obtain $\delta(t)$ for $t \in [0, t_f]$;
4 Solve Problem 2.3 to obtain $\bar{x}(t)$, $\bar{u}(t)$, and $m(t)$ for $t \in [0, t_f]$;
5 Return control law $u(t, x) = \bar{u}(t) + K(t, m(t))(x - \bar{x}(t))$.

Proposition 2.3.10. *The control law $u(t, x)$ returned by Algorithm 1 provides a feasible solution to Problem 2.1.*

Proof. Since the mean control is the solution to Problem 2.3, the mean path constraints (2.9) and the final mean state (2.6a) constraint are satisfied. Furthermore, by Theorem 2.3.2, we have that $P_x(t) \leq P_x^\ell(t)$ for all $t \in [0, t_f]$. Taking $t = t_f$ we have that the final state covariance constraint (2.6b) is satisfied.

Next, we show that the throttle constraint (2.8) is satisfied as well. For fixed $\delta > 0$, the

function

$$g(\sigma_u) = \operatorname{erf}\left(\frac{\delta}{\sigma_u\sqrt{2}}\right) - \frac{2\delta}{\sigma_u\sqrt{2\pi}}e^{-\delta^2/2\sigma_u^2} \tag{2.54}$$

is strictly decreasing since

$$\frac{\mathrm{d}g}{\mathrm{d}\sigma_u}(\sigma_u) = -\frac{2\delta^3}{\sqrt{2\pi\sigma_u^2}}e^{-\delta^2/2\sigma_u^2} < 0. \tag{2.55}$$

It follows that $g(\sqrt{\lambda_{\max}(P_u)}) \geq g(\sqrt{\lambda_{\max}(P_{u,\max})})$ since $P_u \leq P_{u,\max}$. Therefore, the inequality (2.45) holds for u distributed as $\mathcal{N}(\bar{u}, P_u)$ and δ as given by Algorithm 1, and thus, by Theorem 2.3.5, we have that $\mathbb{P}(u \in \Omega) \leq 1 - \beta$. Thus, we have shown that all of the constraints in Problem 2.1 are satisfied. □

2.4 Numerical Example

Consider a Mars Science Laboratory-like descent vehicle, with parameters as shown in Table 2.1, performing a powered descent maneuver at Mars. We use a surface-fixed frame with the first coordinate as the altitude, and we construct the maneuver so that the mean trajectory remains in the plane defined by the first and third coordinates. The initial mean position, velocity, and mass of the vehicle are given as

$$\bar{r}_0 = (1.9, 0, 1.5)\ \mathrm{km}, \qquad \bar{v}_0 = (-80, 0, 40)\ \mathrm{m/s}, \qquad m_0 = 1,905\ \mathrm{kg}. \tag{2.56}$$

The initial position and velocity have covariance

$$\operatorname{Cov}\left(\begin{bmatrix} r_0 \\ v_0 \end{bmatrix}\right) = \begin{bmatrix} (15\mathrm{m}/3)^2 I & 0 \\ 0 & (5\mathrm{ms}^{-1}/3)^2 I \end{bmatrix}. \tag{2.57}$$

The target mean position and velocity are

$$\bar{r}_f = (100, 0, 100)\ \mathrm{m}, \qquad \bar{v}_f = (0, 0, 0)\ \mathrm{m/s}, \tag{2.58}$$

and the final covariance of the position and velocity is constrained per (2.6b) by

$$\mathrm{Cov}\left(\begin{bmatrix} r(t_f) \\ v(t_f) \end{bmatrix}\right) \leq P_{x_f} = \begin{bmatrix} (5\mathrm{m}/3)^2 I & 0 \\ 0 & (3\mathrm{ms}^{-1}/3)^2 I \end{bmatrix}, \tag{2.59}$$

that is, the standard deviation of each position and velocity coordinate at the final time should be at most $5/3 \approx 1.67$ m and 1 m/s, respectively. The disturbance intensity γ is set to be 5% of the maximum thrust given in Table 2.1. The constant weighting matrices

$$Q = \begin{bmatrix} 75I & 0 \\ 0 & 0.5I \end{bmatrix}, \qquad R = I \tag{2.60}$$

were used when solving Problem 2.2. These values for Q and R were chosen qualitatively in order to balance the state covariance and the control covariance along the closed-loop trajectory.

Table 2.1: Vehicle properties

Property	Value	Unit
Specific impulse	210	s
Maximum thrust	16,573	N
Minimum throttle	30	%
Maximum throttle	80	%
Pointing angle θ_{pc_0}	75	deg
Glide slope angle θ_{gs_0}	70	deg
Wet mass m_0	1,905	kg
Propellant mass	400	kg

The optimal mean control was solved as a convex program, as in Ref. [19], for a time-discretization of $\Delta t = 1$ s, in Matlab with CVX and Mosek [104, 105, 106]. The optimal times-of-flight were computed by golden section line search. We solved for the closed-loop PDG following Algorithm 1 for probabilities of throttle saturation $\beta = 10\%, 30\%, 50\%,$ and 70%. For comparison, we also solved for the optimal mean control for a range of fixed (not time-varying) throttle margins with the feedback controls given as the solution

to Problem 2.2. The simulation cases are listed in Table 2.2. We compare the targeting performance for each solution by the root-norm error metric given by

$$\text{error} = \sqrt{\lambda_{\max}\big(P_x(t_f) - P_{x_f}\big)}. \tag{2.61}$$

The fuel cost and the position error, the velocity error, and the targeting error (2.61) are shown in Figures 2.5, 2.6, and 2.7 for each of the solution cases listed in Table 2.2. We see that, for a comparable targeting error, the fuel cost is decreased by setting dynamic throttle margins per Algorithm 1. Intuitively, the fixed throttle margins must be large enough to allow for the most extreme corrective control actions, which may only be required for a short segment of the trajectory.

Consider, for example, the solution for $\beta = 30\%$, which is shown in Figure 2.8. The optimal time-of-flight was 53 s. The 3σ position uncertainty is shown every four seconds, where the covariance was computed by both the analytical solution per (2.16), which is shown in gray, and by a 2,000 trial Monte Carlo, which is shown as dotted lines. The trajectory segment during which the thrust is at the minimum value is emphasized. We see that, despite some throttle saturation events, the covariance of the closed-loop trajectory closely tracks the predicted covariance solution. Near the end of the trajectory, the feedback control actions become more aggressive in order to meet the final state-covariance constraint. Therefore, the throttle variance is largest near the end of the trajectory, and the throttle margin increases accordingly; that is, the nominal trajectory is adjusted in response to predicted future disturbances. A planar view of the control sample path trajectories in polar coordinates, with zero degrees corresponding to the vertical, for the PDG solution with $\beta = 30\%$ is shown in Figure 2.9. Here we can see two-dimensional slices of the δ-balls corresponding to the throttle margin as in Figure 2.3, which are shown every four seconds, and samples of the closed-loop control.

The solutions for $\beta = 10\%$ and 70% are shown in Figure 2.10. When $\beta = 10\%$,

the throttle margins are large enough so that the state covariance computed from Monte Carlo closely tracks the predicted solution. On the other hand, when $\beta = 70\%$, the throttle frequently saturates and the state covariance increases. However, as we see in Figures 2.5, 2.6, and 2.7, and as given by Corollary 2.3.9, there is a corresponding decrease in the fuel cost.

Next, we consider the PDG solutions for fixed throttle margins. The trajectories for the two cases with numbers six and eight from Table 2.2 are compared in Figure 2.11. The throttle limits for the nominal trajectory are shown in gray and the absolute throttle limits are shown in black. We see that in the absence of any throttle margin, the state covariance increases and the final targeting error is significant. As expected, increasing the constant throttle margin improves targeting performance. However, for the nonzero fixed margin case shown in Figure 2.11, there is a high probability of control saturation in the final 10 seconds of the trajectory. Consequently, the targeting error is larger than for any of the cases with dynamic margins, including the case that $\beta = 70\%$. For comparison, we increased the fixed throttle margin until the targeting error was comparable to the case when $\beta = 50\%$; the fuel cost was approximately 12 kg, or 4.7%, greater than the fuel cost for the dynamic margin with $\beta = 50\%$.

Finally, recall that as a consequence of the assumption (2.4), the mass dynamics were modeled as a deterministic function of the mean throttle. This assumption is supported by the Monte Carlo results: For the solution with $\beta = 30\%$, for example, the 3σ-error in the final mass as computed from the Monte Carlo was approximately 10 kg, which amounts to a 0.6% deviation from the deterministic predicted final mass value of 1,648 kg. The small error between the targeted final state covariance and the final state covariance computed from Monte Carlo, as reported in Table 2.2, further supports this assumption.

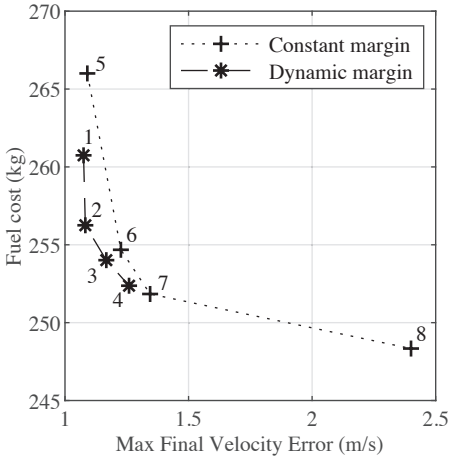

Figure 2.5: Maximum velocity covariance standard deviation for cases listed in Table 2.2.

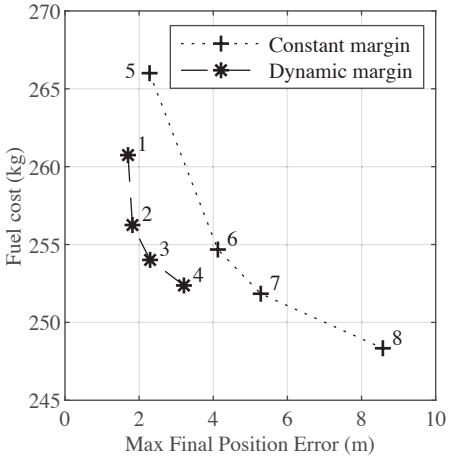

Figure 2.6: Maximum position covariance standard deviation for cases listed in Table 2.2.

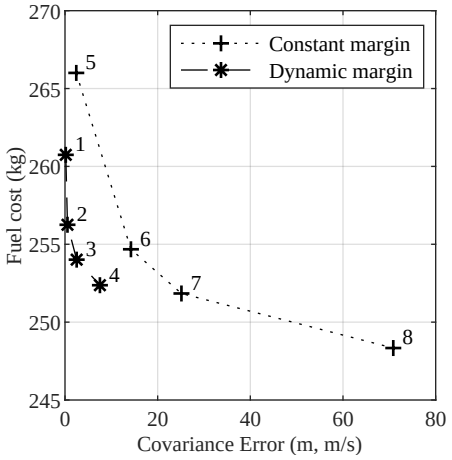

Figure 2.7: Comparison of covariance targeting performance for cases listed in Table 2.2. The error is given by the square root of the maximum eigenvalue of the matrix $P_x(t_f) - P_{x_f}$ as in (2.61).

Table 2.2: Simulation results

Case number	β (%)	Throttle limits (%) Lower	Upper	Fuel cost (kg)	Max std. dev.* Pos. (m)	Vel. (m/s)	Root-norm error
1	10	-	-	260.7	1.70	1.08	0.409
2	30	-	-	256.3	1.82	1.08	0.713
3	50	-	-	254.0	2.30	1.17	1.59
4	70	-	-	252.4	3.20	1.26	2.75
5	-	35	75	266.0	2.28	1.09	1.56
6	-	33	77	254.7	4.12	1.23	3.77
7	-	32	78	251.8	5.28	1.34	5.01
8	-	30	80	248.3	8.57	2.40	8.41

* Square root of the maximum eigenvalue of the covariance matrix.

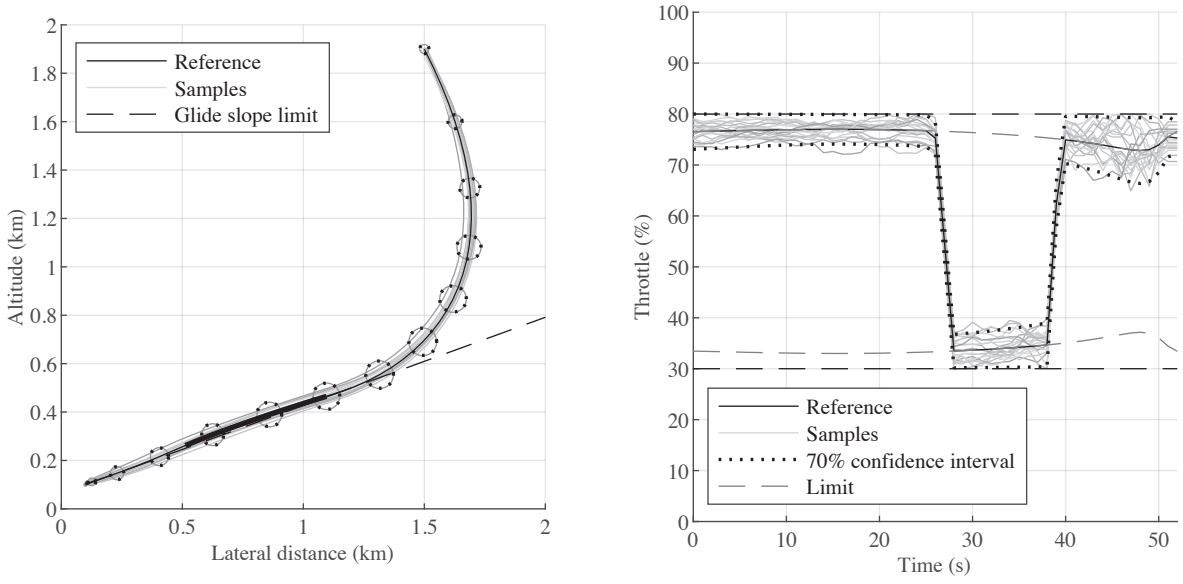

Figure 2.8: Solution with $\beta = 30\%$. (Left:) Powered descent trajectories with 3σ confidence ellipses. (Right:) Closed-loop throttle trajectories with $1 - \beta$ confidence intervals.

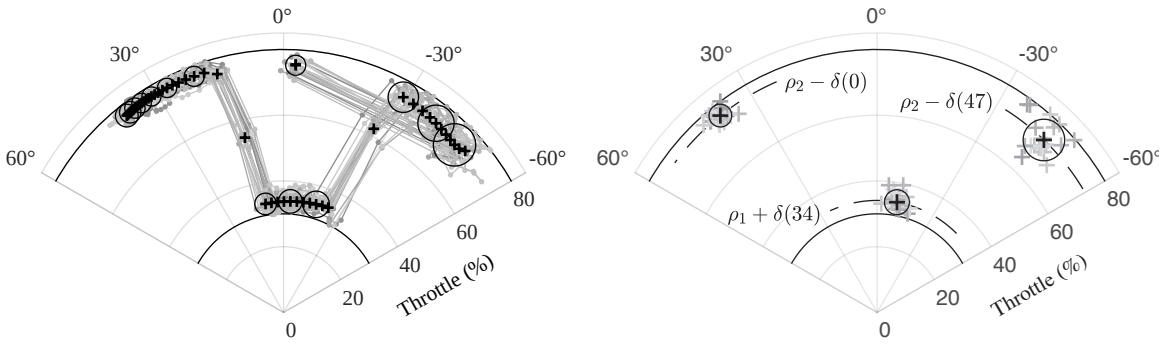

Figure 2.9: Solution with $\beta = 30\%$. (Left:) Planar view of sample control trajectories. (Right:) Control samples at $t = 0$ s, 34 s, and 47 s, and the mean constrained throttle (dashed) at these times.

2.5 Conclusion

In this chapter, a method for adding closed-loop control to existing open-loop powered descent guidance (PDG) solutions was presented. An important property of the closed-loop control law is that the feedback gains are computed before the feed-forward controls, and therefore iteratively solving for the feedback gains and the feed-forward controls can be avoided. Furthermore, the feedback gains are computed by integrating a system of ordinary differential equations with the initial condition given algebraically. The throttle margin is computed by solving for the root of a monotonic function, and the nominal trajectory is solved by any existing method, such as convex programming, using the provided throttle margin. Therefore, the proposed closed-loop PDG can be computed onboard. In numerical simulations, we demonstrated that dynamically setting the throttle margins, per the proposed method, results in lower fuel costs required to meet particular terminal position and velocity covariance requirements when compared to just scaling constant throttle margins.

The proposed method has several limitations that may be addressed in future work. First, aerodynamic forces are not included in the powered descent model, and the disturbance process is assumed to be Brownian with a constant intensity. Furthermore, in order to enable quick on-board computation and to provide performance guarantees, the proposed

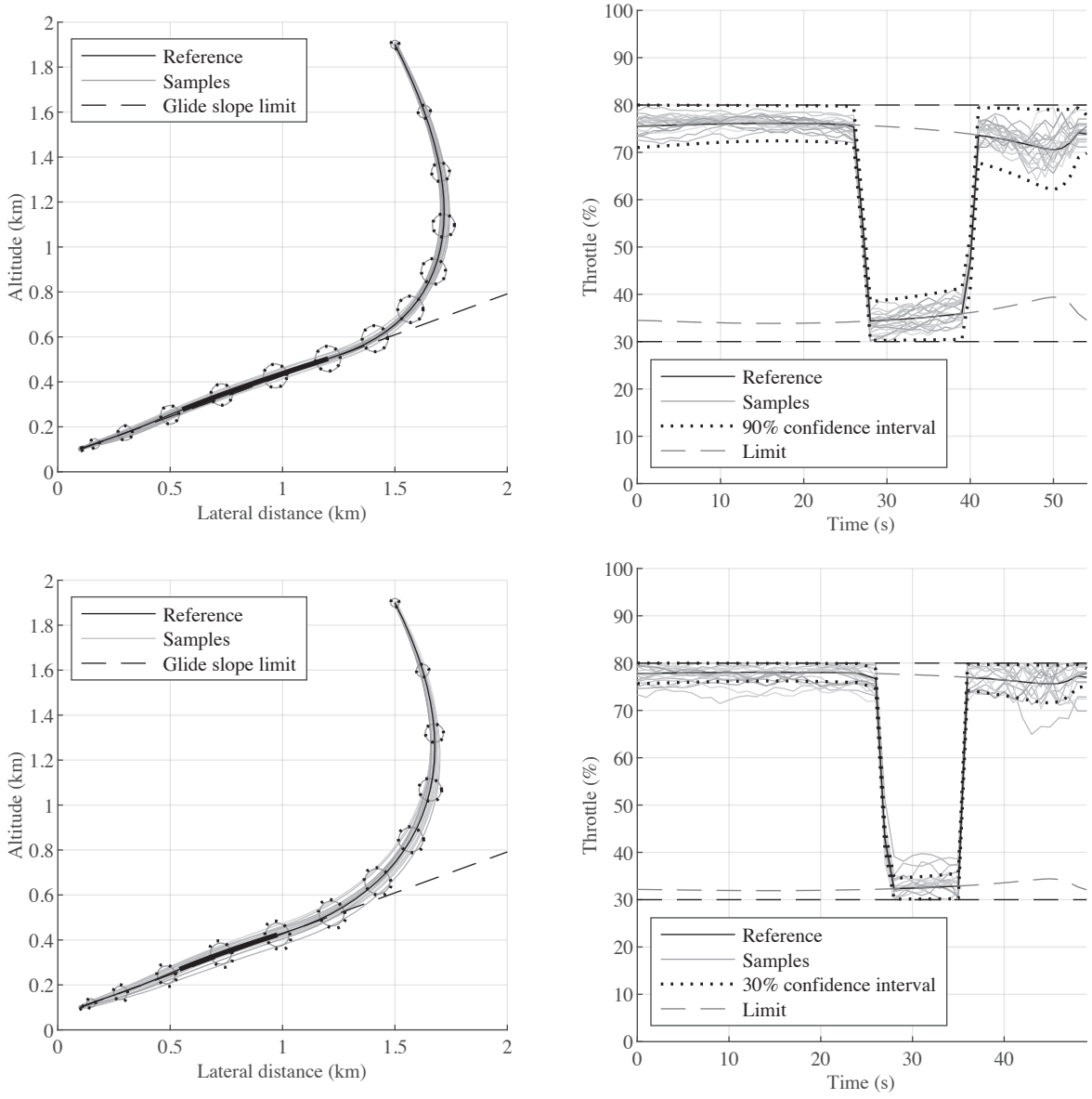

Figure 2.10: Solutions with $\beta = 10\%$ (top) and $\beta = 70\%$ (bottom). (Left:) Powered descent trajectories with 3σ confidence ellipses. (Right:) Closed-loop throttle trajectories with $1 - \beta$ confidence intervals.

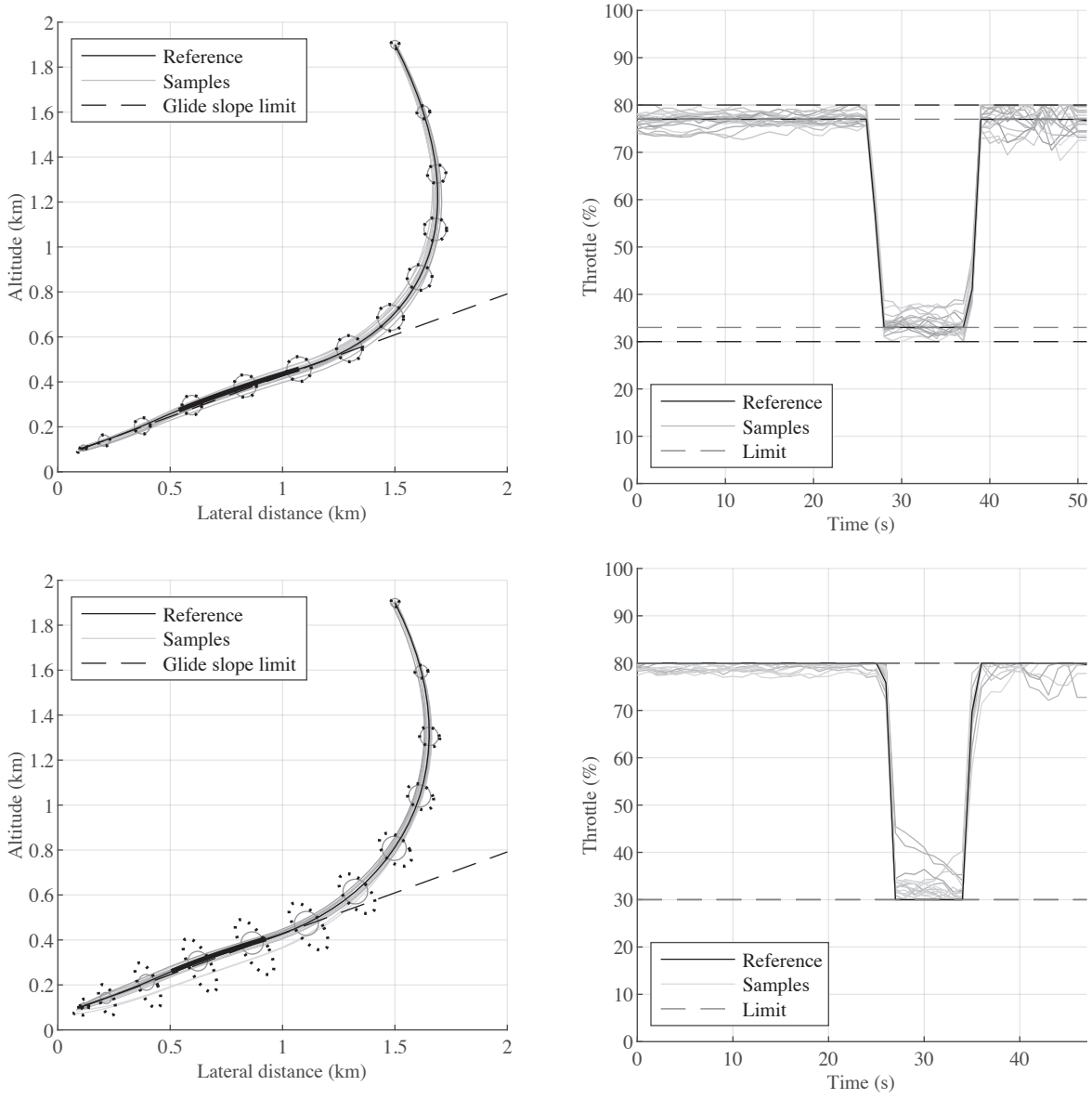

Figure 2.11: Solutions no. 6 (top) and no. 8 (bottom) with fixed margins as given in Table 2.2. (Left:) Powered descent trajectories with 3σ confidence ellipses. (Right:) Closed-loop throttle trajectories.

method solves for the feedback gains before solving for the nominal control; however, in principle, performance may be improved by jointly optimizing the feedback gains and the nominal control.

Looking forward, the framework presented in this chapter can be applied to other non-singular optimal control problems with external disturbances, since, for general optimal control problems with constrained control inputs, the nominal control is coupled to the statistics of the closed-loop system. The proposed method constitutes a computationally straightforward method for computing a closed-loop control law by means of setting open-loop control margins while avoiding iterative methods.

CHAPTER 3
STOCHASTIC ENTRY GUIDANCE

The material in this chapter is based on Refs. [107, 108].

3.1 Introduction

In this chapter, we take a stochastic control approach to entry guidance following the theory of covariance control. As for the Apollo final phase algorithm, the proposed stochastic entry guidance algorithm is assumed to consist of a reference trajectory, a linear feedback law, and table lookup; but the feedback gains in this proposed law are designed to steer the *covariance* of the entry trajectory rather than steer a particular sample path. By considering the closed-loop evolution of the state covariance, we are able to enforce constraints on the probability distributions of the closed-loop state and control, while minimizing the final range error variance. Furthermore, we are able to quantify the effect of terminating the entry trajectory as a function of the state, which is referred to as a state trigger, rather than simply a final time; in particular, the structure of the state trigger defines a transformation on the final state covariance. The drift term (i.e., the deterministic dynamics) in the stochastic model is obtained by a linear approximation of the longitudinal entry dynamics evaluated about a given reference trajectory, similar to the Apollo final phase algorithm. But for a stochastic treatment, it is also necessary to include the approximate effect of random atmospheric disturbances during entry, which is a nontrivial problem.

Monte Carlo studies indicate that for robotic class missions to Mars, dispersions in the atmospheric density and in the initial state of the vehicle are leading drivers of landing position uncertainty (along with aerodynamic modeling and navigation uncertainty) [9]. While the initial vehicle state uncertainty may be simply modeled as a Gaussian random vector, the atmospheric density uncertainty is traditionally modeled by the Global Refer-

ence Atmosphere Models (GRAMs), which include random variations in the density as a function of altitude [68]. Thus, the density variations are a spatially-dependent random process, but, due to the vehicle motion through the atmosphere, the density variations at the vehicle position become a random process in time. Based on this observation, we derive an expression for the diffusion coefficient (i.e., the noise intensity) as a function of the vehicle sink (descent) rate so that the entry trajectory can be expressed as a stochastic differential equation (SDE) driven by Brownian noise.

The proposed stochastic entry guidance depends on the given reference trajectory, the covariance of the initial vehicle states, and the intensity of density variations as a function of altitude. From an operational perspective, the entry guidance feedback gains thus depend not only on the nominal trajectory, but also on the interplanetary delivery performance. If an additional course correction is performed that decreases the delivery uncertainty, for example, then entry guidance performance could be improved by recomputing gains under the assumption of a smaller initial state uncertainty. If, on the other hand, a scheduled correction burn is canceled, then updating the feedback gain values could ensure that the bank angle commands do not saturate while attempting to make larger corrections due to the degraded delivery performance.

In contrast to the modern NPC approach to entry guidance, the proposed stochastic entry guidance is more closely related to the Apollo final phase guidance. For instance, while NPC approaches remove the requirement of supplying a reference trajectory, the proposed method is based on linear perturbations about a given reference trajectory. It follows that the applicability of the proposed method is restricted to correcting for relatively small deviations from this reference, whereas NPC-based entry guidance methods have shown to be robust to large state deviations [35, 42]. On the other hand, NPC entry guidance requires more complex onboard calculations and does not always have theoretical guarantees on convergence. In summary, the proposed method is not a general purpose guidance solution, but rather is an evolution of the Apollo final phase approach with improved range

control performance.

Contributions

The contributions of this chapter are summarized as follows. A novel stochastic process model of density variations is introduced, inspired by the GRAM density variation models, but which is given in an explicit form as an SDE. This model is leveraged to derive a closed-form linear covariance model for atmospheric entry, which includes the effects of random density variations — such a model is broadly applicable for use in preliminary trade studies that may include a first-order approximation of uncertainty [109, 110]. Lastly, we leverage this stochastic model to derive closed-loop entry guidance, while considering the effect of a state-dependent termination condition, which we demonstrate in a Monte Carlo simulation.

Organization

This chapter is organized as follows. In Section 3.2, a stochastic process model for atmospheric entry is developed, based on the proposed SDE model for the atmospheric density. Next, in Section 3.3, this stochastic entry model is used to derive a range control guidance using bank angle modulation. A brief review of the Apollo final phase algorithm is included for completeness. The effect of state triggers on the final state distribution, and hence on the range control law, is considered in Section 3.4. Then, in Section 3.5, the proposed stochastic entry guidance method is compared to the Apollo final phase guidance for a Mars entry mission based on MSL. Finally, we conclude in Section 3.6.

3.2 Entry as a Stochastic Process

The motion of an entry vehicle in atmospheric flight around a spherical, rotating planet is described in planet-relative coordinates by the system of equations [111, 112]

$$\dot{r} = V \sin\gamma \tag{3.1a}$$

$$\dot{\theta} = \frac{V \cos\gamma \sin\psi}{r \cos\phi} \tag{3.1b}$$

$$\dot{\phi} = \frac{V \cos\gamma \cos\psi}{r} \tag{3.1c}$$

$$\dot{V} = -\frac{D}{m} - \frac{\mu \sin\gamma}{r^2} + \Omega^2 r \cos\phi(\sin\gamma\cos\phi - \cos\gamma\sin\phi\cos\psi) \tag{3.1d}$$

$$\dot{\gamma} = \frac{1}{V}\left(\frac{L\cos\sigma}{m} - \frac{\mu\cos\gamma}{r^2} + \frac{V^2\cos\gamma}{r} + 2\Omega V\cos\phi\sin\psi \right. \\ \left. + \Omega^2 r\cos\phi(\cos\gamma\cos\phi + \sin\gamma\sin\phi\cos\psi)\right) \tag{3.1e}$$

$$\dot{\psi} = \frac{1}{V}\left(\frac{L\sin\sigma}{m\cos\gamma} - \frac{V^2\cos\gamma\sin\psi\tan\phi}{r} + 2\Omega V(\tan\gamma\cos\phi\cos\psi - \sin\phi) \right. \\ \left. - \frac{\Omega^2 r\sin\phi\cos\phi\sin\psi}{\cos\gamma}\right) \tag{3.1f}$$

where r is the distance from the planet center to the vehicle, θ is the longitude, ϕ is the latitude, V is the planet-relative velocity, γ is the planet-relative flight path angle, and ψ is the planet-relative heading azimuth. The bank angle σ is the angle between the lift vector and the local vertical, measured about the velocity vector in a right-hand sense; Ω is the planet rotation rate; μ is the planet gravitational parameter; m is the vehicle mass, which is assumed to be constant; and L and D are the lift and drag forces given by

$$L = qA_{\text{ref}}C_L(\alpha), \tag{3.2}$$

$$D = qA_{\text{ref}}C_D(\alpha), \tag{3.3}$$

where $q = \rho V^2/2$ is the dynamic pressure in terms of the atmospheric density ρ, A_{ref} is a reference area, and C_L and C_D are given aerodynamic coefficients which depend on the

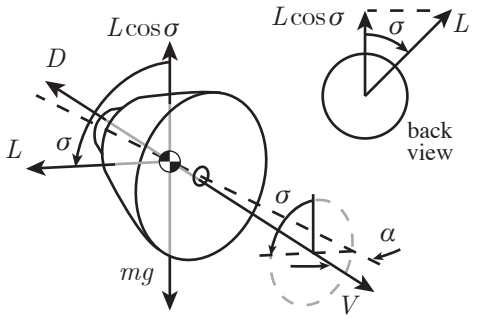

Figure 3.1: Bank angle control

angle of attack α, which we assume to be a function of velocity given by the vehicle trim configuration.

At entry interface (EI), which is the time when the vehicle radius first equals the radius of the edge of the sensible atmosphere r_{atm}, the vehicle state z is assumed to be Gaussian distributed as

$$z_0 = (r_0, \theta_0, \phi_0, V_0, \gamma_0, \psi_0) \sim \mathcal{N}(\bar{x}_0, \Sigma_0), \tag{3.4}$$

in terms of a known mean vector $\bar{x}_0$ and covariance matrix Σ_0. Note that by this definition of the initial time, the initial radius variance is zero.

The density ρ is decomposed into a mean density $\bar{\rho}$ and a multiplicative density variation $\delta\rho$ as follows

$$\rho = \bar{\rho}(1 + \delta\rho). \tag{3.5}$$

The mean density is a function of the radial position and is given as the solution to the ordinary differential equation (ODE)

$$\frac{\mathrm{d}\bar{\rho}}{\mathrm{d}r}(r) = -\frac{\bar{\rho}(r)}{H(r)}, \tag{3.6}$$

where $H(r)$ is the scale height, and with a boundary condition $\bar{\rho}(r_p) = \bar{\rho}_{r_p}$ at the planet surface radius r_p. The density variation, on the other hand, is assumed to be a stochastic process taking values as a function of the radial position. For notational convenience, we

define the *sink distance* as

$$s(r) = r_{\text{atm}} - r, \tag{3.7}$$

where r_{atm} is the radius of the edge of the sensible atmosphere. Since the sink distance and the radius have a unique correspondence, we will use s and r interchangeability when the context is clear.

The density variation process is assumed to be a zero-mean Ornstein–Uhlenbeck (OU) process given by the stochastic differential equation (SDE)

$$\mathrm{d}\delta\rho(s) = -\lambda(s)\delta\rho(s)\mathrm{d}s + \sqrt{\varphi(s)}\,\mathrm{d}w(s), \tag{3.8}$$

where $w(s)$ is a standard Brownian motion, and where $\lambda(s)$ and $\varphi(s)$ are both non-negative functions which determine the structure of the atmospheric uncertainty. The density variation at the zero sink position (the edge of the atmosphere) is normally distributed as

$$\delta\rho(0) \sim \mathcal{N}(0, \zeta_0), \tag{3.9}$$

for some initial variance $\zeta_0 \geq 0$. The density variation process (3.8) is assumed to be an OU process since the OU process is both linear and Gaussian, and since the resulting model closely resembles the existing GRAM dispersion model; in Section 3.5, this model is successfully used to represent MarsGRAM density dispersions.

Remark 2. *Setting $\lambda(s) = 2/H(s)$ results in density variations statistically similar to the GRAM [68] density variation samples [107]. Furthermore, for constant $H(s) \equiv H_0$ and $\varphi(s) \equiv \varphi_0$, it can be shown that*

$$\lim_{s\to\infty} \mathbb{E}(\delta\rho^2(s)) = \frac{\varphi_0 H_0}{4}. \tag{3.10}$$

Assuming rapid convergence of this limit, we set

$$\varphi(s) = \frac{4\zeta_d(s)}{H(s)}, \tag{3.11}$$

so that the variance $\mathbb{E}(\delta\rho^2(s))$ *approximates a desired altitude-dependent variance profile* $\zeta_d(s)$.

The density process may also be represented by an SDE. Applying Itô's formula to the function $F(s, \delta\rho) = \bar{\rho}(s)(1 + \delta\rho)$, and substituting (3.6) and (3.8), we obtain

$$\begin{aligned} \mathrm{d}\rho(s) &= \frac{\partial F}{\mathrm{d}s}(s, \delta\rho(s))\,\mathrm{d}s + \frac{\partial F}{\partial \delta\rho}(s, \delta\rho(s))\,\mathrm{d}\delta\rho(s) && (3.12) \\ &= \underbrace{\left(\left(\frac{1}{H(s)} - \lambda(s)\right)\rho(s) + \lambda(s)\bar{\rho}(s)\right)}_{f_\rho(s,\rho(s))}\mathrm{d}s + \underbrace{\bar{\rho}(s)\sqrt{\varphi(s)}}_{g_\rho(s)}\mathrm{d}w(s). && (3.13) \end{aligned}$$

It remains to combine the density process model with the vehicle dynamics in order to describe the motion of the vehicle in the random atmosphere. First, we compactly rewrite the dynamics (3.1) as

$$\dot{z} = f_z(z, \rho, u), \tag{3.14}$$

where $u = \sigma$ is the control input. Let $s(t) = s(r(t))$ be the sink distance of the vehicle at time t, which has derivative $\dot{s}(t) = -V(t)\sin\gamma(t)$. Applying a change of variables to the drift part of the density SDE (3.13), we obtain the time integral

$$\int_{s(t_0)}^{s(t)} f_\rho(y, \rho(y))\,\mathrm{d}y = \int_{t_0}^{t} f_\rho(s(\tau), \rho(s(\tau)))\dot{s}(z(\tau))\,\mathrm{d}\tau, \tag{3.15}$$

which, when substituted into the integral form of (3.13), results in the expression for the density at the vehicle position:

$$\rho(s(t)) = \rho(s(t_0)) + \int_{t_0}^{t} f_\rho(s(\tau), \rho(s(\tau)))\dot{s}(z(\tau))\,\mathrm{d}\tau + \int_{s(t_0)}^{s(t)} g_\rho(y)\,\mathrm{d}w(y). \tag{3.16}$$

Finally, concatenating (3.16) with the vehicle dynamics, we obtain an integral equation for the joint evolution of the density and the vehicle state as

$$\begin{bmatrix} z(t) \\ \rho(s(t)) \end{bmatrix} = \begin{bmatrix} z_0 \\ \rho(s(t_0)) \end{bmatrix} + \int_{t_0}^{t} \begin{bmatrix} f_z(z(\tau), \rho(s(\tau)), u(\tau)) \\ f_\rho(s(\tau), \rho(s(\tau)))\dot{s}(z(\tau)) \end{bmatrix} \mathrm{d}\tau + \int_{s(t_0)}^{s(t)} \begin{bmatrix} 0 \\ g_\rho(y) \end{bmatrix} \mathrm{d}w(y), \tag{3.17}$$

with the combined state at the initial time being distributed as

$$\begin{bmatrix} z_0 \\ \rho(s_0) \end{bmatrix} = x_0 \sim \mathcal{N}(\bar{x}_0, P_0), \tag{3.18}$$

where

$$\bar{x}_0 = \begin{bmatrix} \bar{z}_0 \\ \bar{\rho}(s_0) \end{bmatrix}, \qquad P_0 = \begin{bmatrix} \Sigma_0 & 0 \\ 0 & \mathrm{Var}(\rho(s_0)) \end{bmatrix}. \tag{3.19}$$

The initial vehicle state z_0 is uncorrelated with density since, by construction, the initial altitude is known exactly.

This equation represents the coupled nature of the density variations and the vehicle trajectory. However, since the limits of the stochastic integral (3.17) depend on the state, it is difficult to solve this equation in its present form.

3.2.1 Non-climbing Flight

In general, the density $\rho(s(t))$ at the vehicle position is a random process taking values as a function of time, however, this process is not necessarily Markovian, nor can it be given as the solution to an SDE. Indeed, since the density is defined as a function of altitude, if the vehicle enters a period of lofting, where it descends and then climbs, the density process will, in effect, reverse through previous values.

This poses both technical and practical issues. If increments of the density process in time are not independent, then the covariance of the joint vehicle-density process cannot be

described by an ODE, and methods from stochastic control theory developed for Brownian motion-driven random processes cannot be applied. Practically, we risk an over-fitting effect since the true atmospheric density likely depends also on the longitude and latitude in addition to the altitude. If the vehicle descends and then climbs, it may be unreasonable to take a past value of density to be exactly equal to the present value since the vehicle may have traveled hundreds of kilometers before reaching the previously experienced altitude. A complete stochastic atmosphere model for such a situation should therefore include statistical correlations which depend on downrange distance traveled.

We leave this spatial modeling issue as a problem for future work (see Chapter 5), and instead, in this chapter we focus primarily on the case of direct entry when the vehicle is monotonically descending. While this assumption excludes from consideration certain lofting or skip-to-entry trajectories, our primary concern is range control for low L/D vehicles at Mars, which traditionally do not include significant enough lofting to invalidate our assumptions. Indeed, in Section 3.5, the proposed range control is successfully applied to an MSL-like entry scenario.

Following this line of reasoning, and assuming that the vehicle is not climbing, we have

$$\dot{s}(t) \geq 0 \quad \text{for all} \quad t \geq t_0. \tag{3.20}$$

Strict adherence to this assumption is largely technical; in practice, as will be shown in Section 3.5, lofting flight may be reasonably captured by this model. This assumption allows us to write the density process using a stochastic integral over a Brownian motion (i.e., as an SDE), as is justified by the following lemma.

Lemma 3.2.1. *(Time-Changed Brownian Motion) Let $\tilde{w}(s)$ be a Brownian motion and let $s : [t_0, t_f] \to [0, s_f]$ be a smooth, non-decreasing function. Then, there exists a Brownian*

motion $w(t)$ *such that, almost surely, for all* $t \in [t_0, t_f]$,

$$\tilde{w}(s(t)) = \int_{t_0}^{t} \sqrt{\dot{s}(z)}\, \mathrm{d}w(z). \tag{3.21}$$

Proof. The Dambis-Dubins-Schwarz theorem [113, p. 5.13] states that all continuous local martingales may be given as a time-changed Brownian motion: for a martingale $y(t)$ with $t \in [t_0, t_f]$, there exists a Brownian motion ζ such that, almost surely (a.s), for all $t \in [t_0, t_f]$, $y(t) = \zeta(\xi(t))$, where $\xi(t) = \langle y, y \rangle(t)$ is the quadratic variation of y [1]. To show (3.21), we let the martingale be given by

$$y(t) = \int_{t_0}^{t} \sqrt{\dot{s}(a)}\, \mathrm{d}w(a). \tag{3.22}$$

This martingale has quadratic variation $\langle y, y \rangle(t) = s(t) - s(t_0)$. Since Brownian motion is a stationary process, we can drop the constant term $s(t_0)$, and then we take the time changed Brownian motion $\tilde{w}(s(t))$ to be $\zeta(s(t))$, which gives the desired result. □

Applying the time-change formula (3.21) to the stochastic integral in (3.17), we obtain

$$\int_{s(t_0)}^{s(t)} \begin{bmatrix} 0 \\ g_\rho(y) \end{bmatrix} \mathrm{d}w(y) = \int_{t_0}^{t} \begin{bmatrix} 0 \\ g_\rho(s(\tau)) \end{bmatrix} \sqrt{\dot{s}(z(\tau))}\, \mathrm{d}w(\tau). \tag{3.23}$$

Finally, we substitute the time-changed integral from (3.23) into (3.17) to obtain the SDE

$$\mathrm{d}x = f(x, u)\, \mathrm{d}t + g(x)\, \mathrm{d}w(t), \tag{3.24}$$

with the coefficient functions

$$f(x, u) = \begin{bmatrix} f_z(z, \rho, u) \\ f_\rho(s, \rho)\dot{s}(z) \end{bmatrix}, \qquad g(x) = \begin{bmatrix} 0 \\ g_\rho(s)\sqrt{\dot{s}(z)} \end{bmatrix}. \tag{3.25}$$

[1] For a definition of quadratic variation see [113, Theorem 4.9].

This SDE completely defines the stochastic process describing the vehicle entry trajectory under the assumption that the atmospheric density variations are as in (3.8) and that the vehicle trajectory is monotonically descending.

3.3 Bank-Angle Range Control

In this section, we consider the problem of range control using bank angle feedback. The vehicle is assumed to be in trimmed flight with positive lift (at zero bank) and zero sideslip, and control is affected by banking to tilt the lift vector. Changes to the vertical component of the lift are made by setting the magnitude of the bank angle, while the direction (left or right) of the lift force follows from the sign of the bank angle.

Vertical lift, which depends on the cosine of the bank angle, affects the vehicle's sink rate and thus its altitude. Increasing the altitude decreases the density and thus decreases drag. It follows that the velocity, and hence the range flown, may be affected by the vertical lift by means of setting the bank angle magnitude [38]. In other words, the vehicle can affect the range flown by increasing (or decreasing) the bank angle in order to fly through thicker (or thinner) atmosphere. We therefore set the cosine of the bank angle to be the longitudinal control input:

$$u_\ell = \cos\sigma. \tag{3.26}$$

Then, during flight, the bank angle command is given by

$$\sigma = b_{\text{dir}} \cos^{-1} u_\ell, \tag{3.27}$$

where the bank direction $b_{\text{dir}} \in \{-1, +1\}$ is set by a separate lateral control logic. For the purposes of range control, we use the simplified system for the longitudinal dynamics given by

$$\dot{r} = V \sin\gamma, \tag{3.28a}$$

$$\dot{V} = -\frac{\rho V^2 S C_D}{2m} - \frac{\mu \sin\gamma}{r^2}, \tag{3.28b}$$

$$\dot{\gamma} = \frac{\rho V S C_L}{2m}\cos\sigma - \left(\frac{\mu}{r^2} - \frac{V^2}{r}\right)\frac{\cos\gamma}{V}, \tag{3.28c}$$

$$\dot{R} = V\cos\gamma, \tag{3.28d}$$

where R is the downrange distance traveled. In terms of the longitudinal vehicle state

$$z_\ell = (r, V, \gamma, R), \tag{3.29}$$

the longitudinal dynamics (3.28) are compactly rewritten as

$$\dot{z}_\ell = f_{z_\ell}(z_\ell, \rho, u_\ell). \tag{3.30}$$

The range control problem is concerned with determining the longitudinal control inputs u_ℓ that steer the evolution of the longitudinal dynamics to reach the target conditions. In the following subsections, the control will be parameterized as a linear function of the state, and thus the range control problem will reduce to identifying the state feedback gains. First, the longitudinal dynamics (3.30) are approximated by a linear discrete-time system with an associated finite sequence of feedback gains.

3.3.1 Linear Discrete-Time Model

We assume that a reference trajectory $\hat{z}_\ell(t)$, with corresponding nominal density $\hat{\rho}(t) = \bar{\rho}(\hat{r}(t))$, and reference bank profile $\hat{\sigma}(t)$ are provided, as is done in the Apollo direct entry method [38, 39]. See Ref. [3] for a discussion of the reference bank profile design process.

The deviation of the combined vehicle and density state from this reference is denoted by

$$\tilde{x}_\ell(t) = \begin{bmatrix} z_\ell(t) - \hat{z}_\ell(t) \\ \rho(t) - \hat{\rho}(t) \end{bmatrix} \tag{3.31}$$

and the corrective control input is denoted by $\tilde{u}_\ell(t)$. The closed-loop bank angle magnitude is given by the sum of the nominal part and the corrective part:

$$u_\ell = \cos\hat{\sigma} + \tilde{u}_\ell. \tag{3.32}$$

The combined longitudinal vehicle dynamics and density process are linearized about this reference to obtain a linear stochastic system for the state deviation dynamics, given by

$$\mathrm{d}\tilde{x}_\ell(t) = (A_\ell(t)\tilde{x}_\ell(t) + B_\ell(t)\tilde{u}_\ell(t))\mathrm{d}t + G_\ell(t)\mathrm{d}w(t), \tag{3.33}$$

where the coefficient matrices

$$A_\ell(t) = \frac{\partial}{\partial z_\ell}\begin{bmatrix} f_{z_\ell} \\ f_\rho\dot{s} \end{bmatrix}, \quad B_\ell(t) = \frac{\partial}{\partial u_\ell}\begin{bmatrix} f_{z_\ell} \\ f_\rho\dot{s} \end{bmatrix}, \quad G_\ell(t) = \begin{bmatrix} 0_{4\times 1} \\ g_\rho\sqrt{\dot{s}} \end{bmatrix} \tag{3.34}$$

are evaluated along the reference trajectory, and where, as before, $w(t)$ is a one-dimensional standard Brownian motion.

The corrective control input is assumed to be constant on the subintervals of a partition $\mathcal{P} = (t_k^p)_{k=0}^{N_p}$ of the interval $[t_0, t_f]$ given by

$$t_0 = t_0^p < t_1^p < \cdots < t_{N_p}^p = t_f. \tag{3.35}$$

In the derivation of the Apollo final phase entry guidance, in contrast, the corrective control at any time is assumed to be constant for the remainder of the flight [38, 39]. However, the bank angle corrections realized in flight are *not* constant in the Apollo implementation,

whereas the control corrections in the present derivation *will* in fact be constant on the subintervals of the partition $\mathscr{P}$. Maintaining this more representative model of the closed-loop bank angle corrections will allow us to leverage the degrees of freedom given by the number of subintervals in $\mathscr{P}$ to enforce constraints on the entry trajectory and on the closed-loop bank angle.

Since, for any step $k \in \{0, \dots, N_p - 1\}$, the control correction $\tilde{u}_\ell(t)$ is constant on the interval $[t_k^p, t_{k+1}^p]$, we can integrate the continuous-time system (3.33) from t_k^p to t_{k+1}^p and obtain the discrete-time system

$$\tilde{x}_{\ell,k+1} = A_{\ell,k}\tilde{x}_{\ell,k} + B_{\ell,k}\tilde{u}_{\ell,k} + G_{\ell,k}w_k, \tag{3.36}$$

where

$$\tilde{x}_{\ell,k} = \tilde{x}_\ell(t_k^p), \quad \tilde{u}_{\ell,k} = \tilde{u}_\ell(t_k^p), \tag{3.37}$$

$$A_{\ell,k} = \Phi_\ell(t_{k+1}^p, t_k^p), \quad B_{\ell,k} = \int_{t_k^p}^{t_{k+1}^p} \Phi_\ell(t_{k+1}^p, \tau) B_\ell(\tau)\, \mathrm{d}\tau, \tag{3.38}$$

and where $\Phi_\ell(t, \tau)$ is the state transition matrix corresponding to the state matrix $A_\ell(t)$, which is the solution to the ODE

$$\frac{\partial}{\partial t}\Phi_\ell(t, t_0) = A_\ell(t)\Phi_\ell(t, t_0), \quad \Phi_\ell(t_0, t_0) = I, \tag{3.39}$$

and which satisfies the property that $\Phi_\ell(t, \tau) = \Phi_\ell(t, t_0)\Phi_\ell^{-1}(\tau, t_0)$. The noise increments w_k are independent standard Gaussian random vectors, and the matrices $G_{\ell,k}$ are set so that the random vector $G_{\ell,k}w_k$ has covariance

$$\int_{t_k^p}^{t_{k+1}^p} \Phi_\ell(t_{k+1}^p, \tau) G_\ell(\tau) G_\ell^\intercal(\tau) \Phi_\ell^\intercal(t_{k+1}^p, \tau)\, \mathrm{d}\tau. \tag{3.40}$$

It follows that $G_{\ell,k}$ can be any matrix such that $G_{\ell,k}G_{\ell,k}^\intercal$ equals the integral (3.40), and,

accordingly, only the matrix product $G_{\ell,k}G_{\ell,k}^{\mathsf{T}}$ affects the evolution of the state covariance.

The control corrections are parameterized as linear functions of the state deviation, which results in the linear feedback law

$$\tilde{u}_{\ell,k} = K_{\ell,k}\tilde{x}_{\ell,k}, \tag{3.41}$$

in terms of the yet to-be-determined feedback gain matrices $K_{\ell,k} \in \mathbb{R}^{1\times 5}$ for $k = 0, \ldots, N_p - 1$. Provided this feedback law, the covariance of the combined vehicle-density state

$$P_{\ell,k} = \mathbb{E}(\tilde{x}_{\ell,k}\tilde{x}_{\ell,k}^{\mathsf{T}}), \tag{3.42}$$

is obtained as the solution to the difference equation

$$P_{\ell,k+1} = (A_{\ell,k} + B_{\ell,k}K_{\ell,k})P_{\ell,k}(A_{\ell,k} + B_{\ell,k}K_{\ell,k})^{\mathsf{T}} + G_{\ell,k}G_{\ell,k}^{\mathsf{T}}, \tag{3.43}$$

with the initial condition

$$P_{\ell,0} = \begin{bmatrix} \Sigma_{\ell,0} & 0 \\ 0 & \mathrm{Var}\left(\rho(t_0)\right) \end{bmatrix}, \tag{3.44}$$

where the value of the initial longitudinal state covariance matrix $\Sigma_{\ell,0}$ follows from the full state covariance matrix Σ_0. There is initially no correlation between the vehicle states and the density since the initial vehicle radius is by definition fixed to be equal to the radius of the edge of atmosphere. The variance of the density at the initial altitude is a function of the density variation variance $\zeta(s) = \mathrm{Var}\left(\delta\rho(s)\right)$ given by

$$\mathrm{Var}\left(\rho(t_0)\right) = \zeta(s(t_0))\bar{\rho}^2(s(t_0)). \tag{3.45}$$

The closed-loop control $u_\ell(t)$ is also Gaussian distributed with mean $\cos\hat{\sigma}(t)$ and variance

$$\mathrm{Var}\left(u_\ell(t)\right) = K_{\ell,k}P_{\ell,k}K_{\ell,k}^{\mathsf{T}}, \tag{3.46}$$

for all times in the interval $[t_k^p, t_{k+1}^p]$. The distribution of the closed-loop control therefore depends on the state covariance and the feedback gain.

3.3.2 Apollo Range Control

Before presenting the stochastic approach to range control, and for the sake of completeness, we briefly review the derivation of the Apollo final phase range control as presented in Refs. [38, 39]. As before, a nominal bank angle profile and the corresponding longitudinal trajectory are provided. The dynamics are linearized about this reference to obtain a linear time-varying system as in (3.33), except that the stochastic term is neglected. Without the stochastic term, there is no longer a reason to include density as a state, and as such, the Apollo direct entry derivation takes the state to be equal to the vehicle state. However, in an effort to keep the notation consistent, we will use the system matrices $A_\ell(t)$ and $B_\ell(t)$ as in (3.34) and the state transition matrix $\Phi_\ell(t, \tau)$ as in (3.39).

At any time t, the corrective control input $\tilde{u}_{\ell,\mathrm{ap}}(t)$ is assumed to remain constant for the remainder of the flight. The state deviation at the final time is therefore given by

$$\tilde{x}_\ell(t_f) = \Phi_\ell(t_f, t)\tilde{x}_\ell(t) + \left(\int_t^{t_f} \Phi_\ell(t_f, \tau) B_\ell(\tau)\, \mathrm{d}\tau \right) \tilde{u}_{\ell,\mathrm{ap}}(t). \tag{3.47}$$

Define the final total range error ΔR_f to be a linear function of the final state, given by

$$\Delta R_f = \vartheta_f^\intercal \tilde{x}_\ell(t_f), \tag{3.48}$$

for some influence-weighting vector ϑ_f. Note that ΔR_f is not necessarily equal to $\tilde{R}(t_f)$, since errors in the altitude may also contribute to the range error following parachute deployment [38, 39]; the relationship between ΔR_f and $\tilde{R}(t_f)$ will be described in Section 3.4. It follows that the total range error can be computed as a linear function of the state and control at any time along the trajectory in terms of the *adjoint* functions $\vartheta(t)$ and

$\vartheta_u(t)$ by

$$\Delta R_f = \vartheta^{\mathsf{T}}(t)\tilde{x}_\ell(t) + \vartheta_u(t)\tilde{u}_{\ell,\mathrm{ap}}(t). \tag{3.49}$$

The adjoint system is obtained as the solution to the backwards ODE [15]

$$\frac{\mathrm{d}}{\mathrm{d}t}\begin{bmatrix}\vartheta(t)\\ \vartheta_u(t)\end{bmatrix} = -\begin{bmatrix}A_\ell^{\mathsf{T}}(t) & 0\\ B_\ell^{\mathsf{T}}(t) & 0\end{bmatrix}\begin{bmatrix}\vartheta(t)\\ \vartheta_u(t)\end{bmatrix}, \qquad \begin{bmatrix}\vartheta(t_f)\\ \vartheta_u(t_f)\end{bmatrix} = \begin{bmatrix}\vartheta_f\\ 0\end{bmatrix}. \tag{3.50}$$

Finally, the feedback law

$$\tilde{u}_{\ell,\mathrm{ap}}(t) = K_{\ell,\mathrm{ap}}(t)\tilde{x}_\ell(t), \quad K_{\ell,\mathrm{ap}}(t) = -K_{\mathrm{oc}}\frac{\vartheta^{\mathsf{T}}(t)}{\vartheta_u(t)}, \tag{3.51}$$

is obtained by setting $\Delta R_f = 0$ in (3.49) and solving for the control, and where K_{oc}, which is referred to as the overcontrol gain, is a user-defined parameter which may be tuned to improve performance. In practice, the feedback law (3.51) is rewritten in terms of range, drag, and climb rate feedback. In addition, the feedback gain and the nominal trajectory are recast as functions of velocity with the nominal trajectory serving as the mapping between time and velocity.

3.3.3 Stochastic Range Control

In the absence of the stochastic forcing term in the linearized system (3.33), the predicted range traveled by the vehicle would be controlled by the selection of a particular bank angle correction to be made during flight. Accordingly, from a deterministic perspective, the central model for range control is the mapping defined by the linearized system (3.33) of bank angle corrections to a predicted final range error; in the derivation of the Apollo final phase entry guidance this mapping is defined via the adjoint state, which determines the feedback gains.

When including the stochastic term, in contrast, there is no longer a unique mapping from bank angle corrections to range-error predictions, since, for any particular bank angle,

the range flown is random. The central model for stochastic range control instead becomes the state covariance evolution equation (3.43), which defines a mapping from bank angle *feedback gains* to the predicted final range error *variance*. The stochastic range control problem is thus to solve for the feedback gains $K_{\ell,k}$ that minimize a function of final state covariance subject to constraints on the probability distribution of the final state and of the control inputs.

Constraints on the final state error are given in the form

$$\mathbb{P}(|d_i^{\mathsf{T}}\tilde{x}_\ell(t_f)| \leq \Delta_i^x) \geq 1 - p_i^x, \tag{3.52}$$

for $i = 1, \ldots, N_x$. The vectors $d_i \in \mathbb{R}^5$ and scalars Δ_i^x define regions which the state error must lie within, and $p_i^x \in (0, 1]$ is the maximum probability with which this constraint may be violated. For example, constraining the final altitude error to be less than 5 km with 99% probability translates to the values $d_i = (1, 0, 0, 0, 0)$, $\Delta_i^x = 5$ km, and $p_i^x = 0.01$.

Assuming the state to be Gaussian distributed, the linear feedback law (3.41) implies that the control corrections are also Gaussian distributed. However, the range of allowable closed-loop bank angles may be limited due to concerns of lateral control authority [3]. In flight, of course, commanded control corrections which are outside of a user-defined interval will be saturated, but including a saturation function in the law (3.41) would invalidate the linear structure. Instead, the *probability* that closed-loop bank angle commands saturate will be constrained, and through this constraint we establish a balance between the intensity of planned corrective controls and the allowable range of bank angles; in other words, this constraint establishes for the feedback gains a dependence on the allowable control inputs. To this end, longitudinal control input deviations (i.e., deviations of the cosine of the bank angle) from the nominal value are constrained at each control decision time t_k^p by

$$\mathbb{P}(|\tilde{u}_{\ell,k}| \leq \Delta_k^u) \geq 1 - p_k^u, \tag{3.53}$$

for $k = 0, \ldots, N_p - 1$, where $p_k^u \in (0, 1]$ is a user-defined maximum allowable probability that the commanded control is outside the allowable range. This constraint assumes a symmetric constrained region $[-\Delta_k^u, +\Delta_k^u]$ about the nominal control value, since the control is Gaussian distributed and the selection of the feedback gains only affects the variance of $\tilde{u}_{\ell,k}$. The closed-loop longitudinal control can be constrained to lie in the interval $[u_{\ell,k,\min}, u_{\ell,k,\max}]$ with probability at least $1 - p_k^u$ by taking $\Delta_k^u = \min\{u_{\ell,k,\max} - \cos\hat{\sigma}(t_k^p), \cos\hat{\sigma}(t_k^p) - u_{\ell,k,\min}\}$.

The range control cost is a function of the sequence of feedback gains $K = (K_{\ell,k})$ given by

$$J_\ell(K) = \mathrm{Var}\left(a_f^\mathsf{T}\tilde{x}_\ell(t_f)\right) + \sum_{k=0}^{N_p-1} \mathcal{R}_k \,\mathrm{Var}\left(\tilde{u}_{\ell,k}\right), \tag{3.54}$$

where the vector a_f weights the coordinates of the final state error, and $(\mathcal{R}_k)$ is a sequence of non-negative control cost weights. The vector a_f may be defined, for instance, so that $a_f^\mathsf{T}\tilde{x}_\ell(t_f) = \tilde{R}(t_f)$, and the control weights $(\mathcal{R}_k)$ can be set to be a small number so that bank angle corrections will only be commanded if there is a meaningful reduction in the final state covariance. The stochastic range control problem is summarized as follows.

Problem 3.1. *Find the sequence of feedback gains $K = (K_{\ell,k})$ that minimize the cost (3.54), subject to the covariance dynamics (3.43), the control constraints (3.53), and the final state constraints (3.52).*

In general, Problem 3.1 is a discrete-time, chance-constrained, linear-quadratic-Gaussian (LQG) stochastic optimal control problem. In the following, we establish a connection between Problem 3.1 and the *unconstrained* LQG problem, which has a known closed-form solution. This connection allows us to obtain the solution to Problem 3.1 by selecting proper LQG weights. While this class of problems can be solved via convex programming [69, 70], we have observed that for the range control problem, the solution method via LQG is numerically better-behaved, is easier to implement, and is more intuitive (i.e., not a "black-box").

Solution using Unconstrained Linear Quadratic Control

The unconstrained LQG problem is summarized as follows.

Problem 3.2. *Find the sequence of feedback gains $K = (K_{\ell,k})$ that minimize the cost*

$$J_{LQ}(K; \mathbb{Q}, \mathscr{R}) = \operatorname{tr} \mathbb{Q} \operatorname{Cov}(\tilde{x}_\ell(t_f)) + \sum_{k=0}^{N_p-1} \mathscr{R}_k \operatorname{Var}(\tilde{u}_{\ell,k}), \tag{3.55}$$

for a given final state weight matrix $\mathbb{Q} \geq 0$ and sequence of positive, scalar control weights $\mathscr{R} = (\mathscr{R}_k)$, subject to the covariance dynamics (3.43).

The solution to Problem 3.2 is obtained by the backwards equations [15]:

$$K_{\ell,k} = -(B_{\ell,k}^\intercal S_{\ell,k+1} B_{\ell,k} + \mathscr{R}_k) B_{\ell,k}^\intercal S_{\ell,k+1} A_{\ell,k}, \tag{3.56a}$$

$$S_{\ell,k} = A_{\ell,k}^\intercal S_{\ell,k+1} A_{\ell,k} - K_{\ell,k}^\intercal (\mathscr{R}_k + B_{\ell,k}^\intercal S_{\ell,k+1} B_{\ell,k}) K_{\ell,k}, \tag{3.56b}$$

$$S_{N_p} = \mathbb{Q}. \tag{3.56c}$$

Comparing Problems 3.1 and 3.2, we observe that the LQG cost function (3.55) appears to be the Lagrangian for Problem 3.1, which would imply that, for particular values of $\mathbb{Q}$ and $\mathscr{R}$ corresponding to Lagrange multipliers, these problems have the same solution. The following theorem shows that this indeed the case.

Theorem 3.3.1. *For particular values of the weights $\mathbb{Q}$ and $\mathscr{R}$, the solution of Problem 3.2 solves Problem 3.1.*

Proof. First, we rewrite the constraints (3.52) and (3.53) as limits on the covariance of the final state and the variance of the closed-loop control inputs. Since the inner product $d_i^\intercal \tilde{x}_\ell(t_f)$ is a zero-mean Gaussian random variable with variance $d_i^\intercal P_{\ell,N_p} d_i$, we have that

$$\mathbb{P}(|d_i^\intercal \tilde{x}_\ell(t_f)| \leq \Delta_i^x) = \operatorname{erf}\left(\frac{\Delta_i^x}{\sqrt{2 d_i^\intercal P_{\ell,N_p} d_i}}\right), \tag{3.57}$$

in terms of the error function erf. Rearranging, we obtain an equivalent constraint to (3.52), given by

$$d_i^\intercal P_{\ell,N_p} d_i \leq \mathscr{D}_i^2, \quad \text{where} \quad \mathscr{D}_i = \frac{\Delta_i^x}{\sqrt{2}\,\mathrm{erf}^{-1}(1-p_i^x)}, \tag{3.58}$$

for $i = 1, \ldots, N_x$. Similarly, since the control correction $\tilde{u}_{\ell,k}$ is zero-mean Gaussian distributed, we have that

$$\mathbb{P}(|\tilde{u}_{\ell,k}| \leq \Delta_k^u) = \mathrm{erf}\left(\frac{\Delta_k^u}{\sqrt{2\,\mathrm{Var}\,(\tilde{u}_{\ell,k})}}\right). \tag{3.59}$$

Substituting $\mathrm{Var}\,(\tilde{u}_{\ell,k}) = K_{\ell,k} P_{\ell,k} K_{\ell,k}^\intercal$ and rearranging, we obtain an equivalent constraint to (3.53) given by

$$K_{\ell,k} P_{\ell,k} K_{\ell,k}^\intercal \leq \mathscr{U}_k^2, \quad \text{where} \quad \mathscr{U}_k = \frac{\Delta_k^u}{\sqrt{2}\,\mathrm{erf}^{-1}(1-p_k^u)}, \tag{3.60}$$

for $k = 0, \ldots, N_p - 1$.

Next, we relate the LQ cost function (3.55) to the Lagrangian for Problem 3.1, which, with the Lagrange multipliers $\xi \in \mathbb{R}^{N_x+N_p}$, is given as

$$L_\ell(K,\xi) = J_\ell(K) + \sum_{i=1}^{N_x} \xi_i \big(d_i^\intercal P_{\ell,N_p} d_i - \mathscr{D}_i^2\big) + \sum_{k=0}^{N_p-1} \xi_{N_x+k+1} \big(K_{\ell,k} P_{\ell,k} K_{\ell,k}^\intercal - \mathscr{U}_k^2\big). \tag{3.61}$$

The terms in the Lagrangian that depend on the final state covariance are rearranged as

$$\begin{aligned}
&\mathrm{Var}\,(a_f^\intercal \tilde{x}_\ell(t_f)) + \sum_{i=1}^{N_x} \xi_i \big(d_i^\intercal P_{\ell,N_p} d_i - \mathscr{D}_i^2\big) \\
&\qquad = \mathrm{tr}\left(a_f a_f^\intercal P_{\ell,N_p}\right) + \mathrm{tr}\left\{\left(\sum_{i=1}^{N_x} \xi_i d_i d_i^\intercal\right) P_{\ell,N_p}\right\} - \sum_{i=1}^{N_x} \xi_i \mathscr{D}_i^2 \\
&\qquad\qquad = \mathrm{tr}\left\{\left(a_f a_f^\intercal + \sum_{i=1}^{N_x} \xi_i d_i d_i^\intercal\right) P_{\ell,N_p}\right\} - \sum_{i=1}^{N_x} \xi_i \mathscr{D}_i^2.
\end{aligned} \tag{3.62}$$

Similarly, the terms including the control variance $K_{\ell,k}P_{\ell,k}K_{\ell,k}^{\mathsf{T}}$ are rearranged as

$$\sum_{k=0}^{N_p-1} \mathcal{R}_k K_{\ell,k}P_{\ell,k}K_{\ell,k}^{\mathsf{T}} + \sum_{k=0}^{N_p-1} \xi_{N_x+k+1}\big(K_{\ell,k}P_{\ell,k}K_{\ell,k}^{\mathsf{T}} - \mathcal{U}_k^2\big) = \sum_{k=0}^{N_p-1} \big(\mathcal{R}_k + \xi_{N_x+k+1}\big)K_{\ell,k}P_{\ell,k}K_{\ell,k}^{\mathsf{T}} - \sum_{k=0}^{N_p-1} \xi_{N_x+k+1}\mathcal{U}_k^2. \quad (3.63)$$

Let (K^*, ξ^*) be a solution pair to Problem 3.1, and let

$$\mathbb{Q}^* = a_f a_f^{\mathsf{T}} + \sum_{i=1}^{N_x} \xi_i^* d_i d_i^{\mathsf{T}}, \quad \mathcal{R}_k^* = \mathcal{R}_k + \xi_{N_x+k+1}^*. \quad (3.64)$$

Substituting (3.62) and (3.63), we rewrite the Lagrangian (3.61) as

$$L_\ell(K, \xi^*) = J_{LQ}(K; \mathbb{Q}^*, \mathcal{R}_k^*) - Z\xi^*, \quad (3.65)$$

where

$$Z = \begin{bmatrix} \mathcal{D}_1^2 & \cdots & \mathcal{D}_{N_x}^2 & \mathcal{U}_0^2 & \cdots & \mathcal{U}_{N_p-1}^2 \end{bmatrix}. \quad (3.66)$$

Since the term $Z\xi^*$ in (3.65) does not depend on the decision variable K, minimizing the Lagrangian over the decision variable at the optimal value of the multipliers ξ^* is equivalent to minimizing the LQ cost with the weights $\mathbb{Q}^*$ and $\mathcal{R}^*$. Therefore, for the particular weight values $\mathbb{Q}^*$ and $\mathcal{R}^*$, the solution to Problem 3.2 also solves Problem 3.1. □

Corollary 3.3.2. *The solution to Problem 3.1 may be obtained by optimizing the objective (3.54) over $\mathbb{Q}$ and $\mathcal{R}$, with the resulting gain K given by (3.56), subject to the constraints (3.53) and (3.52).*

Proof. Let $\mathscr{F} : (\mathcal{R}, \mathbb{Q}) \mapsto K$ be the mapping from the LQ weights to the optimal LQ gains, which is obtained by evaluating the equations (3.56). By Theorem 3.3.1, for particular LQ weights $\mathbb{Q}^*$ and $\mathcal{R}^*$, the solution to Problem 3.2 also solves Problem 3.1. It follows that the gain K^* which solves Problem 3.1 is in the range of $\mathscr{F}$, and hence, if we replace

the decision variable K with $K = \mathscr{F}(\mathscr{R}, \mathbb{Q})$, then we can obtain the optimal gain ss $K^* = \mathscr{F}(\mathscr{R}^*, \mathbb{Q}^*)$. □

As a consequence of this theorem and its corollary, the optimization variable K for Problem 3.1, which is $5 \times N_p$ dimensional, may be replaced with the pair $\mathbb{Q}$ and $\mathscr{R}$, which is only $N_x(N_x+1)/2 + N_p$ dimensional (since $\mathbb{Q}$ is symmetric). Furthermore, for each guess of the new decision variables, the resulting control law enjoys the properties of optimal LQG solutions, such as smooth feedback gains and negligible corrections when feedback is not beneficial. For example, at low dynamic pressure, changes to the bank angle have a negligible effect on the dynamics. Thus, through an optimization which penalizes control actions against the trajectory response, bank angle corrections will not be commanded when the dynamic pressure is low.

3.3.4 Lateral Control

The lateral control logic sets the bank direction b_{dir} as a function of the crossrange error ε, which, in turn, is a function of the current vehicle state, the target position, and the estimated final time $t_{f,\text{est}}$. See Figure 3.2 and Chapter A for details on the downrange and crossrange calculations. In this chapter, we consider a simple deadband for lateral control, as in Refs. [38, 3], which depends on a user-specified maximum allowable crossrange $\varepsilon_{\max}(t, x)$. The deadband should therefore approximately contain the crossrange error to be bounded as

$$-\varepsilon_{\max}(t, x) \leq \varepsilon \leq +\varepsilon_{\max}(t, x). \tag{3.67}$$

At discrete update times, a new bank direction b_{dir}^{+} is determined as a function of the current bank direction, the crossrange error, and the current deadband value given by

$$b_{\text{dir}}^{+}(t, x, b_{\text{dir}}) = \begin{cases} +1, & \text{if } b_{\text{dir}} = -1 \text{ and } \varepsilon < -\varepsilon_{\max}(t, x), \\ -1, & \text{if } b_{\text{dir}} = +1 \text{ and } \varepsilon > +\varepsilon_{\max}(t, x), \\ b_{\text{dir}}, & \text{otherwise.} \end{cases} \tag{3.68}$$

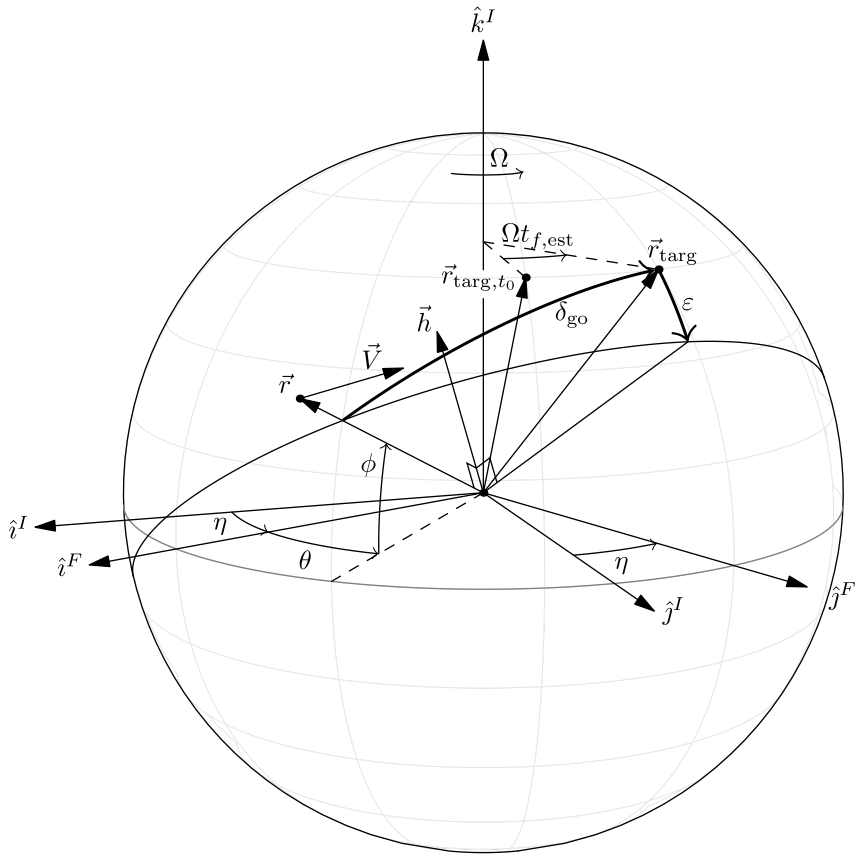

Figure 3.2: Downrange and crossrange definitions (frame definitions are given in appendix A)

3.3.5 Heading Alignment

As the vehicle slows down and approaches the target, bank angle modulation becomes less effective at controlling the downrange position [3]. Therefore, when the vehicle passes

some user-defined threshold, such as a minimum velocity, the guidance mode switches from range control to heading alignment. During the heading alignment segment in Apollo final phase guidance, the bank angle commands are given by the proportional feedback law

$$\sigma = K_{\mathrm{ha}} \tan^{-1}\left(\frac{\delta_{\mathrm{go}}}{\varepsilon}\right), \tag{3.69}$$

where K_{ha} is a user-defined heading alignment gain, and δ_{go} and ε are the downrange-to-go and crossrange angles [3], which are shown in Figure 3.2. The heading alignment law (3.69) is adopted for the proposed stochastic guidance, as the focus of this chapter is the range control phase.

3.4 Range Control with Final State Triggers

In the previous section, the trajectory was considered over a given time interval with a fixed final time. The guidance objective was therefore to steer the state — or, in the stochastic case, the state covariance — to a desired value at this fixed final time. In practice, however, entry trajectories are rarely terminated at a final time. Rather, trajectories are terminated by a condition on the vehicle state. The MSL entry guidance, for example, ended (by initializing the parachute deployment sequence) when the navigated vehicle velocity passed below a threshold [3]. More generally, any condition on the vehicle state, which we refer to as a state trigger, can mark the end of guided entry. Selection of the state trigger criteria can have a significant effect on the final state statistics, as has been demonstrated in Monte Carlo simulations for the Mars 2020 mission, in which switching from a velocity to a range trigger has been shown to significantly improve landing accuracy [9].

We are thus motivated to study the effect of the state trigger on the final state statistics. The following analysis is a generalization of the derivation of the final state weight developed in Ref. [38]. Formally, we define a state trigger by a half-plane in the state space described by the vector ν and the scalar β. The time that the vehicle hits the state trigger is

the stopping time

$$T = \inf\{t \geq t_0 : \nu^\intercal x(t) \leq \beta\}. \tag{3.70}$$

We assume that the nominal trajectory terminates at this stopping time, and thus

$$\nu^\intercal \bar{x}(t_f) = \beta. \tag{3.71}$$

Approximating to first order the state drift from the final time t_f to the stopping time T, we obtain

$$x(T) \approx x(t_f) + \hat{f}_f(T - t_f), \tag{3.72}$$

where $\hat{f}_f = f(\hat{x}(t_f), \hat{u}(t_f))$ is the nominal state derivative at the final time. Note that we neglect the diffusion term, since the effect of density variations during this short period is insignificant. Rearranging the terms in (3.72), and using the condition (3.71), we obtain

$$\nu^\intercal\big(x(T) - x(t_f)\big) = \nu^\intercal\big(\bar{x}(t_f) - x(t_f)\big) \approx \nu^\intercal \hat{f}_f(T - t_f), \tag{3.73}$$

which after simplification yields

$$T \approx t_f - \left(\frac{\nu^\intercal}{\nu^\intercal \hat{f}_f}\right)\tilde{x}(t_f) \tag{3.74}$$

The stopping time T is thus approximately Gaussian distributed with mean t_f and covariance $(\nu^\intercal \hat{f}_f)^{-2}\nu^\intercal P(t_f)\nu$.

Next, we substitute (3.74) into the state approximation (3.72) to obtain an approximate expression of the state at the stopping time as

$$x(T) \approx x(t_f) - \left(\frac{\hat{f}_f \nu^\intercal}{\nu^\intercal \hat{f}_f}\right)\tilde{x}(t_f) = \bar{x}(t_f) + \left(I - \frac{\hat{f}_f \nu^\intercal}{\nu^\intercal \hat{f}_f}\right)\tilde{x}(t_f) \tag{3.75}$$

Since this approximation is a linear function of the nominal final state and the final state

deviation, it follows that $\mathbb{E}\big(x(T)\big) \approx \bar{x}(t_f)$ and

$$\mathrm{Cov}\left(x(T)\right) \approx Z_f P(t_f) Z_f^\mathsf{T}, \quad Z_f = I - \frac{\hat{f}_f \nu^\mathsf{T}}{\nu^\mathsf{T} \hat{f}_f}. \tag{3.76}$$

3.4.1 Stochastic Range Control with a State Trigger

When using a state trigger, the entry guidance should aim to minimize the state errors at the trigger time rather than at the final time. The final state penalty in the range control cost (3.54) is accordingly modified to

$$\mathrm{Var}\left(a_{f,T}^\mathsf{T} \tilde{x}_\ell(T)\right) \approx \mathrm{Var}\left(a_{f,T}^\mathsf{T} Z_{\ell,f} \tilde{x}_\ell(t_f)\right), \tag{3.77}$$

$$Z_{\ell,f} = I - \frac{\hat{f}_{\ell,f} \nu^\mathsf{T}}{\nu^\mathsf{T} \hat{f}_{\ell,f}}, \quad \hat{f}_{\ell,f} = \begin{bmatrix} \hat{f}_{z_\ell} \\ \hat{f}_\rho \dot{\hat{s}} \end{bmatrix}, \tag{3.78}$$

where $\hat{f}_{z_\ell}$ and $\hat{f}_\rho$ are the longitudinal vehicle and density drift terms evaluated at the nominal final states. It follows that the effect of the state trigger can be included by setting the final state error weight a_f in (3.54) as a transformation of the desired weight $a_{f,T}$ on the states at the stopping time:

$$a_f = Z_{\ell,f}^\mathsf{T} a_{f,T} \tag{3.79}$$

3.5 Numerical Example

In this section, we apply both the proposed stochastic range control and the Apollo final phase range control methods for a simulated entry problem at Mars using bank angle control. Separate optimizations and Monte Carlo simulations are performed for both a fixed final time case and a velocity trigger case (as was done for MSL). Further comparison of different state trigger criteria is left for future work. For the simulation, Mars is assumed to be a sphere of uniformly distributed mass with gravitational parameter $\mu = 4.2828 \times 10^{13}$

m^3/s^2, rotating at a fixed rotation rate of $\Omega = 7.0882 \times 10^{-5}$ rad/s. The vehicle properties, which are based on MSL, are listed in Table 3.1 and the nominal entry conditions are listed in Table 3.2. The simulation initializes at entry interface (EI), which is the point where the vehicle radius passes through the radius of the edge of the atmosphere $r_{\mathrm{atm}} = 125$ km, and terminates at the end of heading alignment when the planet-relative velocity drops below 500 m/s. In the fixed final time scenario, the simulation terminates at the time when the nominal trajectory reaches 500 m/s. Sources of uncertainty included in the Monte Carlo simulation are listed in Table 3.3. The heading alignment phase begins at 1.1 km/s, during which the bank angle commands are given by the heading alignment law (3.69) with the gain $K_{\mathrm{ha}} = 50$. Bank angles commanded during the heading alignment phase are saturated to be within $\pm 45^\circ$ for velocities between 1.1 km/s and 0.9 km/s, and within $\pm 35^\circ$ otherwise. We do not consider navigation uncertainty as our focus is guidance performance, and thus the controller has access to the exact vehicle state and atmospheric density for the purposes of feedback.

The target landing site is at the surface radius with position coordinates

$$\theta_{\mathrm{targ}} = 137^\circ, \quad \phi_{\mathrm{targ}} = 0^\circ, \tag{3.80}$$

and the nominal vehicle position at EI was set to

$$\hat{\theta}_0 = 125.973^\circ, \quad \hat{\phi}_0 = 0^\circ, \tag{3.81}$$

so that the simulation would nominally end with the vehicle 10 km uprange of the target point when the other initial vehicle states are as in Table 3.2.

Both the nominal atmospheric density and the density variations are given as functions of altitude by MarsGRAM [68]; resulting density variation samples are shown in Figure 3.3. The assumed density variation process is defined by setting $\lambda(s) = 2/H(s)$ and $\varphi(s)$ as in Remark 2 for a desired variance profile $\zeta_d(s)$ computed from the MarsGRAM

samples. Note that this density variation process model is only used for the purposes of designing the feedback gains, and that when simulating the entry dynamics only the Mars-GRAM density samples are used. Additionally, the trimmed angle of attack was uniformly dispersed on the interval $[-16.5^\circ, -14.5^\circ]$, which, in turn, affected the L/D and the ballistic coefficient.

The bank angle commands are recomputed each second, and the bank angle remains constant until the next command is issued. Increments to the bank angle are constrained by a $\mathcal{L} = 15$ deg/s bank rate limit, and thus the bank angle σ to be flown is a function of the new bank angle command σ_{cmd}, the previous bank angle command $\sigma_{\mathrm{cmd,prev}}$, the rate limit $\mathcal{L}$, and the elapsed time Δt from the time when the previous bank command was issued:

$$\sigma = \begin{cases} \sigma_{\mathrm{cmd,prev}} + \mathcal{L}\Delta t, & \text{if } \sigma_{\mathrm{cmd}} - \sigma_{\mathrm{cmd,prev}} \geq +\mathcal{L}\Delta t, \\ \sigma_{\mathrm{cmd,prev}} - \mathcal{L}\Delta t, & \text{if } \sigma_{\mathrm{cmd,prev}} - \sigma_{\mathrm{cmd}} \leq -\mathcal{L}\Delta t, \\ \sigma_{\mathrm{cmd}}, & \text{otherwise.} \end{cases} \tag{3.82}$$

The nominal trajectory was obtained by integrating the equations of motion (3.1) with the nominal density profile and the longitudinal control (cosine of the bank angle) given as a function of velocity. In particular, the nominal bank angle cosine is equal to $\cos 70^\circ$ for velocities above 5.5 km/s, $\cos 45^\circ$ for velocities below 2.5 km/s, and a linear ramp from $\cos 70^\circ$ to $\cos 45^\circ$ for velocities between 5.5 km/s and 2.5 km/s. The sign of each new bank angle command is determined by the deadband logic (3.68) with the time-dependent deadband shown in Figure 3.4.

For both the Apollo and the stochastic range control methods, the nominal trajectory extends from EI to the end of the heading alignment phase, but the effect of control inputs is set to zero during the latter. Considering the trajectory extended through the heading alignment phase allows for the range control guidance to target conditions at the end of heading alignment, rather than only being able to target conditions at the start of heading

Table 3.1: Vehicle properties

Property	Value	Unit
Mass	3200	kg
Reference area	$\pi 4.5^2/4$	m^2
Trimmed angle of attack	-15.5	deg
L/D	0.24	
Ballistic coefficient	135	kg/m^2

Table 3.2: Initial states

State	Nominal	3σ
Altitude	125 km	0
Velocity	5.8 km/s	20 m/s
Flight path angle	-15.5°	0.5°
Heading azimuth	90.05°	0.01°
Downrange	0	5 km
Crossrange	0.57 km	0.5 km

alignment. The nominal longitudinal trajectories are obtained from the full nominal trajectory, but bank reversals are not included in the nominal control input; that is, the nominal longitudinal state $\hat{x}_\ell(t)$ at any time t is computed as a function of the full nominal state $\hat{x}(t)$, whereas the nominal bank angle is only provided as the nominal bank angle cosine, as in the control law (3.32). The Apollo final phase law is parameterized as a function of velocity, while the stochastic law is parameterized as a function of time. The Apollo overcontrol gain is to $K_{\rm oc} = 5$, and the targeting calculations aim for the target in inertial space at the current time (i.e., $t_{f,\rm est}$ in (A.7) is set to equal t).

Table 3.3: Source of uncertainty included in the Monte Carlo

Source of uncertainty	Method
Vehicle state at EI	Sampled from Gaussian
Atmospheric density	MarsGRAM
Vehicle aerodynamics	Uniform distributed trim-α

3.5.1 Fixed Final Time

First, we consider the range control problem with the final time fixed to be the final time of the nominal trajectory. For the stochastic range control, the weights in the cost (3.54) are set as

$$a_f^\intercal = \begin{bmatrix} 0 & 0 & 0 & 10^6 & 0 \end{bmatrix}, \qquad \mathcal{R}_k = 10^{-2}. \tag{3.83}$$

The 99.73%-ile of the closed-loop controls are constrained to lie within either $[-1, +1]$ (so that $\cos^{-1}$ is defined) or ± 0.45 from the nominal value, whichever results in a smaller deviation from the nominal. The limit ± 0.45 was chosen by trial and error to balance range control against crossrange performance. This results in the control deviation limit given by

$$\Delta_k^u = \min\{0.45,\ 1 - \cos\hat{\sigma}(t_k^p),\ \cos\hat{\sigma}(t_k^p) + 1\}, \tag{3.84}$$

with $p_k^u = 1 - 0.9973$ (3σ) for every step k. The final altitude and flight path angles are constrained to lie within ± 2 km and $\pm 1.55^\circ$ respectively with probability at least $1 - 0.9973$ (3σ), which results in the constraint parameters

$$d_1 = \begin{bmatrix} 1 & 0 & 0 & 0 & 0 \end{bmatrix}^\intercal, \qquad \Delta_1^x = 2\,\mathrm{km}, \tag{3.85}$$

$$d_2 = \begin{bmatrix} 0 & 0 & 1 & 0 & 0 \end{bmatrix}^\intercal, \qquad \Delta_2^x = 1.55^\circ, \tag{3.86}$$

and $p_1^x = p_2^x = 1 - 0.9973$. Per Theorem 3.3.1, the values for $\mathfrak{Q}$ and $\mathfrak{R}$ were found by minimizing the objective (3.54), while satisfying the control and final state constraints, using MATLAB's fmincon function.

Performance of both the Apollo and the stochastic entry guidance methods were evaluated by the linear covariance (LC) approximation as in (3.43) and by Monte Carlo simulation. The control input variances, based on the LC model, are shown in Figure 3.6; while the input variance is different for the final time and the velocity trigger scenarios, both Apollo final phase solutions are similar and so only the final time solution is plot-

ted. Note that, per the control chance constraint (3.53), the $\pm 3\sigma$ bounds for stochastic controllers remain within $[-1, +1]$, whereas the bounds for the Apollo controller at times leave this interval (which, in turn, degrades the LC approximation as it does not include saturation). Interestingly, since the stochastic controller is derived through an optimization which takes dynamic pressure into account, the stochastic controller does not command bank angle corrections immediately following EI when the dynamic pressure is small. Instead, the stochastic controllers both command more aggressive corrections than the Apollo law following the increase in dynamic pressure.

Closed-loop sample trajectories with both $\pm 3\sigma$ bounds computed from the samples and from the LC approximation are shown in Figure 3.8; note that while only 20 sample trajectories are shown, the 3σ bounds are computed from all 1,000 sample trajectories. Bank angle histories are shown in Figure 3.9, and final state errors are listed in Table 3.4. The stochastic controller makes aggressive corrective controls following peak dynamic pressure which result in large altitude and flight path angle deviations, which is required in order to affect drag and thus range. Indeed, when using the stochastic controller, the range error begins to decrease following the increase in flight path angle error around 100 s after EI. Furthermore, there is a trade-off between final altitude error and final range error, which is demonstrated by the final altitude with the stochastic controller error equaling the maximum allowed value of ± 2 km with 3σ confidence. While for most of the states plotted in Figure 3.8 the LC $\pm 3\sigma$ approximation is close to the $\pm 3\sigma$ bounds computed from Monte Carlo, the LC approximation deviates most strongly from the Monte Carlo results for the flight path angle. There are several possible causes for this approximation error: the exclusion of bank reversals from the LC approximation; the effects of closed-loop controls during the heading alignment phase, which are not included in the LC model; the LC approximation does not include the uniformly distributed error in the trimmed angle of attack; or statistical errors due to the finite number of Monte Carlo trials.

As one would expect, the increased intensity of longitudinal control corrections with the

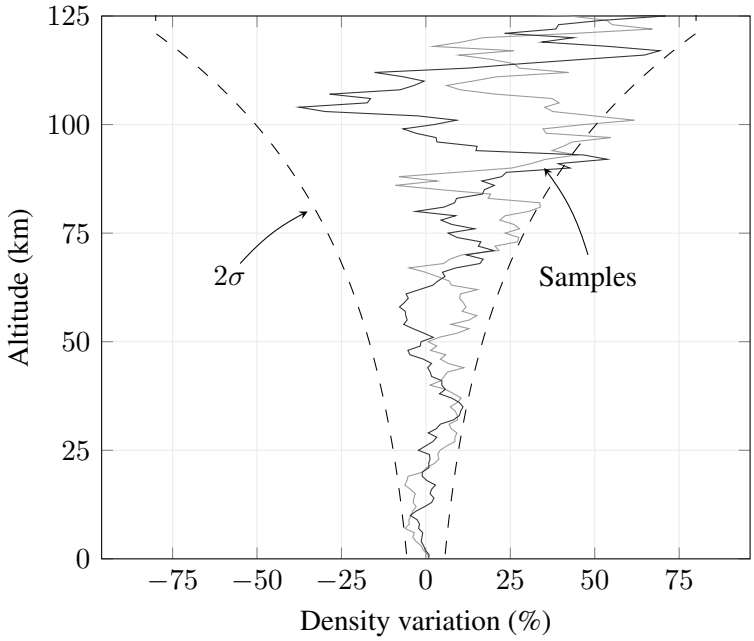

Figure 3.3: MarsGRAM density variation samples

stochastic controller comes with an increase in lateral dispersions. The bank reversal logic together with the heading alignment phase successfully null out the additional crossrange error by the end of the heading alignment phase.

3.5.2 Velocity Trigger

Suppose now that the entry trajectories end when reaching a planet-relative velocity of 500 m/s. This velocity trigger is described, as in (3.70), by the values

$$\nu = \begin{bmatrix} 0 & 1 & 0 & 0 & 0 \end{bmatrix}^{\intercal}, \qquad \beta = 500\,\mathrm{m/s}. \tag{3.87}$$

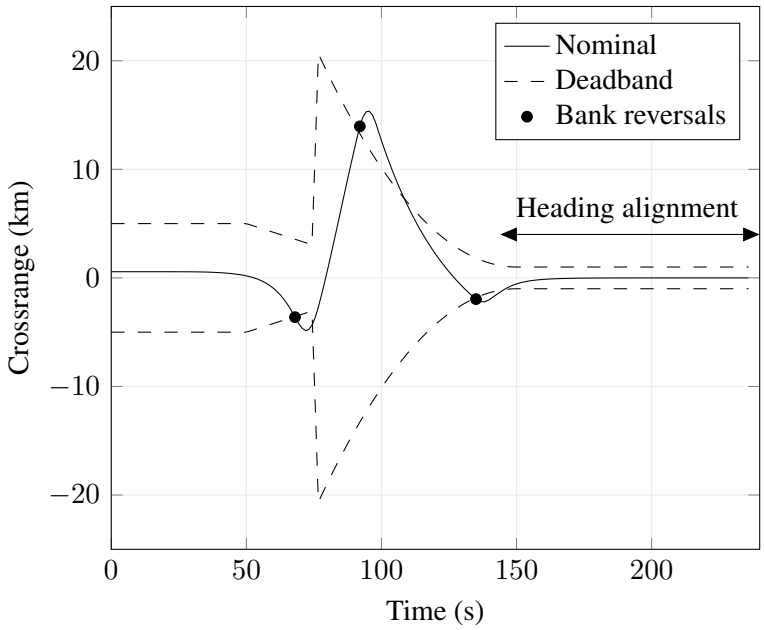

Figure 3.4: Nominal crossrange trajectory with bank reversals

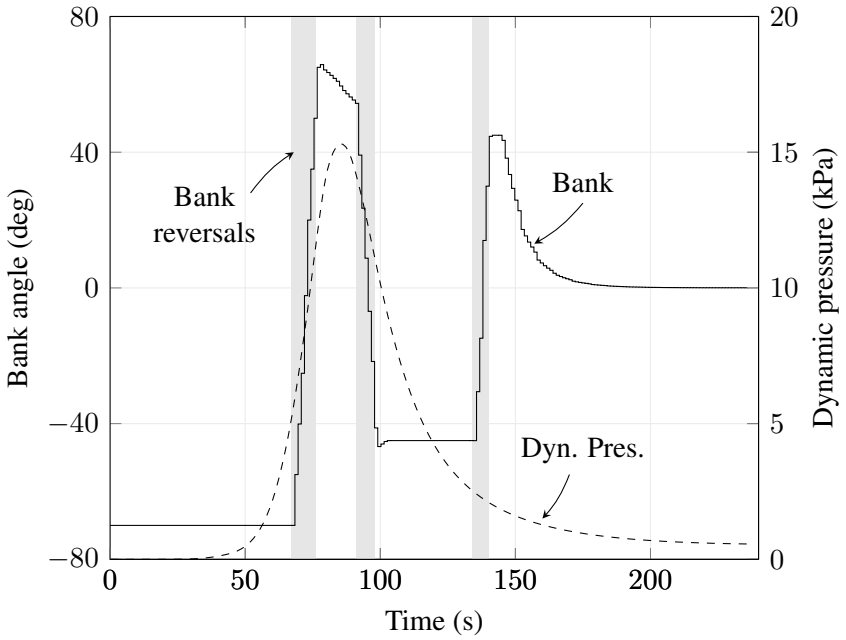

Figure 3.5: Timing of bank reversals with dynamic pressure

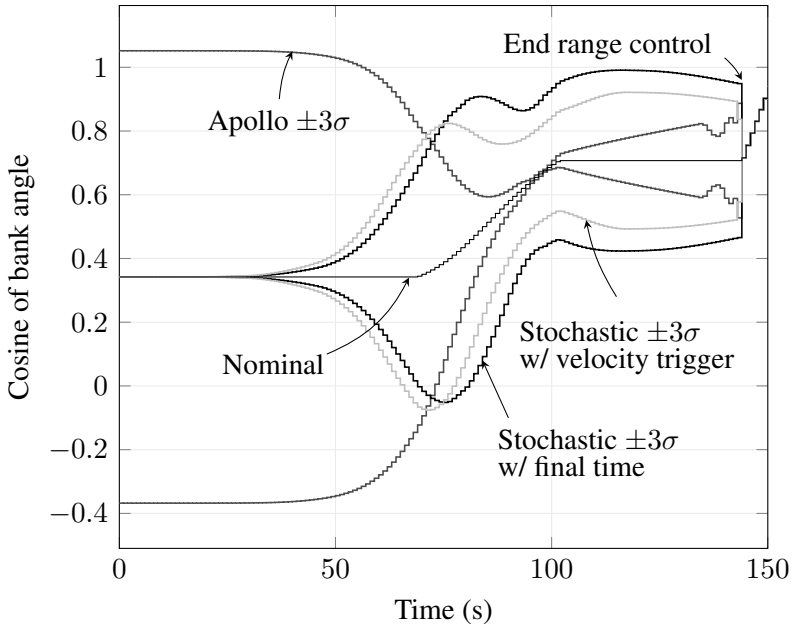

Figure 3.6: Longitudinal control input variance during range control computed via the linear covariance approximation

In units of m/kg/s, the stopping time transform matrix (3.78) is given by

$$Z_f = \begin{bmatrix} 1 & -34.95 & 0 & 0 & 0 \\ 0 & 0 & 0 & 0 & 0 \\ 0 & -0.0015 & 1 & 0 & 0 \\ 0 & 144.75 & 0 & 1 & 0 \\ 0 & 1.5\text{e}{-5} & 0 & 0 & 1 \end{bmatrix}. \tag{3.88}$$

In order to minimize the range control cost (3.54), with the same range-error penalty (3.83) from the fixed time example, except applied to the state error at the time T when the velocity reaches 500 m/s, we apply the transformation (3.79) to obtain the new final state error weight

$$a_f^{\mathsf{T}} = \begin{bmatrix} 0 & 0 & 0 & 10^6 & 0 \end{bmatrix} Z_{\ell,f}. \tag{3.89}$$

The Apollo final phase guidance can similarly be improved by applying the velocity-trigger transformation to the final range error weight, which is given by the final state adjoint value

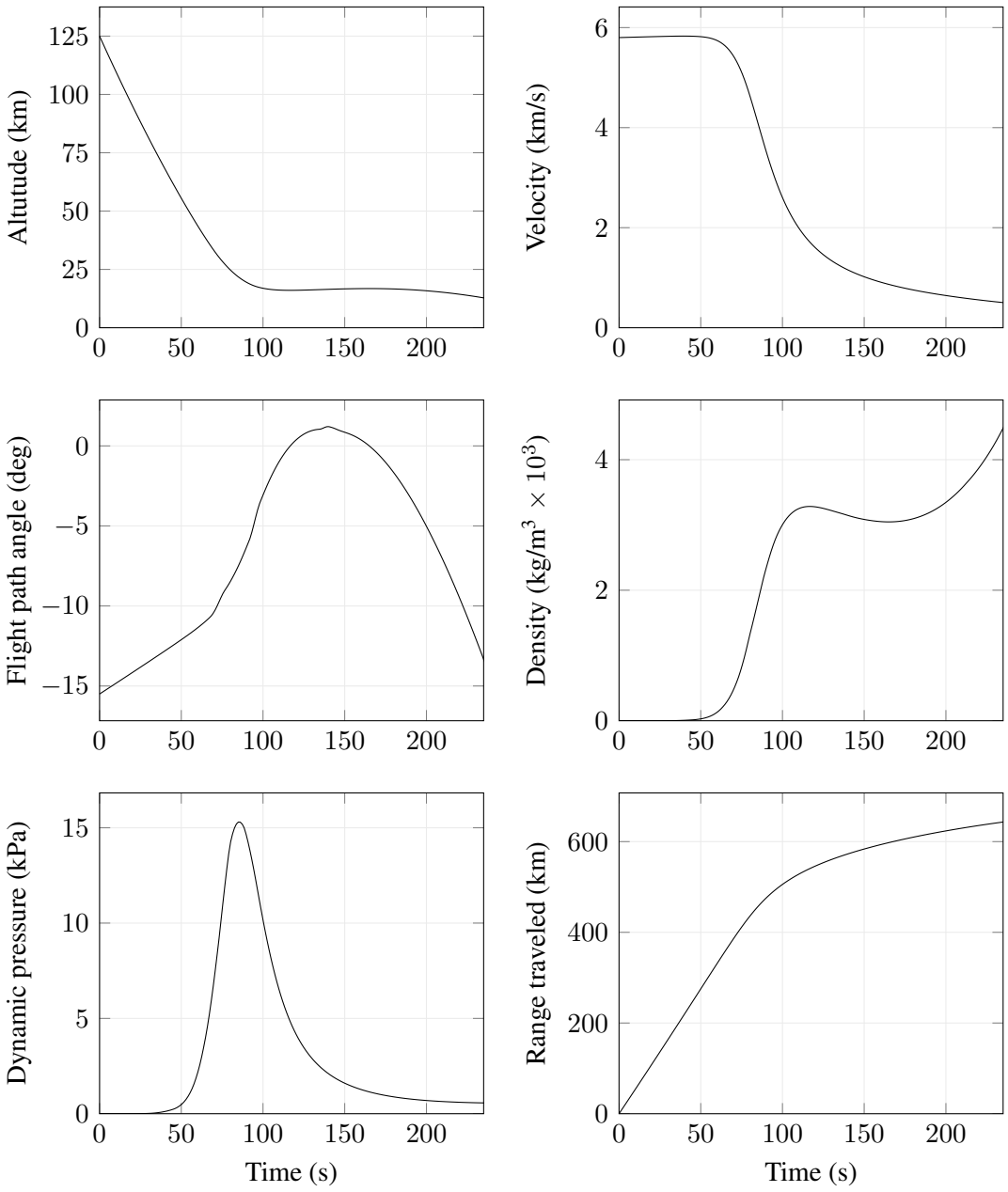

Figure 3.7: Nominal entry trajectory

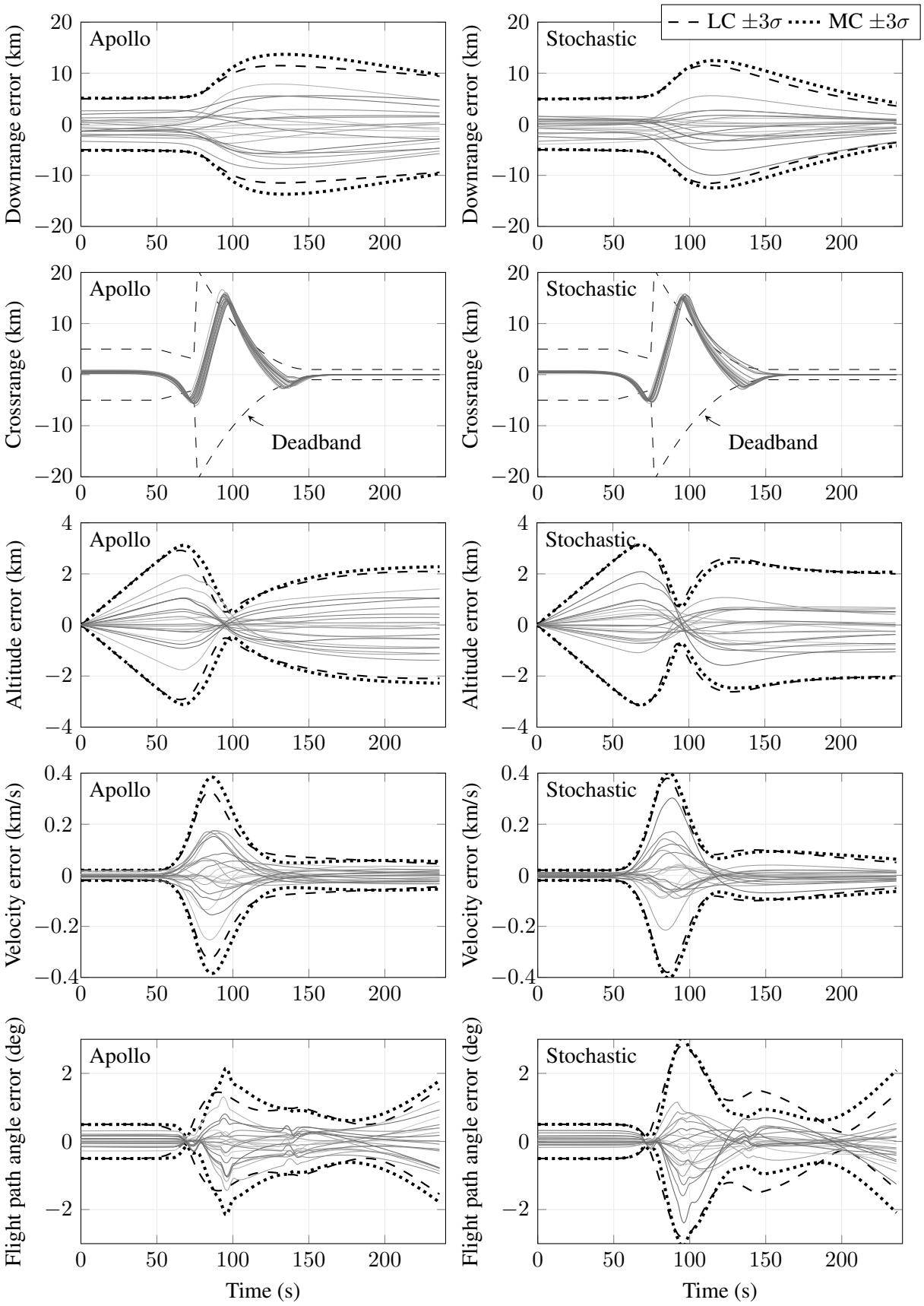

Figure 3.8: Monte Carlo trajectories with a fixed final time

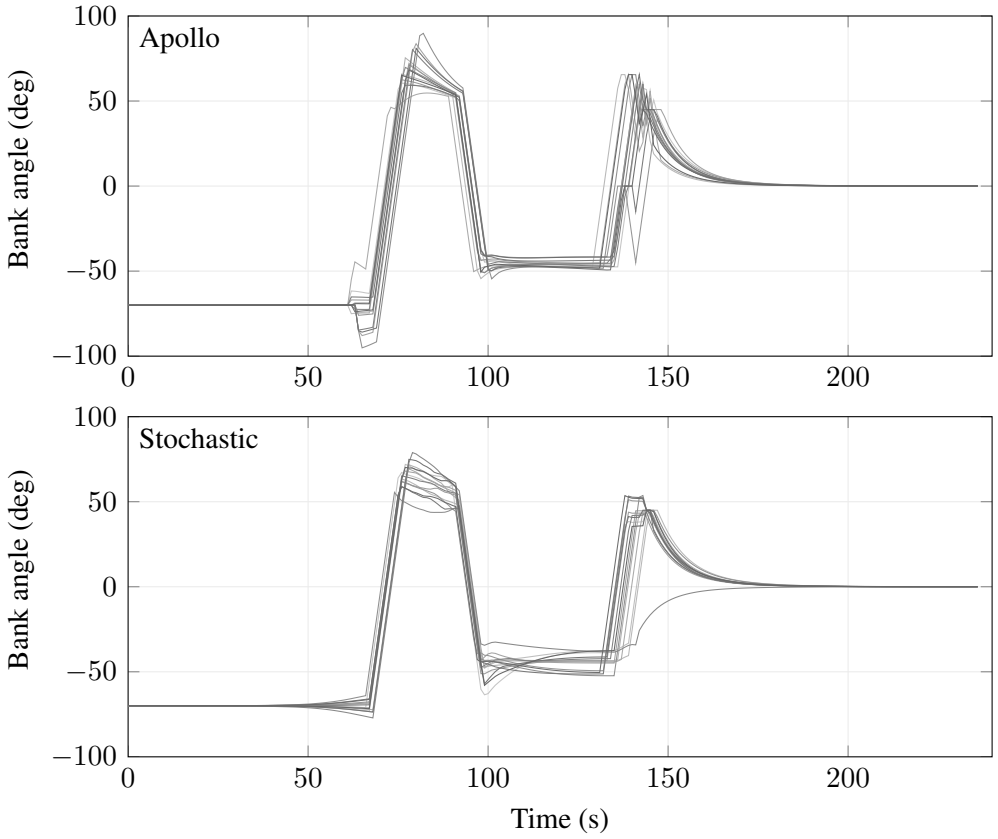

Figure 3.9: Monte Carlo control trajectories with a fixed final time

in (3.48). We thus set

$$\vartheta_f = \begin{bmatrix} 0 & 0 & 0 & 1 & 0 \end{bmatrix} Z_{\ell,f}. \tag{3.90}$$

Sample Monte Carlo trajectories which use the velocity trigger are shown in Figures 3.10 and 3.11, where the improvement in range targeting performance with the stochastic controller is apparent. Final state statistics derived from the full Monte Carlo simulation are listed in Table 3.4. Using the velocity trigger decreased the range errors, in addition to the obvious reduction in velocity error, for both the Apollo and stochastic controllers. Furthermore, when using the velocity trigger, the lower 1%-ile and upper 99%-ile final range errors were approximately halved when using the stochastic controller in compared to the Apollo controller.

The range-velocity covariances at the final time, which are shown in Figure 3.12 (as

Table 3.4: Final state error 1st and 99th percentiles from 1,000 Monte Carlo trials

	Apollo		Stochastic	
Trigger	Time	Velocity	Time	Velocity
Downrange (km)	-8.36 / 6.53	-3.58 / 3.04	-4.64 / 2.56	-1.96 / 1.19
Altitude (km)	-1.59 / 1.99	-0.92 / 0.92	-1.74 / 1.79	-0.87 / 0.82
Velocity (m/s)	-39.54 / 42.89	0 / 0	-54.59 / 51.97	0 / 0
Flight path angle (deg)	-1.28 / 1.55	-2.37 / 2.13	-1.46 / 2.15	-2.07 / 2.05

computed by LC; ellipses contain 99.73% probability), provide intuition behind the differences between the final time and the velocity trigger conditions. While the Apollo final phase guidance naturally results in the range and velocity being negatively correlated — with setting the final adjoint state per the velocity trigger further increasing this negative correlation — there is a clear difference between the final time and velocity trigger stochastic guidance solutions. For the final time case, the guidance is optimized to simply minimize the final range error, which is an objective not dependent on any final state correlations; thus, the range variance is decreased apparently at the expense of range-velocity correlation. On the other hand, when including the effect of the velocity trigger in the optimization, the transformation (3.79) induces a penalty into the range cost, which depends on the final covariances. Intuitively, we expect the velocity trigger cost to induce a strong correlation between velocity and range, since the conditional variance of range, provided the velocity will be fixed, approaches zero as the absolute value of the velocity-range correlation coefficient approaches one. In other words, a strong correlation of two random variables implies that knowing the value of one variable strongly suggests the value of the other; thus, the variance for the final range error decreases when the final velocity is fixed per the trigger condition.

3.6 Conclusion

In this chapter, a stochastic process model for atmospheric entry in a randomly perturbed atmosphere was derived and then applied to develop a novel range control feedback law.

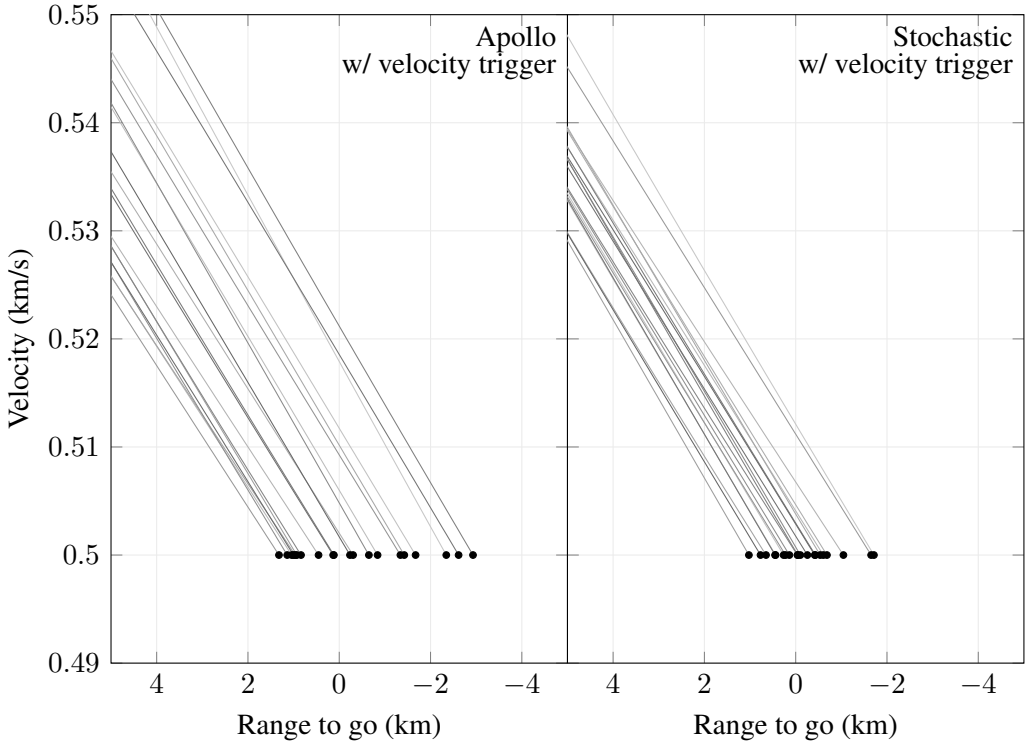

Figure 3.10: Sample trajectories terminating at the velocity trigger

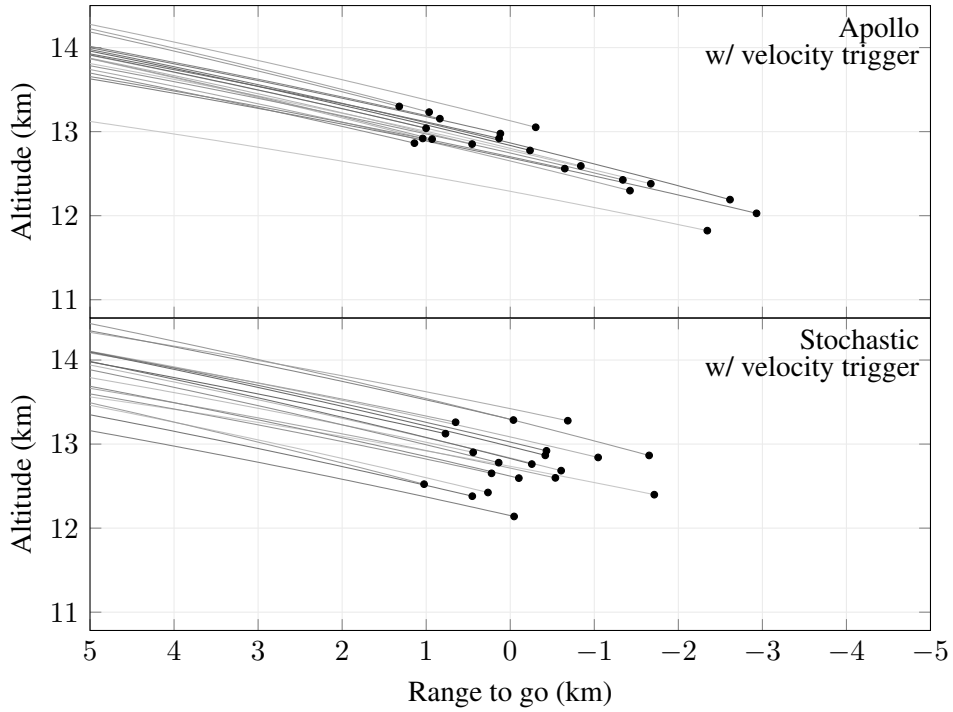

Figure 3.11: Sample trajectories with endpoints at the velocity trigger

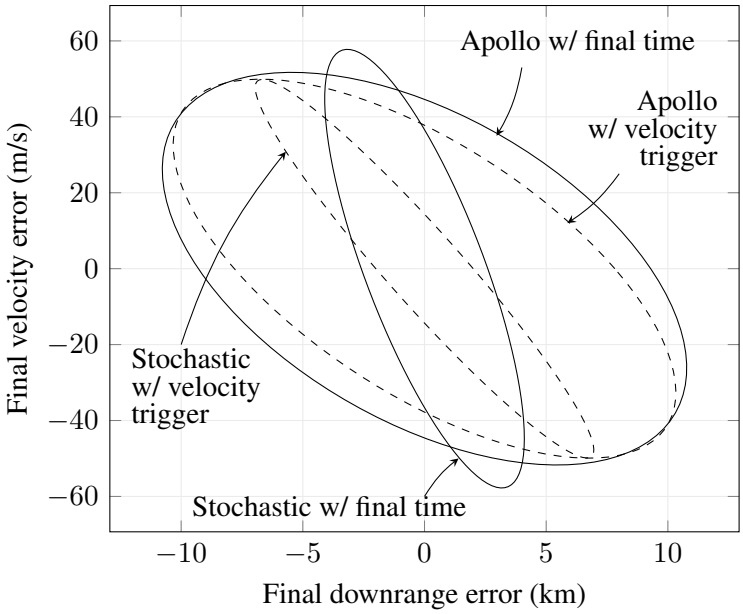

Figure 3.12: Range-velocity covariance at the final time

In contrast to the many existing models that include only parametric uncertainty, such as the scale height of an exponential atmosphere being random, the developed stochastic process model considers the atmospheric density uncertainty as a random function of altitude, similar to the GRAM dispersion models. The effect of altitude-dependent density perturbations on the vehicle trajectory was obtained by setting the diffusion coefficient in the SDE model to be a function of the vehicle sink rate — the faster the vehicle descends through altitude dependent perturbations, the more intense the time dependent perturbations. In future works, this model could enable rapid onboard uncertainty quantification to support decision making during entry.

The proposed guidance algorithm is implemented as a linear feedback law using table lookup, in the same manner as the flight proven Apollo final phase guidance algorithm; the difference being that the feedback gains in the proposed guidance law are derived from an optimization over the feedback gains with respect to the covariance evolution of the closed-loop system. Furthermore, an analytical approximation for the effect of a state triggered termination of the entry trajectory was developed and applied to the proposed guidance algorithm. In a Monte Carlo simulation of an MSL-like entry scenario at Mars,

the proposed stochastic entry guidance results in the 1%-ile and 99%-ile of the final range errors being approximately halved when compared to the Apollo final phase guidance.

CHAPTER 4
COVARIANCE STEERING THEORY

The material in this chapter is based on Refs. [70, 91, 88].

4.1 Introduction

In the previous chapters, we studied both powered descent and atmospheric entry as stochastic processes. The state feedback gain appeared as the control input for the covariance dynamics, leading to the idea of steering the covariance by optimizing over the feedback gains. For both the powered descent and atmospheric entry problems, however, the optimization over the feedback gains was performed independently from the optimization over the nominal controls. This chapter considers the more general case of jointly optimizing over the nominal control the feedback gains.

Departing from the application-specific analysis presented in the previous chapters, the focus of this chapter is on general stochastic systems with additive Gaussian disturbances, and with chance constraints (i.e., limits on the probability that a constraint is violated) on both the state and the control.

Organization

The organization of this chapter is as follows. In Section 4.2, the chance-constrained covariance steering (CS) problem, for linear discrete time systems, is introduced, and the solution is provided by convex programming. This section includes a novel chance constraint on the control magnitude, which is a necessary constraint for modeling spacecraft thrust inputs [88]. The existing CS theory is then extended in Section 4.3 to the output-feedback case, wherein the state is only accessible via noisy measurements [91]. CS theory is further extended to nonlinear systems in Section 4.4 by developing a successive linearization

algorithm, which we refer to as iterative CS (iCS) [70, 100]. Finally, in Section 4.5, we apply the nonlinear CS theory and the iCS algorithm to the problem of low-thrust spacecraft guidance for an Earth-to-Mars transfer [88].

4.2 Covariance Steering with Full State Feedback

In this section, we review the existing results on chance-constrained covariance steering theory for linear discrete-time systems with additive Gaussian disturbances [71, 76]. In addition to the existing theory, this section includes a novel control magnitude chance constraint that was introduced in Ref. [88].

4.2.1 Problem Definition

Consider the stochastic linear discrete-time system given by

$$x_{k+1} = A_k x_k + B_k u_k + G_k w_k, \tag{4.1}$$

for $k = 0, 1, \ldots, N-1$, where $x_k \in \mathbb{R}^n$ and $u_k \in \mathbb{R}^m$ are the state and control, and $A_k \in \mathbb{R}^{n\times n}$, $B_k \in \mathbb{R}^{n\times m}$, and $G_k \in \mathbb{R}^{n\times n}$ are system matrices. Increments of the disturbance process $w_k \in \mathbb{R}^n$ are i.i.d. standard Gaussian random vectors. At the initial step, the state is assumed to be a random vector Gaussian distributed as

$$x_0 \sim \mathcal{N}(\bar{x}_0, P_0), \tag{4.2}$$

where the mean vector $\bar{x}_0$ and positive semi-define covariance matrix P_0 are both fixed and known. The initial state is assumed to be independent from the disturbance process.

The state and control processes are constrained to remain in the convex polytopes $\mathcal{R}_x$

and $\mathcal{R}_u$, which are given by

$$\mathcal{R}_x = \bigcap_{j=1}^{N_x} \{x : a_j^\mathsf{T} x \leq \alpha_j\} \subset \mathbb{R}^n, \tag{4.3}$$

$$\mathcal{R}_u = \bigcap_{j=1}^{N_u} \{u : b_j^\mathsf{T} u \leq \beta_j\} \subset \mathbb{R}^m, \tag{4.4}$$

in terms of the vectors $(a_j \in \mathbb{R}^n : j = 1, \ldots, N_x)$ and scalars $(\alpha_j \in \mathbb{R} : j = 1, \ldots, N_x)$ that define N_x half-planes in $\mathbb{R}^n$, and the vectors $(b_j \in \mathbb{R}^m : j = 1, \ldots, N_u)$ and scalars $(\beta_j \in \mathbb{R} : j = 1, \ldots, N_u)$ that define N_u half-planes in $\mathbb{R}^m$; see Figure 4.1. The maximum probability that the state and the control leave the regions $\mathcal{R}_x$ and $\mathcal{R}_u$ is constrained by

$$\mathbb{P}(x_k \notin \mathcal{R}_x) \leq p_{\text{fail}}^x, \quad k = 1, 2, \ldots, N, \tag{4.5}$$

$$\mathbb{P}(u_k \notin \mathcal{R}_u) \leq p_{\text{fail}}^u, \quad k = 0, 1, \ldots, N-1, \tag{4.6}$$

where $p_{\text{fail}}^x \in (0, 0.5)$ and $p_{\text{fail}}^u \in (0, 0.5)$ are prescribed maximum probabilities of constraint violation. These constraints are referred to as *chance constraints*.

The control is further constrained in Euclidean magnitude by

$$\mathbb{P}(\|u_k\| > \rho) \leq p_{\text{fail}}^{\|u\|}, \quad k = 0, 1, \ldots, N-1, \tag{4.7}$$

where $\rho > 0$ is the maximum control magnitude and $p_{\text{fail}}^{\|u\|} \in (0, 0.5)$ is a prescribed maximum probability of constraint violation. This constraint is useful for modeling systems for which the control input is a directed force with a limited magnitude, such as a gimbaled rocket engine or helicopter rotor.

We require that the mean and the covariance of the state satisfy the terminal constraints

$$\mathbb{E}(x_N) = \bar{x}_f, \tag{4.8a}$$

$$\mathrm{Cov}(x_N) \leq P_f, \tag{4.8b}$$

where the final state mean $\bar{x}_f$ is a given vector and the maximum final state covariance P_f is a given positive-definite matrix.

The control is assumed to follow the state history feedback law

$$u_k = \sum_{i=0}^{k} K_{k,i}\tilde{x}_i + v_k, \tag{4.9}$$

where $\tilde{x}_i = x_i - \bar{x}_i$ is the state deviation from its mean, $K_{k,i} \in \mathbb{R}^{m\times n}$ are feedback gains, and $v_k \in \mathbb{R}^m$ are feedforward controls. While one would expect the feedback law to only depend the current state, the state history feedback law results in a convex formulation of the chance-constrained control problem [76, 71].

Our objective is the find the feedback control law, which is parameterized by the gain matrices $(K_{k,i})$ and the feed-forward controls (v_k), that minimizes the cost function

$$J(K_{k,i}, v_k) = \mathbb{E}\left(\sum_{k=0}^{N-1}(x_k - x_k^d)^\intercal Q_k(x_k - x_k^d) + \tilde{u}_k^\intercal R_k \tilde{u}_k\right) + \sum_{k=0}^{N-1} \bar{u}_k^\intercal \bar{R}_k \bar{u}_k + \eta\|\bar{u}_k\| \tag{4.10}$$

for given state and control weight matrices $Q_k \geq 0$ and $R_k, \bar{R}_k \geq 0$, scalar weight $\eta \geq 0$, and where x_k^d is a desired state trajectory. The term $\tilde{u}_k^\intercal R_k \tilde{u}_k$ penalizes the control variance, since $\tilde{u}_k^\intercal R_k \tilde{u}_k = \mathrm{tr}\, R_k \,\mathrm{Cov}(u_k)$, and the terms $\bar{u}_k^\intercal \bar{R}_k \bar{u}_k$ and $\eta\|\bar{u}_k\|$ penalize the control mean. The resulting stochastic optimal control problem is summarized as follows.

Problem 4.1. *Find the feedback gains $(K_{k,i})$ and the feedforward controls (v_k) for the control law (4.9) that minimize the cost (4.10), subject to the dynamics (4.1), the state chance constraints (4.5), the control chance constraints (4.6), (4.7), and the final state distribution constraints (4.8).*

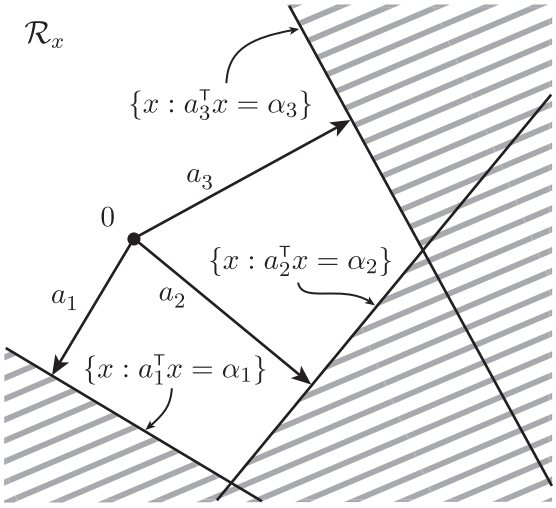

Figure 4.1: State chance-constrained region $\mathcal{R}_x$

Relaxation of the Polytope Chance Constraints

Before attempting to solve Problem 4.1, we consider the following conservative relaxation of the state and control polytopic chance constraints (4.5) and (4.6) given by the conditions

$$\sum_{j=1}^{N_x} p_j^x \leq p_{\text{fail}}^x, \quad \mathbb{P}(a_j^\mathsf{T} x_k > \alpha_j) \leq p_j^x, \quad \forall (k,j) \in \mathcal{X}, \tag{4.11}$$

$$\sum_{j=1}^{N_u} p_j^u \leq p_{\text{fail}}^u, \quad \mathbb{P}(b_j^\mathsf{T} u_k > \beta_j) \leq p_j^u, \quad \forall (k,j) \in \mathcal{U}, \tag{4.12}$$

where $\mathcal{X}$ and $\mathcal{U}$ are index sets given by

$$\mathcal{X} = \{1, \ldots, N\} \times \{1, \ldots, N_x\}, \tag{4.13}$$

$$\mathcal{U} = \{0, \ldots, N-1\} \times \{1, \ldots, N_u\}. \tag{4.14}$$

These constraints represent a decomposition of the original constraints (4.5) and (4.6) into independent half-plane constraints, which we expect to be a conservative approximation due to the subadditivity of probabilities. Indeed, it has been shown in [84] that if (4.11) and (4.12) hold, then the chance constraints (4.5) and (4.6) are satisfied.

4.2.2 Solution by Convex Programming

The following analysis in this subsection is adapted from Refs. [71, 76, 91]. The novel convex formulation of the maximum control magnitude constraint will be treated in the following subsection.

Block-Matrix Formulation

The state process (4.1) may be equivalently written in block-matrix notation as

$$\begin{bmatrix} x_0 \\ x_1 \\ x_2 \\ \vdots \end{bmatrix} = \begin{bmatrix} I \\ A_0 \\ A_1A_0 \\ \vdots \end{bmatrix} x_0 + \begin{bmatrix} 0 & 0 & \\ B_0 & 0 & \\ A_1B_0 & B_1 & \\ & & \ddots \end{bmatrix} \begin{bmatrix} u_0 \\ u_1 \\ \vdots \end{bmatrix} + \begin{bmatrix} 0 & 0 & \\ G_0 & 0 & \\ A_1G_0 & G_1 & \\ & & \ddots \end{bmatrix} \begin{bmatrix} w_0 \\ w_1 \\ \vdots \end{bmatrix}. \quad (4.15)$$

Let $X \in \mathbb{R}^{(N+1)n}$ be a column vector constructed by stacking the states x_k for $k = 0, 1, \ldots, N$, and, similarly, let $U \in \mathbb{R}^{Nm}$ and $W \in \mathbb{R}^{Nn}$ be the column vectors constructed by stacking the controls u_k and disturbances w_k for $k = 0, 1, \ldots, N-1$. Formally, we have that the column vector X is isomorphic to the sequence (x_k), which we denote by $(x_k) \cong X$ (similarly, $(u_k) \cong U$, $(w_k) \cong W$). For appropriately constructed block matrices $\boldsymbol{A}$, $\boldsymbol{B}$, and $\boldsymbol{G}$ as in (4.15), the state process can be written as the linear matrix equation

$$X = \boldsymbol{A}x_0 + \boldsymbol{B}U + \boldsymbol{G}W. \quad (4.16)$$

See Refs. [71, 114, 76] for details on this construction. Furthermore, let

$$\bar{X} = \mathbb{E}(X), \qquad \tilde{X} = X - \bar{X}, \qquad \bar{U} = \mathbb{E}(U), \qquad \tilde{U} = U - \bar{U}. \quad (4.17)$$

Let $V \in \mathbb{R}^{Nm} \cong (v_k)$ be column a vector defined as U, and let

$$\boldsymbol{K} = \begin{bmatrix} K_{0,0} & 0 & 0 & \cdots & 0 \\ K_{1,0} & K_{1,1} & \ddots & \cdots & 0 \\ \vdots & \vdots & \ddots & 0 & 0 \\ K_{N-1,0} & K_{N-1,1} & \cdots & K_{N-1,N-1} & 0 \end{bmatrix} \in \mathbb{R}^{Nm \times (N+1)n}. \tag{4.18}$$

We may then write the control process as the matrix equation

$$U = \boldsymbol{K}\tilde{X} + V. \tag{4.19}$$

Substituting the control process (4.19) into the state equation (4.16), we obtain the closed-loop state process

$$X = \boldsymbol{A}x_0 + \boldsymbol{B}\boldsymbol{K}\tilde{X} + \boldsymbol{B}V + \boldsymbol{G}W. \tag{4.20}$$

Solving for $\bar{X}$ and $\tilde{X}$ from (4.20) yields the state mean and state deviation processes

$$\bar{X} = \boldsymbol{A}\bar{x}_0 + \boldsymbol{B}V, \tag{4.21}$$

$$\tilde{X} = (I - BK)^{-1}(\boldsymbol{A}\tilde{x}_0 + \boldsymbol{G}W). \tag{4.22}$$

In this formulation, the decision variable $\boldsymbol{K}$ is inside of an inverse, which causes the optimization problem to be nonconvex. Following [114], we define the new decision variable $\boldsymbol{L} \in \mathbb{R}^{Nm \times (N+1)n}$ by

$$\boldsymbol{L} = \boldsymbol{K}(I - \boldsymbol{B}\boldsymbol{K})^{-1}. \tag{4.23}$$

Since $\boldsymbol{K}$ is block lower-triangular and $\boldsymbol{B}$ is strictly block lower-triangular, the matrix $I - \boldsymbol{B}\boldsymbol{K}$ is invertible. It follows that $\boldsymbol{L}$ is block lower-triangular and satisfies

$$I + \boldsymbol{B}\boldsymbol{L} = (I - \boldsymbol{B}\boldsymbol{K})^{-1}. \tag{4.24}$$

Furthermore, $\boldsymbol{K}$ is a function of $\boldsymbol{L}$ given by

$$\boldsymbol{K} = \boldsymbol{L}(I + \boldsymbol{B}\boldsymbol{L})^{-1}, \tag{4.25}$$

and therefore we may optimize over $\boldsymbol{L}$ in place of $\boldsymbol{K}$ [114]. Using the decision variable $\boldsymbol{L}$ as in (4.23) results in the state deviation process

$$\tilde{X} = (I + \boldsymbol{B}\boldsymbol{L})(\boldsymbol{A}\tilde{x}_0 + \boldsymbol{G}W). \tag{4.26}$$

The state and control processes X and U are thus Gaussian distributed with mean $\mathbb{E}(X) = \bar{X}$ as in (4.21) and $\mathbb{E}(U) = V$, and covariances

$$\boldsymbol{P_X} = \mathrm{Cov}(X) = (I + \boldsymbol{B}\boldsymbol{L})\boldsymbol{S}(I + \boldsymbol{B}\boldsymbol{L})^\intercal, \tag{4.27}$$

$$\boldsymbol{P_U} = \mathrm{Cov}(U) = \boldsymbol{L}\boldsymbol{S}\boldsymbol{L}^\intercal, \tag{4.28}$$

where

$$\boldsymbol{S} = \boldsymbol{A}P_0\boldsymbol{A}^\intercal + \boldsymbol{G}\boldsymbol{G}^\intercal. \tag{4.29}$$

It will be useful to define the matrices $E_k \in \mathbb{R}^{n\times(N+1)n}$ and $E_k^u \in \mathbb{R}^{m\times Nm}$ such that $E_k X = x_k$ and $E_k^u U = u_k$, which are given as

$$E_k = \begin{bmatrix} 0_{n\times kn} & I_{n\times n} & 0_{n\times(N-k)n} \end{bmatrix}, \tag{4.30}$$

$$E_k^u = \begin{bmatrix} 0_{m\times km} & I_{m\times m} & 0_{m\times(N-k-1)m} \end{bmatrix}. \tag{4.31}$$

State and Control Polytope Chance Constraints

The inner product $a_j^\intercal x_k$ is a Gaussian random variable with mean $a_j^\intercal \mathbb{E}(x_k)$ and covariance $a_j^\intercal \mathrm{Cov}(x_k) a_j$. It follows that the compliment of the probability in (4.11) can be written in

terms of the normal cumulative distribution function cdfn as

$$\mathbb{P}(a_j^\intercal x_k \leq \alpha_j) = \mathrm{cdfn}\left(\frac{\alpha_j - a_j^\intercal E_k \bar{X}}{\sqrt{a_j^\intercal E_k \boldsymbol{P_X} E_k^\intercal a_j}}\right). \tag{4.32}$$

Taking the inverse of the normal cumulative distribution function and rearranging terms, we obtain

$$\mathbb{P}(a_j^\intercal x_k > \alpha_j) \leq p_j^x \iff \mathrm{cdfn}\left(\frac{\alpha_j - a_j^\intercal E_k \bar{X}}{\sqrt{a_j^\intercal E_k \boldsymbol{P_X} E_k^\intercal a_j}}\right) \geq 1 - p_j^x \tag{4.33}$$

$$\iff \frac{\alpha_j - a_j^\intercal E_k \bar{X}}{\sqrt{a_j^\intercal E_k \boldsymbol{P_X} E_k^\intercal a_j}} \geq \mathrm{cdfn}^{-1}(1 - p_j^x) \tag{4.34}$$

$$\iff \mathrm{cdfn}^{-1}(1 - p_j^x)\sqrt{a_j^\intercal E_k \boldsymbol{P_X} E_k^\intercal a_j} + a_j^\intercal E_k \bar{X} \leq \alpha_j. \tag{4.35}$$

It remains to rewrite the square root term in (4.35) containing the state covariance, which depends on the decision variable $\boldsymbol{L}$. Substituting the value of the covariance matrix $\boldsymbol{P_X}$ from (4.27) and rearranging, we find that

$$\begin{aligned} a_j^\intercal E_k \boldsymbol{P_X} E_k^\intercal a_j &= a_j^\intercal E_k (I + \boldsymbol{BL})(\boldsymbol{S}^{1/2})^\intercal \boldsymbol{S}^{1/2}(I + \boldsymbol{BL}) E_k^\intercal a_j \\ &= \|\boldsymbol{S}^{1/2}(I + \boldsymbol{BL})^\intercal E_k^\intercal a_j\|^2, \end{aligned} \tag{4.36}$$

where $\boldsymbol{S}^{1/2}$ denotes a matrix satisfying $\boldsymbol{S} = (\boldsymbol{S}^{1/2})^\intercal \boldsymbol{S}^{1/2}$. Thus, by taking the square root of both sides of (4.36), we obtain

$$\sqrt{a_j^\intercal E_k \boldsymbol{P_X} E_k^\intercal a_j} = \|\boldsymbol{S}^{1/2}(I + \boldsymbol{BL}) E_k^\intercal a_j\|. \tag{4.37}$$

Substituting (4.37) and (4.21) into (4.35) results in the equivalence

$$\begin{aligned} &\mathbb{P}(a_j^\intercal x_k > \alpha_j) \leq p_j^x \\ &\qquad \iff \mathrm{cdfn}^{-1}(1 - p_j^x)\|\boldsymbol{S}^{1/2}(I + \boldsymbol{BL}) E_k^\intercal a_j\| + a_j^\intercal E_k(\boldsymbol{A}\bar{x}_0 + \boldsymbol{B}V) \leq \alpha_j. \end{aligned} \tag{4.38}$$

The right-hand constraint is a second-order cone constraint in $\boldsymbol{L}$ and V, and hence convex.

We follow the same approach for the control polytopic chance constraints. Observing that $u_k \sim \mathcal{N}(E_k^u V, E_k^u \boldsymbol{P_U} E_k^{u\mathsf{T}})$, we rewrite the compliment of the probability in (4.12) as

$$\mathbb{P}(b_j^\mathsf{T} u_k \leq \beta_j) = \text{cdfn}\left(\frac{\beta_j - b_j^\mathsf{T} E_k^u V}{\sqrt{b_j^\mathsf{T} E_k^u \boldsymbol{P_U} E_k^{u\mathsf{T}} b_j}}\right). \tag{4.39}$$

As in (4.36), the control covariance term in (4.39) is expressed as

$$\begin{aligned} b_j^\mathsf{T} E_k^u \boldsymbol{P_U} E_k^{u\mathsf{T}} b_j &= b_j^\mathsf{T} E_k^u \boldsymbol{L} (\boldsymbol{S}^{1/2})^\mathsf{T} \boldsymbol{S}^{1/2} \boldsymbol{L} E_k^{u\mathsf{T}} b_j \\ &= \|\boldsymbol{S}^{1/2} \boldsymbol{L}^\mathsf{T} E_k^{u\mathsf{T}} b_j\|^2. \end{aligned} \tag{4.40}$$

We thus obtain an equivalent expression of the constraint (4.12) as

$$\mathbb{P}(b_j^\mathsf{T} u_k > \beta_j) \leq p_j^u \iff \text{cdfn}^{-1}(1-p_j^u)\|\boldsymbol{S}^{1/2} \boldsymbol{L} E_k^{u\mathsf{T}} b_j\| + b_j^\mathsf{T} E_k^u V \leq \beta_j, \tag{4.41}$$

which is a second-order cone constraint in $\boldsymbol{L}$ and V, and hence convex.

Final State Constraints

Substituting the mean state process (4.21) into the constraint $\mathbb{E}(x_N) = \bar{x}_f$ yields

$$E_N \bar{X} = E_N(\boldsymbol{A}\bar{x}_0 + \boldsymbol{B}V) = \bar{x}_f, \tag{4.42}$$

which is affine in V, and hence convex. Similarly, substituting the state process covariance (4.27) into the maximum final state covariance constraint $\text{Cov}(x_N) \leq P_f$ yields

$$\text{Cov}(x_N) = \text{Cov}(E_N X E_N^\mathsf{T}) = E_N(I + \boldsymbol{BL})\boldsymbol{S}(I + \boldsymbol{BL})^\mathsf{T} E_N^\mathsf{T} \leq P_f, \tag{4.43}$$

or, equivalently [71],

$$\|\boldsymbol{S}^{1/2}(I + \boldsymbol{BL})^\mathsf{T} E_N^\mathsf{T} P_f^{-1/2}\| \leq 1, \tag{4.44}$$

which is a convex constraint in terms of $\boldsymbol{L}$. Note that, by assumption, P_f is positive definite, and hence $P_f^{-1/2}$ exists.

Cost Function

The first quadratic term in the cost funciton (4.10) can be rewritten as

$$\begin{aligned}
&\sum_{k=0}^{N-1}(x_k - x_k^d)^\intercal Q_k (x_k - x_k^d) \\
&\qquad = \begin{bmatrix} x_0 - x_0^d & \cdots & x_N - x_N^d \end{bmatrix} \begin{bmatrix} Q_0 & & & \\ & \ddots & & \\ & & Q_{N-1} & \\ & & & 0 \end{bmatrix} \begin{bmatrix} x_0 - x_0^d \\ \vdots \\ x_N - x_N^d \end{bmatrix} \\
&\qquad = (X - X^d)^\intercal \boldsymbol{Q} (X - X^d), \quad (4.45)
\end{aligned}$$

where $\boldsymbol{Q}$ is a block-diagonal matrix with entries $(Q_0, \ldots, Q_{N-1}, 0)$, and where $X_d \in \mathbb{R}^{(N+1)n} \cong (x_k^d)$ is the desired state process. Taking the expectation of the quadratic form (4.45) yields

$$\begin{aligned}
\mathbb{E}\big((X - X^d)^\intercal \boldsymbol{Q} (X - X^d)\big) &= \mathbb{E}(\tilde{X}^\intercal \boldsymbol{Q} \tilde{X}) + (\bar{X} - X^d)^\intercal \boldsymbol{Q} (\bar{X} - X^d) \quad (4.46) \\
&= \operatorname{tr}(\boldsymbol{P_X Q}) + (\bar{X} - X^d)^\intercal \boldsymbol{Q} (\bar{X} - X^d). \quad (4.47)
\end{aligned}$$

Similarly, the quadratic control penalty terms in (4.10) are rewritten as

$$\mathbb{E}\bigg(\sum_{k=0}^{N-1} \tilde{u}_k^\intercal R_k \tilde{u}_k\bigg) = \operatorname{tr}(\boldsymbol{P_U R}), \quad (4.48)$$

$$\sum_{k=0}^{N-1} \bar{u}_k^\intercal \bar{R}_k \bar{u}_k = V^\intercal \bar{\boldsymbol{R}} V, \quad (4.49)$$

where $\boldsymbol{R}, \bar{\boldsymbol{R}} \in \mathbb{R}^{Nm \times Nm}$ are block-diagonal matrices given by

$$\boldsymbol{R} = \begin{bmatrix} R_0 & & \\ & \ddots & \\ & & R_{N-1} \end{bmatrix}, \qquad \bar{\boldsymbol{R}} = \begin{bmatrix} \bar{R}_0 & & \\ & \ddots & \\ & & \bar{R}_{N-1} \end{bmatrix}. \tag{4.50}$$

The first expected value term in the cost (4.10) is thus rewritten, by substituting (4.47) and (4.48), as

$$\mathbb{E}\left(\sum_{k=0}^{N-1}(x_k - x_k^d)^\intercal Q_k (x_k - x_k^d) + \tilde{u}_k^\intercal R_k \tilde{u}_k\right) = \operatorname{tr}(\boldsymbol{P_X Q} + \boldsymbol{P_U R}) + (\bar{X} - X^d)^\intercal \boldsymbol{Q} (\bar{X} - X^d). \tag{4.51}$$

The trace term in (4.51) is further expanded by substituting the state and control process covariances (4.27) and (4.28), and rearranging, which yields

$$\begin{aligned} \operatorname{tr}(\boldsymbol{P_X Q} + \boldsymbol{P_U R}) &= \operatorname{tr}\left((I + \boldsymbol{BL})\boldsymbol{S}(I + \boldsymbol{BL})^\intercal \boldsymbol{Q} + \boldsymbol{LSL}^\intercal \boldsymbol{R}\right) \\ &= \operatorname{tr}\left((I + \boldsymbol{BL})^\intercal \boldsymbol{Q}(I + \boldsymbol{BL})\boldsymbol{S} + \boldsymbol{L}^\intercal \boldsymbol{RLS}\right) \\ &= \operatorname{tr}\left\{\left((I + \boldsymbol{BL})^\intercal \boldsymbol{Q}(I + \boldsymbol{BL}) + \boldsymbol{L}^\intercal \boldsymbol{RL}\right)\boldsymbol{S}\right\}. \end{aligned} \tag{4.52}$$

The cost function (4.10) is thus written in terms of the decision variables $\boldsymbol{L}$ and V as

$$\begin{aligned} J(\boldsymbol{L}, V) = \operatorname{tr}&\left\{\left((I + \boldsymbol{BL})^\intercal \boldsymbol{Q}(I + \boldsymbol{BL}) + \boldsymbol{L}^\intercal \boldsymbol{RL}\right)\boldsymbol{S}\right\} \\ &+ \|\boldsymbol{A}\bar{x}_0 + \boldsymbol{B}V - X^d\|_{\boldsymbol{Q}}^2 + V^\intercal \bar{\boldsymbol{R}} V + \eta \sum_{k=0}^{N-1} \|E_k^u V\|, \end{aligned} \tag{4.53}$$

which is convex in $\boldsymbol{L}$ and V since the weight matrices $\boldsymbol{Q}$, $\boldsymbol{R}$, and $\bar{\boldsymbol{R}}$ are all positive semi-definite.

4.2.3 Control Magnitude Chance Constraints

Finally, we consider the constraint (4.7) on the probability that the control magnitude exceeds a prescribed maximum value. The following results will be useful for developing a relaxed convex formulation of this control chance constraint.

Theorem 4.2.1. *Let $y \sim \mathcal{N}(\mu, \Sigma)$ be an m-dimensional random vector for $m \geq 1$, let $\sigma = \sqrt{\lambda_{\max}(\Sigma)}$, let $\rho > 0$, and let $1 > \beta > 0$. Then*

$$\|\mu\| + \sigma\left(\sqrt{2\log\frac{1}{\beta}} + \sqrt{m}\right) \leq \rho \implies \mathbb{P}(\|y\| \leq \rho) \geq 1 - \beta. \tag{4.54}$$

Proof. Let $z \sim \mathcal{N}(0, I)$ be an m-dimensional standard Gaussian random vector. Then $\|z\|^2$ is a $\chi^2(m)$-random variable, and thus satisfies the concentration inequality (Ref. [115], Example 2.28):

$$\mathbb{P}(\|z\|^2 \leq m(1+\delta)^2) \geq 1 - e^{-m\delta^2/2} \quad \text{for all } \delta \geq 0. \tag{4.55}$$

Writing $y = \mu + \Sigma^{1/2}z \sim \mathcal{N}(\mu, \Sigma)$, it follows that $\|y\| \leq \|\mu\| + \sigma\|z\|$, and thus

$$\mathbb{P}(\|y\| \leq \rho) \geq \mathbb{P}(\|\mu\| + \sigma\|z\| \leq \rho) = \mathbb{P}(\|z\| \leq (\rho - \|\mu\|)/\sigma). \tag{4.56}$$

Set $\delta = (\rho - \|\mu\|)/\sigma\sqrt{m} - 1$. Since $\sigma\sqrt{2\log(1/\beta)} \geq 0$, the hypothesis implies that $\|\mu\| + \sigma\sqrt{m} \leq \rho$, and hence $\delta \geq 0$. Next, substitute (4.55) into (4.56) to obtain

$$\mathbb{P}(\|y\| \leq \rho) \geq 1 - \exp\left[-\frac{m}{2}\left(\frac{\rho - \|\mu\|}{\sigma\sqrt{m}} - 1\right)^2\right]. \tag{4.57}$$

The hypothesis yields:

$$\|\mu\| + \sigma\left(\sqrt{2\log\frac{1}{\beta}} + \sqrt{m}\right) \leq \rho \implies \sqrt{\frac{2}{m}\log\frac{1}{\beta}} + 1 \leq \frac{\rho - \|\mu\|}{\sigma\sqrt{m}} \tag{4.58}$$

$$\implies \beta \geq \exp\left[-\frac{m}{2}\left(\frac{\rho - \|\mu\|}{\sigma\sqrt{m}} - 1\right)^2\right] \tag{4.59}$$

$$\implies 1 - \beta \leq 1 - \exp\left[-\frac{m}{2}\left(\frac{\rho - \|\mu\|}{\sigma\sqrt{m}} - 1\right)^2\right]. \tag{4.60}$$

Finally, substituting (4.60) into (4.57), we obtain the desired result. □

In the case that control dimension is $m = 1$ or $m = 2$, the following results provide a sharper bound on the allowable controls.

Lemma 4.2.2. *Let $y \sim \mathcal{N}(0, \Sigma)$ be an m-dimensional random vector where $m = 1$ or $m = 2$, let $\sigma = \sqrt{\lambda_{\max}(\Sigma)}$, and let $\rho > 0$. Then*

$$\mathbb{P}(\|y\| \leq \rho) \geq 1 - e^{-\rho^2/2\sigma^2}. \tag{4.61}$$

Proof. For the case $m = 1$, the result immediately follows from the exponential bound of the error function: [116]

$$\mathbb{P}(\|y\| \leq \rho) = \operatorname{erf}\left(\frac{\rho}{\sigma\sqrt{2}}\right) \geq 1 - e^{-\rho^2/2\sigma^2}. \tag{4.62}$$

Next, consider the case $m = 2$. Let $a \geq 0$, and let $z = \Sigma^{-1/2}y = (r\cos\phi, r\sin\phi)$. The

following integral is evaluated by change of variables:

$$\mathbb{P}(y^\intercal \Sigma^{-1} y \leq a^2) = \frac{1}{2\pi\sqrt{\det(\Sigma)}} \int_{\{y^\intercal \Sigma^{-1} y \leq a^2\}} \exp\left(-\frac{y^\intercal \Sigma^{-1} y}{2}\right) \mathrm{d}y \tag{4.63}$$

$$= \frac{1}{2\pi} \int_{\{z^\intercal z \leq a^2\}} e^{-z^\intercal z/2}\, \mathrm{d}z \tag{4.64}$$

$$= \frac{1}{2\pi} \int_0^{a^2} \int_0^{2\pi} r e^{-r^2/2} \mathrm{d}r\, \mathrm{d}\phi \tag{4.65}$$

$$= 1 - e^{-a^2/2}. \tag{4.66}$$

Since $\|y\|^2 / \sigma^2 \leq y^\intercal \Sigma^{-1} y$, it follows that

$$\mathbb{P}(\|y\|^2 \leq \sigma^2 a^2) \geq \mathbb{P}(y^\intercal \Sigma^{-1} y \leq a^2) = 1 - e^{-a^2/2}. \tag{4.67}$$

Setting $\rho^2 = \sigma^2 a^2$ gives the desired result. Intuitively, the level sets $y^\intercal \Sigma^{-1} y = a^2$ define the contours of ellipses having probability $1 - e^{-a^2/2}$, and the level sets $\|y\|^2 = \sigma^2 a^2$ are the smallest circles that contain these ellipses. □

Theorem 4.2.3. *Let $y \sim \mathcal{N}(\mu, \Sigma)$ be an m-dimensional random vector where $m = 1$ or $m = 2$, let $\sigma = \sqrt{\lambda_{\max}(\Sigma)}$, let $\rho > 0$, and let $1 > \beta > 0$. Then*

$$\|\mu\| + \sigma\sqrt{2 \log \frac{1}{\beta}} \leq \rho \implies \mathbb{P}(\|y\| \leq \rho) \geq 1 - \beta. \tag{4.68}$$

Proof. Since $\sigma \geq 0$, the hypothesis implies that $\|\mu\| \leq \rho$. We can therefore rearrange the

hypothesis as follows:

$$\|\mu\| + \sigma\sqrt{2\log\frac{1}{\beta}} \leq \rho \implies \sigma\sqrt{2\log\frac{1}{\beta}} \leq \rho - \|\mu\| \tag{4.69a}$$

$$\implies 2\sigma^2 \log\frac{1}{\beta} \leq (\rho - \|\mu\|)^2 \tag{4.69b}$$

$$\implies \beta \geq \exp\left(-\frac{(\rho - \|\mu\|)^2}{2\sigma^2}\right) \tag{4.69c}$$

$$\implies 1 - \beta \leq 1 - \exp\left(-\frac{(\rho - \|\mu\|)^2}{2\sigma^2}\right). \tag{4.69d}$$

Let $\tilde{y} = y - \mu$. Since $\|y\| = \|\mu + \tilde{y}\| \leq \|\mu\| + \|\tilde{y}\|$, it follows that

$$\mathbb{P}(\|y\| \leq \rho) \geq \mathbb{P}(\|\mu\| + \|\tilde{y}\| \leq \rho) = \mathbb{P}(\|\tilde{y}\| \leq \rho - \|\mu\|). \tag{4.70}$$

Substituting the result of Lemma 4.2.2 into (4.70), with $\rho - \|\mu\|$ in place of ρ, and since $\tilde{y} \sim \mathcal{N}(0, \Sigma)$, we obtain

$$\mathbb{P}(\|y\| \leq \rho) \geq 1 - \exp\left(-\frac{(\rho - \|\mu\|)^2}{2\sigma^2}\right). \tag{4.71}$$

From (4.69d), we finally obtain the desired result:

$$\mathbb{P}(\|y\| \leq \rho) \geq 1 - \exp\left(-\frac{(\rho - \|\mu\|)^2}{2\sigma^2}\right) \geq 1 - \beta. \tag{4.72}$$

□

With these results, we are now prepared to derive a convex relaxation of the control chance constraint (4.7). Let the norm of a square matrix Y be defined as

$$\|Y\| = \sup_{\|x\|=1} \|Yx\| = \sqrt{\lambda_{\max}(Y^\intercal Y)}. \tag{4.73}$$

Since the the control $u_k = E_k^u U$ is normally distributed with mean $\mathbb{E}(u_k) = E_k^u V$ and

covariance

$$\mathrm{Cov}(u_k) = E_k^u \boldsymbol{P_U} E_k^{u\mathsf{T}} = E_k^u \boldsymbol{L}\boldsymbol{S}\boldsymbol{L}^\mathsf{T} E_k^{u\mathsf{T}}, \tag{4.74}$$

it follows, by substituting $Y = \boldsymbol{S}^{1/2}\boldsymbol{L}^\mathsf{T} E_k^{u\mathsf{T}}$ and $\sigma_{u_k}^2 = \lambda_{\max}(\mathrm{Cov}(u_k))$ into (4.73), that

$$\sigma_{u_k} = \sqrt{\lambda_{\max}(E_k^u \boldsymbol{L}\boldsymbol{S}\boldsymbol{L}^\mathsf{T} E_k^{u\mathsf{T}})} = \|\boldsymbol{S}^{1/2}\boldsymbol{L}^\mathsf{T} E_k^{u\mathsf{T}}\|. \tag{4.75}$$

Suppose that the control dimension is $m = 1$ or $m = 2$. In this case, it follows from Theorem 4.2.3, with (4.75) substituted into (4.68), that if

$$\underbrace{\|E_k^u V\|}_{\text{nominal}} + \underbrace{\|\boldsymbol{S}^{1/2}\boldsymbol{L}^\mathsf{T} E_k^{u\mathsf{T}}\|}_{\text{max standard deviation}} \underbrace{\sqrt{2\log\frac{1}{p_{\text{fail}}^{\|u\|}}}}_{\text{weight term}} \leq \rho, \tag{4.76}$$

then the original constraint (4.7) is also satisfied.

In the case that $m \geq 3$, the same result follows from Theorem 4.2.1, except that now the constraint (4.76) is replaced with

$$\|E_k^u V\| + \|\boldsymbol{S}^{1/2}\boldsymbol{L}^\mathsf{T} E_k^{u\mathsf{T}}\|\left(\sqrt{2\log\frac{1}{p_{\text{fail}}^{\|u\|}}} + \sqrt{m}\right) \leq \rho. \tag{4.77}$$

We remark that this bound for $m \geq 3$ is conservative. In practice, the bound (4.76) may reasonably be substituted for (4.77) with a corresponding decrease to $p_{\text{fail}}^{\|u\|}$ for approximate, but less conservative, results.

4.2.4 Summary of Convex Solution

The convex formulation of the chance-constrained covariance steering problem is summarized below. Note that the decision variables are the vector $V \in \mathbb{R}^{Nm}$ and the block

lower-triangular matrix $\boldsymbol{L}$.

$$\begin{aligned}
\underset{\boldsymbol{L},V}{\text{minimize}} \quad & J(\boldsymbol{L},V) = \operatorname{tr}\left\{\left((I+\boldsymbol{B}\boldsymbol{L})^{\intercal}\boldsymbol{Q}(I+\boldsymbol{B}\boldsymbol{L})+\boldsymbol{L}^{\intercal}\boldsymbol{R}\boldsymbol{L}\right)\boldsymbol{S}\right\} && \text{(4.78a)}\\
& \qquad + \|\boldsymbol{A}\bar{x}_0+\boldsymbol{B}V-X^d\|_{\boldsymbol{Q}}^2 + V^{\intercal}\bar{\boldsymbol{R}}V + \eta\sum_{k=0}^{N-1}\|E_k^u V\| \\
\text{subject to} \quad & E_N(\boldsymbol{A}\bar{x}_0+\boldsymbol{B}V)=\bar{x}_f && \text{(4.78b)}\\
& \|\boldsymbol{S}^{1/2}(I+\boldsymbol{B}\boldsymbol{L})^{\intercal}E_N^{\intercal}P_f^{-1/2}\| \le 1 && \text{(4.78c)}\\
& \operatorname{cdfn}^{-1}(1-p_j^x)\|\boldsymbol{S}^{1/2}(I+\boldsymbol{B}\boldsymbol{L})E_k^{\intercal}a_j\| \\
& \qquad + a_j^{\intercal}E_k(\boldsymbol{A}\bar{x}_0+\boldsymbol{B}V) \le \alpha_j \qquad \forall (k,j)\in\mathcal{X} && \text{(4.78d)}\\
& \operatorname{cdfn}^{-1}(1-p_j^u)\|\boldsymbol{S}^{1/2}\boldsymbol{L}E_k^{u\intercal}b_j\| + b_j^{\intercal}E_k^u V \le \beta_j \qquad \forall (k,j)\in\mathcal{U} && \text{(4.78e)}\\
& \begin{cases}
\|E_k^u V\| + \|\boldsymbol{S}^{1/2}\boldsymbol{L}^{\intercal}E_k^{u\intercal}\|\sqrt{2\log\dfrac{1}{p_{\text{fail}}^{\|u\|}}} \le \rho & \text{if } m\le 2\\
\qquad \forall k\in\{0,\dots,N-1\} & \\
\|E_k^u V\| + \|\boldsymbol{S}^{1/2}\boldsymbol{L}^{\intercal}E_k^{u\intercal}\|\left(\sqrt{2\log\dfrac{1}{p_{\text{fail}}^{\|u\|}}}+\sqrt{m}\right) \le \rho & \text{if } m>2\\
\qquad \forall k\in\{0,\dots,N-1\} &
\end{cases} && \text{(4.78f)}\\
\text{where} \quad & \boldsymbol{S} = \boldsymbol{A}P_0\boldsymbol{A}^{\intercal}+\boldsymbol{G}\boldsymbol{G}^{\intercal} && \text{(4.78g)}
\end{aligned}$$

Remark on Problem Size

The controller (4.9) uses feedback of both the current and the past values of the state process at each step. It follows that the computational complexity of the convex formulation of Problem 4.1 as given in (4.78) scales with $\mathcal{O}(N^2nm)$. For problems with a large time horizon, one may restrict the matrix $\boldsymbol{L}$ to be block diagonal; the resulting computational complexity scales by $\mathcal{O}(Nnm)$ [87]. More generally, the matrix $\boldsymbol{L}$ can be set to be block banded, which allows the designer to trade controller performance with computational complexity [114].

4.2.5 Numerical Example

Consider a double integrator system with a pointable and bounded control force, which is described by the discrete-time system (4.1) with system matrices

$$A = \begin{bmatrix} 1 & 0 & \Delta t & 0 \\ 0 & 1 & 0 & \Delta t \\ 0 & 0 & 1 & 0 \\ 0 & 0 & 0 & 1 \end{bmatrix}, \quad B = \begin{bmatrix} \Delta t^2/2 & 0 \\ 0 & \Delta t^2/2 \\ \Delta t & 0 \\ 0 & \Delta t \end{bmatrix}, \quad G = 0.1 \times \begin{bmatrix} 1 & 0 & 0 & 0 \\ 0 & 1 & 0 & 0 \\ 0 & 0 & 1 & 0 \\ 0 & 0 & 0 & 1 \end{bmatrix}, \tag{4.79}$$

and time step size $\Delta t = 0.25$. The final time is $t_f = 5$, and thus the horizon size is $N = 20$. The initial state distribution is given by

$$\bar{x}_0 = \begin{bmatrix} 2 \\ 4 \\ 3 \\ 2 \end{bmatrix}, \qquad P_0 = \begin{bmatrix} 0.1 & 0 & 0 & 0 \\ 0 & 0.1 & 0 & 0 \\ 0 & 0 & 0.02 & 0 \\ 0 & 0 & 0 & 0.02 \end{bmatrix}. \tag{4.80}$$

The final state is constrained to have mean $\bar{x}_f$ and maximum covariance P_f given by

$$\bar{x}_f = \begin{bmatrix} 8 \\ 2 \\ 0 \\ 0 \end{bmatrix}, \quad P_f = \begin{bmatrix} 0.06 & 0 & 0 & 0 \\ 0 & 0.06 & 0 & 0 \\ 0 & 0 & 0.006 & 0 \\ 0 & 0 & 0 & 0.006 \end{bmatrix}. \tag{4.81}$$

The control $u_k \in \mathbb{R}^2$ is constrained to be inside a disk of radius $\rho = 2$ with a maximum probability of constraint violation of $p_{\text{fail}}^{\|u\|} = 1 - 0.9973$. The mean control weight is set to $\eta = 1$. For all steps, the state weight is $Q_k = 0$, the control variance penalty is $R_k = I$, and the mean quadratic control penalty is $\bar{R}_k = 0$. The quadratic mean control weight R_k is set to zero in order to emulate a minimum-fuel type problem with both the mean-fuel (i.e., the

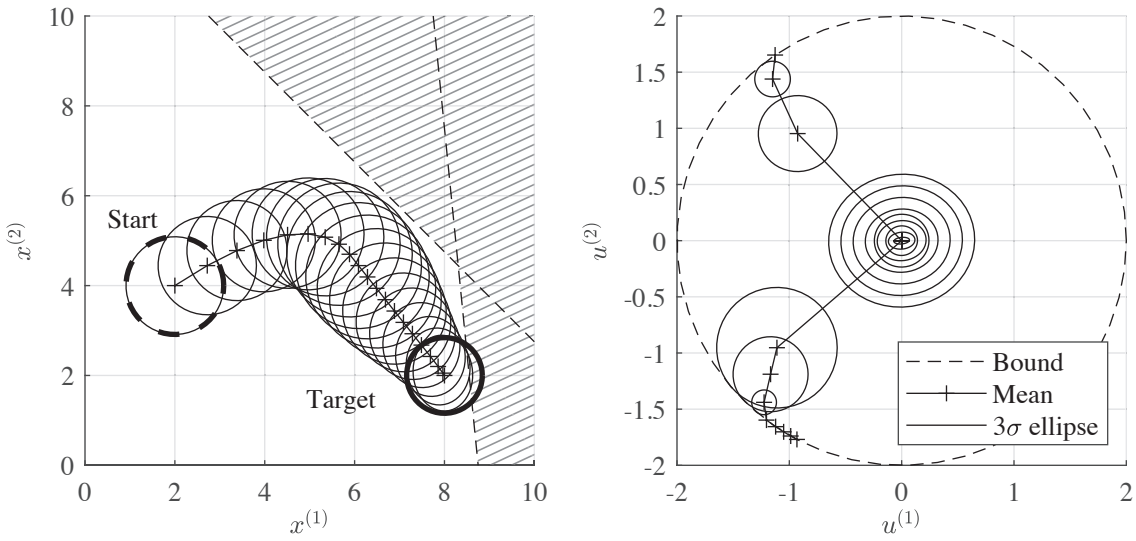

Figure 4.2: Position and control covariance evolution for the closed-loop double integrator system, where $x^{(i)}$ and $u^{(i)}$ denote coordinates of the state and control.

Euclidean norm of expected control) and the control variance penalized.

The state is required to remain in the region $\mathcal{R}_x$ with a probability of at least 99.73% (i.e., $p^x_{\text{fail}} = 1 - 0.9973$), where $\mathcal{R}_x$ is defined as in (4.3) by

$$a_1 = \begin{bmatrix} 1 & 1 & 0 & 0 \end{bmatrix}^\mathsf{T}, \quad \alpha_1 = 12.75, \quad a_2 = \begin{bmatrix} 1 & 0.1 & 0 & 0 \end{bmatrix}^\mathsf{T}, \quad \alpha_2 = 8.75. \tag{4.82}$$

The individual chance constraints are defined by assigning a uniform risk: $p^x_j = p^x_{\text{fail}}/2$ for $j = 1, 2$. The convex program (4.78), with $\boldsymbol{L}$ block lower-triangular, was solved using YALMIP [117] with MOSEK [106].

The resulting closed-loop trajectory is shown in Figure 4.2. The initial covariance is indicated by a dashed 3σ ellipse (i.e., 99.73% of samples are in the ellipse), the maximum final covariance is indicated by a weighted, solid 3σ ellipse, and the compliment of the chance constrained region $\mathcal{R}^c_x$ is indicated by diagonal lines. At the start of the trajectory, the feedback gains are balanced with the feedforward control so that the state distribution both shrinks and shifts to meet the chance constraint, and the mean of the control is distanced from the limiting magnitude accordingly. The feedback gain is increased while the

nominal control is equal to zero in order to shrink to state covariance to meet the endpoint constraint, and then the feedback and feedfoward controls are again balanced during the final segment of the trajectory.

4.3 Covariance Steering with Output Feedback

In the previous section, it was assumed that the value of the state is perfectly known. This section, in contrast, is concerned with covariance steering for the case when the state is only indirectly accessible via noisy measurements (i.e., the output-feedback case).

The main contribution described in this section is the development of a novel covariance steering control policy for linear systems with Gaussian process and measurement noise. The proposed approach is a nontrivial extension of the full-state feedback covariance control policy proposed in [71], which allows one to directly assess the value of the covariance at each time step, while converting the original stochastic control problem to a deterministic convex programming problem. We observe that, as a direct consequence of the constraints on the state covariance, and in contrast to the classical LQG solution [89], the optimal feedback control depends on both the process noise and the observation model.

4.3.1 Problem Definition

As before, we consider the discrete-time linear stochastic system (4.1), except now the state is not directly accessible. Rather, the state is measured through the observation process

$$y_k = C_k x_k + D_k q_k, \tag{4.83}$$

where $y_k \in \mathbb{R}^{n_y}$ is the measurement and $q_k \in \mathbb{R}^{n_y}$ is measurement noise, and $C_k \in \mathbb{R}^{n_y \times n_x}$ and $D_k \in \mathbb{R}^{n_y \times n_y}$ are given. Increments of the measurement noise q_k are i.i.d. standard Gaussian random vectors. In order to simplify the filtering equations, we assume that the matrix D_k is invertible. The case when D_k is rank-deficient can be treated using well-

known approaches [118]. Before the first measurement is taken, we assume that we will be provided with a state estimate $\hat{x}_{0^-}$ with estimation error $\tilde{x}_{0^-} = x_0 - \hat{x}_{0^-}$. We assume that $\hat{x}_{0^-}$ and $\tilde{x}_{0^-}$ are independent random vectors with known distributions given as

$$\hat{x}_{0^-} \sim \mathcal{N}(\bar{x}_0, \hat{P}_{0^-}), \quad \tilde{x}_{0^-} \sim \mathcal{N}(0, \tilde{P}_{0^-}), \tag{4.84}$$

where the positive semi-definite matrices $\tilde{P}_{0^-}$, $\hat{P}_{0^-}$ and the vector $\bar{x}_0$ are all fixed and known. That is, we do not assume to know the initial state estimate when designing the control law, but we know its distribution, which allows for the control law to be designed before any measurements are collected. For example, in the case when we will be provided with the exact value of the state before the initial step, then $\tilde{x}_{0^-} = 0$, $\hat{x}_{0^-} = x_0$, and $\tilde{P}_{0^-} = 0$. On the other hand, if we will not be provided with any new information about the state before step $k = 0$, then $\hat{x}_{0^-} = \bar{x}_0$ and $\hat{P}_{0^-} = 0$. Finally, we assume that $\hat{x}_{0^-}$, $\tilde{x}_{0^-}$, (w_k), and (q_k) are independent.

Define the filtration $(\mathscr{F}_k)_{k=-1}^N$ by $\mathscr{F}_{-1} = \sigma(\hat{x}_{0^-})$ and $\mathscr{F}_k = \sigma(\hat{x}_{0^-}, y_i : 0 \leq i \leq k)$ for $0 \leq k \leq N$. This filtration represents the information that can be used to estimate the state and determine the control action, in the sense that the estimated state and the control at step k are both $\mathscr{F}_k$-measurable random vectors. The initial σ-algebra $\mathscr{F}_{-1}$ is defined for logical consistency, since the initial state estimate is known before any measurements are taken.

As before, let $\bar{x}_k = \mathbb{E}(x_k)$ be the mean state, and now define the estimated (filtered) state as $\hat{x}_k = \mathbb{E}(x_k|\mathscr{F}_k)$ and the estimation error as $\tilde{x}_k = x_k - \hat{x}_k$. The estimated state has mean

$$\mathbb{E}(\hat{x}_k) = \mathbb{E}(\mathbb{E}(x_k|\mathscr{F}_k)) = \mathbb{E}(x_k) = \bar{x}_k, \tag{4.85}$$

and hence the estimation error has zero mean, that is, $\mathbb{E}(\tilde{x}_k) = 0$ for all $0 \leq k \leq N$. Define

the state, estimated state, and estimation error covariances as

$$P_k = \mathrm{Cov}(x_k) = \mathbb{E}\big((x_k - \bar{x}_k)(x_k - \bar{x}_k)^\mathsf{T}\big), \tag{4.86}$$

$$\hat{P}_k = \mathrm{Cov}(\hat{x}_k) = \mathbb{E}\big((\hat{x}_k - \bar{x}_k)(\hat{x}_k - \bar{x}_k)^\mathsf{T}\big), \tag{4.87}$$

$$\tilde{P}_k = \mathrm{Cov}(\tilde{x}_k) = \mathbb{E}\big((\hat{x}_k - x_k)(\hat{x}_k - x_k)^\mathsf{T}\big). \tag{4.88}$$

The estimated state is uncorrelated with the estimation error, since

$$\begin{aligned}
\mathbb{E}(\hat{x}_k \tilde{x}_k^\mathsf{T}) &= \mathbb{E}\big(\hat{x}_k (x_k - \hat{x}_k)^\mathsf{T}\big) \\
&= \mathbb{E}\big(\mathbb{E}\big(\hat{x}_k (x_k - \hat{x}_k)^\mathsf{T} | \mathscr{F}_k\big)\big) \\
&= \mathbb{E}\big(\hat{x}_k \mathbb{E}(x_k^\mathsf{T} - \hat{x}_k^\mathsf{T} | \mathscr{F}_k)\big) \\
&= \mathbb{E}\big(\hat{x}_k (\mathbb{E}(x_k^\mathsf{T} | \mathscr{F}_k) - \hat{x}_k^\mathsf{T})\big) = 0,
\end{aligned} \tag{4.89}$$

and from this expression it can be shown that the state covariance satisfies $P_k = \hat{P}_k + \tilde{P}_k$. Define the prior estimated state and prior estimation error as $\hat{x}_{k^-} = \mathbb{E}(x_k | \mathscr{F}_{k-1})$ and $\tilde{x}_{k^-} = x_k - \hat{x}_{k^-}$, respectively, with corresponding covariances $\hat{P}_{k^-}$ and $\tilde{P}_{k^-}$ as above. It follows that the initial state is distributed as

$$x_0 \sim \mathcal{N}(\bar{x}_0, P_0), \tag{4.90}$$

where $P_0 = \hat{P}_{0^-} + \tilde{P}_{0^-}$.

The initial state distribution is thus the same as in the full-state feedback case considered in Section 4.2. The present case constitutes an extension to the previous theory by decomposing the initial state uncertainty into the part $\hat{x}_{0^-}$ that will be known at the initial time, and a part $\tilde{x}_{0^-}$ that will remain unknown.

As in the previous section, the state and control are constrained as in (4.5) and (4.6) to convex polytopes $\mathcal{R}_x$ and $\mathcal{R}_u$ defined as in (4.3) and (4.4); the probability control magnitude exceeds the limit ρ is constrained as in (4.7); and mean and the covariance of the final state are constrained as in (4.8) for a given final mean vector $\bar{x}_f$ and maximum final state

covariance P_f. However, since the final state covariance consists of both the filtered state and the estimation error covariances, and since the estimation error covariance (as will be shown) cannot be affected by the control, we assume that the final state covariance satisfies

$$P_f > \tilde{P}_N \tag{4.91}$$

so that the constraint $\mathrm{Cov}(x_N) = \hat{P}_N + \tilde{P}_N \leq P_f$ is feasible.

The control is assumed to be an affine function of the *filtered* state history given by the feedback law

$$u_k = \sum_{i=0}^{k} K_{k,i}(\hat{x}_i - \bar{x}_i) + v_k, \tag{4.92}$$

for $k = 0, 1, \ldots, N-1$, where, as before, $K_{k,i} \in \mathbb{R}^{m \times n}$ are feedback gains and $v_k \in \mathbb{R}^m$ are feedforward controls.

Finally, as before, we wish to find the feedback gains $(K_{k,i})$ and the feedforward controls (v_k) to minimize the cost function (4.10). In summary, we are concerned with following stochastic optimal control problem.

Problem 4.2. *Find the feedback gains $(K_{k,i})$ and the feedforward controls (v_k) for the control law (4.92) that minimize the cost (4.10), subject to the dynamics (4.1), the state chance constraints (4.5), the control chance constraints (4.6), (4.7), and the final state distribution constraints (4.8).*

Note that the only difference between this output-feedback problem and Problem 4.1 is that the feedback law (4.92) depends on the filtered state rather than the true state.

4.3.2 Separation of the Observation and Control Problems

Since the system (4.1) is linear and the state is Gaussian distributed, the estimated state is obtained by the Kalman filter. Thus, the filtered estimated satisfies [15]

$$\hat{x}_k = \hat{x}_{k\text{-}} + F_k(y_k - C_k\hat{x}_{k\text{-}}), \tag{4.93}$$

$$\hat{x}_{k\text{-}} = A_{k-1}\hat{x}_{k-1} + B_{k-1}u_{k-1}, \tag{4.94}$$

where

$$F_k = \tilde{P}_{k\text{-}}C_k^\intercal(C_k\tilde{P}_{k\text{-}}C_k^\intercal + D_kD_k^\intercal)^{-1} \tag{4.95}$$

is the Kalman gain, and the error covariances are given by

$$\tilde{P}_k = (I - F_kC_k)\tilde{P}_{k\text{-}}(I - F_kC_k)^\intercal + F_kD_kD_k^\intercal F_k^\intercal, \tag{4.96}$$

$$\tilde{P}_{k\text{-}} = A_{k-1}\tilde{P}_{k-1}A_{k-1}^\intercal + G_{k-1}G_{k-1}^\intercal. \tag{4.97}$$

We see that the estimation error covariance $\tilde{P}_k$ does not depend on the control. It follows that the control objective can be equivalently be given entirely in terms of the filtered state. First, we rewrite the quadratic state penalty term in the cost (4.10) as

$$\mathbb{E}\big((x_k - x_k^d)^\intercal Q_k(x_k - x_k^d)\big) = \mathbb{E}\big((x_k - \hat{x}_k + \hat{x}_k - x_k^d)^\intercal Q_k(x_k - \hat{x}_k + \hat{x}_k - x_k^d)\big). \tag{4.98}$$

Expanding and collecting terms, we obtain

$$\mathbb{E}\big((x_k - x_k^d)^\intercal Q_k(x_k - x_k^d)\big) = \underbrace{\mathbb{E}\big((x_k - \hat{x}_k)^\intercal Q_k(x_k - \hat{x}_k)\big)}_{\operatorname{tr}\tilde{P}_kQ_k} \tag{4.99a}$$

$$+ \underbrace{\mathbb{E}\big(2(x_k - \hat{x}_k)^\intercal Q_k(\hat{x}_k - x_k^d)\big)}_{0} \tag{4.99b}$$

$$+ \mathbb{E}\big((\hat{x}_k - x_k^d)^\intercal Q_k(\hat{x}_k - x_k^d)\big), \tag{4.99c}$$

where the first term (4.99a) reduces to $\operatorname{tr} \tilde{P}_k Q_k$ directly from the definition (4.88) of $\tilde{P}_k$, and where the second term (4.99b) equals zero due to the properties of conditional expectation:

$$\mathbb{E}\big((x_k - \hat{x}_k)^\intercal Q_k(\hat{x}_k - x_k^d)\big) = \mathbb{E}\big(\mathbb{E}\big[(x_k - \hat{x}_k)^\intercal Q_k(\hat{x}_k - x_k^d)|\mathscr{F}_k\big]\big) \tag{4.100}$$

$$= \mathbb{E}\big(\underbrace{\mathbb{E}\big[(x_k - \hat{x}_k)^\intercal|\mathscr{F}_k\big]}_{0} Q_k(\hat{x}_k - x_k^d)\big). \tag{4.101}$$

Therefore, by substituting (4.99), the objective (4.10) may be rewritten as

$$J(K_{k,i}, v_k) = \sum_{k=0}^{N-1} \operatorname{tr} \tilde{P}_k Q_k + \hat{J}(K_{k,i}, v_k), \tag{4.102}$$

where

$$\hat{J}(K_{k,i}, v_k) = \mathbb{E}\left(\sum_{k=0}^{N-1}(\hat{x}_k - x_k^d)^\intercal Q_k(\hat{x}_k - x_k^d) + \tilde{u}_k^\intercal R_k \tilde{u}_k\right) + \sum_{k=0}^{N-1} \bar{u}_k^\intercal \bar{R}_k \bar{u}_k + \eta\|\bar{u}_k\|. \tag{4.103}$$

Since the estimation error covariance $\tilde{P}_k$ is determined by the Kalman filter and not by the control, optimizing over the objective $\hat{J}(K_{k,i}, v_k)$ is equivalent to optimizing over $J(K_{k,i}, v_k)$. Furthermore, we can determine the distribution of the state as a function of the mean and covariance of the *estimated* state process, that is,

$$x_k \sim \mathcal{N}(\bar{x}_k, P_k) \iff \hat{x}_k \sim \mathcal{N}(\bar{x}_k, P_k - \tilde{P}_k). \tag{4.104}$$

It follows that, in order for the final state covariance to satisfy $0 < P_N \leq P_f$, the maximum final covariance P_f must satisfy $P_f > \tilde{P}_N$, which we have already assumed.

Define now the *innovation process* $(\tilde{y}_{k^-})$ by

$$\tilde{y}_{k^-} = y_k - \mathbb{E}(y_k|\mathscr{F}_{k-1}), \tag{4.105}$$

for $k = 0, 1, \ldots, N$. Since

$$\mathbb{E}(y_k|\mathscr{F}_{k-1}) = \mathbb{E}(C_k x_k + D_k q_k|\mathscr{F}_{k-1}) = C_k \hat{x}_{k^-}, \tag{4.106}$$

we obtain, by substituting the observation model (4.83) in (4.105), that

$$\tilde{y}_{k^-} = y_k - C_k \hat{x}_{k^-} = C_k \tilde{x}_{k^-} + D_k q_k. \tag{4.107}$$

The state error $\tilde{x}_{k^-}$ depends linearly on $\tilde{x}_{0^-}$, $(w_i)_{i=1}^{k-1}$, and $(q_i)_{i=1}^{k-1}$, which are each independent of q_k. It follows that $\tilde{x}_{k^-}$ and q_k are independent, and therefore we can compute the covariance of the innovation process as

$$P_{\tilde{y}_{k^-}} = \mathbb{E}(\tilde{y}_{k^-}\tilde{y}_{k^-}^\intercal) = C_k \tilde{P}_{k^-} C_k^\intercal + D_k D_k^\intercal. \tag{4.108}$$

Thus, the distribution of the innovation process is determined by the estimation error covariance $\tilde{P}_{k^-}$, and therefore may be computed prior to solving for the control inputs. We rewrite the estimated state process as

$$\hat{x}_{k+1} = A_k \hat{x}_k + B_k u_k + F_{k+1} \tilde{y}_{(k+1)^-}, \tag{4.109}$$

where $\hat{x}_0 = \hat{x}_{0^-} + F_0 \tilde{y}_{0^-}$. We have thus replaced the state process (4.1) with noise term $G_k w_k$ with a corresponding filtered state process with noise $F_{k+1}\tilde{y}_{(k+1)^-}$. The stochastic optimal control problem may now be posed entirely in terms of the filtered state process (4.109).

4.3.3 Control of the Filtered State

Block-Matrix Formulation

As was done for the state process in Section 4.2, the filtered state process is rewritten in matrix notation as

$$\begin{bmatrix} \hat{x}_0 \\ \hat{x}_1 \\ \hat{x}_2 \\ \vdots \end{bmatrix} = \begin{bmatrix} I \\ A_0 \\ A_1A_0 \\ \vdots \end{bmatrix} \hat{x}_{0\text{-}} + \begin{bmatrix} 0 & 0 & \\ B_0 & 0 & \\ A_1B_0 & B_1 & \\ & & \ddots \end{bmatrix} \begin{bmatrix} u_0 \\ u_1 \\ \vdots \end{bmatrix} + \begin{bmatrix} F_0 & 0 & 0 & \\ A_0F_0 & F_1 & 0 & \\ A_1A_0F_0 & A_1F_1 & F_2 & \\ & & & \ddots \end{bmatrix} \begin{bmatrix} \tilde{y}_{0\text{-}} \\ \tilde{y}_{1\text{-}} \\ \tilde{y}_{2\text{-}} \\ \vdots \end{bmatrix}. \tag{4.110}$$

Let $\hat{X} \in \mathbb{R}^{(N+1)n}$ and $\tilde{Y} \in \mathbb{R}^{(N+1)n_y}$ be column vectors constructed by stacking $\hat{x}_k$ and $\tilde{y}_{k\text{-}}$ for $k = 0, 1, \ldots, N$, and let $\boldsymbol{A}$, $\boldsymbol{B}$, and $\boldsymbol{F}$ be appropriately constructed block matrices as in (4.110). Note that the structure of $\boldsymbol{F}$ differs from that of $\boldsymbol{G}$; otherwise, this construction for the filtered state process is the same as for the state process (4.15).

The filtered state process is then written as the linear matrix equation

$$\hat{X} = \boldsymbol{A}\hat{x}_{0\text{-}} + \boldsymbol{B}U + \boldsymbol{F}\tilde{Y}. \tag{4.111}$$

Let $\boldsymbol{K}$ and $V \cong (v_k)$ be defined as in Subsection 4.2.2, which allows us to write the control process $U \in \mathbb{R}^{Nm} \cong (u_k)$ as

$$U = \boldsymbol{K}(\hat{X} - \bar{X}) + V. \tag{4.112}$$

Substituting the control (4.112) into the filtered state equation (4.111), we obtain the closed-loop filtered state process

$$\hat{X} = \boldsymbol{A}\hat{x}_{0\text{-}} + \boldsymbol{B}\boldsymbol{K}(\hat{X} - \bar{X}) + \boldsymbol{B}V + \boldsymbol{F}\tilde{Y}. \tag{4.113}$$

Solving for $\bar{X}$ and $\hat{X} - \bar{X}$ from (4.113), and using the fact that $\tilde{Y}$ has zero mean, we obtain

$$\bar{X} = \mathbb{E}(\hat{X}) = \boldsymbol{A}\bar{x}_0 + \boldsymbol{B}V, \tag{4.114}$$

$$\hat{X} - \bar{X} = (I - \boldsymbol{B}\boldsymbol{K})^{-1}(\boldsymbol{A}(\hat{x}_{0\text{-}} - \bar{x}_0) + \boldsymbol{F}\tilde{Y}). \tag{4.115}$$

Following the approach in Section 4.2, we again define $\boldsymbol{L}$ as in (4.23) to be a new decision variable. In terms of $\boldsymbol{L}$, the closed-loop system (4.115) is given as

$$\hat{X} - \bar{X} = (I + \boldsymbol{B}\boldsymbol{L})(\boldsymbol{A}(\hat{x}_{0\text{-}} - \bar{x}_0) + \boldsymbol{F}\tilde{Y}). \tag{4.116}$$

Since steps of the innovation process $(\tilde{y}_{k\text{-}})$ are independent [119], the covariance of $\tilde{Y}$ is the block-diagonal matrix

$$\boldsymbol{P}_{\tilde{\boldsymbol{Y}}} = \mathrm{Cov}(\tilde{Y}) = \mathrm{blkdiag}(P_{\tilde{y}_{0\text{-}}}, \ldots, P_{\tilde{y}_{N\text{-}}}), \tag{4.117}$$

where $P_{\tilde{y}_{k\text{-}}}$ as in (4.108). By assumption, $\hat{x}_{0\text{-}}$ is independent from both $\tilde{x}_{0\text{-}}$ and q_0, and therefore by (4.107) we have that $\hat{x}_{0\text{-}}$ is independent from $\tilde{Y}$. It follows that

$$\hat{\boldsymbol{S}} = \mathrm{Cov}(\boldsymbol{A}(\hat{x}_{0\text{-}} - \bar{x}_0) + \boldsymbol{F}\tilde{Y}) = \boldsymbol{A}\hat{P}_{0\text{-}}\boldsymbol{A}^{\intercal} + \boldsymbol{F}\boldsymbol{P}_{\tilde{\boldsymbol{Y}}}\boldsymbol{F}^{\intercal}. \tag{4.118}$$

The filtered state and control processes are thus both Gaussian distributed with mean values $\bar{X}$ and V and with covariances

$$\boldsymbol{P}_{\hat{\boldsymbol{X}}} = \mathrm{Cov}(\hat{X}) = (I + \boldsymbol{B}\boldsymbol{L})\hat{\boldsymbol{S}}(I + \boldsymbol{B}\boldsymbol{L})^{\intercal}, \tag{4.119}$$

$$\hat{\boldsymbol{P}}_{\boldsymbol{U}} = \mathrm{Cov}(U) = \boldsymbol{L}\hat{\boldsymbol{S}}\boldsymbol{L}^{\intercal}. \tag{4.120}$$

Note that while the structure of (4.119) and (4.120) are similar to the state and control process covariance (4.27) and (4.28) for the full state feedback case, the value of $\hat{\boldsymbol{S}}$, which depends on both the process and observation noise models, differs from that of $\boldsymbol{S}$ given in

(4.29) — hence the notation $\hat{\boldsymbol{P}}_{\boldsymbol{U}}$ to differentiate the control process covariance when using output feedback.

State and Control Polytope Chance Constraints

In terms of the column vector $\tilde{X} \cong (\tilde{x}_k)$, the state chance constraints (4.5) may be written as

$$\mathbb{P}(E_k(\hat{X} + \bar{X}) \notin \mathcal{R}_x) \leq p^x_{\text{fail}}, \quad k = 1, 2, \ldots, N. \tag{4.121}$$

The distribution of $\hat{X} + \tilde{X}$ is determined, per (4.104), by the filtered process (4.111) and the sequence $(\tilde{P}_k)$, and therefore the probability in (4.121) depends solely, for fixed problem parameters, on the control sequence U.

As in the full state feedback case, we again relax the state chance constraint (4.121) as in (4.11), enforcing N_x separate half-plane constraints given by

$$\mathbb{P}(a_j^\intercal x_k > \alpha_j) \leq p_j^x \iff \text{cdfn}^{-1}(1 - p_j^x)\|P_k^{1/2} a_j\| + a_j^\intercal \bar{x}_k \leq \alpha_j, \tag{4.122}$$

where P_k is the state covariance at time step k, which we can write as

$$P_k = E_k \boldsymbol{P}_{\hat{\boldsymbol{X}}} E_k^\intercal + \tilde{P}_k. \tag{4.123}$$

In addition, $P_k^{1/2}$ satisfies $(P_k^{1/2})^\intercal P_k^{1/2} = P_k$ and is obtained by

$$P_k^{1/2} = \begin{bmatrix} \hat{\boldsymbol{S}}^{1/2}(I + \boldsymbol{BL})^\intercal E_k^\intercal \\ \tilde{P}_k^{1/2}, \end{bmatrix}, \tag{4.124}$$

since

$$\begin{bmatrix} E_k(I + \boldsymbol{BL})(\hat{\boldsymbol{S}}^{1/2})^\intercal & (\tilde{P}_k^{1/2})^\intercal \end{bmatrix} \begin{bmatrix} \hat{\boldsymbol{S}}^{1/2}(I + \boldsymbol{BL})^\intercal E_k^\intercal \\ \tilde{P}_k^{1/2}, \end{bmatrix} = E_k \boldsymbol{P}_{\hat{\boldsymbol{X}}} E_k^\intercal + \tilde{P}_k = P_k. \tag{4.125}$$

Notice that, because each $p_j < 0.5$, it follows that $\mathrm{cdfn}^{-1}(1-p_j) > 0$. Finally, substituting (4.124) into the chance constraint (4.122), we obtain the second order cone constraint

$$\mathrm{cdfn}^{-1}(1-p_j^x)\left\|\begin{bmatrix}\hat{\boldsymbol{S}}^{1/2}(I+\boldsymbol{BL})^\intercal E_k^\intercal \\ \tilde{P}_k^{1/2}\end{bmatrix} a_j\right\| + a_j^\intercal E_k(\boldsymbol{A}\bar{x}_0 + \boldsymbol{B}V) \leq \alpha_j. \tag{4.126}$$

The control half-plane chance constraint is formulated as in Section 4.2, except the term $\boldsymbol{S}$ is replaced with $\hat{\boldsymbol{S}}$ as in (4.120), which yields

$$\mathrm{cdfn}^{-1}(1-p_j^u)\|\hat{\boldsymbol{S}}^{1/2}\boldsymbol{L}^\intercal E_k^{u\intercal} b_j\| + b_j^\intercal E_k^u V \leq \beta_j, \tag{4.127}$$

which is also a second order cone constraint in $\boldsymbol{L}$ and V.

Control Magnitude Chance Constraints

The convex formulation of the control magnitude constraint (4.7) is the same for the output feedback case as for the state feedback case, except that, as for the half-plane constraints (4.127), the matrix $\boldsymbol{S}$ in (4.76) and (4.77) is substituted with $\hat{\boldsymbol{S}}$.

Final State Constraints

The terminal constraint $\mathbb{E}(x_N) = \bar{x}_f$ is written as

$$E_N\bar{X} = E_N(\boldsymbol{A}\bar{x}_0 + \boldsymbol{B}V) = \bar{x}_f, \tag{4.128}$$

which is affine in V, and hence convex. The terminal covariance constraint may be written as

$$\mathrm{Cov}(\hat{x}_N) = E_N(I+\boldsymbol{BF})\hat{\boldsymbol{S}}(I+\boldsymbol{BF})^\intercal E_N^\intercal \leq P_f - \tilde{P}_N, \tag{4.129}$$

or, equivalently, as

$$\|\hat{\boldsymbol{S}}^{1/2}(I+\boldsymbol{BF})^{\mathsf{T}}E_N^{\mathsf{T}}(P_f-\tilde{P}_N)^{-1/2}\|\leq 1. \tag{4.130}$$

The matrix $(P_f-\tilde{P}_N)^{-1/2}$ exists since, by assumption, $P_f>\tilde{P}_N$.

Cost Function

The filtered state objective (4.103) has the same form as the original objective (4.10), except that the state is replaced by the filtered state. Thus, similar to (4.53), the filtered state objective can be rewritten as

$$\begin{aligned}\hat{J}(\boldsymbol{L},V)=\operatorname{tr}\left\{\left((I+\boldsymbol{BL})^{\mathsf{T}}\boldsymbol{Q}(I+\boldsymbol{BL})+\boldsymbol{L}^{\mathsf{T}}\boldsymbol{RL}\right)\hat{\boldsymbol{S}}\right\}\\ +\|\boldsymbol{A}\bar{x}_0+\boldsymbol{B}V-X^d\|_{\boldsymbol{Q}}^2+V^{\mathsf{T}}\bar{\boldsymbol{R}}V+\eta\sum_{k=0}^{N-1}\|E_k^uV\|.\end{aligned} \tag{4.131}$$

Note that, except for the matrix $\hat{\boldsymbol{S}}$, the structure of this cost function is the same as for the state feedback case. However, as we will see in the following, the optimal controls for the output feedback problem are differentiated from those for the state feedback case due to the interaction between the state constraints and the estimation error uncertainty.

4.3.4 Summary of Convex Solution

The convex formulation of the output feedback, chance-constrained covariance steering problem is summarized as follows.

$$\underset{\boldsymbol{L},V}{\text{minimize}} \quad \hat{J}(\boldsymbol{L},V) = \operatorname{tr}\left\{\left((I+\boldsymbol{B}\boldsymbol{L})^{\intercal}\boldsymbol{Q}(I+\boldsymbol{B}\boldsymbol{L})+\boldsymbol{L}^{\intercal}\boldsymbol{R}\boldsymbol{L}\right)\hat{\boldsymbol{S}}\right\} \tag{4.132a}$$

$$+\|\boldsymbol{A}\bar{x}_0+\boldsymbol{B}V-X^d\|_{\boldsymbol{Q}}^2+V^{\intercal}\bar{\boldsymbol{R}}V+\eta\sum_{k=0}^{N-1}\|E_k^uV\|$$

$$\text{subject to} \quad E_N(\boldsymbol{A}\bar{x}_0+\boldsymbol{B}V)=\bar{x}_f \tag{4.132b}$$

$$\|\hat{\boldsymbol{S}}^{1/2}(I+\boldsymbol{B}\boldsymbol{F})^{\intercal}E_N^{\intercal}(P_f-\tilde{P}_N)^{-1/2}\|\leq 1 \tag{4.132c}$$

$$\operatorname{cdfn}^{-1}(1-p_j^x)\left\|\begin{bmatrix}\hat{\boldsymbol{S}}^{1/2}(I+\boldsymbol{B}\boldsymbol{L})^{\intercal}E_k^{\intercal}\\ \tilde{P}_k^{1/2}\end{bmatrix}a_j\right\| \qquad \forall (k,j)\in\mathcal{X} \tag{4.132d}$$

$$+a_j^{\intercal}E_k(\boldsymbol{A}\bar{x}_0+\boldsymbol{B}V)\leq\alpha_j$$

$$\operatorname{cdfn}^{-1}(1-p_j^u)\|\hat{\boldsymbol{S}}^{1/2}\boldsymbol{L}E_k^{u\intercal}b_j\|+b_j^{\intercal}E_k^uV\leq\beta_j \qquad \forall (k,j)\in\mathcal{U} \tag{4.132e}$$

$$\begin{cases}\|E_k^uV\|+\|\hat{\boldsymbol{S}}^{1/2}\boldsymbol{L}^{\intercal}E_k^{u\intercal}\|\sqrt{2\log\dfrac{1}{p_{\text{fail}}^{\|u\|}}}\leq\rho & \text{if } m\leq 2\\ \qquad\qquad \forall k\in\{0,\dots,N-1\} & \\ \|E_k^uV\|+\|\hat{\boldsymbol{S}}^{1/2}\boldsymbol{L}^{\intercal}E_k^{u\intercal}\|\left(\sqrt{2\log\dfrac{1}{p_{\text{fail}}^{\|u\|}}}+\sqrt{m}\right)\leq\rho & \text{if } m>2\\ \qquad\qquad \forall k\in\{0,\dots,N-1\} & \end{cases} \tag{4.132f}$$

$$\text{where} \quad \hat{\boldsymbol{S}}=\boldsymbol{A}\hat{P}_{0\text{-}}\boldsymbol{A}^{\intercal}+\boldsymbol{F}\boldsymbol{P}_{\tilde{\boldsymbol{Y}}}\boldsymbol{F}^{\intercal} \tag{4.132g}$$

$$\boldsymbol{P}_{\tilde{\boldsymbol{Y}}} \text{ as in } (4.117) \tag{4.132h}$$

4.3.5 Numerical Example

Consider the double integrator system (4.79) described in Subsection 4.2.5 with, in addition, the observation model described by the matrices

$$C = \begin{bmatrix} 0 & 1 & 0 & 0 \\ 0 & 0 & 1 & 0 \\ 0 & 0 & 0 & 1 \end{bmatrix}, \quad D = \begin{bmatrix} 0.5 & 0 & 0 \\ 0 & 0.003 & 0 \\ 0 & 0 & 0.003 \end{bmatrix}. \tag{4.133}$$

Note that the first position coordinate is not measured. The state is initially distributed as in (4.80), with the initial covariance decomposed into the filtered state covariance and estimation error given by

$$\tilde{P}_{0\text{-}} = \begin{bmatrix} 0.03 & 0 & 0 & 0 \\ 0 & 0.01 & 0 & 0 \\ 0 & 0 & 0.014 & 0 \\ 0 & 0 & 0 & 0.014 \end{bmatrix}, \quad \hat{P}_{0\text{-}} = \begin{bmatrix} 0.07 & 0 & 0 & 0 \\ 0 & 0.09 & 0 & 0 \\ 0 & 0 & 0.006 & 0 \\ 0 & 0 & 0 & 0.006 \end{bmatrix}. \tag{4.134}$$

Note that $\tilde{P}_{0\text{-}} + \hat{P}_{0\text{-}} = P_0$. The final state is constrained as in (4.81). The convex optimization problem (4.132), with $\boldsymbol{L}$ block lower-triangular, was solved using YALMIP [117] with MOSEK [106]. Resulting trajectories are shown in Figures 4.3 and 4.4.

In this example it is clear that the resulting control depends on the observation model. Since the first position coordinate is not directly measured, there is a larger uncertainty in the estimated value of the first position coordinate compared to the second position coordinate. The controller compensates accordingly by using sufficient control effort along the first position coordinate so that the chance constraints are satisfied. We can see this by comparing the estimated state covariance and the estimation error covariance in Figure 4.4.

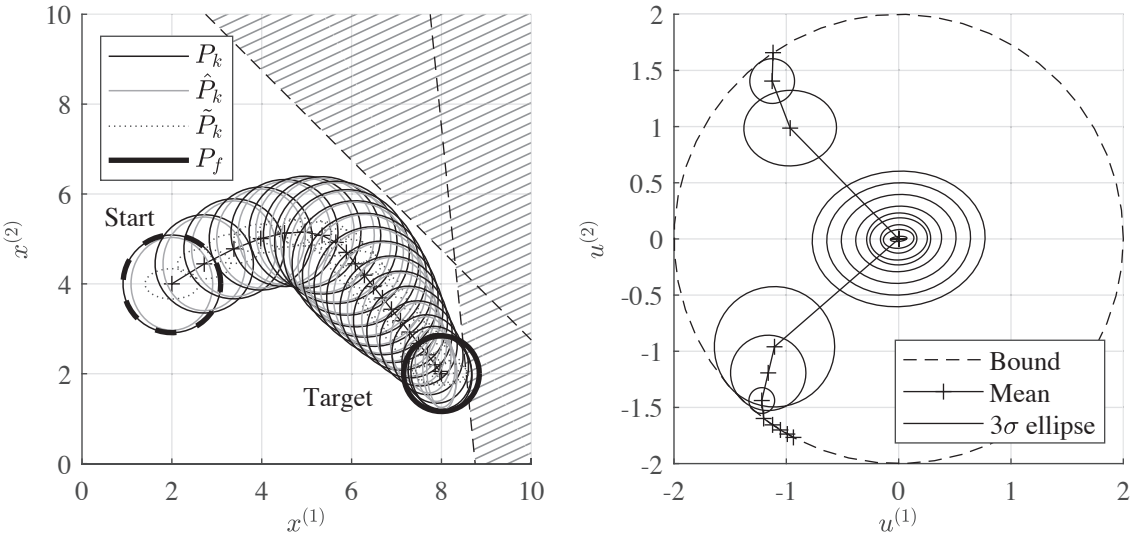

Figure 4.3: Position and control covariance evolution for the closed-loop double integrator system, where $x^{(i)}$ and $u^{(i)}$ denote coordinates of the state and control.

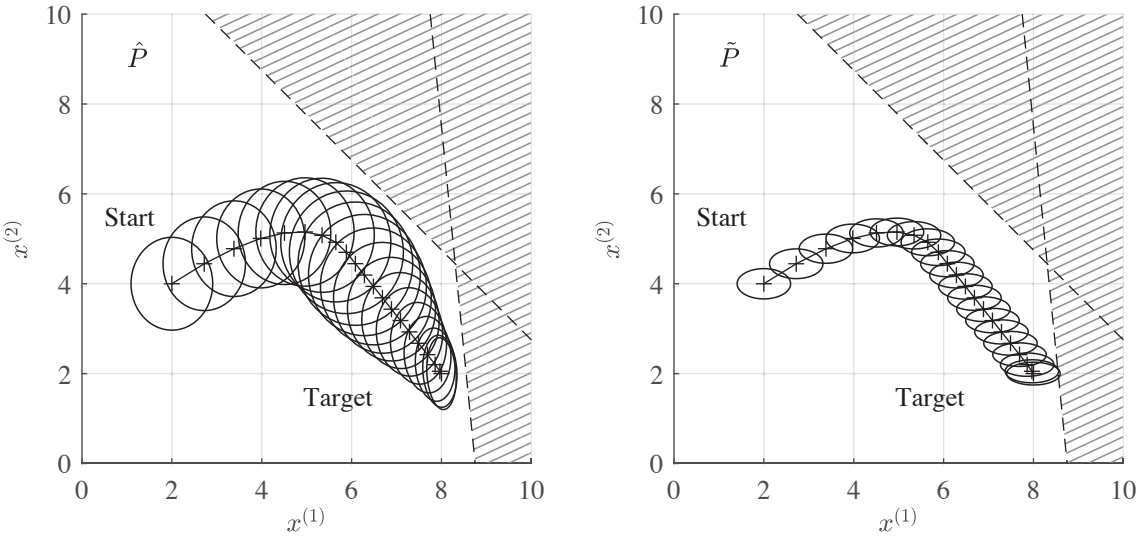

Figure 4.4: Estimated state covariance (left) and estimation error covariance (right).

4.4 Nonlinear Covariance Steering via Successive Linearization

In this section, we propose an algorithmic approach to solve the nonlinear CS problem by iteratively solving the linear CS problem with respect to the reference trajectory of the previous step. This algorithm, which we will refer to as iterative CS (iCS), is a natural extension of linear CS in the spirit of other well known successive approximation methods such as differential dynamic programming (DDP) [120] and iterative LQG (iLQG) [121], which both compute a feedback control by backwards propagating an approximation of the value function. For iCS, we similarly approximate the nonlinear dynamics about a reference trajectory, but, in contrast, the control updates are found by solving a convex program, which has the benefit of allowing direct consideration of probabilistic constraints at the cost of computation time and restricts the approximation of the dynamics to first order.

4.4.1 Problem Definition

Consider the nonlinear continuous-time stochastic system

$$\mathrm{d}x = f(x, u, t)\mathrm{d}t + g(x, t)\mathrm{d}w, \tag{4.135}$$

on the time interval $[t_0, t_f]$, where $x \in \mathbb{R}^n$ is the state, $u \in \mathbb{R}^m$ is the control, $w(t)$ is an n-dimensional Brownian motion, and the functions f and g are known. The state at the initial time $x(t_0)$ is Gaussian distributed as

$$x(t_0) \sim \mathcal{N}(\bar{x}_0, P_0), \tag{4.136}$$

with known mean $\bar{x}_0$ and known covariance P_0. Let $\mathscr{P} = (t_k : k = 0, \ldots, N)$ be a partition of the interval $[t_0, t_f]$, that is,

$$t_0 = t_{k=0} < \cdots < t_k < \cdots < t_{k=N} = t_f. \tag{4.137}$$

The control is assumed to be piecewise constant on subintervals of the partition $\mathscr{P}$, so that

$$u(t) = u(t_k), \quad t \in [t_k, t_{k+1}), \quad k = 0, \ldots, N-1. \tag{4.138}$$

We write $x_k = x(t_k)$ and $u_k = u(t_k)$ for notational simplicity. As in Section 4.2, the control is assumed to follow the state history feedback law

$$u_k = \sum_{\ell=0}^{k} K_{k,\ell} \tilde{x}_\ell + v_k, \tag{4.139}$$

where $\tilde{x}_\ell = x_\ell - \bar{x}_\ell$ is the state deviation from its mean, $K_{k,\ell} \in \mathbb{R}^{m \times n}$ are feedback gains, and $v_k \in \mathbb{R}^m$ are nominal controls. Thus, at each time t_k, the control is computed as a function of the states $x(t_0), \ldots, x(t_k)$, and is then held constant until the next decision time t_{k+1}. Since the control $u_k = u(t_k)$ depends only on state at or before the time t_k, the resulting control process is causal.

Aside from considering the nonlinear continuous-time system (4.135) in place of the linear discrete-time system (4.1), the problem definition in this section is the same as Section 4.2. The state and control are constrained at the discrete times t_k of the partition $\mathscr{P}$ to lie in convex polytopes as in (4.5) and (4.6), and we again relax the polytope chance constraints into N_x and N_u independent half-plane constraints (4.11) and (4.12). The control magnitude is further constrained in probability as in (4.7). The state at the final time t_f is constrained to have a prescribed mean $\bar{x}_f$ and a maximum covariance P_f as in (4.8). Finally, our objective is solve for the feedback gains $K_{k,\ell}$ and the nominal controls v_k that minimize the objective (4.10).

4.4.2 Approximation by a Linear Discrete-Time System

Linearization

Suppose we are provided with a reference control $\hat{u}(t)$ over the time interval $[t_0, t_f]$. The corresponding reference state process $\hat{x}(t)$ is obtained by integrating the deterministic system

$$\dot{\hat{x}} = f(\hat{x}, \hat{u}, t), \tag{4.140}$$

from the initial condition $\hat{x}(t_0) = \bar{x}_0$. The nonlinear system (4.135) is then linearized along the trajectory $(\hat{u}(t), \hat{x}(t))$ to obtain the linear stochastic system

$$\mathrm{d}x \approx (A(t)x + B(t)u + c(t))\mathrm{d}t + G(t)\mathrm{d}w, \tag{4.141}$$

where the system matrices are partial derivatives evaluated along the reference as

$$A(t) = \frac{\partial f}{\partial x}(\hat{x}(t), \hat{u}(t), t), \quad B(t) = \frac{\partial f}{\partial u}(\hat{x}(t), \hat{u}(t), t), \quad G(t) = g(\hat{x}(t), \hat{u}(t)), \tag{4.142}$$

$$c(t) = f(\hat{x}(t), \hat{u}(t), t) - A(t)\hat{x}(t) - B(t)\hat{u}(t). \tag{4.143}$$

Discretization

The state $x(t)$ at any time $t > t_k$ is approximately obtained by integrating the linear SDE (4.141), which admits the exact solution

$$x(t) = \Phi(t, t_k)x(t_k) + \int_{t_k}^{t} \Phi(t, s)\big(B(s)u(s) + c(s)\big)\mathrm{d}s + \int_{t_k}^{t} \Phi(t, s)G(s)\mathrm{d}w(s), \tag{4.144}$$

in terms of the state transition matrix $\Phi(t, s)$ corresponding to the state matrix $A(t)$; that is, $\Phi(t, s)$ is an invertible matrix that satisfies

$$\frac{\partial}{\partial t}\Phi(t, t_0) = A(t)\Phi(t, t_0), \quad \Phi(t_0, t_0) = I, \tag{4.145}$$

from which it can be shown that $\Phi(t,s) = \Phi(t,t_0)\Phi^{-1}(s,t_0)$. Note that the solution in (4.144) is an approximation only due to the linearization (4.141), and not from the integration. Substituting the control $u(t) = u_k$ from (4.138), and letting $t = t_{k+1}$, we obtain the discrete-time system

$$x_{k+1} = \Phi(t_{k+1},t_k)x_k + \int_{t_k}^{t_{k+1}} \Phi(t_{k+1},s)B(s)\mathrm{d}s\, u_k \\ + \int_{t_k}^{t_{k+1}} \Phi(t_{k+1},s)c(s)\mathrm{d}s + \int_{t_k}^{t_{k+1}} \Phi(t_{k+1},s)G(s)\mathrm{d}w(s). \quad (4.146)$$

The stochastic integral in (4.146) is a Gaussian random vector with mean

$$\mathbb{E}\bigg(\int_{t_k}^{t_{k+1}} \Phi(t_{k+1},s)G(s)\mathrm{d}w(s) \bigg) = 0, \quad (4.147)$$

and, using Itô's isometry, covariance

$$\mathbb{E}\bigg(\int_{t_k}^{t_{k+1}} \Phi(t_{k+1},t)G(t)\,\mathrm{d}w(t) \int_{t_k}^{t_{k+1}} \Phi(t_{k+1},t)G(t)\,\mathrm{d}w(t) \bigg) \\ = \int_{t_k}^{t_{k+1}} \Phi(t_{k+1},t)G(t)G^{\mathsf{T}}(t)\Phi^{\mathsf{T}}(t_{k+1},t)\,\mathrm{d}t. \quad (4.148)$$

Thus, if $w_k \in \mathbb{R}^n$ is a standard Gaussian random vector, and if $G_k \in \mathbb{R}^{n\times n}$ is any matrix such that $G_k^{\mathsf{T}}G_k$ equals (4.148), then

$$G_k w_k \overset{\mathrm{d}}{=} \int_{t_k}^{t_{k+1}} \Phi(t_{k+1},s)G(s)\mathrm{d}w(s), \quad (4.149)$$

where $\overset{\mathrm{d}}{=}$ denotes equality in distribution. The matrix G_k may be computed, for example, as the Cholesky decomposition of the integral (4.148). We rewrite (4.146) as

$$x_{k+1} = A_k x_k + B_k u_k + c_k + G_k w_k, \quad (4.150)$$

in terms of the matrices

$$A_k = \Phi(t_{k+1}, t_k), \quad B_k = \int_{t_k}^{t_{k+1}} \Phi(t_{k+1}, s)B(s)\mathrm{d}s, \quad c_k = \int_{t_k}^{t_{k+1}} \Phi(t_{k+1}, s)c(s)\mathrm{d}s. \tag{4.151}$$

Since segments $\big(w(t) : t \in [t_k, t_{k+1})\big)$ and $\big(w(s) : s \in [t_\ell, t_{\ell+1})\big)$, for $k \neq \ell$, of the Brownian motion $w(t)$ are independent, it follows that the Gaussian random vectors (w_k) in (4.151) are independent.

In summary, the solution (x_k) of the difference equation (4.150), with the initial condition $x_0 = x(t_0)$, equals, in distribution, the solution $x(t)$ of the linear SDE (4.141) at the times t_k for $k = 0, \ldots, N$.

Block Matrix Formulation

The linear discrete-time system (4.150) may be equivalently written in block-matrix notation as

$$\begin{bmatrix} x_0 \\ x_1 \\ x_2 \\ \vdots \end{bmatrix} = \begin{bmatrix} I \\ A_0 \\ A_1A_0 \\ \vdots \end{bmatrix} x_0 + \begin{bmatrix} 0 & 0 & \\ B_0 & 0 & \\ A_1B_0 & B_1 & \\ & & \ddots \end{bmatrix} \begin{bmatrix} u_0 \\ u_1 \\ \vdots \end{bmatrix}$$
$$+ \begin{bmatrix} 0 & 0 & \\ I & 0 & \\ A_1I & I & \\ & & \ddots \end{bmatrix} \begin{bmatrix} c_0 \\ c_1 \\ \vdots \end{bmatrix} + \begin{bmatrix} 0 & 0 & \\ G_0 & 0 & \\ A_1G_0 & G_1 & \\ & & \ddots \end{bmatrix} \begin{bmatrix} w_0 \\ w_1 \\ \vdots \end{bmatrix}. \tag{4.152}$$

For appropriately constructed block matrices $\boldsymbol{A}$, $\boldsymbol{B}$, and $\boldsymbol{G}$, as in Section 4.2, and with the column vector $C \in \mathbb{R}^{(N+1)n}$ resulting from the matrix multiplication involving the (c_k)

terms in (4.152), the filtered state process can be written as the linear matrix equation

$$X = \boldsymbol{A}x_0 + \boldsymbol{B}U + C + \boldsymbol{G}W. \tag{4.153}$$

This system is the same as that treated in the previous sections, except for the addition of the drift term C. We therefore proceed following the analysis from Section 4.2, with the new decision variable $\boldsymbol{L}$ in place of $\boldsymbol{K}$. Since the addition of the drift term C only affects the mean state process by

$$\bar{X} = \boldsymbol{A}\bar{x}_0 + \boldsymbol{B}V + C, \tag{4.154}$$

we omit the details and instead present the resulting convex optimization problem, following the introduction of additional constraints.

4.4.3 Iterative Covariance Steering

Trust Region Constraints

The linear approximation of the system dynamics is only valid in a neighborhood around the reference trajectory, so care must be taken to ensure that the optimal controls for the linear problem are relevant to the nonlinear problem. For this reason, variations in the state and the control from the previous solution are bounded inside a *trust region* [24] defined by the constraints

$$\|\bar{x}_k - \hat{x}_k\|_{M_k^x} \leq \Delta^x, \quad k = 1, \ldots, N, \tag{4.155}$$

$$\|\bar{u}_k - \hat{u}_k\|_{M_k^u} \leq \Delta^u, \quad k = 0, \ldots, N-1, \tag{4.156}$$

where M_k^x and M_k^u are positive semi-definite weight matrices, Δ^x and Δ^u are given deviation limits, and $\hat{x}_k = \hat{x}(t_k)$ and $\hat{u}_k = \hat{u}(t_k)$ are the nominal state and control at the discrete times t_k.

Summary of Convex Solution

In summary, the original continuous-time stochastic optimal control problem has been approximated in the neighborhood of a provided reference trajectory as the following deterministic convex optimization problem.

$$\underset{\boldsymbol{L},V}{\text{minimize}} \quad J(\boldsymbol{L},V) = \operatorname{tr}\left\{\left((I+\boldsymbol{B}\boldsymbol{L})^\intercal \boldsymbol{Q}(I+\boldsymbol{B}\boldsymbol{L}) + \boldsymbol{L}^\intercal \boldsymbol{R}\boldsymbol{L}\right)\boldsymbol{S}\right\} \tag{4.157a}$$
$$+\|\boldsymbol{A}\bar{x}_0 + \boldsymbol{B}V + C - X^d\|_{\boldsymbol{Q}}^2 + V^\intercal \bar{\boldsymbol{R}} V + \eta \sum_{k=0}^{N-1} \|E_k^u V\|$$

$$\text{subject to} \quad E_N(\boldsymbol{A}\bar{x}_0 + \boldsymbol{B}V + C) = \bar{x}_f \tag{4.157b}$$

$$\|\boldsymbol{S}^{1/2}(I+\boldsymbol{B}\boldsymbol{L})^\intercal E_N^\intercal P_f^{-1/2}\| \le 1 \tag{4.157c}$$

$$\operatorname{cdfn}^{-1}(1-p_j^x)\|\boldsymbol{S}^{1/2}(I+\boldsymbol{B}\boldsymbol{L})E_k^\intercal a_j\| + a_j^\intercal E_k(\boldsymbol{A}\bar{x}_0 + \boldsymbol{B}V + C) \le \alpha_j \qquad \forall (k,j) \in \mathcal{X} \tag{4.157d}$$

$$\operatorname{cdfn}^{-1}(1-p_j^u)\|\boldsymbol{S}^{1/2}\boldsymbol{L}E_k^{u\intercal} b_j\| + b_j^\intercal E_k^u V \le \beta_j \qquad \forall (k,j) \in \mathcal{U} \tag{4.157e}$$

$$\begin{cases} \|E_k^u V\| + \|\boldsymbol{S}^{1/2}\boldsymbol{L}^\intercal E_k^{u\intercal}\| \sqrt{2\log\dfrac{1}{p_{\text{fail}}^{\|u\|}}} \le \rho & \text{if } m \le 2 \\ \qquad\qquad \forall k \in \{0,\dots,N-1\} & \\ \|E_k^u V\| + \|\boldsymbol{S}^{1/2}\boldsymbol{L}^\intercal E_k^{u\intercal}\| \left(\sqrt{2\log\dfrac{1}{p_{\text{fail}}^{\|u\|}}} + \sqrt{m}\right) \le \rho & \text{if } m > 2 \\ \qquad\qquad \forall k \in \{0,\dots,N-1\} & \end{cases} \tag{4.157f}$$

$$\|E_k(\boldsymbol{A}\bar{x}_0 + \boldsymbol{B}V + C) - \hat{x}_k\|_{M_k^x} \le \Delta^x \qquad \forall k \in \{0,\dots,N-1\} \tag{4.157g}$$

$$\|E_k^u V - \hat{u}_k\|_{M_k^u} \le \Delta^u \qquad \forall k \in \{1,\dots,N\} \tag{4.157h}$$

$$\text{where} \quad \boldsymbol{S} = \boldsymbol{A}P_0\boldsymbol{A}^\intercal + \boldsymbol{G}\boldsymbol{G}^\intercal \tag{4.157i}$$

After solving this problem, the gain matrices $(K_{k,i})$ are computed from $\boldsymbol{L}$ per (4.25) and the feedforward controls v_k and expected states $\bar{x}_k = \mathbb{E}(x(t_k))$ are given in V and $\bar{X}$, respectively, thus obtaining a feedback law of the desired form (4.139).

Iterative Covariance Steering Algorithm

The solution to the original optimal control problem is obtained by successively solving the approximate convex problem, where the optimal control obtained during each iteration is used to propagate the nonlinear system, as in (4.140), in order to obtain the reference trajectory for the following iteration [70]. In the context of deterministic optimal control, this method is often referred to as successive linearization or successive convexification [24, 122]; in the absence of constraints, this procedure reduces to iterative linear quadratic Gaussian control (iLQG) [121]. The resulting iterative solution procedure, which we refer to as iterative covariance steering (iCS) [70], is summarized in Algorithm 2.

Algorithm 2: Iterative covariance steering (iCS)

Input: Initial state mean and covariance $\bar{x}_0$, P_0, initial control guess $\hat{u}$, time partition $\mathscr{P}$

Output: Control law parameters $(K_{k,\ell})$, (v_k), $(\bar{x}_k)$

while *termination criteria not met* **do**
- Propagate nominal trajectory (4.140);
- Linearize (4.141);
- Discretize and construct block matrix system (4.152);
- Solve convex program (4.157);
- Solve feedback gain $\boldsymbol{K}$ from $\boldsymbol{L}$ as in (4.25);
- Set control law (4.139);
- Set new nominal control $\hat{u}_k \leftarrow \bar{u}_k$;

end

4.5 Application to Spacecraft Guidance

In this section, we apply the iCS method developed in Section 4.4 to the problem of guiding a spacecraft on an Earth-to-Mars transfer with a low-thrust engine. For simplicity, the orbits of Earth and Mars are assumed to be co-planar and the spacecraft mass-change dynamics are neglected. The position $r \in \mathbb{R}^2$ and velocity $v \in \mathbb{R}^2$ of the spacecraft are given in a Sun-centered inertial frame, and external perturbing accelerations are modeled as a two-dimensional Brownian motion $w(t)$. At the initial time t_0, the spacecraft state $x = (r, v)$ is

assumed to be normally distributed as

$$x(t_0) = x_0 \sim \mathcal{N}(\bar{x}_0, P_0), \tag{4.158}$$

where the vector $\bar{x}_0 = (\bar{r}_0, \bar{v}_0)$ and the positive semi-definite matrix P_0 are both fixed and known. From this initial time, the spacecraft trajectory is described by the SDE

$$\mathrm{d}\begin{bmatrix} r \\ v \end{bmatrix} = \begin{bmatrix} v \\ -\mu r / \|r\|^3 + u \end{bmatrix} \mathrm{d}t + \begin{bmatrix} 0 \\ \sigma I \end{bmatrix} \mathrm{d}w, \tag{4.159}$$

where μ is the gravitational parameter of the Sun, σ is a positive scalar indicating the disturbance intensity, and $u \in \mathbb{R}^2$ is the commanded thrust acceleration, which is constrained in magnitude by

$$\|u\| \leq u_{\max}. \tag{4.160}$$

The initial state covariance is given as

$$P_0 = \mathrm{diag}(10^2\,\mathrm{km}^2, 10^2\,\mathrm{km}^2, 0.1^2\,\mathrm{km}^2/\mathrm{s}^2, 0.1^2\,\mathrm{km}^2/\mathrm{s}^2), \tag{4.161}$$

and the final covariance is constrained by to be less than

$$P_{x_f} = \mathrm{diag}(0.0447\,\mathrm{AU}^2, 0.0447\,\mathrm{AU}^2, 0.3336\,\mathrm{AU}^2/\mathrm{day}^2, 0.3336\,\mathrm{AU}^2/\mathrm{day}^2) \times 10^{-4}. \tag{4.162}$$

The running cost weights are give by

$$Q = \mathrm{diag}(0.1\,\mathrm{AU}^{-2}, 0.1\,\mathrm{AU}^{-2}, 0.001\,\mathrm{day}^2/\mathrm{AU}^2, 0.001\,\mathrm{day}^2/\mathrm{AU}^2), \tag{4.163}$$

$$R = 0.1I\,\mathrm{day}^2/\mathrm{AU}. \tag{4.164}$$

Table 4.1: Parameters for Earth-to-Mars transfer example [95]

Property	Value	Unit
$\bar{r}_0$	$(-0.94052, -0.34502)$	AU
$\bar{v}_0$	$(9.7746, -28.078)$	km/s
$\bar{r}_f$	$(-1.1543, 1.1829)$	AU
$\bar{v}_f$	$(-16.427, -14.861)$	km/s

Property	Value	Unit
$t_f - t_0$	348.79	days
$u_{\max}$	1×10^{-3}	m/s^2
σ	$0.2 \times u_{\max}$	-
μ	1.3271×10^{20}	m^3/s^2
N	40	-

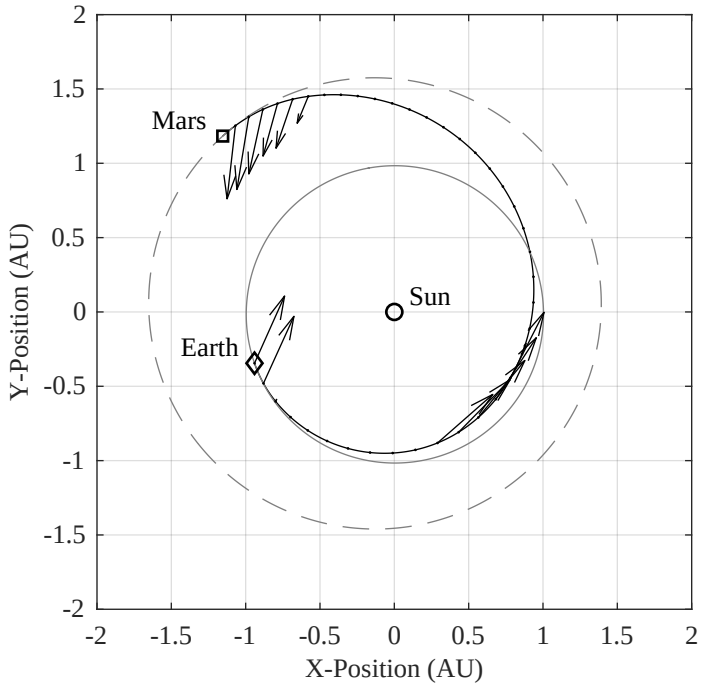

Figure 4.5: Nominal trajectory and controls with discrete times indicated as dots along the trajectory.

Following the initial covariance provided in km and km/s, the problem was converted into astronomical units and days, and hence the final covariance and running costs are provided in these units. The remainder of the problem parameters are listed in Table 4.1. We remark that these parameters are approximately equal to the parameters from the numerical example presented in Ref. [95]. The disturbance intensity, final covariance, and running cost weights, however, are arbitrarily set for the purposes of numerical demonstration.

The initial control guess was obtained as the solution to the nominal optimal control problem using an existing solver with a fixed margin on the maximum throttle[1]. The al-

[1]GPOPS-II [123] was used to solve for the initial trajectory.

gorithm ran for five iterations, and the resulting nominal trajectory is shown in Figure 4.5. The nominal control with Monte Carlo samples is shown in Figure 4.6 and the evolution of the position covariance for both open and closed-loop control simulations is shown in Figure 4.7. The final state covariance is

$$\mathrm{Cov}\left(x(t_f)\right) = \begin{bmatrix} 0.4468 & 0.0000 & 0.0128 & 0.0078 \\ 0.0000 & 0.4468 & 0.0051 & 0.0102 \\ 0.0128 & 0.0051 & 0.0022 & 0.0014 \\ 0.0078 & 0.0102 & 0.0014 & 0.0011 \end{bmatrix} \times 10^{-5}, \tag{4.165}$$

in units of AU for position values and AU/day for velocity values, which is less than the maximum allowed covariance (4.162).

Due to the control magnitude chance constraint, the controller plans for more aggressive feedback when the optimal open-loop control is not near the maximum value. Furthermore, as we can see in Figure 4.6, the nominal control does not immediately increase to its maximum value during the final approach segment as would be the case for an optimal deterministic controller. Instead, the nominal control is set so as to reserve a margin for the corrective actions that are necessary to meet the final covariance constraint. If the final covariance constraint is tightened, then we expect that a larger margin will be left on the nominal control. This behavior demonstrates the benefit of coupling the design of the reference trajectory to the design of the feedback gains.

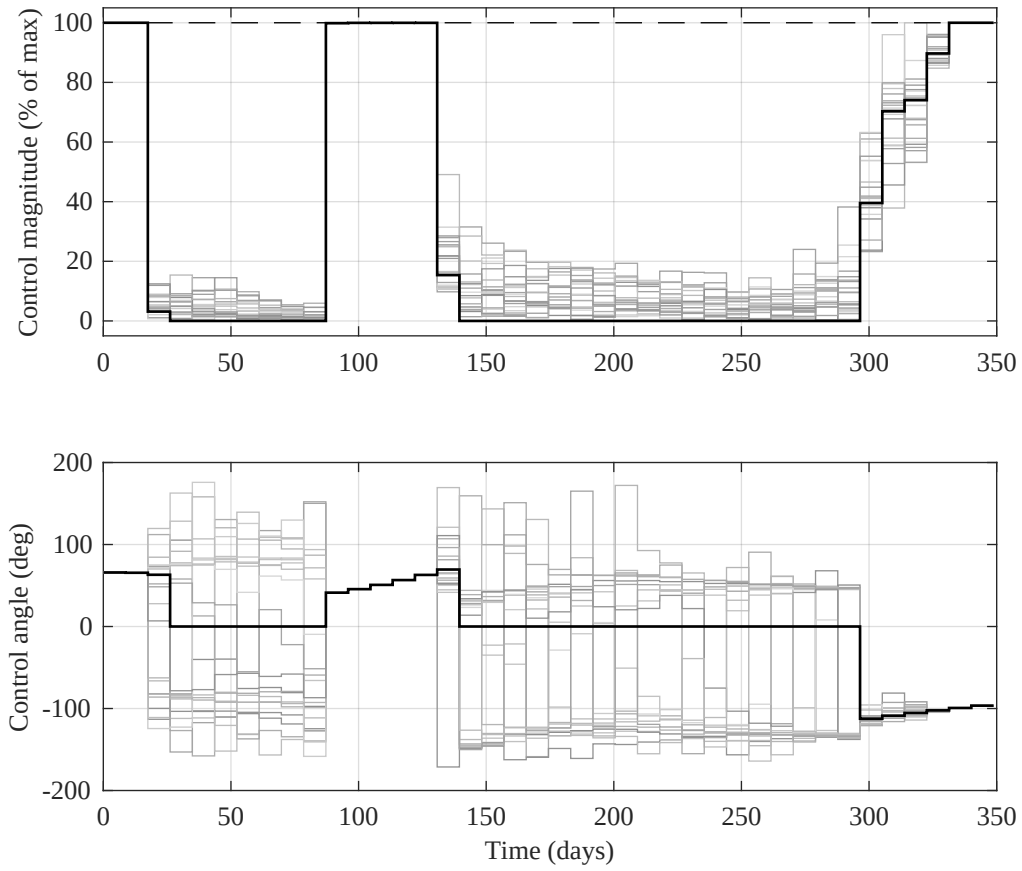

Figure 4.6: Nominal control (black) with sample control trajectories (gray).

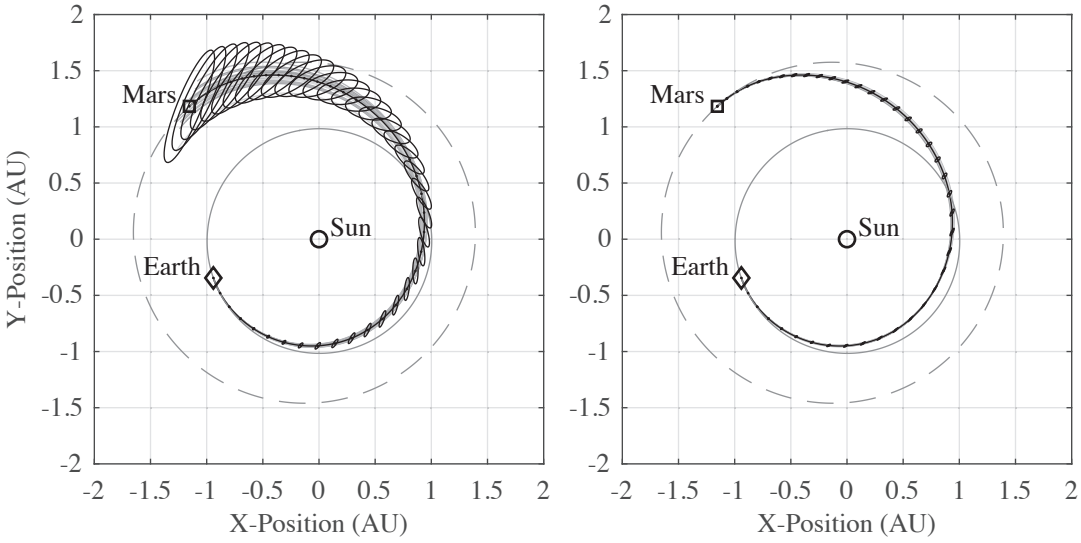

Figure 4.7: Open-loop (left) and closed-loop (right) position covariances at each time step.

CHAPTER 5
COVARIANCE STEERING WITH SPATIALLY-DEPENDENT UNCERTAINTY

The material in this chapter is based on Ref. [124].

5.1 Introduction

Random disturbances acting on autonomous systems are often spatially dependent. Examples include variations in atmospheric properties [66], underwater currents [125], and gravitational fields [126]. The uncertain nature of these disturbances leads the system state to be a random variable with statistics determined by the system dynamics, the probabilistic structure of the disturbances, and the system control law. While system dynamics and the probabilistic structure of the disturbances are fixed, it is possible to design the feedback controls to desirably shape the evolution of the system probability distribution. Indeed, as we have shown in the previous chapter, steering the state covariance of a Gaussian distributed system can be formulated as a convex optimization over the nominal control and the feedback gains. However, the stochastic control literature — including the work in the previous chapter — is primarily concerned with systems affected by temporal disturbances, such as Brownian motion, rather than spatial disturbances. The aim of this chapter is to bridge the gap between the treatment of spatial and temporal disturbances for feedback control design, and to solve for affine feedback laws that explicitly steer the mean and covariance of the system state, subject to chance constraints, while the system is affected by spatially-dependent uncertainty.

In this chapter, we model spatial uncertainty as a Gaussian random field (GRF), which can be thought of as a generalization of the Gaussian distribution to function spaces [127]. Similarly to a Gaussian random vector, a GRF is fully characterized by a mean and a covariance function. Indeed, for any finite number of inputs, such as a set of position

vectors, the values of the GRF at the input points are jointly Gaussian distributed with mean and covariance determined by evaluating the mean and covariance functions at the input points.

GRF models are widely applied in the fields of spatial analysis [128, 129], machine learning [127], robotics [130, 131, 132], and state estimation [126, 133]. For many applications, including the aforementioned references, GRF models are primarily used for either regression or for characterization of a to-be-explored unknown environment. This chapter, in contrast, is concerned with using a GRF to characterize disturbances to be handled by feedback control, similar to how disturbances are treated in classical stochastic control, such as Linear Quadratic Gaussian (LQG) control.

We take as a motivating example the problem of aerocapture, which is an orbital aeroassist maneuver where a spacecraft uses a planet's atmosphere to decelerate from a hyperbolic orbit into a captured elliptical orbit around the planet [50]. By design, the spacecraft must fly through the atmosphere of another planet, which may not be well characterized, at orbital velocity. Descending into the lower atmosphere results in (exponentially) higher density and thus more drag, which increases the effectiveness of the maneuver — but the perturbing effect of density variations is also much greater at the lower attitudes. Furthermore, assuming that atmospheric density variations depend, at least partly, on the altitude, the density variations seen by the vehicle following periapsis are correlated to previously encountered variations [66, 107]. While the atmospheric density uncertainty is a major driver of performance, no methodology currently exists to *explicitly* treat the atmospheric uncertainty for guidance and control optimization. Rather, the state-of-the-art closed-loop predictor-corrector guidance successively treats the atmosphere as being equal to an onboard current best estimate, and performs a deterministic optimization [64]. The resulting guidance performance is evaluated through Monte Carlo that does include spatial density variations, and guidance parameters are tuned based on the Monte Carlo results [59, 68].

This chapter takes a sequential optimization approach to solve for both a feedforward

(nominal) control and corresponding state feedback gains. We begin with a nominal trajectory that does not account for uncertainty, and which takes the GRF to be equal to its mean value. This trajectory may be the solution to a deterministic optimal control problem, for example. Assuming that, in the presence of uncertainty, the trajectory will not deviate too far from its nominal value, the perturbing effect of the GRF can be approximated by the statistics of the GRF evaluated along the nominal trajectory. In other words, the nominal trajectory serves as a mapping between time and space, which is used to reduce the spatial GRF to a temporal process. Trajectory disturbances due to the GRF are then approximated by a sequence of jointly Gaussian random vectors, the statistics of which depend on both the structure of the GRF and the nominal trajectory. Thus, the linearized optimal control subproblem is reduced to the more tractable situation of a linear system being affected by temporal disturbances.

For linear stochastic systems with additive Gaussian disturbances, it is well known that the nominal control steers the state mean while the feedback gains steer the state covariance. Chance constraints, however, depend on both the state mean and the covariance. Thus, the chance-constrained optimal control of a linear stochastic system involves a joint optimization over the nominal control and the feedback gains. This problem is referred to as chance-constrained covariance steering, since the control law is designed to explicitly steer the dynamics of the state covariance [75, 101]. Previous works have shown that state history feedback laws result in a convex formulation of the chance constrained covariance steering problem [76, 71, 70, 91]. For the present problem, we may therefore jointly optimize updates to the nominal control and the feedback gains, while considering the local effect of the GRF-induced disturbances, and while enforcing chance constraints. Finally, the optimal control from each linearized subproblem is used to propagate the nominal, nonlinear dynamics to obtain the reference trajectory for the subsequent iterate.

This chapter is organized as follows. Properties of GRFs are reviewed in Section 5.2. The stochastic optimal control problem of chance-constrained covariance steering in a GRF

is introduced in Section 5.3. In Section 5.4, a solution to this problem is developed by successive convexification. The proposed method is first applied to a simple double integrator problem in Section 5.5.1, and is then applied to the aerocapure guidance problem in Section 5.5.2. Finally, we conclude in Section 5.6.

5.2 Gaussian Random Fields

A collection of random variables $\big(\Psi(z) : z \in \mathcal{F}\big)$ is a *Gaussian random field* (GRF), also referred to as a Gaussian process, if any finite linear combination of the variables $\Psi(z_i)$ with $\{z_i\} \subset \mathcal{F}$ is Gaussian distributed — that is, if the variables $\Psi(z_i)$ are *jointly Gaussian* [113, 127]. A GRF is fully characterized by a mean function

$$\mu : \mathcal{F} \to \mathbb{R}, \quad \mu(z) = \mathbb{E}\big(\Psi(z)\big), \tag{5.1}$$

and a positive semi-definite covariance function

$$\Sigma : \mathcal{F} \times \mathcal{F} \to \mathbb{R}, \quad \Sigma(z_1, z_2) = \mathrm{Cov}\left(\Psi(z_1), \Psi(z_2)\right). \tag{5.2}$$

Thus, the values of the field $\Psi_* = \big(\Psi(z_1^*), \ldots, \Psi(z_n^*)\big)$ at any n input points $\{z_1^*, \ldots, z_n^*\} \subset \mathcal{F}$ are Gaussian distributed as $\Psi_* \sim \mathcal{N}(\mu_*, \Sigma_{*,*})$, where

$$\mu_* = \begin{bmatrix} \mu(z_1^*) \\ \vdots \\ \mu(z_n^*) \end{bmatrix}, \qquad \Sigma_{*,*} = \begin{bmatrix} \Sigma(z_1^*, z_1^*) & \cdots & \Sigma(z_1^*, z_n^*) \\ \vdots & \ddots & \vdots \\ \Sigma(z_n^*, z_1^*) & \cdots & \Sigma(z_n^*, z_n^*) \end{bmatrix}. \tag{5.3}$$

Suppose that $y \in \mathbb{R}^m$ is a vector of measurements $y_i = \Psi(z_i^m) + \varepsilon_i$ taken at the points $\{z_1^m, \ldots, z_m^m\} \subset \mathcal{F}$, with the measurement noise $\varepsilon_i \overset{i.i.d}{\sim} \mathcal{N}(0, \sigma^2)$. Let $\mu_m \in \mathbb{R}^m$ be a vector with coordinates $\mu(z_i)$, and let $\Sigma_{*,m} = \Sigma_{m,*}^\intercal \in \mathbb{R}^{n \times m}$ and $\Sigma_{m,m} \in \mathbb{R}^{m \times m}$ be matrices with entries $\Sigma(z_i^*, z_j^m)$ and $\Sigma(z_i^m, z_j^m)$. Then, the values Ψ_*, conditioned on the measurement

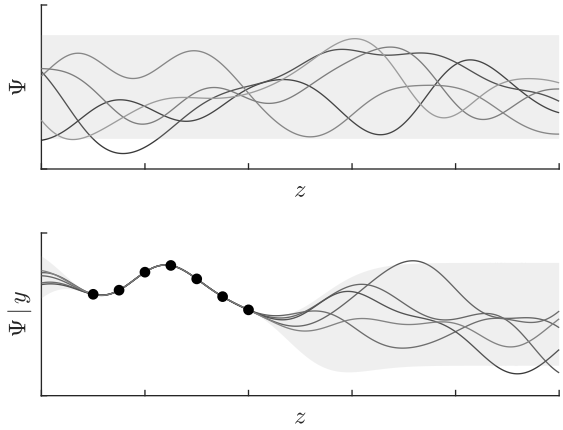

Figure 5.1: Single-dimensional GRF Ψ conditioned on measurements

data, are distributed as $\Psi_* \mid y \sim \mathcal{N}(\mu_{*|m}, \Sigma_{*,*|m})$, where

$$\mu_{*|m} = \mu_* + \Sigma_{*,m}(\Sigma_{m,m} + \sigma^2 I)^{-1}(y - \mu_m), \tag{5.4}$$

$$\Sigma_{*,*|m} = \Sigma_{*,*} - \Sigma_{*,m}(\Sigma_{m,m} + \sigma^2 I)^{-1}\Sigma_{m,*}. \tag{5.5}$$

Examples of conditioning on measurements are shown in Figures 5.1 and 5.2. Computing the matrix inverse $(\Sigma_{m,m} + \sigma^2 I)^{-1}$, however, incurs cubic computational complexity in the number of measurements.

5.3 Problem Formulation

Consider a system with state $x \in \mathbb{R}^n$, and let $\big(\Psi(z) \in \mathbb{R} : z \in \mathbb{R}^d\big)$ be a GRF with known mean function $\mu : \mathbb{R}^d \to \mathbb{R}$ and known covariance function $\Sigma : \mathbb{R}^d \times \mathbb{R}^d \to \mathbb{R}$. The independent variable z of the GRF Ψ is a function of the system state, given by $z = \phi(x)$. Let the system state evolve according to

$$\dot{x} = f\big(x, u, \Psi(\phi(x))\big), \tag{5.6}$$

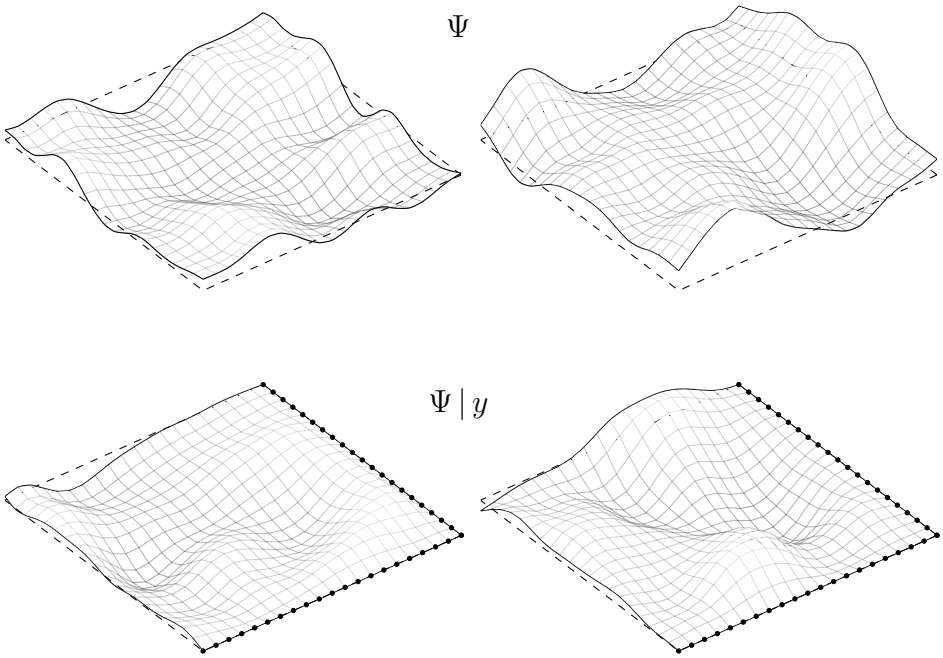

Figure 5.2: Two-dimensional GRF Ψ conditioned to have the right-most edges be constant

with the initial condition

$$x(t_0) \sim \mathcal{N}(\bar{x}_0, P_0), \tag{5.7}$$

where $u \in \mathbb{R}^m$ is the control input, and where the mean vector $\bar{x}_0$ and covariance matrix P_0 are both fixed and known. The initial state x_0 is assumed to be independent of the field Ψ. The evolution of the system (5.6) is considered on the discrete time partition

$$\mathscr{P} = \big(t_0, \ldots, t_N\big), \tag{5.8}$$

for a given time horizon N, and such that $t_N = t_f > 0$ is a given, fixed final time.

The control is assumed to be piecewise constant on subintervals of the partition $\mathscr{P}$, so that

$$u(t) = u(t_k), \quad t \in [t_k, t_{k+1}), \quad k = 0, \ldots, N-1. \tag{5.9}$$

We write $x_k = x(t_k)$ and $u_k = u(t_k)$ for notational simplicity. The control is assumed to

follow the state history feedback law

$$u_k = \sum_{\ell=0}^{k} K_{k,\ell}\tilde{x}_\ell + v_k, \tag{5.10}$$

where $\tilde{x}_\ell = x_\ell - \bar{x}_\ell$ is the state deviation from its mean, $K_{k,\ell} \in \mathbb{R}^{m\times n}$ are feedback gains, and where $v_k \in \mathbb{R}^m$ are nominal controls. As will be shown in the following sections, state history feedback results in a convex formulation of the chance-constrained covariance steering problem. Intuitively, and in contrast to Brownian-disturbance driven processes, state history feedback is required since, due to the GRF Ψ, the state process may not be Markovian.

The state and controls must satisfy the chance constraints

$$\mathbb{P}\big(a_{i,k}^\mathsf{T} x_k \geq \alpha_{i,k}\big) \leq p_{i,k}^x, \quad \forall (i,k) \in \mathcal{X}, \tag{5.11}$$

$$\mathbb{P}\big(b_{i,k}^\mathsf{T} u_k \geq \beta_{i,k}\big) \leq p_{i,k}^u, \quad \forall (i,k) \in \mathcal{U}, \tag{5.12}$$

where the vectors $a_{i,k} \in \mathbb{R}^n$, $b_{i,k} \in \mathbb{R}^m$ and scalars $\alpha_{i,k}$, $\beta_{i,k}$ define half-plane constraints, and $p_{i,k}^x, p_{i,k}^u \in (0, 0.5)$ are maximum probabilities of constraint violation; the index sets $\mathcal{X}$ and $\mathcal{U}$ determine the number of half-plane constraints to enforce at each decision time t_k. Furthermore, the mean and covariance of the state at the final time $x_f = x(t_f)$ are constrained by

$$\mathbb{E}(x_f) = \bar{x}_f, \tag{5.13a}$$

$$\mathrm{Cov}(x_f) \leq P_f, \tag{5.13b}$$

for a given target mean state $\bar{x}_f$ and positive definite maximum final covariance matrix P_f. Subject to the aforementioned constraints, we are concerned with finding the feedback

gains $K_{k,\ell}$ and feedforward controls v_k to minimize the quadratic cost

$$J_1(K_{k,\ell}, v_k) = \mathbb{E}\left(\sum_{k=0}^{N-1} (x_k - x_k^d)^\intercal Q_k (x_k - x_k^d) + \tilde{u}_k^\intercal R_k \tilde{u}_k \right) + \sum_{k=0}^{N-1} \bar{u}_k^\intercal \bar{R}_k \bar{u}_k, \tag{5.14}$$

for user-defined state and control weight matrices $Q_k \geq 0$ and $R_k, \bar{R}_k \geq 0$, and where x_k^d is a given defined desired trajectory. The cost weight is separated into R_k and $\bar{R}_k$ so that, if desired, the control variance may be penalized without penalizing the nominal control. Alternatively, the upper $1 - p_f$ percentile of a functional of the state may be minimized by considering the cost

$$J_2(K_{k,\ell}, v_k) = \inf\{\gamma \in \mathbb{R} : \mathbb{P}(\xi^\intercal x_f > \gamma) \leq p_f\}, \tag{5.15}$$

where $\xi \in \mathbb{R}^n$ and $p_f \in (0, 1)$ are user-defined constants. Note that, when seeking to minimize the upper percentile cost (5.15), the final state mean should not be constrained, since changing the final state mean may affect the cost value.

Without loss of generality, we take the cost to be the weighted sum

$$J = J_1 + \eta J_2, \tag{5.16}$$

for some non-negative scalar η. Indeed, setting Q_k, R_k, and $\bar{R}_k$ to zero and $\eta = 1$, we recover the $1 - p_f$ percentile cost (5.15), whereas setting $\eta = 0$ results in the purely quadratic cost (5.14).

5.4 Solution via Successive Convex Programming

5.4.1 Approximation About a Nominal Trajectory

Assume that a nominal control input $\hat{u}$ is provided on the time interval $[t_0, t_f]$, and let the corresponding nominal state be the solution to the system

$$\dot{\hat{x}} = f\big(\hat{x}, \hat{u}, \mathbb{E}(\Psi(\phi(\hat{x})))\big), \tag{5.17}$$

with the initial value $\hat{x}(t_0) = \bar{x}_0$. The GRF Ψ, its mean function μ, and its covariance function Σ, evaluated along the nominal trajectory $\hat{x}$, are denoted as

$$\hat{\Psi}(t) = \Psi\big(\phi(\hat{x}(t))\big), \tag{5.18a}$$

$$\hat{\mu}(t) = \mu\big(\phi(\hat{x}(t))\big), \tag{5.18b}$$

$$\hat{\Sigma}(t, \tau) = \Sigma\big(\phi(\hat{x}(t)), \phi(\hat{x}(\tau))\big). \tag{5.18c}$$

Note that, unlike $\hat{x}$ and $\hat{u}$, the function $\hat{\Psi}$ is random: the function $\hat{\Psi}$ is an approximation of Ψ in the sense that the statistics of $\hat{\Psi}$ are evaluated along the nominal trajectory rather than the perturbed trajectory. In other words, the nominal trajectory $\hat{x}$ determines a mapping from the spatially-dependent random field Ψ to the time-dependent random process $\hat{\Psi}$; this relationship is shown graphically in Figure 5.3. The following result establishes the consistency of the definitions (5.18).

Proposition 5.4.1. *The function $\hat{\Psi}(t)$ is a Gaussian random process with mean $\hat{\mu}(t)$ and covariance $\hat{\Sigma}(t, \tau)$.*

Proof. The process $\hat{\Psi}$ is Gaussian since the random field Ψ is Gaussian; it remains only to show that the mean and covariance of $\hat{\Psi}$ are given by $\hat{\mu}$ and $\hat{\Sigma}$. From the definitions (5.18),

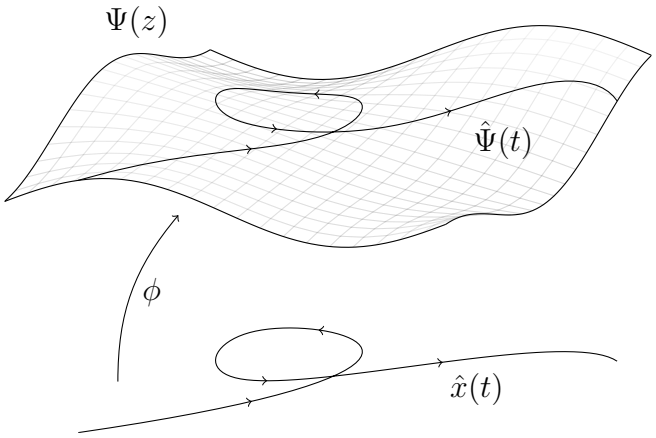

Figure 5.3: Samples of the GRF Ψ and random process $\hat{\Psi}$ along the nominal trajectory $\hat{x}$

we obtain

$$\mathbb{E}\big(\hat{\Psi}(t)\big) = \mathbb{E}\big(\Psi\big(\phi(\hat{x}(t))\big)\big) = \mu\big(\phi(\hat{x}(t))\big) = \hat{\mu}(t), \tag{5.19}$$

and

$$\begin{aligned} \operatorname{Cov}\big(\hat{\Psi}(t), \hat{\Psi}(\tau)\big) &= \operatorname{Cov}\big(\Psi\big(\phi(\hat{x}(t))\big), \Psi\big(\phi(\hat{x}(\tau))\big)\big) \\ &= \Sigma\big(\phi(\hat{x}(t)), \phi(\hat{x}(\tau))\big) \\ &= \hat{\Sigma}(t, \tau), \end{aligned} \tag{5.20}$$

which yields the desired result. □

Next, we linearly approximate the system dynamics about the nominal trajectory $\big(\hat{x}, \hat{u}, \hat{\mu}\big)$ to obtain

$$\dot{x} \approx f(\hat{x}, \hat{u}, \hat{\mu}) + \frac{\partial f}{\partial x}(x - \hat{x}) + \frac{\partial f}{\partial u}(u - \hat{u}) + \frac{\partial f}{\partial \Psi}(\hat{\Psi} - \hat{\mu}). \tag{5.21}$$

Define the functions

$$A(t) = \frac{\partial f}{\partial x}, \quad B(t) = \frac{\partial f}{\partial u}, \quad G(t) = \frac{\partial f}{\partial \Psi}, \tag{5.22}$$

evaluated at $\big(\hat{x}(t), \hat{u}(t), \hat{\mu}(t)\big)$, and let

$$c(t) = f(\hat{x}, \hat{u}, \hat{\mu}) - A(t)\hat{x} - B(t)\hat{u} - G(t)\hat{\mu}. \tag{5.23}$$

The linearized system (5.21) is integrated from time t_k to t_{k+1} to obtain the approximate system evolution

$$x_{k+1} \approx \Phi(t_{k+1}, t_k)x_k + \int_{t_k}^{t_{k+1}} \Phi(t_{k+1}, t)\big(B(t)u_k + c(t)\big)\,\mathrm{d}t + \int_{t_k}^{t_{k+1}} \Phi(t_{k+1}, t)G(t)\hat{\Psi}(t)\,\mathrm{d}t, \tag{5.24}$$

where Φ is the state transition matrix corresponding to $A(t)$. Simplifying, (5.24) is written as the stochastic difference equation

$$x_{k+1} = A_k x_k + B_k u_k + c_k + w_k, \tag{5.25}$$

with the values A_k, B_k and c_k taken from (5.24), and where the Gaussian disturbance term w_k is given by

$$w_k = \int_{t_k}^{t_{k+1}} \Phi(t_{k+1}, t)G(t)\hat{\Psi}(t)\,\mathrm{d}t. \tag{5.26}$$

As shown in the following result, the mean and covariances of the disturbance terms w_k depend on the system dynamics and on the statistics of the GRF Ψ, via the functions $\hat{\mu}$ and $\hat{\Sigma}$.

Proposition 5.4.2. *The vectors w_k, for $k = 0, \ldots, N-1$, are jointly Gaussian with mean values*

$$\mathbb{E}(w_k) = \int_{t_k}^{t_{k+1}} \Phi(t_{k+1}, t)G(t)\hat{\mu}(t)\,\mathrm{d}t, \tag{5.27}$$

and covariances

$$\mathrm{Cov}(w_k, w_\ell) = \int_{t_k}^{t_{k+1}} \int_{t_\ell}^{t_{\ell+1}} \Phi(t_{k+1}, t)G(t)\hat{\Sigma}(t, \tau)G^{\intercal}(\tau)\Phi^{\intercal}(t_{\ell+1}, \tau)\,\mathrm{d}\tau\,\mathrm{d}t. \tag{5.28}$$

Proof. The mean term (5.27) follows from taking the expectation of w_k in (5.26) and substituting (5.19). Furthermore,

$$w_k - \mathbb{E}(w_k) = \int_{t_k}^{t_{k+1}} \Phi(t_{k+1}, t) G(t) \big(\hat{\Psi}(t) - \hat{\mu}(t)\big) \, \mathrm{d}t. \tag{5.29}$$

The covariance of w_k and w_ℓ is computed from (5.29) as

$$\begin{aligned}
\mathrm{Cov}(w_k, w_\ell) &= \mathbb{E}\big\{ \big(w_k - \mathbb{E}(w_k)\big) \big(w_\ell - \mathbb{E}(w_\ell)\big)^\mathsf{T} \big\} && (5.30) \\
&= \mathbb{E}\bigg\{ \int_{t_k}^{t_{k+1}} \Phi(t_{k+1}, t) G(t) \big(\hat{\Psi}(t) - \hat{\mu}(t)\big) \, \mathrm{d}t \\
&\qquad \int_{t_\ell}^{t_{\ell+1}} \big(\hat{\Psi}(\tau) - \hat{\mu}(\tau)\big) G^\mathsf{T}(\tau) \Phi^\mathsf{T}(t_{\ell+1}, \tau) \, \mathrm{d}\tau \bigg\} && (5.31) \\
&= \int_{t_k}^{t_{k+1}} \int_{t_\ell}^{t_{\ell+1}} \Phi(t_{k+1}, t) G(t) \mathbb{E}\big\{ \big(\hat{\Psi}(t) - \hat{\mu}(t)\big) \big(\hat{\Psi}(\tau) - \hat{\mu}(\tau)\big) \big\} \\
&\qquad G^\mathsf{T}(\tau) \Phi^\mathsf{T}(t_{\ell+1}, \tau) \, \mathrm{d}\tau \, \mathrm{d}t. && (5.32)
\end{aligned}$$

Substituting the covariance function $\hat{\Sigma}$ from (5.20) into (5.32), we obtain the desired result. Finally, by the definition of a GRF, any finite collection of evaluations of $\big(\Psi(z_i)\big)$ are jointly Gaussian, and thus integrals over Ψ are also jointly Gaussian. □

The system (5.25) is therefore simply a stochastic difference equation with Gaussian disturbances — but the disturbances are neither (necessarily) independent nor identically distributed.

5.4.2 Block-Matrix Formulation

The state process (5.25) may be equivalently written in block-matrix notation as

$$\begin{bmatrix} x_0 \\ x_1 \\ x_2 \\ \vdots \end{bmatrix} = \begin{bmatrix} I \\ A_0 \\ A_1A_0 \\ \vdots \end{bmatrix} x_0 + \begin{bmatrix} 0 & 0 & \\ B_0 & 0 & \\ A_1B_0 & B_1 & \\ & & \ddots \end{bmatrix} \begin{bmatrix} u_0 \\ u_1 \\ \vdots \end{bmatrix} + \begin{bmatrix} 0 \\ c_0 \\ A_1c_1 \\ \vdots \end{bmatrix} + \begin{bmatrix} 0 & 0 & \\ I & 0 & \\ A_1 & I & \\ & & \ddots \end{bmatrix} \begin{bmatrix} w_0 \\ w_1 \\ \vdots \end{bmatrix}. \quad (5.33)$$

Let X be a column vector constructed by stacking the states x_k for $k = 0, 1, \ldots, N$, and, similarly, let U and W be the column vectors constructed by stacking the controls u_k and disturbances w_k for $k = 0, 1, \ldots, N-1$. For appropriately constructed block matrices $\boldsymbol{A}$, $\boldsymbol{B}$, and $\boldsymbol{G}$ as in (5.33), and with C an appropriately constructed vector, the state process can be written as the linear matrix equation

$$X = \boldsymbol{A}x_0 + \boldsymbol{B}U + C + \boldsymbol{G}W. \quad (5.34)$$

See Refs. [71, 114, 76] for details on this construction. Letting the block lower-triangular matrix $\boldsymbol{K} \in \mathbb{R}^{Nm \times (N+1)n}$ be given by

$$\boldsymbol{K} = \begin{bmatrix} K_{0,0} & 0 & & \cdots & 0 \\ K_{1,0} & K_{1,1} & 0 & \cdots & 0 \\ \vdots & & & & \vdots \\ K_{N-1,0} & K_{N-1,1} & K_{N-1,2} & \cdots & 0 \end{bmatrix}, \quad (5.35)$$

and letting $U \in \mathbb{R}^{Nm}$, $V \in \mathbb{R}^{Nm}$, and $\tilde{X} \in \mathbb{R}^{(N+1)n}$ be the vectors obtained by stacking the closed-loop controls (u_k), the feedforward controls (v_k), and the state deviation $(\tilde{x}_k)$, the control law (5.10) is given in block-matrix notation as

$$U = \boldsymbol{K}\tilde{X} + V. \quad (5.36)$$

Substituting the control (5.36) into the state equation (5.34) gives the closed-loop system

$$\bar{X} = \boldsymbol{A}\bar{x}_0 + \boldsymbol{B}V + C + \boldsymbol{G}\bar{W}, \tag{5.37}$$

$$\tilde{X} = (I - \boldsymbol{B}\boldsymbol{K})^{-1}(\boldsymbol{A}\tilde{x}_0 + \boldsymbol{G}\tilde{W}). \tag{5.38}$$

Note that the mean state $\bar{X}$ depends on the nominal control V, whereas the random state deviation $\tilde{X}$ depends on the feedback gain $\boldsymbol{K}$.

Following [114], we define the new decision variable $\boldsymbol{L} \in \mathbb{R}^{Nm\times(N+1)n}$ as

$$\boldsymbol{L} = \boldsymbol{K}(I - \boldsymbol{B}\boldsymbol{K})^{-1}. \tag{5.39}$$

Since $\boldsymbol{K}$ is block lower-triangular and $\boldsymbol{B}$ is strictly block lower-triangular, the matrix $I - \boldsymbol{B}\boldsymbol{K}$ is invertible. It follows that $\boldsymbol{L}$ is block lower-triangular and satisfies

$$I + \boldsymbol{B}\boldsymbol{L} = (I - \boldsymbol{B}\boldsymbol{K})^{-1}, \tag{5.40}$$

$$\boldsymbol{K} = \boldsymbol{L}(I + \boldsymbol{B}\boldsymbol{L})^{-1}. \tag{5.41}$$

Therefore, we optimize over $\boldsymbol{L}$ in place of $\boldsymbol{K}$ [114].

Using the decision variable $\boldsymbol{L}$ as in (5.39) results in the closed-loop system

$$\bar{X} = \boldsymbol{A}\bar{x}_0 + \boldsymbol{B}V + C + \boldsymbol{G}\bar{W}, \tag{5.42}$$

$$\tilde{X} = (I + \boldsymbol{B}\boldsymbol{L})(\boldsymbol{A}\tilde{x}_0 + \boldsymbol{G}\tilde{W}). \tag{5.43}$$

The state and control processes X and U are thus Gaussian distributed with mean $\mathbb{E}(X) =$

$\bar{X}$ as in (5.42), $\mathbb{E}(U) = V$, and covariances

$$\boldsymbol{P_X} = \mathrm{Cov}(X) = (I + \boldsymbol{BL})\boldsymbol{S}(I + \boldsymbol{BL})^\intercal, \tag{5.44}$$

$$\boldsymbol{P_U} = \mathrm{Cov}(U) = \boldsymbol{LSL}^\intercal, \tag{5.45}$$

where

$$\boldsymbol{S} = \boldsymbol{A}P_0\boldsymbol{A}^\intercal + \boldsymbol{G}\,\mathrm{Cov}(W)\boldsymbol{G}^\intercal. \tag{5.46}$$

The elements of the mean disturbance vector $\bar{W}$ and the covariance matrix $\mathrm{Cov}(W)$ are obtained from the integrals (5.27) and (5.28).

5.4.3 Chance Constraints

The inner product $a_{i,k}^\intercal x_k$ is a Gaussian random variable with mean $a_{i,k}^\intercal \mathbb{E}(x_k)$ and covariance $a_{i,k}^\intercal \mathrm{Cov}(x_k) a_{i,k}$. It follows that

$$\mathbb{P}(a_{i,k}^\intercal x_k \leq \alpha_{i,k}) = \mathrm{cdfn}\left(\frac{\alpha_{i,k} - a_{i,k}^\intercal E_k \bar{X}}{\sqrt{a_{i,k}^\intercal E_k \boldsymbol{P_X} E_k^\intercal a_{i,k}}}\right), \tag{5.47}$$

where cdfn is the normal cumulative distribution function. Taking the inverse of the normal cumulative distribution function and rearranging terms, we obtain

$$\begin{aligned} &\mathbb{P}(a_{i,k}^\intercal x_k > \alpha_{i,k}) \leq p_{i,k}^x \\ \iff\ &\mathrm{cdfn}^{-1}(1-p_{i,k}^x)\|\boldsymbol{S}^{1/2}(I+\boldsymbol{BL})^\intercal E_k^\intercal a_{i,k}\| + a_{i,k}^\intercal E_k(\boldsymbol{A}\bar{x}_0 + \boldsymbol{B}V + C + \boldsymbol{G}\bar{W}) \leq \alpha_{i,k}, \end{aligned} \tag{5.48}$$

where $\boldsymbol{S}^{1/2}$ denotes a matrix satisfying $\boldsymbol{S} = (\boldsymbol{S}^{1/2})^\intercal \boldsymbol{S}^{1/2}$, and where $E_k \in \mathbb{R}^{n\times(N+1)n}$ is a matrix defined such that $E_k X = x_k$. Similarly, for the control constraints,

$$\mathbb{P}(b_{i,k}^\intercal u_k > \beta_{i,k}) \leq p_{i,k}^u \iff \mathrm{cdfn}^{-1}(1-p_{i,k}^u)\|\boldsymbol{S}^{1/2}\boldsymbol{L}^\intercal E_k^{u\intercal} b_{i,k}\| + b_{i,k}^\intercal E_k^u V \leq \beta_{i,k}, \tag{5.49}$$

where $E_k^u \in \mathbb{R}^{m \times Nm}$ such that $E_k^u U = u_k$.

5.4.4 Terminal Distribution Constraints

The final state mean constraint is given by

$$\mathbb{E}(x_f) = E_N(\boldsymbol{A}\bar{x}_0 + \boldsymbol{B}V + C + \boldsymbol{G}\bar{W}) = \bar{x}_f, \tag{5.50}$$

which is convex in the decision variable V. The final state covariance constraint is given by

$$E_N(I + \boldsymbol{B}\boldsymbol{L})\boldsymbol{S}(I + \boldsymbol{B}\boldsymbol{L})^\intercal E_N^\intercal \leq P_f, \tag{5.51}$$

which may be equivalently written as [71]

$$\|\boldsymbol{S}^{1/2}(I + \boldsymbol{B}\boldsymbol{L})^\intercal E_N^\intercal P_f^{-1/2}\| \leq 1, \tag{5.52}$$

which is a convex constraint in terms of $\boldsymbol{L}$. Note that, by assumption, P_f is positive definite, and hence $P_f^{-1/2}$ exists.

5.4.5 Cost Function

The cost J_1 is written in terms of the decision variables $\boldsymbol{L}$ and V as

$$\begin{aligned} J_1(\boldsymbol{L}, V) = \operatorname{tr}\left\{\left((I + \boldsymbol{B}\boldsymbol{L})^\intercal \boldsymbol{Q}(I + \boldsymbol{B}\boldsymbol{L}) + \boldsymbol{L}^\intercal \boldsymbol{R}\boldsymbol{L}\right)\boldsymbol{S}\right\} \\ + \|\boldsymbol{A}\bar{x}_0 + \boldsymbol{B}V + C + \boldsymbol{G}\bar{W} - X^d\|_{\boldsymbol{Q}}^2 + V^\intercal \bar{\boldsymbol{R}}V. \end{aligned} \tag{5.53}$$

where $\boldsymbol{Q} \in \mathbb{R}^{(N+1)n \times (N+1)n}$ and $\boldsymbol{R} \in \mathbb{R}^{Nm \times Nm}$ are block-diagonal matrices given by

$$\boldsymbol{Q} = \begin{bmatrix} Q_0 & & & \\ & \ddots & & \\ & & Q_{N-1} & \\ & & & 0 \end{bmatrix}, \qquad \boldsymbol{R} = \begin{bmatrix} R_0 & & \\ & \ddots & \\ & & R_{N-1} \end{bmatrix}, \tag{5.54}$$

and where $\bar{\boldsymbol{R}}$ is defined as $\boldsymbol{R}$ with the weights $\bar{R}_k$. Next, we consider the expression of the cost J_2. Following the analysis in subsection 5.4.3, and since $\xi^\mathsf{T} x_f$ is a Gaussian random variable, we have the relationship

$$\mathbb{P}(\xi^\mathsf{T} x_f \leq \gamma) = \operatorname{cdfn}\left(\frac{\gamma - \xi^\mathsf{T}\mathbb{E}(x_f)}{\sqrt{\xi^\mathsf{T} \operatorname{Cov}(x_f)\xi}}\right). \tag{5.55}$$

We can thus rewrite the inequality in the cost definition (5.15) as

$$\mathbb{P}(\xi^\mathsf{T} x_f > \gamma) \leq p_f \iff \xi^\mathsf{T}\mathbb{E}(x_f) + \sqrt{\xi^\mathsf{T} \operatorname{Cov}(x_f)\xi}\, \operatorname{cdfn}^{-1}(1-p_f) \leq \gamma. \tag{5.56}$$

The minimum value $\gamma^* = J_2$ that satisfies the inequality (5.56) is obtained by setting equality in (5.56). After substituting the decision variables $\boldsymbol{L}$ and V from (5.42) and (5.43) into (5.56) and simplifying, we obtain the cost J_2 as the convex function

$$J_2(\boldsymbol{L}, V) = \xi^\mathsf{T}(\boldsymbol{A}\bar{x}_0 + \boldsymbol{B}V + C + \boldsymbol{G}\bar{W}) + \operatorname{cdfn}^{-1}(1-p_f)\|\boldsymbol{S}^{1/2}(I + \boldsymbol{B}\boldsymbol{L})^\mathsf{T} E_N^\mathsf{T} \xi\|. \tag{5.57}$$

5.4.6 Iterative Covariance Steering

In the precious subsections, we have formulated the original stochastic optimal control problem as a convex program with respect to a provided nominal control input. A solution to the original, nonlinear problem can be obtained by iteratively solving the convexified problem; this procedure is, in general, referred to as successive convex programming [122, 24, 70].

First, we must introduce the following trust region constraints that serve to restrict each successive convex problem to a domain in which the convex approximation remains valid:

$$\|\bar{u}_k - \hat{u}_k\|_{M_k^u} \leq \Delta^u, \tag{5.58}$$

$$\|\bar{x}_k - \hat{x}_k\|_{M_k^x} \leq \Delta^x, \tag{5.59}$$

where M_k^u and M_k^x are positive semi-definite weight matrices and where Δ^u and Δ^x are given deviation limits. The subproblem to be solved, which we refer to as the covariance steering problem, is therefore given as the following convex optimization problem.

$$\begin{aligned}
\underset{\boldsymbol{L},V}{\text{minimize}} \quad & J(\boldsymbol{L},V) = \operatorname{tr}\left\{\left((I+\boldsymbol{B}\boldsymbol{L})^\intercal \boldsymbol{Q}(I+\boldsymbol{B}\boldsymbol{L}) + \boldsymbol{L}^\intercal \boldsymbol{R}\boldsymbol{L}\right)\boldsymbol{S}\right\} && && \text{(5.60a)}\\
& \quad + \|\bar{X} - X^d\|_{\boldsymbol{Q}}^2 + V^\intercal \bar{\boldsymbol{R}} V \\
& \quad + \eta\left\{\xi^\intercal \bar{X} + \operatorname{cdfn}^{-1}(1-p_f)\|\boldsymbol{S}^{1/2}(I+\boldsymbol{B}\boldsymbol{L})^\intercal E_N^\intercal \xi\|\right\} \\
\text{subject to} \quad & E_N \bar{X} = \bar{x}_f && && \text{(5.60b)}\\
& \|\boldsymbol{S}^{1/2}(I+\boldsymbol{B}\boldsymbol{L})^\intercal E_N^\intercal P_f^{-1/2}\| \leq 1 && && \text{(5.60c)}\\
& \operatorname{cdfn}^{-1}(1-p_{i,k}^x)\|\boldsymbol{S}^{1/2}(I+\boldsymbol{B}\boldsymbol{L})E_k^\intercal a_{i,k}\| && \forall (i,k) \in \mathcal{X} && \text{(5.60d)}\\
& \qquad + a_{i,k}^\intercal E_k \bar{X} \leq \alpha_j \\
& \operatorname{cdfn}^{-1}(1-p_{i,k}^u)\|\boldsymbol{S}^{1/2}\boldsymbol{L}E_k^{u\intercal} b_{i,k}\| && \forall (i,k) \in \mathcal{U} && \text{(5.60e)}\\
& \qquad + b_j^\intercal E_k^u V \leq \beta_{i,k} \\
& \|E_k \bar{X} - \hat{x}_k\|_{M_k^x} \leq \Delta^x && \forall k \in \{0,\ldots,N-1\} && \text{(5.60f)}\\
& \|E_k^u V - \hat{u}_k\|_{M_k^u} \leq \Delta^u && \forall k \in \{1,\ldots,N\} && \text{(5.60g)}\\
\text{where} \quad & \boldsymbol{S} = \boldsymbol{A}P_0\boldsymbol{A}^\intercal + \boldsymbol{G}\operatorname{Cov}(W)\boldsymbol{G}^\intercal && && \text{(5.60h)}\\
& \bar{X} = \boldsymbol{A}\bar{x}_0 + \boldsymbol{B}V + C + \boldsymbol{G}\bar{W} && && \text{(5.60i)}
\end{aligned}$$

The resulting successive convex programming algorithm is summarized in Algorithm 3.

Algorithm 3: Iterative Covariance Steering in a Gaussian Random Field

Input: Initial state mean and covariance $\bar{x}_0$, P_0, initial control guess $\hat{u}$, time partition $\mathscr{P}$

Output: Control law parameters $(K_{k,\ell})$, (v_k), $(\bar{x}_k)$

while *termination criteria not met* **do**
- Propagate nominal trajectory (5.17);
- Linearize (5.21);
- Discretize (5.24);
- Calculate disturbance statistics (5.27), (5.28);
- Solve convex program (5.60);
- Solve feedback gain $\boldsymbol{K}$ from $\boldsymbol{L}$ as in (5.41);
- Set control law (5.10);
- Set new nominal control $\hat{u}_k \leftarrow \bar{u}_k$;

end

5.5 Numerical Examples

In this section we illustrate the developed theory with two examples. The first of which is a double integrator subjected to random, position-dependent external force. The second example treats aerocapture guidance around a planet with altitude-dependent density variations.

5.5.1 Double Integrator

Consider a single-dimensional double integrator with position r and velocity v. A GRF $\Psi(r)$ acts as an external force on the system, as a function of the position, in addition to a control force u. This system is described by the equations

$$\dot{r} = v, \tag{5.61a}$$

$$\dot{v} = u + \Psi(r). \tag{5.61b}$$

The state is normally distributed at the initial time by

$$\begin{bmatrix} r(t_0) \\ v(t_0) \end{bmatrix} \sim \mathcal{N}\left(\begin{bmatrix} 0.1 \\ 0.1 \end{bmatrix}, \begin{bmatrix} \sigma_r^2 & 0 \\ 0 & \sigma_v^2 \end{bmatrix} \right), \tag{5.62}$$

where $3\sigma_r = 0.05$ and $3\sigma_v = 0.01$. The force input Ψ is assumed to have zero mean and locally-periodic covariance

$$\Sigma(r, r') = \sigma_\Psi^2 \exp\left(- \frac{2\sin^2\left(\pi|r - r'|/p\right)}{\ell_p^2} \right) \exp\left(- \frac{(r - r')^2}{2\ell_e^2} \right), \tag{5.63}$$

where $\sigma_\Psi^2 = 2 \times 10^{-6}$ is the variance, $p = 0.35$ is the period, $\ell_p = 0.8$ is the periodic length scale, and $\ell_e = 1$ is the exponential-quadratic length scale. Samples of Ψ are plotted in Figure 5.4.

We consider the system over the time interval $[0, 5]$ with $\mathscr{P} = (0, 1, \ldots, 5)$, and so $N = 5$. The distribution of the state at the final time is constrained by

$$\bar{x}(t_f) = \begin{bmatrix} 0.6 \\ 0.1 \end{bmatrix}, \quad P(t_f) \leq P_f = \begin{bmatrix} \sigma_r^2 & 0 \\ 0 & \sigma_v^2 \end{bmatrix}. \tag{5.64}$$

At each step k, the state is constrained to lie in the region between two lines passing through the point $(0.7, 0.1)$ and with slopes $\pm 0.05/0.1$, which is shown by dashed lines in Figure 5.5, with a probability of at least 0.9973. Translating into the format (5.11), and leveraging the subadditivity of probability, this chance constraint is represented by

$$a_{1,k} = \begin{bmatrix} 0.212766 \\ 8.51064 \end{bmatrix}, \quad a_{2,k} = \begin{bmatrix} 0.30303 \\ -12.1212 \end{bmatrix}, \tag{5.65}$$

and $\alpha_{1,k} = 1$, $\alpha_{2,k} = -1$, and $p_{i,k}^x = (1 - 0.9973)/2$ for $i = 1, 2$. The running control weight is $R_k = \bar{R}_k = 1$ and the state weight Q_k is zero. We only consider the quadratic cost J_1, and therefore we set $\eta = 0$.

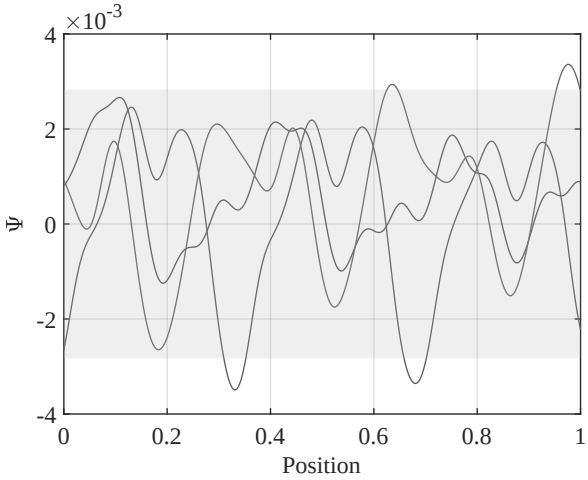

Figure 5.4: Samples of Ψ with shaded 2σ confidence interval

Algorithm 3 was run for a single iteration, and the resulting open and closed-loop trajectories are shown in Figure 5.5. While for the closed-loop trajectory the confidence ellipses are not entirely within the constrained region, the chance constraints were satisfied based on 5,000 Monte Carlo trails.

5.5.2 Aerocapture

In this subsection, we apply Algorithm 3 to the problem of aerocapture guidance, which was briefly described in Section 5.1 and Subsection 1.1.3.

Mission Design

The aerocapture mission profile is shown in Figure 5.6. Following atmospheric flight, the vehicle will perform a periapsis raising burn (to raise the periapsis out of the planet's atmosphere) followed by an apoapsis clean up burn. Both the final orbit and the Δv cost are determined by the target periapsis and target apoapsis; the Δv cost is also determined by the vehicle states following the atmospheric flight segment.

Let r, v, and γ be the vehicle radius, planet-relative velocity, and planet-relative flight path angle (FPA). The apoapsis radius of the orbit following atmospheric flight is a function

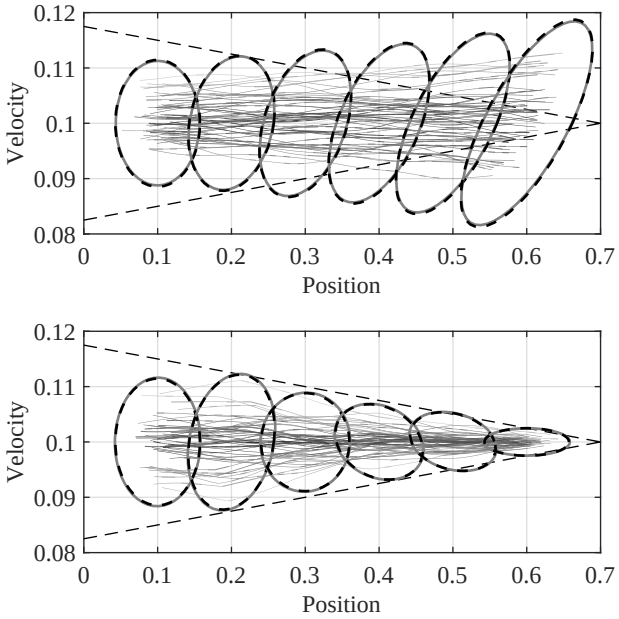

Figure 5.5: Open-loop (top) and closed-loop (bottom) trajectories of the double integrator system with 99.73% confidence ellipses computed from linear covariance (black, dashed) and 5,000 trial Monte Carlo (gray, solid).

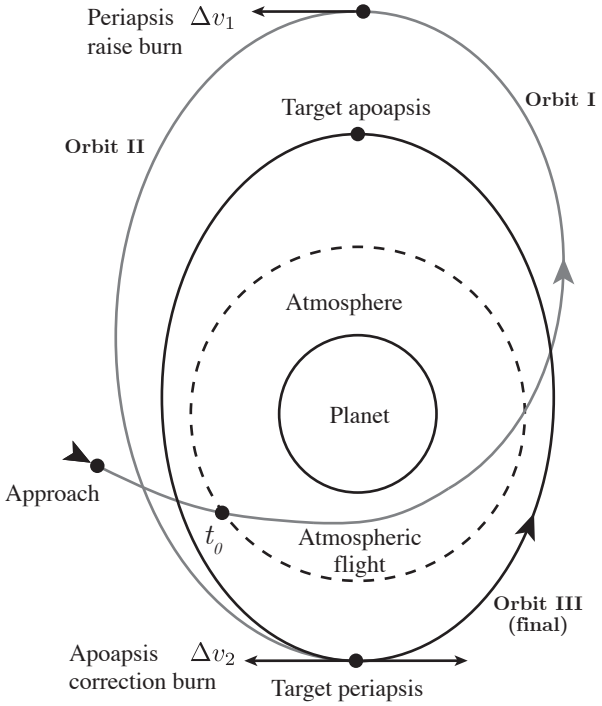

Figure 5.6: Aerocapture mission overview

of the states $x_f = (r_f, v_f, \gamma_f)$ at the final time given by

$$r_{a,\text{ex}} = a_{\text{ex}}\left(1 + \sqrt{1 - \frac{r_f^2 v_f^2 \cos^2 \gamma_f}{\mu_{\text{grav}} a_{\text{ex}}}}\right), \tag{5.66}$$

where μ_{grav} is the planet's gravitational parameter, and where a_{ex} is the semi-major axis at atmospheric exit given by

$$a_{\text{ex}} = \frac{\mu_{\text{grav}}}{2\mu_{\text{grav}}/r_f - v_f^2}. \tag{5.67}$$

Following the atmospheric flight segment, the vehicle coasts to its apoapsis, where it has the velocity

$$v_{a_1}^- = \sqrt{v_f^2 + 2\mu_{\text{grav}}\left(\frac{1}{r_{a,\text{ex}}} - \frac{1}{r_f}\right)}. \tag{5.68}$$

However, the required velocity at the radius $r_{a,\text{ex}}$ for the periapsis to equal to the desired periapsis $r_{p,\text{targ}}$ is

$$v_{a_1}^+ = \sqrt{2\mu_{\text{grav}}\left(\frac{1}{r_{a,\text{ex}}} - \frac{1}{r_{a,\text{ex}} + r_{p,\text{targ}}}\right)}. \tag{5.69}$$

The first impulsive maneuver increases the velocity from $v_{a_1}^-$ to $v_{a_1}^+$, and hence

$$\Delta v_1 = v_{a_1}^+ - v_{a_1}^-. \tag{5.70}$$

Next, the vehicle coasts to the periapsis $r_{p,\text{targ}}$, where it has velocity

$$v_{p_1}^- = \sqrt{2\mu_{\text{grav}}\left(\frac{1}{r_{p,\text{targ}}} - \frac{1}{r_{a,\text{ex}} + r_{p,\text{targ}}}\right)}, \tag{5.71}$$

whereas the velocity at this point required for the apoapsis to be equal to the target apoapsis $r_{a,\text{targ}}$ is

$$v_{p_1}^+ = \sqrt{2\mu_{\text{grav}}\left(\frac{1}{r_{p,\text{targ}}} - \frac{1}{r_{a,\text{targ}} + r_{p,\text{targ}}}\right)}. \tag{5.72}$$

The second impulsive maneuver corrects the discrepancy in the velocity at periapsis, and

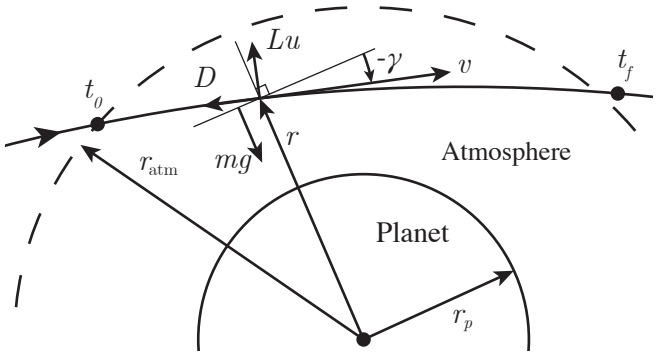

Figure 5.7: Atmospheric flight coordinates with lift L and drag D

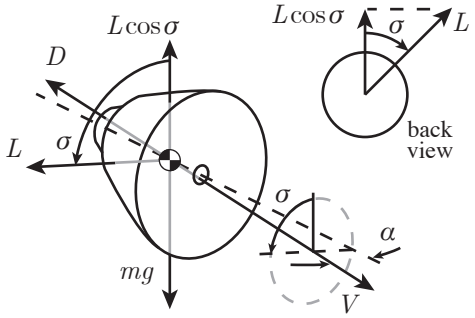

Figure 5.8: Bank angle control with bank angle σ and angle of attack α

thus

$$\Delta v_2 = |v_{p_1}^+ - v_{p_1}^-|. \tag{5.73}$$

The total fuel cost is the sum

$$\Delta v = \Delta v_1 + \Delta v_2. \tag{5.74}$$

Atmospheric Flight

During atmospheric flight, which is described in Figure 5.7, a vehicle flying at a trimmed angle of attack can steer by banking the lift vector about the velocity vector, as shown in Figure 5.8. The vertical component in the lift vector is set via the cosine of the bank angle, and the sign of the bank angle is set for lateral control. In this example, we only consider the longitudinal guidance, and so the control input during atmospheric flight is the bank angle cosine.

The vehicle dynamics during atmospheric flight are described by the system of equations

$$\dot{r} = v \sin\gamma, \tag{5.75a}$$

$$\dot{v} = -\frac{\rho(r) v^2}{2B_c} - \frac{\mu_{\text{grav}} \sin\gamma}{r^2}, \tag{5.75b}$$

$$\dot{\gamma} = \frac{\rho(r) v (L/D)}{2B_c} u - \left(\frac{\mu_{\text{grav}}}{r^2} - \frac{v^2}{r} \right) \frac{\cos\gamma}{v}, \tag{5.75c}$$

where the input u is the cosine of the bank angle, ρ is atmospheric density, L/D is the lift-to-drag ratio, and $B_c = m/SC_D$ is the spacecraft ballistic coefficient in terms of mass m, reference area S, and drag coefficient C_D. In this example, we set $B_c = 150$ kg/m^2 and $L/D = 0.2$. We take the planet to be Mars, which we model as a sphere of radius $r_p = 3397$ km and gravitational parameter $\mu_{\text{grav}} = 4.2828 \times 10^{13}$ m^3/s^2. At the initial time, the state has mean $\bar{x}_0 = (\bar{r}_0, \bar{v}_0, \bar{\gamma}_0)$, with $\bar{r}_0 = 125\,\text{km} + r_p$, $\bar{v}_0 = 6.1\,\text{km/s}$, and $\bar{\gamma}_0 = -10.0128°$. The initial flight path angle is set so that a constant control input $u \equiv 0$ results in the apoapsis after atmospheric exit $r_{a,\text{ex}}$ being equal to the target apoapsis $r_{a,\text{targ}}$. While the proposed method allows for the initial state to be Gaussian distributed, for this example we set the initial state covariance to be zero so that the effect of the atmospheric disturbances is more clear.

The atmospheric density is given by

$$\rho = \bar{\rho}(1 + \delta\rho), \tag{5.76}$$

where $\bar{\rho}$ is a known, smooth function describing the nominal density. The *density variation* $\delta\rho$ is a zero-mean GRF taking values as a function of the altitude $h = r - r_p$, where r_p is the planet radius. Based on the MarsGRAM atmosphere model [68] we define the density

variation covariance function as

$$\Sigma(h_1, h_2) = \exp\left(- \frac{|h_1 - h_2|}{H_{\text{scale}}} \right) \times \begin{cases} b\big(\min(h_1, h_2)\big), & \min(h_1, h_2) < h_{\text{trans}}, \\ \sigma^2_{\rho,\max}, & \min(h_1, h_2) \geq h_{\text{trans}}, \end{cases} \tag{5.77}$$

where H_{scale} is the scale height, and where

$$b(h) = \sigma^2_{\rho,\max} \exp\left(\frac{h - h_{\text{trans}}}{c_{\text{scale}}} \right). \tag{5.78}$$

The constants h_{trans} and c_{scale} determine the scale of the exponential variance model and $\sigma^2_{\rho,\max}$ is the maximum density variance, which is realized for altitudes $h \geq h_{\text{trans}}$. We use the values $H_{\text{scale}} = 11.1$ km, $\sigma^2_{\rho,\max} = 1480$ (kg/m^3)^2, $h_{\text{trans}} = 120$ km, and $c_{\text{scale}} = 20$ km. Samples of $\delta\rho$ are shown in Figure 5.9. The nominal density $\bar{\rho}(h)$ is provided by MarsGRAM [68]. We remark that while in this example the atmosphere is taken as a function of altitude, more general models including longitude and latitude dependence could also be used, provided an appropriate covariance function.

Without loss of generality, we let $t_0 = 0$. The final time is set to $t_f = 400$ s and $\mathcal{P} = (0, 50, 75, \ldots, 425, 450, 400)$ s.

Feedback Control Design

The bank angle control during atmospheric flight is determined to minimize the Δv required to reach the target orbit apoapsis $r_{a,\text{targ}} = 5r_p$ and periapsis $r_{p,\text{targ}} = 2r_p$. Since, in the stochastic setting, Δv is a random variable, we are able to explicitly minimize the 99$^{\text{th}}$ percentile of the total Δv cost, rather than simply minimizing the expected Δv cost. To this end, we approximate Δv from (5.74) to first order as

$$\Delta v(x_f) \approx \Delta v(\hat{x}_f) + \left. \frac{\partial \Delta v}{\partial x_f} \right|_{\hat{x}_f} (x_f - \hat{x}_f), \tag{5.79}$$

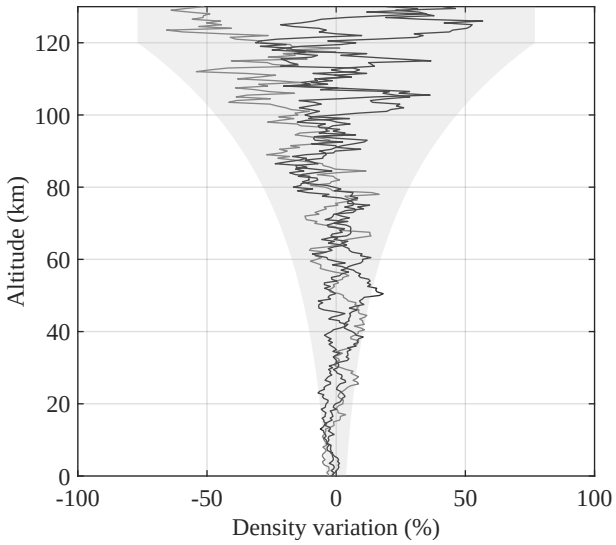

Figure 5.9: Samples from the density variation process with the 2σ confidence interval shaded

where $\hat{x}_f$ is obtained from integrating the nominal dynamics (5.17), and set

$$\xi^\intercal = \frac{\partial \Delta v}{\partial x_f}. \tag{5.80}$$

The cost J_2 as in (5.15) with ξ as in (5.80) and with $p_f = 0.1$ is thus approximately equal to the 99$^{\text{th}}$ percentile of Δv. Since, in this case, the final state mean and covariance are included in the cost function, we do not enforce the final state constraints (5.13).

Leveraging the subadditivity of probability, we constrain the probability that $u_k \in [-1, +1]$ to be at least 0.9973 by enforcing the constraints

$$\mathbb{P}(u_k \leq 1) \geq 1 - p^u/2, \;\; \text{and} \;\; \mathbb{P}(u_k \geq -1) \geq 1 - p^u/2, \tag{5.81}$$

for $p^u = 1 - 0.9973$, and for $k = 0, \ldots, N-1$.

The desired trajectory is set as $x_k^d = \bar{x}_k$ so that the state-error penalty Q_k penalizes the running state covariance. In particular, we penalize variations in the dynamic pressure $q = \rho v^2/2$, since excessive deviation from the nominal lift and drag forces will invalidate

the linear approximation of the dynamics. We thus set

$$Q_k = \hat{q}^{-2}\left(\frac{\partial q}{\partial x}\right)^{\mathsf{T}}\left(\frac{\partial q}{\partial x}\right), \tag{5.82}$$

where $\hat{q}$ is the dynamic pressure along the nominal trajectory, and where the terms on the right-hand side of (5.82) are evaluated at $\hat{x}_k$. The running control weights are set to $R_k = 2 \times 10^{-2}$ and $\bar{R}_k = 0$ for each step k, and $\eta = 1$.

Finally, the change in the mean control for each iteration was limited as in (5.58) with $\Delta_u = 0.1$ and $M_k^u = 1$; the change in the mean final state was constrained as in (5.59) with $\Delta_x = 0.1 r_p$, $M_N^x = (\partial r_{a,\text{ex}}/\partial x)^{\mathsf{T}}(\partial r_{a,\text{ex}}/\partial x)$, and $M_k^x = 0$ for $k = 1, \ldots, N-1$.

Results

Algorithm 3 was run for three iterations, starting with the initial control guess $\hat{u}_k = 0$ for all $k = 0, \ldots, N-1$. The nominal aerocapture trajectory resulting from both the initial guess and from the final nominal control are shown in Figure 5.10. The resulting probability distributions of Δv following each iteration, including the initial open-loop guess, were computed by both the linear covariance approximation and by 5,000 trial Monte Carlo, and are plotted in Figure 5.11. First, we note that the linear covariance approximation (plotted as a PDF) reasonably approximates the empirical distribution (shown as a histogram) obtained from Monte Carlo. One source of error between the linear covariance and the Monte Carlo distributions follows from the absolute value in the Δv cost corresponding to the apoapsis cleanup burn. Regardless, as shown by Figure 5.11, the linear covariance approximation serves a useful surrogate for the optimization. Despite, for example, the mismatch of the linear covariance probability density in Figure 5.11(c), the Monte Carlo distribution is consistently shifted and shaped in each iteration to have a lower upper percentile cost.

Next, consider the control inputs for each iteration, shown in Figure 5.12. With progressive iterations, the nominal control tends to increase the vertical lift in the first part of the

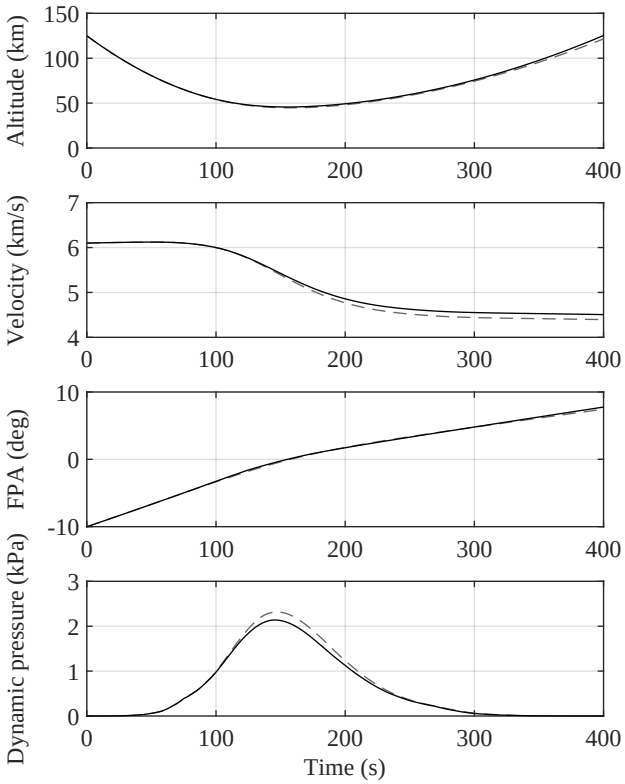

Figure 5.10: Nominal aerocapture trajectories for the initial control guess (dashed) and the final iteration (solid).

trajectory while decreasing the lift in the final part of the trajectory. Around the maximum dynamic pressure, which occurs nominally at 147 s, the nominal vertical lift is set to almost zero by the final iteration, which allows for the maximum amount of feedback control to be effected while ensuring that the control remains between ± 1 with high probability.

Using the final control law, the 99$^{\text{th}}$ percentile of Δv from the 5,000 Monte Carlo trails was 314 m/s, whereas to the open loop 99$^{\text{th}}$ percentile was 717 m/s.

5.6 Conclusion

In this chapter, a method is presented for chance-constrained stochastic control of systems subjected to a spatially-dependent uncertainty modeled as a GRF. Along a fixed nominal trajectory, spatially-dependent uncertainty becomes time-dependent, and accordingly, spatial correlations are approximated as temporal correlations. An integral equation is derived

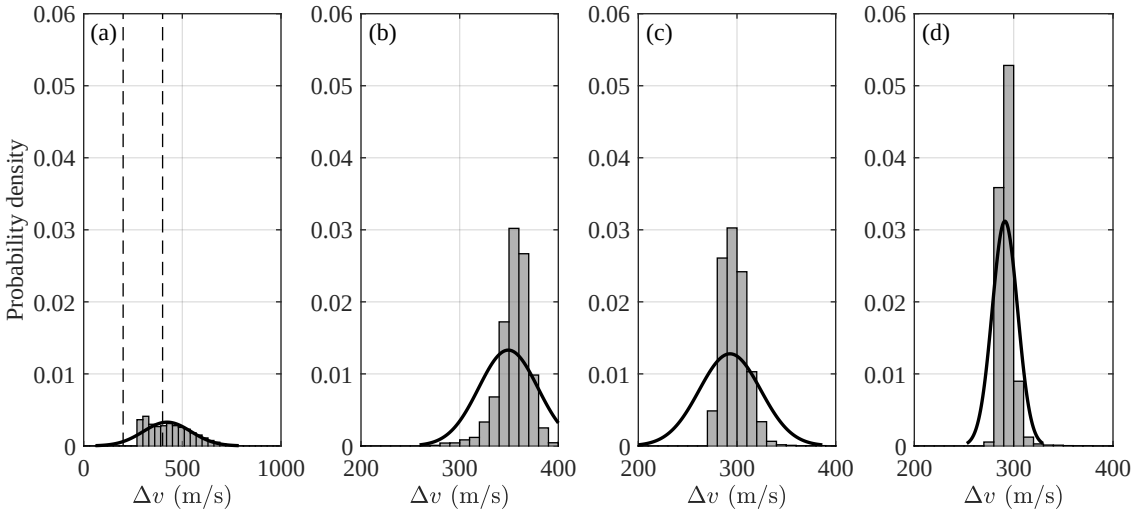

Figure 5.11: Δv probability density for each iteration of Algorithm 3. Note that plots (b–d) only show from 200 to 400 m/s, which is the interval between the dashed lines in plot (a).

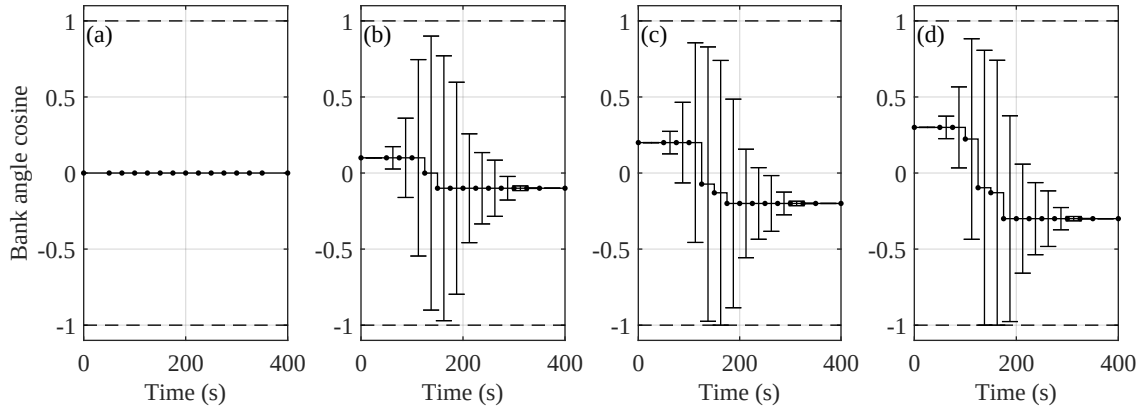

Figure 5.12: Control inputs with $\pm 3\sigma$ confidence intervals for each iteration of Algorithm 3.

to compute the temporal correlations of random disturbances on a dynamical system due to a GRF. Following a linear approximation of the system dynamics, the joint optimization of the nominal and feedback controls is derived as a convex program. The solution to the original stochastic optimal control problem is obtained by successively performing convex optimization with respect to the linearized system. The proposed method was demonstrated on both a simple double integrator example and on a realistic aerocapture problem. In future work, the proposed method can be applied to problems with more sophisticated disturbance models, such as aerocapture or hypersonic vehicle guidance with a three-dimensional atmosphere model.

CHAPTER 6
CONCLUSIONS

In this chapter, we review the contributions presented in the previous chapters and outline some potential future research directions.

6.1 Summary of Contributions

In the previous chapters, we have applied stochastic optimal control for spacecraft guidance during powered descent, atmospheric entry, and aerocapture. In addition, motivated by the technical challenges posed by these applications, we have developed contributions to the general theory of covariance steering. The existing linear methods were extended to nonlinear systems via a successive approximation scheme, which permits applicability to, for example, low-thrust spacecraft guidance. Atmospheric flight problems, including entry and aerocapture, include spatially-dependent uncertainty in the atmosphere as a leading driver of trajectory dispersions. In order to apply stochastic control methods for these applications involving atmospheric flight, we developed a chance-constrained covariance steering theory with the uncertainty being due to a spatially-defined Gaussian random field.

Moving beyond the specific application areas presented in the preceding chapters, the direction taken in this dissertation follows a wider trend in the guidance and controls community: management of uncertainty is taking a larger role, particularly in early-stage guidance and trajectory design. Entry, descent, and landing, which is a notoriously complex endeavor defined by the problem of managing uncertainty, has served in this dissertation as an illuminating and motivating example for bringing uncertainty into the guidance design process.

By focusing on applications, we have confronted challenges not often considered by the stochastic controls community. For example, as we have seen when studying the entry and

aerocapture problems, the underlying uncertainty affecting the vehicle trajectory cannot simply be modeled by adding standard Brownian noise, as is often done in the stochastic controls literature. Rather, we derived the statistics of the disturbance vectors from fundamental models of the underlying uncertainty, which for entry and aerocapture is the altitude-dependent atmospheric density. Looking forward, future applications of stochastic control theory to spacecraft systems may similarly involve a thorough treatment of modeling the underlying uncertainty.

The stochastic control approach taken in this dissertation differs from the numerical-predictor corrector (NPC) based guidance proposed in the EDL and aerocapture literature, which does not explicitly consider uncertainty but is rather founded solely on deterministic optimal control theory. A thorough comparison of performance between stochastic guidance and NPC-based guidance is left for future work. Regardless, one of the aims of this dissertation is to bring a stochastic perspective into the EDL literature, and to provide a basis for future inclusion of uncertainty into the spacecraft guidance design process.

6.2 Future Research Directions

6.2.1 Chance-Constrained Powered Descent Guidance

The powered descent guidance (PDG) method developed in Chapter 2 used covariance steering theory to design the closed-loop control and thus the throttle margins, whereas the nominal, minimum-fuel descent trajectory was solved as a separate convex optimization that does not consider uncertainty. On the other hand, the chance-constrained covariance steering theory from Chapter 4 cannot be directly applied to solve PDG as a single convex program, due to the nonlinearity of the PDG dynamics.

The convex solution to minimum-fuel PDG problem is obtained by applying several changes of variables, which complicate the linear covariance analysis [19]. However, if an approximation of the state and control covariances can be included in the analysis, then it may be possible to jointly solve for the nominal trajectory and the feedback law as a convex

program, with chance-constraints on the state.

6.2.2 Tighter Maximum Magnitude Chance Constraint in Three Dimensions

A convex formulation of the chance constraint

$$\mathbb{P}(\|u_k\| \geq \rho) \leq p_{\text{fail}}^{\|u\|} \tag{6.1}$$

was presented in Chapter 4. This convex formulation is conservative, but the conservatism is relatively small for the case that u_k is one or two-dimensional. However, for higher dimensions, the convex formulation of (6.1) given in Chapter 4 is very conservative. This conservatism is problematic when applying the theory to spacecraft systems with three dimensional control inputs, resulting in suboptimal solutions.

For greater insight into the construction of this bound in three dimensions, we draw parallels to the convex formulation of the bound for one and two dimensions, as was done in Subsection 4.2.3. Let $y \sim \mathcal{N}(\mu, \Sigma)$ be a three-dimensional random vector, and consider the chance constraint

$$\mathbb{P}(\|y\| \leq \rho) \geq 1 - \beta, \tag{6.2}$$

for a maximum magnitude $\rho > 0$ and maximum failure probability $0 \leq \beta \leq 1$.

First, we write $y = \mu + \Sigma^{1/2} z$ for $z \sim \mathcal{N}(0, I)$. In terms of $\sigma = \sqrt{\lambda_{\max}(\Sigma)}$, we can bound the magnitude of y from above as

$$\|y\| \leq \|\mu\| + \sigma\|z\|. \tag{6.3}$$

If $\|\mu\| + \sigma\|z\| \leq \rho$, then $\|y\| \leq \rho$ as well. Thus, the event $\{\|y\| \leq \rho\}$ contains the event $\{\|\mu\| + \sigma\|z\| \leq \rho\}$. It follows that we can bound the probability that $\|y\| \leq \rho$ from below by

$$\mathbb{P}(\|y\| \leq \rho) \geq \mathbb{P}(\|\mu\| + \sigma\,\|z\| \leq \rho) = \mathbb{P}(\|z\| \leq (\rho - \|\mu\|)/\sigma). \tag{6.4}$$

The probability on the right-hand side of (6.4) can be evaluated by integrating the three-dimensional Gaussian probability density function over a ball of radius $(\rho - \|\mu\|)/\sigma$, which we have done in Theorem 2.3.4. Furthermore, using the bound $\operatorname{erf}(x) \geq 1 - \exp(-x^2)$ [116], we have that

$$\mathbb{P}(\|y\| \leq \rho) \geq \mathbb{P}(\|z\| \leq (\rho - \|\mu\|)/\sigma) \tag{6.5}$$

$$= \operatorname{erf}\left(\frac{\rho - \|\mu\|}{\sigma\sqrt{2}}\right) - \frac{2(\rho - \|\mu\|)}{\sigma\sqrt{2\pi}} \exp\left(-\frac{(\rho - \|\mu\|)^2}{2\sigma^2}\right) \tag{6.6}$$

$$\geq \underbrace{1 - \exp\left(-\frac{(\rho - \|\mu\|)^2}{2\sigma^2}\right)}_{\text{same as 2d case}} - \underbrace{\frac{2(\rho - \|\mu\|)}{\sigma\sqrt{2\pi}} \exp\left(-\frac{(\rho - \|\mu\|)^2}{2\sigma^2}\right)}_{\text{additional term}}. \tag{6.7}$$

Therefore, if

$$\left(1 + \frac{2(\rho - \|\mu\|)}{\sigma\sqrt{2\pi}}\right) \exp\left(-\frac{(\rho - \|\mu\|)^2}{2\sigma^2}\right) \leq \beta, \tag{6.8}$$

then the chance constraint (6.2) is satisfied. Rearranging terms, we rewrite the inequality (6.8) as

$$\|\mu\| + \sigma\sqrt{2\log\left(\frac{1 + \frac{2(\rho - \|\mu\|)}{\sigma\sqrt{2\pi}}}{\beta}\right)} \leq \rho. \tag{6.9}$$

The term

$$\frac{2(\rho - \|\mu\|)}{\sigma\sqrt{2\pi}} \tag{6.10}$$

inside the logarithm prevents an obvious convex formulation of the constraint (6.9).

The distance of the mean from the limit is $\rho - \|\mu\|$, and the semi-major axis of a 99.73 percentile confidence ellipse centered at μ is approximately 3σ. It follows that, heuristically, we may approximate the term $\rho - \|\mu\| \approx 3\sigma$ to describe the situation when the chance constraint is active, which in turn yields the approximation

$$\frac{2(\rho - \|\mu\|)}{\sigma\sqrt{2\pi}} \approx \frac{6}{\sqrt{2\pi}} \approx 2.39. \tag{6.11}$$

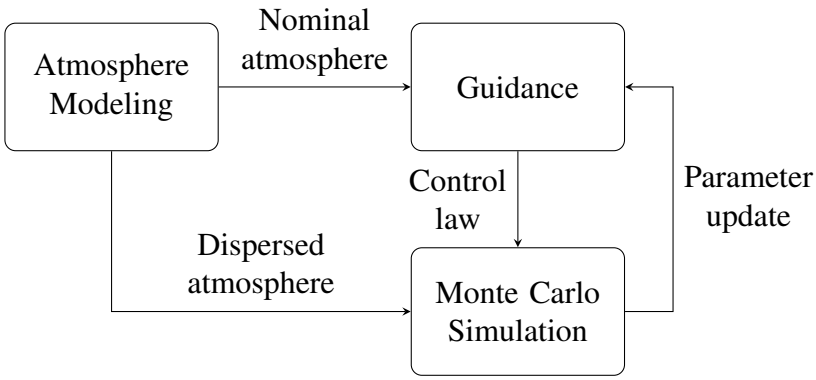

Figure 6.1: Current role of atmosphere modeling for entry and aerocapture guidance

While this approximation appears to be effective in preliminary simulations, further work is required to establish performance guarantees.

6.2.3 Stochastic Atmosphere Modeling

The role of stochastic atmosphere modeling in the state-of-the-art approach to planetary entry is shown in Figure 6.1. As current entry guidance algorithms depend only on a deterministic model of the atmosphere, the dispersed atmosphere statistics only enter the design process through Monte Carlo simulation. Based on the results of the Monte Carlo, with the dispersed atmosphere, guidance parameters may be tuned to improve performance or to reduce the probability of failure or constraint violation.

Looking forward, and based on the developments presented in this dissertation, future approaches to entry and aerocapture guidance may depend explicitly on the probabilistic structure of the atmosphere. Then, stochastic atmosphere modeling will directly affect the derivation of the guidance, as is shown in Figure 6.2. This architecture raises several questions which should be addressed in future work:

- If the guidance is derived based on an assumed stochastic atmosphere model, how robust is the guidance to atmosphere modeling error?

- The current "black-box" stochastic atmosphere models were intended to be applied as in the architecture shown in Figure 6.1. Are these models sufficient for application

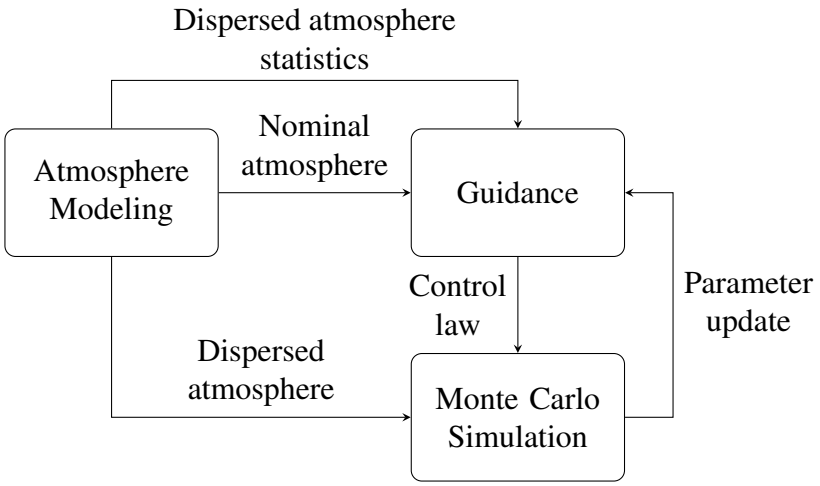

Figure 6.2: Proposed role of atmosphere modeling for entry and aerocapture guidance

in the new architecture shown in Figure 6.2?

- Is it possible to derive stochastic atmosphere models, from first principles, with the intent of application to stochastic guidance?

6.2.4 Fast Computation of Covariance Integrals

The method for chance-constrained covariance steering in a Gaussian random field presented in Chapter 5 required the computation of the covariance matrix

$$\mathrm{Cov}(W) = \begin{bmatrix} \mathbb{Q}_{0,0} & \mathbb{Q}_{0,1} & \cdots & \mathbb{Q}_{0,N-1} \\ \mathbb{Q}_{1,0} & \mathbb{Q}_{1,1} & & \vdots \\ \vdots & & \ddots & \vdots \\ \mathbb{Q}_{N-1,0} & \cdots & \cdots & \mathbb{Q}_{N-1,N-1} \end{bmatrix} \in \mathbb{R}^{Nn \times Nn}, \tag{6.12}$$

which consists of the matrix-valued, two-dimensional integrals $\mathbb{Q}_{k,\ell} \in \mathbb{R}^{n \times n}$ given by

$$\mathbb{Q}_{k,\ell} = \int_{t_k}^{t_{k+1}} \int_{t_\ell}^{t_{\ell+1}} \Phi(t_{k+1}, t) G(t) \Sigma\big(\phi(\hat{x}(t)), \phi(\hat{x}(\tau))\big) G^{\mathsf{T}}(\tau) \Phi^{\mathsf{T}}(t_{\ell+1}, \tau) \, \mathrm{d}\tau \, \mathrm{d}t, \tag{6.13}$$

where $\Phi(t, s)$ is a state transition matrix corresponding to the state matrix $A(t)$, $G(t)$ is a diffusion matrix, $\Sigma(z_1, z_2)$ is the known covariance function of a random field, and $\phi(\hat{x}(t))$ is the position in the random field of the nominal trajectory $\hat{x}(t)$ at time t.

Since the matrix $\mathrm{Cov}(W)$ is symmetric, it follows that $\mathbb{Q}_{k,\ell} = \mathbb{Q}_{\ell,k}^{\intercal}$. Computing $\mathrm{Cov}(W)$ thus requires evaluating $N(N+1)/2$ integrals of the form (6.13), where N is the number of discrete time steps considered by the algorithm. The two-dimensional integration is time consuming, and the accuracy of the integration determines the accuracy of the resulting uncertainty quantification and control method. Thus, improving the computational efficiency of (6.13) is an important consideration for future research. One possible avenue is the piecewise-constant approximation method presented in Section B.3.

6.2.5 Stochastic Control for Skip-to-Entry Guidance

In the derivation of the stochastic entry guidance presented in Chapter 3, the vehicle was assumed to be strictly descending for the entire guided entry. This assumption was made so that the changes in density variations seen by the vehicle are uncorrelated with previous density variations. If, on the other hand, the vehicle were to climb after descending, then, assuming the density variations depend on the altitude, the density variations experienced by the vehicle during the climb may be correlated to density variations seen during the descent.

Take for example the skip-to-entry mission profile, shown in Figure 6.3. Following an initial dip into the atmosphere, the vehicle leaves the atmosphere, coasts under orbital motion, and then reenters the atmosphere [38]. The vehicle thus flies through certain altitude ranges multiple times.

This situation poses both modeling and analysis challenges. If the vehicle constructs an onboard atmosphere estimate, how reasonable is an assumption that future density variations equal previous density variations? Furthermore, is it possible to characterize a probabilistic model of the atmosphere that accounts for three-dimensional spatial correlations?

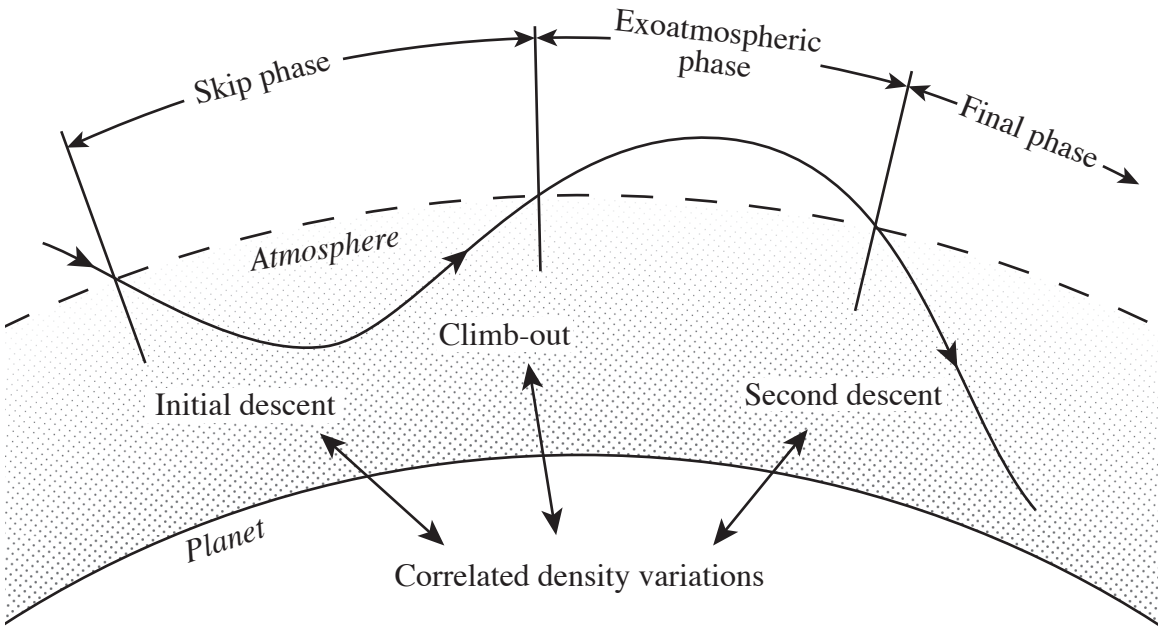

Figure 6.3: Skip-to-entry

Is is possible to leverage a spatial-correlative stochastic model to improve skip-to-entry performance?

We attempted to address these questions in Chapter 5 by using the theory for covariance steering in a Gaussian random field (CS-GRF), which includes a notion of spatial correlations of the density variations. In contrast to the state-of-the-art guidance methods [64, 42], a skip-to-entry guidance based on CS-GRF theory would not necessarily include onboard atmosphere estimation and re-planning. Rather, the effect of spatial correlations on the control law are encoded through a state-history feedback law, which could be stored onboard and accessed through table lookup, similar to as is done for the Apollo final phase entry guidance [38, 3].

However, the CS-GRF approach requires solving a convex optimization problem which scales with the square of the number of time steps. Thus, in order to apply the CS-GRF theory to a skip-to-entry mission, with several hundred decision times (e.g., 1 Hz guidance updates for the duration of the guided entry), significant advances in computational efficiency and parallelization are required.

Appendices

APPENDIX A
ENTRY TARGETING CALCULATIONS

In this section, we review the targeting calculations to solve for downrange and crossrange distances, based on Ref. [38]. See also Figure 3.2.

First, consider the following reference frame definitions: The planet-centered inertial frame *I* with basis $\{\hat{\imath}^I, \hat{\jmath}^I, \hat{k}^I\}$; the planet-centered planet fixed frame *F* with basis $\{\hat{\imath}^F, \hat{\jmath}^F, \hat{k}^F\}$, which is defined relative to the planet-centered inertial frame by the planet rotation angle η about the $\hat{k}^I$ axis; and the vehicle rotating frame *R* (also known as the up-east-north frame), which is defined relative to the planet-centered planet fixed frame by two rotations for the vehicle longitude and latitude so that $\hat{\imath}^R$ is aligned with the vehicle position $\vec{r}$. We use in this section the notation that a subscript denotes reference frame, and a superscript outside of brackets denotes a vector being expressed in a coordinate system.

A vector in planet-centered, planet-fixed coordinates is transformed into planet-centered inertial coordinates by the matrix

$$T^{IF}(\eta) = \begin{bmatrix} \cos\eta & -\sin\eta & 0 \\ \sin\eta & \cos\eta & 0 \\ 0 & 0 & 1 \end{bmatrix}. \tag{A.1}$$

Similarly, when the vehicle is at longitude θ and latitude ϕ (planet-fixed), then vectors in vehicle-rotating coordinates *R* are transformed to planet-centered, planet-fixed coordinates *F* by the matrix

$$T^{FR}(\theta,\phi) = \begin{bmatrix} \cos\theta\cos\phi & -\sin\theta & -\cos\theta\sin\phi \\ \cos\phi\sin\theta & \cos\theta & -\sin\theta\sin\phi \\ \sin\phi & 0 & \cos\phi \end{bmatrix}. \tag{A.2}$$

The vehicle position in planet-centered inertial coordinates is therefore given by

$$[\vec{r}]^I = T^{IF}(\eta)T^{FR}(\theta,\phi)\begin{bmatrix} r \\ 0 \\ 0 \end{bmatrix} = \begin{bmatrix} r\cos\phi\cos(\eta+\theta) \\ r\cos\phi\sin(\eta+\theta) \\ r\sin\phi \end{bmatrix}. \tag{A.3}$$

The vehicle velocity in the planet-fixed frame is given in vehicle rotating coordinates as

$$[\vec{V}_F]^R = \begin{bmatrix} V\sin\gamma \\ V\cos\gamma\sin\psi \\ V\cos\gamma\cos\psi \end{bmatrix}, \tag{A.4}$$

and it follows that the planet-relative vehicle velocity is planet-centered inertial coordinates is obtained by

$$[\vec{V}_F]^I = T^{IF}(\eta)T^{FR}(\theta,\phi)[\vec{V}_F]^R. \tag{A.5}$$

Finally, the vehicle velocity in the planet-centered inertial frame and in planet-centered inertial coordinates is

$$[\vec{V}_I]^I = [\vec{V}_F]^I + [\vec{\Omega}]^I \times [\vec{r}]^I, \tag{A.6}$$

where $[\vec{\Omega}]^I = [0\ 0\ \Omega]^\intercal$ is the planet rotation vector in planet-centered inertial coordinates.

The target position is defined by a target longitude θ_{targ} and target latitude ϕ_{targ}. This position is given in planet-fixed inertial coordinates at an estimated final time $t_{f,\text{est}}$ as

$$[\hat{r}_{\text{targ}}]^I = T^{IF}(\eta_0 + t_{f,\text{est}}\Omega)\begin{bmatrix} \cos\phi_{\text{targ}}\cos\theta_{\text{targ}} \\ \cos\phi_{\text{targ}}\sin\theta_{\text{targ}} \\ \sin\phi_{\text{targ}} \end{bmatrix}, \tag{A.7}$$

where η_0 is the planet rotation angle at the initial time. The downrange angle is given as

$$\delta_{\text{go}} = \cos^{-1}\left([\hat{r}_{\text{targ}}]^I \cdot [\hat{r}]^I\right), \tag{A.8}$$

where $[\hat{r}]^I = [\vec{r}]^I/r$, and the crossrange angle is

$$\varepsilon = \frac{\pi}{2} - \cos^{-1}\left([\hat{r}_{\text{targ}}]^I \cdot [\hat{h}]^I\right), \tag{A.9}$$

where $[\hat{h}]^I$ is a unit vector pointing towards the vehicle angular momentum vector in planet-centered inertial coordinates, which is given as $[\vec{h}]^I = [\vec{r}]^I \times [\vec{V}_I]^I$. The downrange and crossrange distances are then obtained by multiplying the angles δ_{go} and ε by the planet radius, or more generally, by any reference radius.

APPENDIX B

USEFUL MATHEMATICAL RESULTS

B.1 Discretization of a Linear Stochastic System

In this section, we review the procedure for the discretization of the continuous-time stochastic system

$$\mathrm{d}x(t) = \big(A(t)x(t) + B(t)u(t) + c(t)\big)\mathrm{d}t + G(t)\mathrm{d}w(t), \tag{B.1}$$

where $A(t) \in \mathbb{R}^{n\times n}$, $B(t) \in \mathbb{R}^{n\times m}$, and $G(t) \in \mathbb{R}^{n\times n}$ are known system matrices, $c(t) \in \mathbb{R}^n$ is a known drift term, $x(t) \in \mathbb{R}^n$ is the system state, $u(t) \in \mathbb{R}^m$ is the control input, and $w(t)$ is an n-dimensional Brownian motion. Let (t_k) be a sequence of times for which we wish to evaluate the state $x_k = x(t_k)$. Furthermore, assume that the control is piecewise constant on the intervals $[t_k, t_{k+1})$ so that $u_k = u(t)$ for $t \in [t_k, t_{k+1})$. Integrating the system (B.1) from t_k to t_{k+1}, we obtain

$$\begin{aligned} x_{k+1} = \underbrace{\Phi(t_{k+1}, t_k)}_{A_k} x_k + \underbrace{\int_{t_k}^{t_{k+1}} \Phi(t_{k+1}, t)B(t)\,\mathrm{d}t}_{B_k} u_k \\ + \underbrace{\int_{t_k}^{t_{k+1}} \Phi(t_{k+1}, t)c(t)\,\mathrm{d}t}_{c_k} + \underbrace{\int_{t_k}^{t_{k+1}} \Phi(t_{k+1}, t)G(t)\,\mathrm{d}w(t)}_{G_k w_k}, \end{aligned} \tag{B.2}$$

where $w_k \overset{i.i.d.}{\sim} \mathcal{N}(0, I)$, and where

$$\frac{\partial}{\partial t}\Phi(t, t_0) = A(t)\Phi(t, t_0), \qquad \Phi(t_0, t_0) = I. \tag{B.3}$$

Thus the discrete system

$$x_{k+1} = A_k x_k + B_k u_k + c_k + G_k w_k \tag{B.4}$$

is obtained with

$$A_k = \Phi(t_{k+1}, t_k), \tag{B.5}$$

$$B_k = \int_{t_k}^{t_{k+1}} \Phi(t_{k+1}, t) B(t) \, \mathrm{d}t, \tag{B.6}$$

$$c_k = \int_{t_k}^{t_{k+1}} \Phi(t_{k+1}, t) c(t) \, \mathrm{d}t, \tag{B.7}$$

and where G_k is any matrix such that

$$G_k w_k \overset{\mathrm{d}}{=} \int_{t_k}^{t_{k+1}} \Phi(t_{k+1}, t) G(t) \, \mathrm{d}w(t), \tag{B.8}$$

where $\overset{\mathrm{d}}{=}$ denotes equality in distribution. It follows that G_k satisfies

$$G_k G_k^{\mathsf{T}} = \int_{t_k}^{t_{k+1}} \Phi(t_{k+1}, t) G(t) G^{\mathsf{T}}(t) \Phi^{\mathsf{T}}(t_{k+1}, t) \, \mathrm{d}t, \tag{B.9}$$

and thus G_k can be obtained by taking any matrix square root, such as the Cholesky decomposition, of the integral on the right hand of (B.9). Computing the discrete representation (B.4) of the system (B.1) thus requires evaluating the integrals (B.5), (B.6), (B.7), and (B.9).

B.2 Piecewise-Constant Approximation for Discretization

In this section, we present a computationally efficient method for approximating the discretization of the continuous-time stochastic system (B.1). In the case that $A(t)$, $B(t)$, $c(t)$, and $G(t)$ are constant, then we can use the result that the integrals

$$M_1(t; A) = \int_0^t e^{A(t-s)} \, \mathrm{d}s, \qquad M_2(t; A, G) = \int_0^t e^{A(t-s)} G G^{\mathsf{T}} e^{-A^{\mathsf{T}} s} \, \mathrm{d}s \tag{B.10}$$

are obtained by the matrix exponential [134]

$$e^{Yt} = \begin{bmatrix} - & M_1(t;A) & - & - \\ 0 & - & - & - \\ 0 & 0 & - & M_2(t;A,G) \\ 0 & 0 & 0 & - \end{bmatrix}, \quad \text{where} \quad Y = \begin{bmatrix} A & I & 0 & 0 \\ 0 & 0 & 0 & 0 \\ 0 & 0 & A & GG^\intercal \\ 0 & 0 & 0 & -A^\intercal \end{bmatrix}. \tag{B.11}$$

We proceed to approximate the discrete system (B.4) by taking $A(t)$, $B(t)$, $c(t)$, and $G(t)$ to be constant on a finer time grid than (t_k), and then computing the integrals (B.5), (B.6), (B.7), and (B.9) in terms of the integrals (B.10).

Let (t_i^k) be a partition of $[t_k, t_{k+1}]$ such that

$$t_k = t_0^k < t_1^k < \cdots < t_{N_k}^k = t_{k+1}. \tag{B.12}$$

Integrating (B.1) from t_i^k to t_{i+1}^k results in the discrete-system characterized by

$$A_i^k = \Phi(t_{i+1}^k, t_i^k) \qquad \approx \exp\big(A(t_i^k)(t_{i+1}^k - t_i^k)\big), \tag{B.13}$$

$$B_i^k = \int_{t_i^k}^{t_{i+1}^k} \Phi(t_{i+1}^k, t) B(t)\,\mathrm{d}t \qquad \approx \int_{t_i^k}^{t_{i+1}^k} \exp\big(A(t_i^k)(t_{i+1}^k - t)\big)\,\mathrm{d}t\, B(t_i^k), \tag{B.14}$$

$$c_i^k = \int_{t_i^k}^{t_{i+1}^k} \Phi(t_{i+1}^k, t) c(t)\,\mathrm{d}t \qquad \approx \int_{t_i^k}^{t_{i+1}^k} \exp\big(A(t_i^k)(t_{i+1}^k - t)\big)\,\mathrm{d}t\, c(t_i^k), \tag{B.15}$$

where

$$\int_{t_i^k}^{t_{i+1}^k} \exp\big(A(t_i^k)(t_{i+1}^k - t)\big)\,\mathrm{d}t = M_1\big(t_{i+1}^k - t_i^k; A(t_i^k)\big), \tag{B.16}$$

and

$$G_i^k G_i^{k\intercal} = \int_{t_i^k}^{t_{i+1}^k} \Phi(t_{i+1}^k, t) G(t) G^\intercal(t) \Phi^\intercal(t_{i+1}^k, t)\,\mathrm{d}t \tag{B.17}$$

$$\approx \int_{t_i^k}^{t_{i+1}^k} \exp\big(A(t_i^k)(t_{i+1}^k - t)\big) G(t_i^k) G^\intercal(t_i^k) \exp\big(A^\intercal(t_i^k)(t_{i+1}^k - t)\big)\,\mathrm{d}t \tag{B.18}$$

$$= \int_{t_i^k}^{t_{i+1}^k} \exp\big(A(t_i^k)(t_{i+1}^k - t)\big) G(t_i^k) G^{\mathsf{T}}(t_i^k) \exp\big(-A^{\mathsf{T}}(t_i^k)t\big)\,\mathrm{d}t\, \exp\big(A^{\mathsf{T}}(t_i^k)t_i^k\big) \quad \text{(B.19)}$$

$$= M_2\big(t_{i+1}^k - t_i^k; A(t_i^k), G(t_i^k)G^{\mathsf{T}}(t_i^k)\big) \exp\big(A^{\mathsf{T}}(t_i^k)t_i^k\big). \quad \text{(B.20)}$$

It remains to describe the original discrete system (B.4) in terms of the values A_i^k, B_i^k, c_i^k, and $G_i^k G_i^{k\mathsf{T}}$. First, the matrices A_k and B_k are rewritten as

$$A_k = \Phi(t_{k+1}, t_k) = \Phi(t_{N_k}^k, t_{N_k-1}^k)\Phi(t_{N_k-1}^k, t_{N_k-1}^k)\cdots\Phi(t_1^k, t_0^k) \quad \text{(B.21)}$$

$$= \prod_{i=0}^{N_k-1} \Phi(t_{i+1}^k, t_i^k) \quad \text{(B.22)}$$

$$= \prod_{i=0}^{N_k-1} A_i^k, \quad \text{(B.23)}$$

and

$$B_k = \int_{t_k}^{t_{k+1}} \Phi(t_{k+1}, t)B(t)\,\mathrm{d}t \quad \text{(B.24)}$$

$$= \sum_{i=0}^{N_k-1} \int_{t_i^k}^{t_{i+1}^k} \Phi(t_{k+1}, t)B(t)\,\mathrm{d}t \quad \text{(B.25)}$$

$$= \sum_{i=0}^{N_k-1} \Phi(t_{k+1}, t_{i+1}^k) \int_{t_i^k}^{t_{i+1}^k} \Phi(t_{i+1}^k, t)B(t)\,\mathrm{d}t \quad \text{(B.26)}$$

$$= \sum_{i=0}^{N_k-1} \left(\prod_{j=i+1}^{N_k-1} \Phi(t_{i+1}^k, t_i^k)\right) \int_{t_i^k}^{t_{i+1}^k} \Phi(t_{i+1}^k, t)B(t)\,\mathrm{d}t \quad \text{(B.27)}$$

$$= \sum_{i=0}^{N_k-1} \left(\prod_{j=i+1}^{N_k-1} A_j^k\right) B_i^k. \quad \text{(B.28)}$$

Similarly, the vector c_k is given by

$$c_k = \sum_{i=0}^{N_k-1} \left(\prod_{j=i+1}^{N_k-1} A_j^k\right) c_i^k. \quad \text{(B.29)}$$

Finally, the product $G_k G_k^\intercal$ is written as

$$G_k G_k^\intercal = \int_{t_k}^{t_{k+1}} \Phi(t_{k+1}, t) G(t) G^\intercal(t) \Phi^\intercal(t_{k+1}, t)\, \mathrm{d}t \tag{B.30}$$

$$= \sum_{i=0}^{N_k-1} \int_{t_i^k}^{t_{i+1}^k} \Phi(t_{k+1}, t) G(t) G^\intercal(t) \Phi^\intercal(t_{k+1}, t)\, \mathrm{d}t \tag{B.31}$$

$$= \sum_{i=0}^{N_k-1} \Phi(t_{k+1}, t_{i+1}^k) \bigg(\int_{t_i^k}^{t_{i+1}^k} \Phi(t_{i+1}^k, t) G(t) G^\intercal(t) \Phi^\intercal(t_{i+1}^k, t)\, \mathrm{d}t \bigg) \Phi^\intercal(t_{k+1}, t_{i+1}^k) \tag{B.32}$$

$$= \sum_{i=0}^{N_k-1} \bigg(\prod_{j=i+1}^{N_k-1} A_j^k \bigg) G_i^k G_i^{k\intercal} \bigg(\prod_{j=i+1}^{N_k-1} A_j^k \bigg)^\intercal. \tag{B.33}$$

In summary, the integrals (B.5), (B.6), (B.7), and (B.9) describing the discrete system (B.4) have been approximated by N_k evaluations of the matrix exponential (B.11).

B.3 Piecewise-Constant Approximation for Covariance Integrals

In this section, we provide an approximate expression for integrals of the form

$$\mathbb{Q}_{k,\ell} = \int_{t_k}^{t_{k+1}} \int_{t_\ell}^{t_{\ell+1}} \Phi(t_{k+1}, t) G(t) \Sigma\big(\phi(\hat{x}(t)), \phi(\hat{x}(\tau))\big) G^\intercal(\tau) \Phi^\intercal(t_{\ell+1}, \tau)\, \mathrm{d}\tau\, \mathrm{d}t, \tag{B.34}$$

where $\Phi(t, s)$ is a state transition matrix corresponding to the state matrix $A(t)$, $G(t)$ is a diffusion matrix, $\Sigma(z_1, z_2)$ is the known covariance function of a random field, and $\phi(\hat{x}(t))$ is the position in the random field of the nominal trajectory.

As in the previous section, we use the fact that the integral

$$M(t) = \int_0^t e^{A(t-s)}\, \mathrm{d}s \tag{B.35}$$

is obtained by the matrix exponential

$$e^{Yt} = \begin{bmatrix} - & M(t) & - & - \\ 0 & - & - & - \\ 0 & 0 & - & - \\ 0 & 0 & 0 & - \end{bmatrix}, \quad \text{where} \quad Y = \begin{bmatrix} A & I & 0 & 0 \\ 0 & 0 & 0 & 0 \\ 0 & 0 & 0 & 0 \\ 0 & 0 & 0 & 0 \end{bmatrix}. \tag{B.36}$$

We subdivide the intervals $[t_k, t_{k+1}]$ into N_k subintervals $[t_i^k, t_{i+1}^k]$, where (t_i^k) is a partition given by

$$t_k = t_0^k < t_1^k < \cdots < t_{N^k}^k = t_{k+1}. \tag{B.37}$$

The integral (B.34) over $[t_k, t_{k+1}] \times [t_\ell, t_{\ell+1}]$ can be written as $N_k \times N_\ell$ separate integrals given by

$$\mathbb{Q}_{k,\ell} = \int_{t_k}^{t_{k+1}} \int_{t_\ell}^{t_{\ell+1}} f(t,\tau)\,\mathrm{d}t\,\mathrm{d}\tau = \sum_{i=0}^{N_k-1} \sum_{j=0}^{N_\ell-1} \int_{t_i^k}^{t_{i+1}^k} \int_{t_j^\ell}^{t_{j+1}^\ell} f(t,\tau)\,\mathrm{d}t\,\mathrm{d}\tau, \tag{B.38}$$

where

$$f(t,\tau) = \Phi(t_{k+1},t)G(t)\Sigma\big(\phi(\hat{x}(t)),\phi(\hat{x}(\tau))\big)G^\intercal(\tau)\Phi^\intercal(t_{\ell+1},\tau)\,\mathrm{d}\tau\,\mathrm{d}t. \tag{B.39}$$

Next, we approximate the integrand $f(t,\tau)$ so that each of the $N_k \times N_\ell$ integrals in (B.38) can be computed by matrix exponentiation as in (B.36). The covariance function Σ and the diffusion matrices G are taken to be constant on the sets $[t_i^k, t_{i+1}^k] \times [t_j^\ell, t_{j+1}^\ell]$, and the state transition matrix is approximated to first order as

$$\Phi(t_{k+1},t)G(t) = \Phi(t_{k+1},t_{i+1}^k)\Phi(t_{i+1}^k,t)G(t) \tag{B.40}$$

$$\approx \Phi(t_{k+1},t_{i+1}^k)\exp\big(A(t_i^k)(t_{i+1}^k - t)\big)G(t_i^k), \tag{B.41}$$

which, upon substitution into (B.39), results in the approximation

$$f(t,\tau) \approx \Phi(t_{k+1}, t^k_{i+1}) \exp\big(A(t^k_i)(t^k_{i+1} - t)\big) G(t^k_i) \Sigma\big(\phi(\hat{x}(t^k_i)), \phi(\hat{x}(t^\ell_j))\big) \\ G^\mathsf{T}(t^\ell_j) \exp\big(A^\mathsf{T}(t^\ell_j)(t^\ell_{j+1} - \tau)\big) \Phi^\mathsf{T}(t_{\ell+1}, t^\ell_{j+1}). \quad \text{(B.42)}$$

Substituting (B.42) into (B.38), we obtain

$$\int_{t^k_i}^{t^k_{i+1}} \int_{t^k_j}^{t^k_{j+1}} f(t,\tau)\,\mathrm{d}t\,\mathrm{d}\tau \approx \\ \Phi(t_{k+1}, t^k_{i+1}) \bigg(\int_{t^k_i}^{t^k_{i+1}} \exp\big(A(t^k_i)(t^k_{i+1} - t)\big)\,\mathrm{d}t \bigg) G(t^k_i) \Sigma\big(\phi(\hat{x}(t^k_i)), \phi(\hat{x}(t^\ell_j))\big) \\ G^\mathsf{T}(t^\ell_j) \bigg(\int_{t^\ell_j}^{t^\ell_{j+1}} \exp\big(A(t^\ell_j)(t^\ell_{j+1} - \tau)\big)\,\mathrm{d}\tau \bigg)^\mathsf{T} \Phi^\mathsf{T}(t_{\ell+1}, t^\ell_{j+1}), \quad \text{(B.43)}$$

where the remaining integral terms on the right-hand side of (B.43) can be quickly computed as in (B.36). The term $\mathbb{Q}_{k,\ell}$ is thus computed by evaluating and summing $N_k \times N_\ell$ matrix exponentials — a procedure which can be parallelized.

APPENDIX C
AUTHOR'S PUBLICATIONS

C.1 Journals

1. **J. Ridderhof** and P. Tsiotras, "Minimum-Fuel Closed-Loop Powered Descent Guidance with Stochastically Derived Throttle Margins," *Journal of Guidance, Control, and Dynamics*, vol. 44, no. 3, pp 537–547, 2021. doi:10.2514/1.G005400

2. **J. Ridderhof**, P. Tsiotras, and B. Johnson, "Stochastic Entry Guidance," *Journal of Guidance, Control, and Dynamics* (under review).

3. **J. Ridderhof** and P. Tsiotras, "Chance-Constrained Covariance Steering in a Gaussian Random Field via Successive Convex Programming," *Journal of Guidance, Control, and Dynamics* (under review).

C.2 Conferences

1. **J. Ridderhof** and P. Tsiotras, "Uncertainty Quantification and Control During Mars Powered Descent and Landing using Covariance Steering," in *AIAA Guidance, Navigation, and Control Conference*, Kissimmee, FL, Jan. 2018. doi:10.2514/6.2018-0611

2. **J. Ridderhof** and P. Tsiotras, "Minimum-fuel Powered Descent in the Presence of Random Disturbances," in *AIAA Guidance, Navigation, and Control Conference*, San Diego, CA, Jan. 2019. (1^{st} place in student paper competition) doi:10.2514/6.2019-0646

3. **J. Ridderhof**, K. Okamoto, and P. Tsiotras, "Nonlinear Uncertainty Control with Iterative Covariance Steering," in *IEEE Conference on Decision and Control*, Nice,

France, Dec. 2019. doi:10.1109/CDC40024.2019.9029993

4. **J. Ridderhof** and P. Tsiotras, "Stochastic Atmosphere Modeling for Risk Adverse Aerocapture Guidance", in *IEEE Aerospace Conference*, Big Sky, MT, Mar. 2020. doi:10.1109/AERO47225.2020.9172724

5. **J. Ridderhof**, J. Pilipovsky, and P. Tsiotras, "Chance-Constrained Covariance Control for Low-Thrust Minimum-Fuel Trajectory Optimization", in *AAS/AIAA Astrodynamics Specialist Conference*, Virtual event, Aug. 2020.

6. **J. Ridderhof**, K. Okamoto, and P. Tsiotras, "Chance Constrained Covariance Control for Linear Stochastic Systems With Output Feedback", in *IEEE Conference on Decision and Control*, Virtual event, Dec. 2020. doi:10.1109/CDC42340.2020.9303731

7. **J. Ridderhof** and P. Tsiotras, "Planetary Entry in a Randomly Perturbed Atmosphere," in *AIAA Guidance, Navigation, and Control Conference*, Virtual event, Jan. 2021. (2^{nd} place in student paper competition) doi:10.2514/6.2021-1218

8. V.M. Makkapati, **J. Ridderhof**, P. Tsiotras, J. Hart, and B. Waanders, "Desensitized Trajectory Optimization for Hypersonic Vehicles", in *IEEE Aerospace Conference*, Virtual event, Mar. 2021.

9. D. Zheng, **J. Ridderhof**, P. Tsiotras, and A. Agha-mohammadi, "Belief Space Planning: A Covariance Steering Approach", in *Robotics: Science and Systems*, Virtual event, July 2021. (under review)

REFERENCES

[1] V. G. Perminov, *The Difficult Road to Mars: A Brief History of Mars Exploration in the Soviet Union*, ser. Monographs in Aerospace History 15. NASA, 1999.

[2] R. N. Ingoldby, "Guidance and control system design of the Viking planetary lander," *Journal of Guidance, Control, and Dynamics*, vol. 1, no. 3, pp. 189–196, 1978. DOI: 10.2514/3.55763.

[3] G. F. Mendeck and L. Craig McGrew, "Entry guidance design and postflight performance for 2011 Mars Science Laboratory mission," *Journal of Spacecraft and Rockets*, vol. 51, no. 4, pp. 1094–1105, 2014. DOI: 10.2514/1.A32737.

[4] D. Way, S. Dutta, C. Zumwalt, and S. Santini De León, "EDL simulation results for the Mars 2020 landing site safety assessment," in *IEEE Aerospace Conference*, Big Sky, MT, 2020. DOI: 10.1109/AERO47225.2020.9172525.

[5] "Human exploration of Mars design reference architecture 5.0," NASA, Tech. Rep. SP-2009-566, 2009.

[6] T. Martin-Mur, G. Kruizinga, P. Burkhart, F Abilleira, M. Wong, and J. Kangas, "Mars Science Laboratory interplanetary navigation," *Journal of Spacecraft and Rockets*, vol. 51, no. 4, pp. 1014–1028, 2014. DOI: 10.2514/1.A32631.

[7] S. W. Sell, J. Davis, A. Miguel San Martin, and F. Serricchio, "Powered flight design and performance summary for the Mars Science Laboratory mission," *Journal of Spacecraft and Rockets*, vol. 51, no. 4, pp. 1197–1207, 2014. DOI: 10.2514/1.A32682.

[8] D. W. Way, J. L. Davis, and J. D. Shidner, "Assessment of the Mars Science Laboratory entry, descent, and landing simulation," in *23rd AAS/AIAA Space Flight Mechanics Meeting*, Kauai, HI, 2013.

[9] S. Dutta and D. W. Way, "Comparison of the effects of velocity and range triggers on trajectory dispersions for the Mars 2020 mission," in *AIAA Atmospheric Flight Mechanics Conference*, Grapevine, Texas, 2017. DOI: 10.2514/6.2017-0245.

[10] A. R. Klumpp, "Apollo lunar descent guidance," *Automatica*, vol. 10, no. 2, pp. 133–146, 1974. DOI: 10.1016/0005-1098(74)90019-3.

[11] E. C. Wong, G. Singh, and J. P. Masciarelli, "Guidance and control design for hazard avoidance and safe landing on Mars," *Journal of Spacecraft and Rockets*, vol. 43, no. 2, pp. 378–384, 2006. DOI: 10.2514/1.19220.

[12] G. Singh, A. Miguel San Martin, and E. C. Wong, "Guidance and control design for powered descent and landing on Mars," in *2007 IEEE Aerospace Conference*, Big Sky, MT, 2007. DOI: 10.1109/AERO.2007.352818.

[13] I. Ross, "How to find minimum-fuel controllers," in *AIAA Guidance, Navigation, and Control Conference and Exhibit*, Providence, RI, 2004. DOI: 10.2514/6.2004-5346.

[14] J. P. Marec, *Optimal Space Trajectories*, ser. Studies in Astronautics. Elsevier Scientific Pub. Co., 1979, ISBN: 0444418121.

[15] A. E. Bryson and Y.-C. Ho, *Applied Optimal Control: Optimization, Estimation and Control*. Ginn and Company, 1975. DOI: 10.1201/9781315137667.

[16] J Meditch, "On the problem of optimal thrust programming for a lunar soft landing," *IEEE Transactions on Automatic Control*, vol. 9, no. 4, pp. 477–484, 1964. DOI: 10.1109/TAC.1964.1105758.

[17] U. Topcu, J. Casoliva, and K. D. Mease, "Minimum-fuel powered descent for Mars pinpoint landing," *Journal of Spacecraft and Rockets*, vol. 44, no. 2, pp. 324–331, 2007. DOI: 10.2514/1.25023.

[18] Z. Song, C. Wang, S. Theil, D. Seelbinder, M. Sagliano, X. Liu, and Z. Shao, "Survey of autonomous guidance methods for powered planetary landing," *Frontiers of Information Technology & Electronic Engineering*, 2020. DOI: 10.1631/FITEE.1900458.

[19] B. Açıkmeşe and S. R. Ploen, "Convex programming approach to powered descent guidance for Mars landing," *Journal of Guidance, Control, and Dynamics*, vol. 30, no. 5, pp. 1353–1366, 2007. DOI: 10.2514/1.27553.

[20] B. Açıkmeşe, J. M. Carson III, and L. Blackmore, "Lossless convexification of nonconvex control bound and pointing constraints of the soft landing optimal control problem," *IEEE Transactions on Control Systems Technology*, vol. 21, no. 6, pp. 2104–2113, 2013. DOI: 10.1109/TCST.2012.2237346.

[21] D. P. Scharf, B. Açıkmeşe, D. Dueri, J. Benito, and J. Casoliva, "Implementation and experimental demonstration of onboard powered-descent guidance," *Journal of Guidance, Control, and Dynamics*, vol. 40, no. 2, pp. 213–229, 2017. DOI: 10.2514/1.G000399.

[22] T. Reynolds, M. Szmuk, D. Malyuta, M. Mesbahi, B. Açıkmeşe, and J. M. Carson, "A state-triggered line of sight constraint for 6-dof powered descent guidance problems," in *AIAA Scitech 2019 Forum*, San Diego, CA, 2019. DOI: 10.2514/6.2019-0924.

[23] U. Lee and M. Mesbahi, "Constrained autonomous precision landing via dual quaternions and model predictive control," *Journal of Guidance, Control, and Dynamics*, vol. 40, no. 2, pp. 292–308, 2017. DOI: 10.2514/1.G001879.

[24] M. Szmuk, B. Açıkmeşe, and A. W. Berning, "Successive convexification for fuel-optimal powered landing with aerodynamic drag and non-convex constraints," in *AIAA Guidance, Navigation, and Control Conference*, San Diego, CA, 2016. DOI: 10.2514/6.2016-0378.

[25] M. Szmuk, T. Reynolds, B. Açıkmeşe, M. Mesbahi, and J. M. Carson, "Successive convexification for 6-dof powered descent guidance with compound state-triggered constraints," in *AIAA Scitech 2019 Forum*, San Diego, CA, 2019. DOI: 10.2514/6.2019-0926.

[26] P. Lu, "Propellant-optimal powered descent guidance," *Journal of Guidance, Control, and Dynamics*, vol. 41, no. 4, pp. 813–826, 2018. DOI: 10.2514/1.G003243.

[27] P. Lu, R. R. Sostaric, and G. F. Mendeck, "Adaptive powered descent initiation and fuel-optimal guidance for Mars applications," in *2018 AIAA Guidance, Navigation, and Control Conference*, Kissimmee, FL, 2018. DOI: 10.2514/6.2018-0616.

[28] P. Lu, "Augmented apollo powered descent guidance," *Journal of Guidance, Control, and Dynamics*, vol. 42, no. 3, pp. 447–457, 2019. DOI: 10.2514/1.G004048.

[29] ——, "Theory of fractional-polynomial powered descent guidance," *Journal of Guidance, Control, and Dynamics*, vol. 43, no. 3, pp. 398–409, 2019. DOI: 10.2514/1.G004556.

[30] B. J. Johnson, R. R. Sostaric, and P. Lu, "Mid lift-to-drag ratio rigid vehicle 6-dof performance for human Mars entry, descent, and landing: A fractional polynomial powered descent guidance approach," in *AIAA Scitech 2020 Forum*, Orlando, FL, 2020. DOI: 10.2514/6.2020-1513.

[31] H. Johnston, E. Schiassi, R. Furfaro, and D. Mortari, "Fuel-efficient powered descent guidance on large planetary bodies via theory of functional connections," *The Journal of the Astronautical Sciences*, vol. 67, no. 4, pp. 1521–1552, 2020. DOI: 10.1007/s40295-020-00228-x.

[32] I. Exarchos, E. Theodorou, and P. Tsiotras, "L^1-optimal control via forward and backward stochastic differential equations," *Systems and Control Letters*, vol. 118, pp. 101–108, 2018. DOI: 10.1016/j.sysconle.2018.06.005.

[33] ——, "Optimal thrust profile for planetary soft landing under stochastic disturbances," *Journal of Guidance, Control, and Dynamics*, vol. 42, no. 1, pp. 209–216, 2019. DOI: 10.2514/1.g003598.

[34] B. Açıkmeşe, J. M. Carson III, and D. S. Bayard, "A robust model predictive control algorithm for incrementally conic uncertain/nonlinear systems," *International Journal of Robust and Nonlinear Control*, vol. 21, no. 5, pp. 563–590, 2011. DOI: 10.1002/rnc.1613.

[35] P. Lu, "Entry guidance: A unified method," *Journal of Guidance, Control, and Dynamics*, vol. 37, no. 3, pp. 713–728, 2014. DOI: 10.2514/1.62605.

[36] R. D. Braun and R. M. Manning, "Mars exploration entry, descent and landing challenges," in *IEEE Aerospace Conference*, Big Sky, MT, 2006. DOI: 10.1109/AERO.2006.1655790.

[37] A. D. Cianciolo and T. T. Polsgrove, "Human Mars entry, descent, and landing architecture study overview," in *AIAA SPACE*, Long Beach, CA, 2016. DOI: 10.2514/6.2016-5494.

[38] P. E. Moseley, *The Apollo entry guidance: A review of the mathematical development and its operational characteristics*, TRW Note No. 69-FMT-791, 1969.

[39] G. L. Carman, D. G. Ives, and D. K. Geller, "Apollo-derived precision lander guidance," in *23rd Atmospheric Flight Mechanics Conference*, Boston, MA, 1998. DOI: 10.2514/6.1998-4570.

[40] R. Powell, "Numerical roll reversal predictor corrector aerocapture and precision landing guidance algorithms for the mars surveyor program 2001 missions," in *23rd Atmospheric Flight Mechanics Conference*, Boston, MA, 1998. DOI: 10.2514/6.1998-4574.

[41] S. Xue and P. Lu, "Constrained predictor-corrector entry guidance," *Journal of Guidance, Control, and Dynamics*, vol. 33, no. 4, pp. 1273–1281, 2010. DOI: 10.2514/1.49557.

[42] Z. R. Putnam, M. D. Neave, and G. H. Barton, "PredGuid entry guidance for Orion return from low Earth orbit," in *IEEE Aerospace Conference*, Big Sky, MT, 2010. DOI: 10.1109/AERO.2010.5447010.

[43] J. C. Harpold and C. A. J. Graves, "Shuttle entry guidance," *Journal of the Astronautical Sciences*, vol. 37, no. 3, pp. 239–268, 1979.

[44] J. C. Harpold and D. E. Gavert, "Space shuttle entry guidance performance results," *Journal of Guidance, Control, and Dynamics*, vol. 6, no. 6, pp. 442–447, 1983. DOI: 10.2514/3.8523.

[45] P. Lu, "Entry guidance and trajectory control for reusable launch vehicle," *Journal of Guidance, Control, and Dynamics*, vol. 20, no. 1, pp. 143–149, 1997. DOI: 10.2514/2.4008.

[46] K. D. Mease and J.-P. Kremer, "Shuttle entry guidance revisited using nonlinear geometric methods," *Journal of Guidance, Control, and Dynamics*, vol. 17, no. 6, pp. 1350–1356, 1994. DOI: 10.2514/3.21355.

[47] K.-Y. Tu, M. S. Munir, K. D. Mease, and D. S. Bayard, "Drag-based predictive tracking guidance for Mars precision landing," *Journal of Guidance, Control, and Dynamics*, vol. 23, no. 4, pp. 620–628, 2000. DOI: 10.2514/2.4607.

[48] M. K. Lockwood, K. T. Edquist, B. R. Starr, B. R. Hollis, G. A. Hrinda, R. W. Bailey, J. L. Hall, T. R. Spilker, M. A. Noca, and N O'Kongo, "Aerocapture systems analysis for a Neptune mission," NASA, Tech. Rep. TM-2006-214300, 2006.

[49] J. Masciarelli, C. Westhelle, and C. Graves, "Aerocapture guidance performance for the Neptune orbiter," in *AIAA Atmospheric Flight Mechanics Conference and Exhibit*, Providence, RI, 2004. DOI: 10.2514/6.2004-4954.

[50] M. K. Lockwood, "Neptune aerocapture systems analysis," in *AIAA Atmospheric Flight Mechanics Conference and Exhibit*, Providence, RI, 2004. DOI: 10.2514/6.2004-4951.

[51] H. S. Wright, D. Y. Oh, C. H. Westhelle, J. L. Fisher, R. E. Dyke, K. T. Edquist, J. L. Brown, H. L. Justh, and M. M. Munk, "Mars aerocapture systems study," NASA, Tech. Rep. TM-2006-214522, 2006.

[52] M. K. Lockwood, "Titan aerocapture systems analysis," in *39th AIAA/ASME/SAE/ASEE Joint Propulsion Conference and Exhibit*, Huntsville, AL, 2003. DOI: 10.2514/6.2003-4799.

[53] M. K. Lockwood, E. M. Queen, D. W. Way, R. W. Powell, K. Edquist, B. W. Starr, B. R. Hollis, E. V. Zoby, G. A. Hrinda, and R. W. Bailey, "Aerocapture systems analysis for a titan mission," Tech. Rep. TM-2006-214273, 2006.

[54] R. D. Braun and R. W. Powell, "Predictor-corrector guidance algorithm for use in high-energy aerobraking system studies," *Journal of Guidance, Control, and Dynamics*, vol. 15, no. 3, pp. 672–678, 1992. DOI: 10.2514/3.20890.

[55] R. W. Powell and R. D. Braun, "Six-degree-of-freedom guidance and control analysis of Mars aerocapture," *Journal of Guidance, Control, and Dynamics*, vol. 16, no. 6, pp. 1038–1044, 1993. DOI: 10.2514/3.21125.

[56] E. Roelke, M. Werner, and R. D. Braun, "Single-stage drag modulation GNC performance for Venus aerocapture demonstration," in *AIAA Scitech 2019 Forum*, San Diego, CA, 2019. DOI: 10.2514/6.2019-0016.

[57] D. T. Ward and J. Shipley Buford W., "Control algorithms for aerobraking in the Martian atmosphere," NASA, Technical Report NASA-CR-185665, 1991.

[58] J. M. Lafleur, "The conditional equivalence of ΔV minimization and apoapsis targeting in numerical predictor-corrector aerocapture guidance," NASA, Technical Report TM-2011-216156, 2011.

[59] D. A. Matz and C. Cerimele, "Development of a numeric predictor-corrector aerocapture guidance for direct force control," in *AIAA Scitech 2020 Forum*, Orlando, FL, 2020. DOI: 10.2514/6.2020-0847.

[60] R. G. Deshmukh, D. A. Spencer, and S. Dutta, "Investigation of direct force control for aerocapture at Neptune," *Acta Astronautica*, vol. 175, pp. 375–386, 2020. DOI: 10.1016/j.actaastro.2020.05.047.

[61] Z. R. Putnam, I. G. Clark, and R. D. Braun, "Drag modulation flight control for aerocapture," in *IEEE Aerospace Conference*, Big Sky, MT, 2012. DOI: 10.1109/AERO.2012.6186999.

[62] A. Austin, A. Nelessen, B. Strauss, J. Ravich, M. Jesick, E. Venkatapathy, R. Beck, P. Wercinski, M. Aftosmis, M. Wilder, *et al.*, "Smallsat aerocapture to enable a new paradigm of planetary missions," in *IEEE Aerospace Conference*, Big Sky, MT, 2019. DOI: 10.1109/AERO.2019.8742220.

[63] E Roelke and R. Braun, "Discrete-event drag-modulated guidance performance for Venus aerocapture," *Journal of Spacecraft and Rockets*, 2020. DOI: 10.2514/1.A34761.

[64] P. Lu, C. J. Cerimele, M. A. Tigges, and D. A. Matz, "Optimal aerocapture guidance," *Journal of Guidance, Control, and Dynamics*, vol. 38, no. 4, pp. 553–565, 2015. DOI: 10.2514/1.G000713.

[65] C. R. Heidrich and R. D. Braun, "Aerocapture trajectory design in uncertain entry environments," in *AIAA Scitech 2020 Forum*, Orlando, FL, 2020. DOI: 10.2514/6.2020-1741.

[66] J. Ridderhof and P. Tsiotras, "Stochastic atmosphere modeling for risk adverse aerocapture guidance," in *2020 IEEE Aerospace Conference*, Big Sky, MT, 2020. DOI: 10.1109/AERO47225.2020.9172724.

[67] S. W. Albert, A. Doostan, and H. Schaub, "Finite-dimensional density representation for aerocapture uncertainty quantification," in *AIAA Scitech 2021 Forum*, Virtual event, 2021. DOI: 10.2514/6.2021-0932.

[68] C. Justus, B. James, S. Bougher, A. Bridger, R. Haberle, J. Murphy, and S Engel, "Mars-GRAM 2000: A Mars atmospheric model for engineering applications," *Advances in Space Research*, vol. 29, no. 2, pp. 193–202, 2002. DOI: 10.1016/S0273-1177(01)00569-5.

[69] Y. Chen, T. T. Georgiou, and M. Pavon, "Optimal steering of a linear stochastic system to a final probability distribution, Part II," *IEEE Transactions on Automatic Control*, vol. 61, no. 5, pp. 1170–1180, 2016. DOI: 10.1109/TAC.2015.2457791.

[70] J. Ridderhof, K. Okamoto, and P. Tsiotras, "Nonlinear uncertainty control with iterative covariance steering," in *IEEE 58th Conference on Decision and Control*, Nice, France, 2019, pp. 3484–3490. DOI: 10.1109/CDC40024.2019.9029993.

[71] K. Okamoto, M. Goldshtein, and P. Tsiotras, "Optimal covariance control for stochastic systems under chance constraints," *IEEE Control Systems Letters*, vol. 2, no. 2, pp. 266–271, 2018. DOI: 10.1109/LCSYS.2018.2826038.

[72] F. Alabau-Boussouira, R. Brockett, O. Glass, J. Le Rousseau, and E. Zuazua, *Control of Partial Differential Equations*, J.-M. C. Piermarco Cannarsa, Ed., ser. Lecture Notes in Mathematics. Cetraro, Italy: Springer, 2012, vol. 2048. DOI: 10.1007/978-3-642-27893-8.

[73] A. F. Hotz and R. E. Skelton, "A covariance control theory," in *IEEE Conference on Decision and Control*, vol. 24, Fort Lauderdale, FL, 1985, pp. 552–557. DOI: 10.1109/CDC.1985.268547.

[74] A. Hotz and R. E. Skelton, "Covariance control theory," *International Journal of Control*, vol. 46, no. 1, pp. 13–32, 1987. DOI: 10.1080/00207178708933880.

[75] Y. Chen, T. T. Georgiou, and M. Pavon, "Optimal steering of a linear stochastic system to a final probability distribution, Part I," *IEEE Transactions on Automatic Control*, vol. 61, no. 5, pp. 1158–1169, 2016. DOI: 10.1109/TAC.2015.2457784.

[76] E. Bakolas, "Optimal covariance control for discrete-time stochastic linear systems subject to constraints," in *IEEE Conference on Decision and Control*, Las Vegas, NV, 2016, pp. 1153–1158. DOI: 10.1109/CDC.2016.7798422.

[77] ——, "Finite-horizon separation-based covariance control for discrete-time stochastic linear systems," in *IEEE Conference on Decision and Control*, Miami Beach, FL, 2018, pp. 3299–3304. DOI: 10.1109/CDC.2018.8619542.

[78] A Beghi, "On the relative entropy of discrete-time Markov processes with given end-point densities," *IEEE Transactions on Information Theory*, vol. 42, no. 5, pp. 1529–1535, 1996. DOI: 10.1109/18.532893.

[79] M. Goldshtein and P. Tsiotras, "Finite-horizon covariance control of linear time-varying systems," in *IEEE Conference on Decision and Control*, Melbourne, Australia, 2017, pp. 3606–3611. DOI: 10.1109/CDC.2017.8264189.

[80] A. Halder and E. D. Wendel, "Finite horizon linear quadratic Gaussian density regulator with Wasserstein terminal cost," in *American Control Conference*, Boston, MA, 2016, pp. 7249–7254. DOI: 10.1109/ACC.2016.7526817.

[81] Y. Chen, T. T. Georgiou, and M. Pavon, "Optimal steering of a linear stochastic system to a final probability distribution, Part III," *IEEE Transactions on Automatic Control*, vol. 63, no. 9, pp. 3112 –3118, 2016. DOI: 10.1109/TAC.2018.2791362.

[82] L. Blackmore, M. Ono, and B. C. Williams, "Chance-constrained optimal path planning with obstacles," *IEEE Transactions on Robotics*, vol. 27, no. 6, pp. 1080–1094, 2011. DOI: 10.1109/TRO.2011.2161160.

[83] A. Mesbah, "Stochastic model predictive control: An overview and perspectives for future research," *IEEE Control Systems*, vol. 36, no. 6, pp. 30–44, 2016. DOI: 10.1109/MCS.2016.2602087.

[84] L. Blackmore and M. Ono, "Convex chance constrained predictive control without sampling," in *AIAA Guidance, Navigation, and Control Conference*, Chicago, IL, 2009. DOI: 10.2514/6.2009-5876.

[85] A. Geletu, M. Klöppel, H. Zhang, and P. Li, "Advances and applications of chance-constrained approaches to systems optimisation under uncertainty," *International Journal of Systems Science*, vol. 44, no. 7, pp. 1209–1232, 2013. DOI: 10.1080/00207721.2012.670310.

[86] M. Farina, L. Giulioni, and R. Scattolini, "Stochastic linear model predictive control with chance constraints–a review," *Journal of Process Control*, vol. 44, pp. 53–67, 2016. DOI: 10.1016/j.jprocont.2016.03.005.

[87] K. Okamoto and P. Tsiotras, "Optimal stochastic vehicle path planning using covariance steering," *IEEE Robotics and Automation Letters*, vol. 4, no. 3, pp. 2276–2281, 2019. DOI: 10.1109/LRA.2019.2901546.

[88] J. Ridderhof, J. Pilipovsky, and P. Tsiotras, "Chance-constrained covariance control for low-thrust minimum-fuel trajectory optimization," in *2020 AAS/AIAA Astrodynamics Specialist Conference*, 2020.

[89] E. Tse, "On the optimal control of stochastic linear systems," *IEEE Transactions on Automatic Control*, vol. 16, no. 6, pp. 776–785, 1971. DOI: 10.1109/TAC.1971.1099840.

[90] H. A. Simon, "Dynamic programming under uncertainty with a quadratic criterion function," *Econometrica, Journal of the Econometric Society*, vol. 24, no. 1, pp. 74–81, 1956. DOI: 10.2307/1905261.

[91] J. Ridderhof, K. Okamoto, and P. Tsiotras, "Chance constrained covariance control for linear stochastic systems with output feedback," in *IEEE 59th Conference on Decision and Control*, Jeju Island, South Korea, 2020, pp. 1758–1763. DOI: 10.1109/CDC42340.2020.9303731.

[92] Y. Chen, T. Georgiou, and M. Pavon, "Steering state statistics with output feedback," in *IEEE Conference on Decision and Control*, Osaka, Japan, 2015, pp. 6502–6507. DOI: 10.1109/CDC.2015.7403244.

[93] E. Bakolas, "Covariance control for discrete-time stochastic linear systems with incomplete state information," in *American Control Conference*, Seattle, WA, 2017, pp. 432–437. DOI: 10.23919/ACC.2017.7962991.

[94] M. Farina, L. Giulioni, L. Magni, and R. Scattolini, "An approach to output-feedback MPC of stochastic linear discrete-time systems," *Automatica*, vol. 55, pp. 140–149, 2015. DOI: 10.1016/j.automatica.2015.02.039.

[95] N. Ozaki, S. Campagnola, R. Funase, and C. H. Yam, "Stochastic differential dynamic programming with unscented transform for low-thrust trajectory design," *Journal of Guidance, Control, and Dynamics*, vol. 41, no. 2, pp. 377–387, 2018. DOI: 10.2514/1.G002367.

[96] N. Ozaki, S. Campagnola, and R. Funase, "Tube stochastic optimal control for nonlinear constrained trajectory optimization problems," *Journal of Guidance, Control, and Dynamics*, vol. 43, no. 4, pp. 645–655, 2020. DOI: 10.2514/1.G004363.

[97] E. Theodorou, Y. Tassa, and E. Todorov, "Stochastic differential dynamic programming," in *American Control Conference*, Baltimore, MD, 2010, pp. 1125–1132. DOI: 10.1109/ACC.2010.5530971.

[98] Z. Yi, Z. Cao, E. Theodorou, and Y. Chen, "Nonlinear covariance control via differential dynamic programming," in *American Control Conference*, IEEE, Denver, CO, 2020, pp. 3571–3576. DOI: 10.23919/ACC45564.2020.9147531.

[99] M. Ono, M. Pavone, Y. Kuwata, and J. Balaram, "Chance-constrained dynamic programming with application to risk-aware robotic space exploration," *Autonomous Robots*, vol. 39, no. 4, pp. 555–571, 2015. DOI: 10.1007/s10514-015-9467-7.

[100] J. Ridderhof and P. Tsiotras, "Minimum-fuel powered descent in the presence of random disturbances," in *AIAA Guidance, Navigation, and Control Conference*, San Diego, CA, 2019. DOI: 10.2514/6.2019-0646.

[101] ——, "Minimum-fuel closed-loop powered descent guidance with stochastically derived throttle margins," *Journal of Guidance, Control, and Dynamics*, vol. 44, no. 3, pp. 537–547, 2021. DOI: 10.2514/1.G005400.

[102] G. Freiling, G. Jank, and H. Abou-Kandil, "Generalized Riccati difference and differential equations," *Linear Algebra and its Applications*, vol. 241, pp. 291–303, 1996. DOI: 10.1016/0024-3795(95)00587-0.

[103] G. S. Chirikjian, *Stochastic Models, Information Theory, and Lie Groups, Volume 1 Classical Results and Geometric Methods*, ser. Applied and Numerical Harmonic Analysis. Birkhäuser, 2009, ISBN: 0-8176-4803-8. DOI: 10.1007/978-0-8176-4803-9.

[104] CVX Research, Inc., *CVX: Matlab Software for Disciplined Convex Programming, version 2.0*, http://cvxr.com/cvx, Aug. 2012.

[105] M. Grant and S. Boyd, "Graph implementations for nonsmooth convex programs," in *Recent Advances in Learning and Control*, ser. Lecture Notes in Control and Information Sciences, V. Blondel, S. Boyd, and H. Kimura, Eds., http://stanford.edu/~boyd/graph_dcp.html, Springer-Verlag Limited, 2008, pp. 95–110. DOI: 10.1007/978-1-84800-155-8_7.

[106] Mosek ApS, *The MOSEK Optimization Toolbox for MATLAB Manual*, Version 9.1, 2019.

[107] J. Ridderhof and P. Tsiotras, "Planetary entry in a randomly perturbed atmosphere," in *AIAA Guidance, Navigation, and Control Conference*, Virtual event, 2021. DOI: 10.2514/6.2021-1218.

[108] J. Ridderhof, P. Tsiotras, and B. J. Johnson, "Stochastic entry guidance," 2021. arXiv: 2103.05168.

[109] D. Woffinden, S. Robinson, J. Williams, and Z. R. Putnam, "Linear covariance analysis techniques to generate navigation and sensor requirements for the safe and precise landing integrated capabilities evolution (SPLICE) project," in *AIAA Scitech Forum*, San Diego, CA, 2019, p. 0662. DOI: 10.2514/6.2019-0662.

[110] J. M. Carson, M. M. Munk, R. R. Sostaric, J. N. Estes, F. Amzajerdian, J. B. Blair, D. K. Rutishauser, C. I. Restrepo, A. M. Dwyer-Cianciolo, G. Chen, *et al.*, "The SPLICE project: Continuing NASA development of GN&C technologies for safe

and precise landing," in *AIAA Scitech Forum*, San Diego, CA, 2019. DOI: 10.2514/6.2019-0660.

[111] N. Vinh, A. Busemann, and R. Culp, *Hypersonic and Planetary Entry Flight Mechanics*. University of Michigan Press, 1980.

[112] B. J. Johnson, D. Rocca-Bejar, P. Lu, B. Nikaido, Z. B. Hays, S. D'Souza, and R. R. Sostaric, "Pterodactyl: Development and performance of guidance algorithms for a mechanically deployed entry vehicle," in *AIAA SciTech Forum*, Orlando, FL, 2020. DOI: 10.2514/6.2020-1011.

[113] J.-F. Le Gall, *Brownian Motion, Martingales, and Stochastic Calculus*, ser. Graduate Texts in Mathematics. Springer International Publishing, 2016, ISBN: 9783319310893. DOI: 10.1007/978-3-319-31089-3.

[114] J. Skaf and S. P. Boyd, "Design of affine controllers via convex optimization," *IEEE Transactions on Automatic Control*, vol. 55, no. 11, pp. 2476–2487, 2010.

[115] M. J. Wainwright, *High-Dimensional Statistics: A Non-Asymptotic Viewpoint*, ser. Cambridge Series in Statistical and Probabilistic Mathematics. Cambridge University Press, 2019. DOI: 10.1017/9781108627771.

[116] M. Chiani, D. Dardari, and M. K. Simon, "New exponential bounds and approximations for the computation of error probability in fading channels," *IEEE Transactions on Wireless Communications*, vol. 2, no. 4, pp. 840–845, 2003. DOI: 10.1109/TWC.2003.814350.

[117] J. Lofberg, "YALMIP: A toolbox for modeling and optimization in MATLAB," in *IEEE International Conference on Robotics and Automation*, IEEE, Taipei, Taiwan, 2004, pp. 284–289. DOI: 10.1109/CACSD.2004.1393890.

[118] F. W. Fairman and L. Luk, "On reducing the order of Kalman filters for discrete-time stochastic systems having singular measurement noise," *IEEE Transactions on Automatic Control*, vol. 30, no. 11, pp. 1150–1152, 1985. DOI: 10.1109/TAC.1985.1103832.

[119] K. J. Åström, *Introduction to Stochastic Control Theory*, ser. Mathematics in Science and Engineering. Academic Press, 1970, vol. 70.

[120] E. Theodorou, Y. Tassa, and E. Todorov, "Stochastic differential dynamic programming," in *American Control Conference*, Baltimore, MD, 2010, pp. 1125–1132. DOI: 10.1109/ACC.2010.5530971.

[121] E. Todorov and W. Li, "A generalized iterative LQG method for locally-optimal feedback control of constrained nonlinear stochastic systems," in *American Control Conference*, Portland, OR, 2005, pp. 300–306. DOI: 10.1109/ACC.2005.1469949.

[122] Y. Mao, M. Szmuk, and B. Açıkmeşe, "Successive convexification of non-convex optimal control problems and its convergence properties," in *IEEE 55th Conference on Decision and Control*, Las Vegas, NV, 2016, pp. 3636–3641. DOI: 10.1109/CDC.2016.7798816.

[123] M. A. Patterson and A. V. Rao, "GPOPS-II: A MATLAB software for solving multiple-phase optimal control problems using hp-adaptive gaussian quadrature collocation methods and sparse nonlinear programming," *ACM Trans. Math. Softw.*, vol. 41, no. 1, Oct. 2014. DOI: 10.1145/2558904.

[124] J. Ridderhof and P. Tsiotras, "Chance-constrained covariance steering in a Gaussian random field via successive convex programming," 2021. arXiv: 2101.09634.

[125] K. M. B. Lee, C. Yoo, B. Hollings, S. Anstee, S. Huang, and R. Fitch, "Online estimation of ocean current from sparse GPS data for underwater vehicles," in *IEEE International Conference on Robotics and Automation*, Montreal, Canada, 2019, pp. 3443–3449. DOI: 10.1109/ICRA.2019.8794308.

[126] K. J. DeMars and R. H. Bishop, "Projecting high-dimensional parametric uncertainties for improved state estimation error confidence," *Journal of Guidance, Control, and Dynamics*, vol. 38, no. 9, pp. 1659–1672, 2015. DOI: 10.2514/1.G000994.

[127] C. E. Rasmussen and C. K. I. Williams, *Gaussian Processes for Machine Learning*, ser. Adaptive Computation and Machine Learning. The MIT Press, 2005. DOI: 10.7551/mitpress/3206.001.0001.

[128] D. G. Krige, "A statistical approach to some basic mine valuation problems on the Witwatersrand," *Journal of the Southern African Institute of Mining and Metallurgy*, vol. 52, no. 6, pp. 119–139, 1951. DOI: 10520/AJA0038223X_4792.

[129] G. Camps-Valls, J. Verrelst, J. Munoz-Mari, V. Laparra, F. Mateo-Jimenez, and J. Gomez-Dans, "A survey on Gaussian processes for Earth-observation data analysis: A comprehensive investigation," *IEEE Geoscience and Remote Sensing Magazine*, vol. 4, no. 2, pp. 58–78, 2016. DOI: 10.1109/MGRS.2015.2510084.

[130] S. Anderson, T. D. Barfoot, C. H. Tong, and S. Särkkä, "Batch nonlinear continuous-time trajectory estimation as exactly sparse Gaussian process regression," *Autonomous Robots*, vol. 39, no. 3, pp. 221–238, 2015. DOI: 10.1007/s10514-015-9455-y.

[131] M. Mukadam, X. Yan, and B. Boots, "Gaussian process motion planning," in *IEEE International Conference on Robotics and Automation*, Stockholm, Sweden, 2016, pp. 9–15. DOI: 10.1109/ICRA.2016.7487091.

[132] E. Kreuzer and E. Solowjow, "Learning environmental fields with micro underwater vehicles: A path integral—Gaussian Markov random field approach," *Autonomous Robots*, vol. 42, no. 4, pp. 761–780, 2018. DOI: 10.1007/s10514-017-9685-2.

[133] C. G. Olson, R. P. Russell, and J. R. Carpenter, "Precomputing process noise covariance for onboard sequential filters," *Journal of Guidance, Control, and Dynamics*, vol. 40, no. 8, pp. 2062–2075, 2017. DOI: 10.2514/1.G002144.

[134] C. Van Loan, "Computing integrals involving the matrix exponential," *IEEE Transactions on Automatic Control*, vol. 23, no. 3, pp. 395–404, 1978. DOI: 10.1109/TAC.1978.1101743.

VITA

Jack Ridderhof earned his bachelor's and master's degrees in Aerospace Engineering and master's degree in Mathematics all from the Georgia Institute of Technology, where he is currently a Ph.D. candidate in Aerospace Engineering. Jack is a NASA Space Technology Fellow.